



UNIVERSITY OF
LEICESTER

Graduate School

Exploiting Quantitative Trait Analysis in Yeast to Identify Genetic Modifiers of Huntington's and Parkinson's Disease

Thesis submitted for the degree of

Doctor of Philosophy

at the University of Leicester

by

Mónica Alfonso Núñez (MSc, BSc)

Department of Genetics and Genome Biology

University of Leicester

December 2021

Abstract

Exploiting Quantitative Trait Analysis in Yeast to Identify Genetic Modifiers of Huntington's and Parkinson's Disease by Mónica Alfonso Núñez.

Huntington's disease (HD) and Parkinson's disease (PD) are neurodegenerative diseases (NDs) in which protein misfolding/accumulation are associated with neuronal dysfunction and loss. HD is a hereditary disease caused by the expansion of a CAG trinucleotide repeat in the *huntingtin* (*HTT*) gene. Although the number of repeats correlates with the severity of the disease, there is still variability amongst individuals with the same number of repeats. PD is the second most common ND and, although there are familial forms, most PD cases are sporadic, caused by a combination of environmental and genetic risk factors, one of which is the *SNCA* gene that encodes α-Synuclein (αSyn).

To find candidate genetic modifiers responsible for the variability in severity/risk in HD and PD, quantitative trait loci (QTL) analysis was performed in yeast. The effect of mutant HTT (mHTT) and αSyn on growth was assessed in 14 genetically diverse natural isolates using PHENOS - a software that allows the analysis of yeast growth on solid media -. The strains that showed the most extreme phenotypes (SX1, HN6 and BJ20) were intercrossed to generate a large population of stains with new combinations of alleles. The QTL analysis was performed using the effect on growth of mHTT and αSyn separately, and the possible modifier genes that were present in both lists were further validated in yeast and fruit flies by overexpressing or downregulating them.

Through this work we identified four genes whose deletion enhanced the toxicity of the proteins: *PPM1* and *TIF6* enhanced both mHTT and αSyn toxicity, while *PER1* and *GIN4* only enhanced αSyn toxicity. The overexpression (OE) of *TIF6* was protective against mHTT and αSyn toxicity in yeast. In conclusion, these four genes, specially *TIF6*, are interesting therapeutic targets for HD and PD and should be validated in more complex models.

Acknowledgements

Firstly, I would like to thank my supervisors Flav and Ed for giving me this opportunity and for all the support they have provided me during the PhD. I'm going to miss the stories about how science was decades ago and the guitar concerts in the lab. I would also like to thank everyone else in both labs for making such an amazing work environment. And especially to Yue Hu for her help with the QTL analysis, I would have thrown the computer out of the window without your help.

I also thank the University of Leicester for awarding me the scholarship that made this possible. And I appreciate the collaboration of Lina, Sarah, Fiora, Nyasha and Ali, the undergraduate and Erasmus students that helped me with the project.

Finally, I want to thank my friends and family for all their support. I would have gone crazy without all the stupid jokes and baseless scientific facts.

Jesús, Mercedes and Ricardo, thank you for supporting me when I decided to go to a different country alone because there was something I wanted to study there. You are the best family anyone can hope to have, although you have the weirdest sense of humour.

To all my friends, thanks for keep talking to me even when I keep mixing Spanish and English. I know I don't make sense most of the time and I promise I will learn how to speak only in Spanish again soon!

It's the questions we can't answer that teach us the most. They teach us how to think. If you give a man an answer, all he gains is a little fact. But give him a question and he'll look for his own answers. Patrick Rothfuss (*The Wise Man's Fear*)

List of contents

Abstract	I
Acknowledgements	II
List of contents	III
List of tables	VII
List of figures	VIII
List of abbreviations	XI
1. Introduction	1
1.1. Study of heritable traits	1
1.1.1. Differences between Mendelian and quantitative traits	1
1.1.2. Genome-wide association studies.....	4
1.2. Neurodegenerative diseases.....	4
1.2.1. Huntington's Disease	7
1.2.1.1. Symptoms of HD.....	9
1.2.1.1.1. Psychiatric disturbances	10
1.2.1.1.2. Cognitive loss.....	10
1.2.1.1.3. Motor impairment	10
1.2.1.2. Genetics of HD	11
1.2.1.3. Histopathological hallmarks of HD	13
1.2.1.4. Characteristics and role of wildtype HTT	14
1.2.1.5. Mechanisms of cellular pathogenesis in HD	15
1.2.1.6. Genetic modifiers found in previous studies	17
1.2.2. Parkinson's Disease	19
1.2.2.1. Symptoms of PD	21
1.2.2.2. Pathological hallmarks of PD	22
1.2.2.3. Aetiology of PD	23
1.2.2.3.1. Genes involved in familial forms of PD	23
1.2.2.3.2. GWAS studies in PD.....	24
1.3. Organisms used to model NDs	27
1.3.1. <i>Saccharomyces cerevisiae</i> as a model of NDs	28
1.3.1.1. Yeast as a model of HD and PD	29
1.3.2. <i>Drosophila melanogaster</i> as a model of neurodegenerative diseases	32
1.3.2.1. <i>GAL4/UAS</i> system	33
1.3.2.2. Flies as a model of HD	36
1.4. Aims and objectives	38
2. Materials and methods	40
2.1. <i>Saccharomyces cerevisiae</i> strains	40
2.1.1. Yeast Maintenance	41
2.1.1.1. Media for yeast	41
2.1.1.1.1. Types of plates and tubes.....	42
2.1.1.1.2. Yeast extract peptone dextrose (YPD) and yeast extract peptone galactose (YPGal) media	42
2.1.1.1.3. Synthetic defined (SD) complete (SC) and dropout (SD-aa) media.....	43
2.1.1.1.4. Complete powder and dropout powders.....	43
2.1.1.1.5. FoA (5-Fluoroorotic acid) media for <i>ura3Δ0</i> selection	44

2.1.1.1.6. Potassium acetate (KAc) media for sporulation	44
2.1.1.1.7. Minimal media.....	44
2.1.1.2. Growth, storage, and recovery of yeast strains	44
2.1.1.2.1. Growth conditions	44
2.1.1.2.2. Storage conditions and sample recovery.....	45
2.1.1.2.3. Obtaining single colonies.....	45
2.1.2. Plasmids and deletion cassettes	46
2.1.2.1. Maintenance of <i>Escherichia coli</i>.....	46
2.1.2.1.1. Media for bacteria	46
2.1.2.1.2. Growth, storage, and recovery of <i>E. coli</i>	46
2.1.2.2. Gene cloning and bacterial transformation	47
2.1.2.2.1. PCR amplification of candidate genes.....	47
2.1.2.2.2. Transformation of the gene into an intermediate vector for easier digestion	48
2.1.2.2.3. RE digestion and integration into the final vector	49
2.1.2.3. Amplification of DNA cassettes for gene deletion by homologous recombination	50
2.1.2.3.1. Cassette for the deletion of the <i>URA3</i> gene (<i>ura3Δ0</i>)	50
2.1.2.3.2. Cassette for the substitution of the gene with <i>LEU2</i> (<i>gene::LEU2</i>)	51
2.1.2.4. List of plasmids and DNA cassettes	53
2.1.2.4.1. Auxotrophic markers	54
2.1.2.4.2. Plasmids	56
2.1.2.4.3. Deletion of possible modifier genes	57
2.1.3. Transformation of yeast strains	57
2.1.3.1. Lithium Acetate (LiAc) transformation protocol	57
2.1.3.2. High-throughput transformation protocol	58
2.1.4. Phenotyping yeast strains	59
2.1.4.1. Spotting assay	59
2.1.4.2. Phenotyping in solid media (PHENOS)	60
2.1.4.3. Aggregation assessment	62
2.1.4.3.1. Fluorescence microscopy	62
2.1.4.3.2. Filter trap	63
2.1.4.4. Flow Cytometry	65
2.1.5. Intercrosses of yeast strains	67
2.1.5.1. Yeast crossing protocol	67
2.1.5.2. Tetrad dissection	68
2.1.5.3. Mating type test	69
2.1.6. Genotyping yeast strains	70
2.1.6.1. Genomic DNA extraction	70
2.1.6.2. DNA quantification	70
2.1.6.3. Sequencing	71
2.1.7. Bioinformatics	71
2.1.7.1. QTL analysis	71
2.1.7.2. Study of the interactome and the pathways enriched in the QTL	72
2.1.7.3. Other bioinformatic tools	73
2.2. <i>Drosophila melanogaster</i>	73
2.2.1. Fly lines	73
2.2.2. Maintenance of fruit flies	75
2.2.3. Fly crosses	75
2.2.3.1. Cross to express HTT in neurons	76
2.2.3.2. Cross to downregulate the expression of the modifier genes in neurons	77
2.2.3.3. Cross to express HTT and downregulate the modifiers in neurons	77
2.2.3.3.1. Genotyping of the HTT and modifier recombinants	78
2.2.4. Phenotyping of flies	80
2.2.4.1. Viability assay	80
2.2.4.2. Survival assay	80
2.2.4.3. Pseudopupil assay	81
2.2.4.4. Locomotor activity assay	82

3. Selection of parental strains for QTL analysis	84
3.1. Results.....	84
3.1.1. Selection of strains able to use galactose as a source of carbon	84
3.1.2. Deletion of <i>URA3</i> in the <i>GAL+</i> strains	86
3.1.3. Effect of mHTT expression in yeast.....	87
3.1.3.1. The effect of mHTT on viability is affected by the genotype	87
3.1.3.2. The effect on growth of mHTT is affected by the genotype	89
3.1.3.3. Cellular distribution and kinetics of mHTT are affected by the genotype	90
3.1.4. Effect of alpha-synuclein expression in the parental strains	94
3.1.4.1. The effect of α Syn on viability is affected by the genotype	95
3.1.4.2. The effect on growth of α Syn is affected by the genotype	97
3.1.4.3. Cellular distribution and kinetics of α Syn are similar between genotypes	98
3.1.5. Further characterization of the selected parental strains	99
3.1.5.1. The parental strains carry the [PIN+] prion	100
3.1.5.2. The expression levels from pRS426 and pRS327 are unrelated to the decrease in toxicity	101
3.2. Discussion.....	103
4. Intercrosses and QTL analysis	105
4.1. Results.....	105
4.1.1. Parental strain preparation and intercrosses.....	105
4.1.2. PHENOS of F12 strains	106
4.1.3. Aggregation of mHTT is unrelated to growth or survival.....	108
4.1.4. QTL analysis.....	110
4.1.4.1. mHTT QTL analysis	110
4.1.4.2. α Syn QTL analysis	115
4.2. Discussion.....	117
4.2.1. <i>SLMAP (FAR10)</i>	119
4.2.2. <i>LCMT1 (PPM1)</i>	120
4.2.3. <i>RAB1F (DSS4)</i>	121
4.2.4. <i>EIF6 (TIF6)</i>	124
4.2.5. <i>POLR1B (RPA135)</i>	125
4.2.6. <i>TAF2 (TAF2)</i>	127
4.2.7. <i>GYS1 and GYS2 (GYS2)</i>	127
4.2.8. <i>SLC25A42 (MRX21)</i>	128
5. QTL validation in <i>Saccharomyces cerevisiae</i>	130
5.1. Results.....	130
5.1.1. Effect of the deletion of the modifier gene candidates on mHTT and α Syn toxicity in the parental strains	130
5.1.2. Effect of the OE of the modifier gene candidates on mHTT and α Syn toxicity in the parental strains	137
5.1.3. Effect of the deletion of other possible modifier genes on mHTT and α Syn toxicity in BY4741	144
5.2. Discussion.....	147
6. QTL validation in <i>Drosophila melanogaster</i>	155
6.1. Results.....	155
6.1.1. Characterization of the HTT lines	155
6.1.1.1. Cross to obtain the flies that express HTT in the neurons	156
6.1.1.2. Expression of mHTT Ex1 in neurons reduces the viability of flies	157
6.1.1.3. Expression of mHTT in neurons reduces the lifespan of flies	158
6.1.1.4. Expression of mHTT Ex1 in neurons causes neurodegeneration from day one	159

6.1.1.5. Expression of mHTT in neurons causes locomotor impairment.....	160
6.1.2. Characterization of the modifier lines	161
6.1.2.1. Cross to obtain the flies that express the different shRNA in neurons ...	162
6.1.2.2. The downregulation of <i>DPCoAC</i> in neurons reduces the viability of flies	162
6.1.2.3. The downregulation of <i>DPCoAC</i> in neurons reduces the lifespan of flies	163
6.1.2.4. There is no neuronal loss caused by the downregulation of the genes in flies.....	164
6.1.3. Effect of the downregulation of the modifier genes on the toxicity of HTT 165	
6.1.3.1. Cross to obtain the flies that express HTT and the shRNA in neurons ...	166
6.1.3.2. Downregulation of <i>Strat</i> and <i>eIF6</i> does not modulate the viability of mHTT flies.....	167
6.1.3.3. Downregulation of <i>Strat</i> and <i>eIF6</i> does not modulate the lifespan of mHTT flies.....	168
6.1.3.4. Downregulation of <i>Strat</i> partially rescues the neurodegeneration caused by mHTT	169
6.2. Discussion.....	170
7. Discussion and future directions	175
8. Bibliography	185

List of tables

Table 2.1-1. Yeast strains information.....	40
Table 2.1-2. Amino acid composition of the complete powder	43
Table 2.1-3. Primers and Ta for gene cloning	48
Table 2.1-4. RE digestion protocol	50
Table 2.1-5. Primers for the amplification of the deletion cassettes	52
Table 2.1-6. Primers and fragment sizes for the deletion-check PCR.....	53
Table 2.1-7. List of plasmids and DNA cassettes.....	53
Table 2.1-8. Rotor protocols for PHENOS	61
Table 2.2-1. Fly lines.....	74
Table 2.2-2. Fly food recipe.....	75
Table 2.2-3. Primers for genotyping the recombinant flies	79
Table 4.1-1. Number of loci and genes identified during the QTL analysis	110
Table 4.1-2. Pathways enriched in the mHTT QTL list.....	111
Table 4.1-3. Pathways enriched in the α Syn QTL list	115
Table 5.1-1. Effect of the deletion of the possible modifier genes on mHTT and α Syn toxicity in the parental strains.....	133
Table 5.1-2. Effect of the OE of the possible modifier genes on mHTT and α Syn toxicity in the parental strains.....	140
Table 5.1-3. Effect of the deletion of possible modifier genes in mHTT and α Syn toxicity in the laboratory strain BY4741.....	146

List of figures

Figure 1.1-1. Inheritance of Mendelian and quantitative traits.....	2
Figure 1.2-1. Aggregate formation mechanism in NDs.	6
Figure 1.3-1. Crosses for neuronal expression using the GAL4/UAS system ..	34
Figure 2.1-1. Phylogenetic diversity of the natural yeast strain isolates	41
Figure 2.1-2. Auxotrophic markers deletion protocol.....	55
Figure 2.1-3. Spotting assay protocol.....	59
Figure 2.1-4. Punch-in method to normalize mass for PHENOS experiments .	60
Figure 2.1-5. Illustration of the growth curves provided by PHENOS with all the parameters analysed by the software	62
Figure 2.1-6. Yeast crossing protocol to generate the F12	68
Figure 2.1-7. Dissection YPD plates	69
Figure 2.2-1. Crossing scheme to obtain flies that express the HTT constructs in neurons	76
Figure 2.2-2. Crossing scheme to obtain flies that express the different RNAi in neurons	77
Figure 2.2-3. Crossing scheme to obtain the flies that express both the RNAi construct and HTT in the neurons	78
Figure 2.2-4. Counter current climbing apparatus protocol	83
Figure 3.1-1. Not all yeast strains have the ability to use galactose as source of carbon.....	85
Figure 3.1-2. Yeast strains present a wide range of viability phenotypes while expressing mHTT.....	88
Figure 3.1-3. Differences in growth due to mHTT toxicity can be assessed using PHENOS.....	90
Figure 3.1-4. There are differences in the aggregation dynamics of the strains.	93
Figure 3.1-5. Agarose electrophoresis gels of the amplification and integration of GFP into pRS426.	95
Figure 3.1-6. Yeast strains present a wide range of viability phenotypes while expressing α Syn.....	96
Figure 3.1-7. SX1 is resistant to α Syn expression.	97
Figure 3.1-8. Differences in growth due to α Syn toxicity can be assessed using PHENOS.	98
Figure 3.1-9. There are no differences in the aggregation dynamics of WT α Syn in the parental strains.....	99

Figure 3.1-10. All the parental strains are [PIN+].	100
Figure 3.1-11. Comparison of the level of expression from pRS426 and pRS327 plasmids on the parental strains.....	102
Figure 4.1-1. α Syn and mHTT toxicity is variable among the F12 strains of the three intercrosses.....	107
Figure 4.1-2. Aggregation of mHTT is unrelated to its toxicity.....	109
Figure 4.1-3. Human orthologues interaction network of the mHTT QTL.....	113
Figure 4.1-4. Human orthologues' interaction network of the α Syn QTL.....	116
Figure 5.1-1. Most of the non-essential genes were deleted in all the strains using the homologous recombination transformation protocol.....	131
Figure 5.1-2. The deletion of <i>GYS2</i> , <i>TAF2</i> and <i>PPM1</i> in the resistant strain SX1 enhances toxicity of mHTT and α Syn.	134
Figure 5.1-3. The deletion of <i>TIF6</i> , <i>PPM1</i> and <i>GYS2</i> reduces toxicity of mHTT, and the deletion of <i>TIF6</i> and <i>DSS4</i> reduces the toxicity of α Syn in the sensitive strain HN6.	135
Figure 5.1-4. The deletions of <i>TAF2</i> , <i>GYS2</i> , <i>DSS4</i> , <i>PPM1</i> and <i>MRX21</i> in the sensitive strain BJ20 decrease toxicity of mHTT, and all except <i>PPM1</i> decrease α Syn toxicity.....	137
Figure 5.1-5. There is expression of GFP and α Syn to confirm the cloning of those genes into the pRS426 <i>L</i> YS2 plasmids in the parental strains.....	139
Figure 5.1-6. The OE of <i>TAF2</i> and <i>MRX21</i> in the resistant strain SX1 enhances toxicity of mHTT, and the OE of <i>DSS4</i> and <i>MRX21</i> of α Syn.....	141
Figure 5.1-7. The OE of <i>TIF6</i> , <i>TAF2</i> , <i>DSS4</i> and <i>MRX21</i> is protective against mHTT toxicity in the sensitive strain HN6.....	142
Figure 5.1-8. OE of <i>TIF6</i> in the sensitive strain BJ20 decreases toxicity of mHTT.	143
Figure 5.1-9. The deletion of SNT1 is protective against mHTT and α Syn toxicity in the laboratory strain BY4741.	147
Figure 6.1-1. Expression of mHTT Ex1 causes a reduction in the number of flies that make it to adulthood.....	157
Figure 6.1-2. Expression of mHTT causes a significant reduction in the lifespan of the flies.....	158
Figure 6.1-3. The expression of mHTT Ex1 causes neurodegeneration from day one.	160
Figure 6.1-4. Expression of mHTT causes movement impairment in flies.	161
Figure 6.1-5. Downregulation of <i>DPCoAC</i> causes a reduction in the number of flies that make it to adulthood.....	163

Figure 6.1-6. Downregulation of <i>DPCoAC</i> causes a significant reduction in the lifespan of the flies.....	164
Figure 6.1-7. Downregulating the expression of <i>Strat</i> , <i>DPCoAC</i> or <i>eIF6</i> has no neurodegenerative effects in the fly eye.....	165
Figure 6.1-8. Agarose electrophoresis gels of the recombination PCR.....	167
Figure 6.1-9. There is no rescue in the percentage of flies that make it to adulthood when downregulating <i>Strat</i> or <i>eIF6</i>	168
Figure 6.1-10. No significant rescue in longevity was found due to the downregulation of <i>Strat</i> or <i>eIF6</i>	169
Figure 6.1-11. Downregulating the expression of <i>Strat</i> partially rescues the neurodegeneration caused by mHTT.....	170

List of abbreviations

3-HK	3-hydroxykynurenone
3M	Empty vector control for flies
AD	Alzheimer's disease
ALS	Amyotrophic lateral sclerosis
BDNF	Brain-derived neurotrophic factor
CelAc	Cellulose acetate
Chr	Chromosome
CNV	Copy number variation
CoA	Coenzyme A
dH ₂ O	Deionized water
dMG	Difference in maximum growth
dMS	Difference in maximum slope
dsRNA	Double-stranded RNA
EDTA	Ethylenediaminetetraacetic acid
ER	Endoplasmic reticulum
EtBr	Ethidium bromide
F1	First generation
F12	Twelfth generation
FDR	False discovery rate
FoA	5-Fluoroorotic acid
GAL+	Able to grow using galactose as the source of carbon
GAP	GTP activating protein
GDNF	Glial cell line-derived neurotrophic factor
GEF	Guanine exchange factor
GPI	Glycosylphosphatidylinositol
GPI-AP	GPI-anchored proteins
GWAS	Genome-wide association studies
HD	Huntington's disease
HTT	Huntingtin
Kac	Potassium acetate
KP	Kynurenine pathway
KYNA	Kynurenic acid
LB	Lewy body
LBr	Luria Broth
LBr-Amp	LBr with ampicillin

LD	Linkage disequilibrium
LiAc	Lithium acetate
LN	Lewy neurites
LOD	Logarithm of the odds
MG	Maximum growth
mHTT	Mutant Huntingtin
mPP2A	Methylated PP2A
MPTP	1-methyl-4-phenyl-1,2,3,6-tetrahydropyridine
mRNA	Messenger RNA
MS	Maximum slope
NA	North American
NC	Nitrocellulose
ND	Neurodegenerative disease
OD600	Optic density at 600 nm
OE	Overexpression
ORF	Open reading frame
PAP	Adenosine 3', 5' -diphosphate
PD	Parkinson's disease
PEG	Polyethylene glycol
PHENOS	Phenotyping in Solid Media (software)
pMST2	Phosphorylated MST2
PolyQ	Polyglutamine
QTL	Quantitative trait loci
QUIN	Quinolinic acid
rDNA	Ribosomal DNA
RE	Restriction enzyme
RNA Pol I	RNA Polymerase I
RNAi	RNA-mediated interference
rRNA	Ribosomal RNA
SA	Sake
SC	Synthetic complete
SD	Synthetic defined
SD-aa	Synthetic define media without an amino acid
SDS	Sodium dodecyl sulphate
shRNA	Short hairpin RNA
SNCA	α -Synuclein (gene)
SNP	Single nucleotide polymorphism

ssDNA	Single-stranded carrier DNA
TRED	Trinucleotide repeat expansion diseases
TWAS	Transcriptome-wide association study
UAS	Upstream activation sequence
UPR	Unfolded-protein response
WA	West African
WE	Wine European
WT	Wildtype
YFG	Your favourite gene
YNB	Yeast nitrogen base without amino acids
YPD	Yeast extract peptone dextrose
YPG	Yeast extract peptone galactose
α Syn	α -Synuclein (protein)

1. Introduction

During this thesis yeast and fly models are used to identify and validate genes that modify the phenotype of two neurodegenerative diseases (NDs), Huntington's (HD) and Parkinson's disease (PD), using a technique called quantitative trait loci (QTL) analysis.

Hence, this introductory chapter will review the research on which the experiments of this thesis are based, including how to study heritably traits and how that can be applied to the study of NDs, the core facts about NDs focusing on HD and PD, and the reasons behind using yeast and flies as a model in this study.

1.1. Study of heritable traits

1.1.1. Differences between Mendelian and quantitative traits

Heritable traits can be divided between Mendelian and quantitative traits (Fisher, 1919; Visscher & Goddard, 2019; Weldon, 1902). Mendelian traits are those in which one or a few genes are responsible for large variations on the phenotype, having high or complete penetrance (Weldon, 1902) (Figure 1.1-1 A). The best-known example is the genetics of pea colour described by Mendel: if you cross two homozygote lines of peas, one green (recessive) and one yellow (dominant), all the descendants will be yellow because that allele has complete dominance and only one copy is necessary to show the phenotype. Mendelian inheritance is what is observed in HD and the familial forms of PD, where mutation of one gene is sufficient to cause the disease whether it is in a dominant -*Huntingtin (HTT)* and *alpha-synuclein (SNCA)*- or a recessive -*Parkin (PRKK)*- manner (HDCRG, 1993; Jankovic & Tan, 2020; Polymeropoulos et al., 1996). On the other hand, quantitative traits, which present a continuous variation, depend on the combined effect of many genes

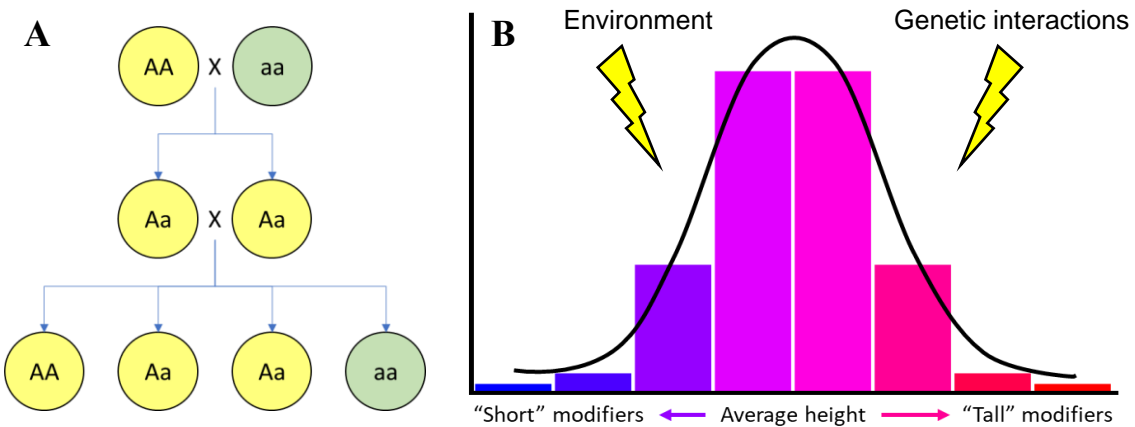


Figure 1.1-1. Inheritance of Mendelian and quantitative traits

A) Mendelian traits are dominated by one or few genes. For example, in peas, the presence of the dominant allele (A) will give you a yellow phenotype while the presence of the recessive allele (a) will give you a green phenotype but only in homozygotes. **B)** Quantitative traits are controlled by several genes, for example, the average height of an individual will depend on the final combination of “short” and “tall” alleles and the interactions between them. However, it will also be influenced by the environment.

to determine the phenotype (Figure 1.1-1 B) (Özsoy et al., 2021; Taylor & Ehrenreich, 2014). That can be because each gene has a small effect on the phenotype, or because they present complex interactions acting as modifiers of one another, producing a phenotype that is stronger than the sum of each of their effects alone. In addition, the influence of environmental factors on the phenotype is easier to perceive in qualitative traits. One of the best-known examples of quantitative traits is height (Fisher, 1919). It is known that the height of a person is influenced by environmental factors like nutrition, but genetics have a major influence on it too (Fisher, 1919). However, since height is a quantitative trait, there is no one specific gene that correlates with it, but a great number of them. There is still no clear answer to how many genes are involved in height and what proportion of the inheritance they are responsible for. In the beginning, Fisher thought 95% of height was hereditary, however, recent genome-wide association studies (GWAS) have been unable to account for all that variability (Fisher, 1919; Wood et al., 2014; Yengo et al., 2018).

A study performed on 450,000 individuals discovered 3290 nearly independent SNPs related to height that explain 25.6% of the phenotypical variance (Yengo et al., 2018).

A different study with more than 250,000 participants identified 697 variants in 423 loci that together explained 60% of the heritability (Wood et al., 2014). Although not all the variability has been accounted for, researchers believe that interactions between the identified genes could explain at least part of it.

Quantitative traits are considerably more common than Mendelian ones in yeast, where only 8.9% of traits presented Mendelian inheritance (Hou et al., 2016). Furthermore, some Mendelian genes can also present more complex inheritance patterns in different yeast strains depending on the background - some genes are inherited in a Mendelian way in one strain but present incomplete penetrance and act as modifiers in a different one - meaning that the separation between Mendelian and quantitative traits is not as clear as it was previously thought.

The genetic cause of traits is being researched in two different ways, depending on the population employed for the studies (Londin et al., 2013). Pedigree studies recruit members of the same family, in which there are several cases of a specific trait, while GWAS recruit large populations of non-related individuals also with and without the trait. The advantage of pedigree studies is that the sample size is smaller, however, this means that the markers discovered might not have a high prevalence in the general population even among those with the trait. Family studies are more useful to uncover risk alleles related to Mendelian traits. On the other hand, GWAS are more useful to study complex traits. They require large populations since they are based on the principle of linkage disequilibrium (LD) - some loci associated and segregate together, usually due to close proximity in the chromosome - to identify the modifier genes.

1.1.2. Genome-wide association studies

The development of GWAS has become a valuable resource to discover the genes responsible for quantitative traits (Londin et al., 2013; Plomin et al., 2009; Visscher et al., 2012). GWAS are studies in which the whole genome of a considerable number of individuals is scanned for variants, usually single nucleotide polymorphisms (SNPs) and sometimes copy number variations (CNVs), that might be related to a specific phenotype. As mentioned before, these studies need to be carried out in large populations because they are based on LD. Since there are several groups of linked genes that tend to be inherited together, a large population in which many recombination events have happened is necessary in order to break the linkage groups into small enough regions so that a SNP can be used to mark just a few genes. The more recombination there is in the population, the more variability there is, making it easier to identify the responsible gene associated with a marker. An SNP with a significantly higher presence in individuals with the phenotype than in those without it indicates that a gene in that region is related to the trait, so then they should be further studied to validate the discovery. GWAS provide several variants with different risk factors associated to the trait, the effect of the variants increases when more of them are present in an individual.

1.2. Neurodegenerative diseases

Neurodegenerative disorders are a group of diseases that affect the central or peripheral nervous system (Dugger & Dickson, 2017; Skovronsky et al., 2006). A key feature of these diseases is the loss of function or death of specific neuronal populations. They can be classified based on the main symptoms present in the patients, including impaired movement, cognitive and behavioural disorders, although often they present a mix of these clinical features. NDs mostly happen past

middle age and, while some of them are hereditary, most of them are idiopathic with age being one of the most important risk factors for developing the disease. Interestingly, not all the NDs have genetic causes, some of them are caused by prions - infective misfolded proteins that are able to replicate by misfolding normal variants of the same protein (NIH, 2019) -, and some are caused by environmental factors (Dugger & Dickson, 2017; Skovronsky et al., 2006).

Even though the causes and symptoms of NDs are widely variable, many have in common that there is an accumulation of insoluble filamentous aggregates of protein in the central nervous system that is associated with neuronal dysfunction and loss, which predominantly affects a specific brain region (Dugger & Dickson, 2017; Skovronsky et al., 2006). The proteins - or peptides - that aggregate are soluble in their native form, and some are expressed ubiquitously but only aggregate in the central nervous system in the context of disease. The aggregation begins with the protein of interest being misfolded (Karamanos et al., 2015; Skovronsky et al., 2006). This misfolded protein has the tendency of self-associating, forming oligomers that, similarly, associate with one another forming protofibrils, and finally creating fibrils (Figure 1.2-1). In order to get rid of the aggregates, the options are stabilizing the native protein to avoid its misfolding, using chaperones to correctly fold the misfolded protein, degrading the protein, or dissolving the fibrils into oligomers or monomers and clear them.

The presence of misfolded proteins is not only a problem because of its potential loss of normal function, but also because the aggregates can impair cellular mechanisms and even sequester other proteins causing the impairment of several mechanisms in the cell (Karamanos et al., 2015; Skovronsky et al., 2006). It is still unknown which aggregation stage of the protein constitutes the toxic species, but it affects several important mechanisms of the cell: the accumulation of a misfolded

protein causes proteotoxic stress and the collapse of the protein degradation systems (proteasomal and lysosomal systems), it also causes impairments in axonal transport, defects in DNA transcription and increased levels of oxidative stress, and together, these dysfunctions lead to programmed cell death and neuroinflammation.

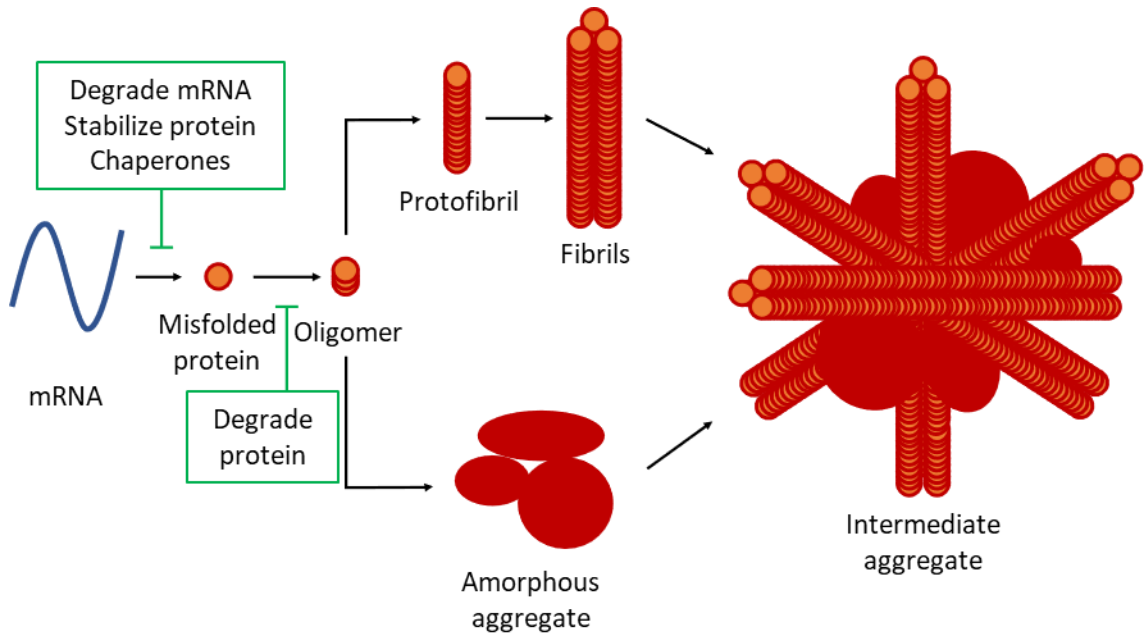


Figure 1.2-1. Aggregate formation mechanism in NDs.

After the translation of the mRNA, the protein misfolds. Misfolded proteins associate and form oligomers. If the oligomers continue associating without forming a structure, they become amorphous aggregates. If the oligomers associate forming a structure they become protofibrils, that can associate into fibrils (a.k.a. filamentous aggregates). Intermediate aggregates are structures made out of fibrils and amorphous aggregates. Aggregate formation can be prevented by degrading the mRNA so the protein can not be synthesised, stabilizing the protein in its native state so it keeps its original structure, refolding the protein with chaperones, or degrading the protein before it forms more resilient structures.

Even though the protein aggregates can appear several years prior to the onset of the symptoms of the disease, there are no biomarkers for many NDs - although some can be detected thanks to mutations in the causative gene, analysis of the cerebrospinal fluid, or via imaging - and the diagnosis needs to be confirmed during autopsy (Dugger & Dickson, 2017).

Even though the pathogenic mechanism appears to be similar, the protein that aggregates, the location of the aggregates - intra or extracellular - and the timing and

region where those aggregates appear are different for each ND (Dugger & Dickson, 2017; Skovronsky et al., 2006). Notably, there can be several diseases associated with the same aggregation-prone protein, as is the case of tauopathies (Alzheimer's disease (AD), Prick's disease), α -synucleinopathies (PD, dementia with Lewy bodies), and transactivation response DNA binding protein 43 proteinopathies (Amyotrophic lateral sclerosis (ALS), Frontotemporal lobar degeneration), or they can be caused by different proteins that have the same motif, such as CAG triplet repeat expansion diseases (HD, X-linked spinal-bulbar muscular atrophy), or by prions (Creutzfeldt–Jakob disease, Gerstmann–Straüssler–Scheinker disease).

CAG triplet expansion diseases, also known as polyglutamine (polyQ) diseases, are a type of trinucleotide repeat expansion diseases (TREDs). TREDs are caused by an increase in the number of a specific triplet above a certain threshold (Budworth & McMurray, 2013). These diseases are classified depending on the sequence of the triplet: CGG (arginine) expansion is related to fragile X syndrome, CAG (glutamine) to X-linked spinal-bulbar muscular atrophy and HD, and CTG (leucine) to myotonic dystrophy type 1. Although they share a cause, the toxicity can occur for different reasons, such as RNA silencing - Fragile X syndrome - or protein misfolding and aggregation – polyQ diseases -. In TREDs, the age at onset and severity of the disease inversely correlates with the number of repeats and, although these diseases are hereditary, the number of repeats is unstable, which makes it possible for an individual barely below the threshold to produce gametes with a number of repeats above the threshold.

1.2.1. Huntington's Disease

HD (OMIM 143100) is a ND first described by George Huntington in 1872. He reported it as a severe, rare hereditary form of chorea that causes the progressive

degeneration, leading to spasms of the voluntary muscles and psychological problems. Unlike other forms of chorea known at the time, HD onset happens during adult life and is always fatal.

HD has a prevalence in the general population of five to ten cases per 100,000 individuals (Parsons & Raymond, 2015) and, similar to what Huntington described, the hallmarks of HD currently include the progressive degeneration of the patient due to movement disorders, a variety of psychiatric syndromes, and cognitive impairment (Bonelli & Beal, 2013). Among the movement disorders, the involuntary choreic movements are the most characteristic of the disease and are often considered the clinical onset of HD, which occurs during midlife - the average being 30 to 50 years but presenting a wide range from two to 85 years (Bonelli & Beal, 2013; Roos, 2010). The disease takes 17 to 20 years to develop on average, and as it progresses, the patient's condition worsens until the patient dies. The choreic movements are substituted by movement impairment, and the cognitive dysfunction worsens, leading to more dependency and finally to death. The leading cause of death of HD patients is pneumonia, followed by suicide.

Although almost 30 years have passed since the HD collaborative research group (1993) discovered that HD is caused by the presence of an expansion of a trinucleotide CAG repeat region in the *HTT* gene, which can be used to validate HD diagnosis by genetic testing, there are still no cures or treatments available to delay the appearance or progression of this disease. However, there are a few treatments available to relieve the symptoms (Dash & Mestre, 2020). One of the main drugs being used for treating chorea is tetrabenazine, an inhibitor of the vesicular monoamine transporter, which has been proved to ameliorate the choreic symptoms and is well tolerated as a long-term treatment, although it has neuropsychiatric and motor side effects (Frank, 2009; Huntington Study Group, 2006). There is also a

deuterated version of the drug, deutetrabenazine, that has been reported to have similar therapeutic effects that last for longer and have less severe side effects (Shao & Hewitt, 2010). In addition, dopamine blocking agents and Benzodiazepines have been utilised for the treatment of chorea (Dash & Mestre, 2020). Surgical treatment is being used for severe refractory chorea, and consists of pallidal deep brain stimulation, although it is under study because it might worsen gait and parkinsonism (Schrader et al., 2011; Wojtecki et al., 2016). There are no effective treatments for cognitive impairment, and the treatments suitable for the psychiatric disorders depend on the patient. Fortunately, a treatment might be available soon since currently several pharmaceutical companies are performing experimental trials with HTT lowering drugs (Pan and Feiging 2021; Bennett, Kordasiewicz and Cleveland 2021). There are two types of HTT lowering drugs, those that target HTT in an unspecific manner and those that specifically target mHTT, in both cases, the drug consists of antisense oligonucleotides that bind to a specific sequence of HTT RNA triggering its degradation via RNase H and, therefore, lowering the level of HTT protein. This is a novel and interesting approach, however, Roche's tominersen (RG6042) clinical trial, which was the most promising, was recently interrupted due to the inefficiency of the drug.

1.2.1.1. Symptoms of HD

HD patients suffer from psychiatric manifestations, motor disturbance and cognitive loss (Bonelli & Beal, 2013; HDCRG, 1993; Huntington, 1872). Both psychiatric symptoms and cognitive loss can begin before the motor onset of the disease (Bonelli & Beal, 2013).

1.2.1.1.1. Psychiatric disturbances

Among the psychiatric disturbances, depression is the most common (Anderson & Marder, 2001; Bonelli & Beal, 2013). However, other disturbances have been reported: a higher rate of suicide or attempted suicide, psychotic symptoms, irritability and aggressive behaviour, apathy or personality change, problems in planning and organization, obsession and compulsiveness, and anxiety. Not all patients suffer from all the disturbances, and they tend to change as the disease develops.

1.2.1.1.2. Cognitive loss

This cognitive loss in HD is progressive, affecting mainly attention and executive functions during the asymptomatic stage, and cognitive functions after the first three years (Bonelli & Beal, 2013; Roos, 2010). As the disease progresses, cognitive decline worsens to the point where almost all patients suffer from dementia during the late stages (Bonelli & Beal, 2013; Huntington, 1872; Roos, 2010). Although the cognitive impairment varies significantly between patients, a higher number of CAG repeats correlates with a faster cognitive decline (Bonelli & Beal, 2013; Roos, 2010). This decline is independent of the parental mode of inheritance and of the age at onset but related to the number of years the patient has been affected.

1.2.1.1.3. Motor impairment

Choreic movements begin at the early stages of HD (Huntington, 1872). These involuntary movements are quick and infrequent in the beginning, but their frequency increases gradually with the development of the disease (Bonelli & Beal, 2013; Roos, 2010). During the later stages, choreic movements are replaced by bradykinesia and dystonia that cause immobility and can lead to aspiration pneumonia in the late stages of the illness, which is the most common cause of death for HD patients. Although chorea is the most striking motor symptom, HD patients also suffer from

ocular movement disorders, problems with complex, voluntary movements, impaired standing and walking that worsens over time, problems swallowing and speaking, and in the terminal phase weight loss and hypokinesia (Bonelli & Beal, 2013). The progression of the disease is usually faster in the juvenile cases than in adult-onset HD (Bonelli & Beal, 2013; Roos, 2010).

1.2.1.2. Genetics of HD

Knowing that HD is inherited in a Mendelian autosomal dominant way, researchers tried to find the gene responsible for the disease. In 1983, Gusella's group tracked the gene to a region of chromosome 4. Later, in 1993, the HDCRG identified a gene (~210Kb) in that region that encoded a previously undescribed protein (~348Kd). They called it *IT15*, (now known as *HTT*). This gene presents a polymorphic (CAG)n triplet repeat consisting of 40 repeats or more in HD patients - over 60 in the case of juvenile-onset - and 34 or less in people not at risk of HD (HDCRG, 1993). People with 35 to 39 repeats present incomplete penetrance so they may or may not develop the disease. Contrary to what was previously assumed, it is the number of CAG repeats, and not the length of the polyQ track that correlates better with the age of onset of the motor symptoms (GeM-HD Consortium, 2019). Similar polyQ expansions have been identified in proteins that cause different NDs: spinocerebellar ataxia, dentatorubral-pallidoluysian atrophy and spinal and bulbar muscular atrophy, among others (Saudou & Humbert, 2016). In patients with 40 CAG repeats or more, the age of onset and the severity of HD inversely correlates to the number of repeats, the higher number of CAG, the earlier the onset regardless of the length of the repeat in the other *HTT* allele (GeM-HD Consortium, 2019; Gusella & MacDonald, 2006; HDCRG, 1993; Langbehn et al., 2004; Lee, J. M. et al., 2012). However, ~50% of the remaining variability in the age at onset in patients with the

same number of repeats is also heritable, which indicates the presence of modifier genes.

Researchers from the HDCRG (1993) found that individuals that were hemizygotes for 4p16.3 -the region where *IT15* was mapped did not, in fact, develop an HD phenotype, meaning that HD is not caused only by a loss of function due to the polyQ expansion in the HTT protein, but to a gain of toxic function. It has also been established that HD has a complete dominant inheritance since patients heterozygous and homozygous for the mutant protein display the same clinical phenotype, meaning that the presence of only one mutant allele is enough to cause the disease and suggesting that there is no interaction between the normal and the mutant HTT (mHTT) (Lee et al., 2012; Myers et al., 1989; Wexler et al., 1987).

Similar to other CAG-triplet diseases such as fragile X syndrome, spino-bulbar muscular atrophy and myotonic dystrophy, there is an instability of the CAG triplet length, causing variability in its length between generations (HDCRG, 1993). This variation usually consists of an expansion of the number of CAG triplets in the descendant - although there are cases of contraction too - and it happens without the need for recombination. These expansions and contractions lead to gonadal and somatic mosaicism in HD patients (Monckton, 2021; Telenius et al., 1994). Somatic mosaicism affects selected regions of the brain -there is an overall expansion in most regions but a contraction in the cerebellum when compared to the number of triplets found in peripheral blood- (Monckton, 2021; Telenius et al., 1994). However, there is no clear evidence of this expansion being higher in the areas more affected by HD and the studies were done in tissue samples containing both neurons and glia, so mosaicism can not be determined as the cause of selective neuronal loss. On the other hand, as a consequence of these expansions in the germ line, *de novo* mutations happen at a rate of 1 in 5372 individuals, with a higher frequency in the

fathers than the mothers (Kay et al., 2018). The increase in the number of CAG triplets in the germline of parents that are in the incomplete penetrance range can lead to the CAG track being over the HD threshold in the child. This expansion of the CAG triplet across generations, leading to an early age of onset is known as anticipation.

1.2.1.3. Histopathological hallmarks of HD

Although HTT is a ubiquitous protein, some types of cells are more vulnerable to its toxic effects (Gusella et al., 1983; Gusella & MacDonald, 2006; HDCRG, 1993). Medium spiny neurons of the striatum and cortical neurons that project to the striatum are particularly affected. This is thought to be due to decreased levels of the brain-derived neurotrophic factor (BDNF) and an increase in glutamate released by the cortical pyramidal neurons, which reduce the survival signals and lead to excitotoxicity, respectively, of the medium spiny neurons (Ross & Tabrizi, 2011). The loss of functionality and death of these cells begins up to 10 years before the appearance of symptoms, correlating with the development of cognitive dysfunction (Gusella et al., 1983; Gusella & MacDonald, 2006; HDCRG, 1993). It has been estimated that at the beginning of the motor symptoms, 20 - 30 % of the GABAergic medium spiny neurons of the caudate nucleus have been lost (Gusella & MacDonald, 2006). This cell loss leads to less inhibition of the Globus Pallidus and the Substantia Nigra and therefore causes involuntary movements. By the time of death, HD patients have lost 10 - 20% of their brain mass (Reiner et al., 2011). Intracellular inclusions of mHTT have been described in the brain of HD patients, specifically in the striatum and the cortex, which are the regions that are more affected by neurodegeneration (DiFiglia et al., 1997).

1.2.1.4. Characteristics and role of wildtype HTT

Although HTT is ubiquitously expressed, its highest concentration is found in the central nervous system, where it is expressed in both neurons and glia cells (Schulte & Littleton, 2011; Zheng & Diamond, 2012). HTT is an essential protein, but its wildtype (WT) role is not yet clear. However, HTT is known to interact with proteins related to cellular dynamics, metabolism, gene expression, signal transduction and the formation of protein complexes (Saudou & Humbert, 2016).

HTT is a large protein (350 kDa) that is highly conserved in vertebrates (Schulte & Littleton 2011; Zheng & Diamond 2012). There are HEAT repeats distributed along the protein that mediate protein-protein interactions, suggesting that HTT might have a role as scaffold for protein complex formation (Schulte & Littleton, 2011; Zheng & Diamond, 2012). In humans, it has an N-terminal polyQ tract encoded by the CAG repeat region that forms a polar zipper that allows the interaction with other polar factors. On the C-terminus, HTT has a nuclear export signal, which suggests that this protein may traffic between the nucleus and the cytoplasm (Xia et al., 2003). It is thought that this protein might change its conformation depending on its subcellular localization since different epitopes colocalize with many organelles including the nucleus, cytoplasm, endoplasmic reticulum (ER), Golgi complex, endosomes, axon, and synapses (Zheng & Diamond, 2012). There is a highly conserved region of 17 amino acids between the polyQ and the exon 1 that is thought to be involved in the aggregation of mHTT (Schulte & Littleton, 2011). Under pathological conditions, the length of the polyQ tract correlates with the aggregation kinetics and with the severity of the disease (Giorgini & Muchowski, 2009; Krobitsch & Lindquist, 2000).

1.2.1.5. Mechanisms of cellular pathogenesis in HD

HD is not primarily caused by the loss of WT function, but by a gain of toxic function since mHTT interferes with several normal cellular processes including, but not limited to autophagy, homeostasis of the ER, mitochondrial transport, and transcription (Giorgini & Muchowski, 2009; Schulte & Littleton, 2011).

HTT can undergo several post-translational modifications such as cleavage, ubiquitination, phosphorylation and SUMOylation (Schulte & Littleton, 2011; Zheng & Diamond, 2012). SUMOylation of mHTT has been related to an increase in neurodegeneration in fly models (Steffan et al., 2004), while reduced phosphorylation of serine 421 is associated with toxicity in mice and humans (Warby et al., 2005). In addition to those mechanisms, proteolysis has an important role in HD pathogenesis. Cleaved mHTT fragments of different sizes have been observed in the brains of mice and patients which formed inclusions, with aggregation preceding the motor onset and correlating with the areas of neurodegeneration (DiFiglia et al., 1997; Landles et al., 2010; Lunkes et al., 2002). Caspase-3 cleavage of mHTT occurs in the human brain before HD clinical onset (Wellington et al., 2002), and cleavage at amino acid 586 by caspase-6 is necessary for neuronal dysfunction and neurodegeneration in HD mice (Graham et al., 2006). N-terminal fragments display more aggregation and toxicity than the full-length protein, with exon 1 being the shortest and most toxic fragment, these discoveries suggest that preventing the cleavage of mHTT could ameliorate the disease (Sathasivam et al., 2013; Zheng & Diamond, 2012). However, it is still uncertain if this exon 1 polyQ fragment is synthesised via post-translational modification, such as proteolytic cleavage, or due to aberrant splicing (Landles et al., 2010; Sathasivam et al., 2013).

Interestingly, mHTT aggregates contain other proteins apart from mHTT, including ubiquitin and CREB binding protein, which reduces the amount of these proteins

available altering the homeostasis of the cell (Schulte & Littleton, 2011). The presence of ubiquitin in the aggregates implies that mHTT is marked for degradation, however, the ubiquitin-proteasome system is impaired – perhaps because polyQ tracts are degraded inefficiently and block the catalytic region of the proteasome - leading to an increase in the concentration of mHTT in the cell (Schulte & Littleton, 2011; Zheng & Diamond, 2012) Since the cell is unable to clear the misfolded protein, it accumulates and interferes with the normal function of the cell (DiFiglia et al., 1977; Schulte & Littleton, 2011).

Although HD is considered to be caused by a gain of toxic function, the loss of WT function may be responsible for several mechanisms of cellular pathogenesis (Zheng & Diamond, 2012). PolyQ regions of HTT mediate the interaction between transcription factors and transcriptional regulators, however, this is impaired by the polyQ expansion, leading to the transcriptional dysregulation seen in HD. One of the consequences of this transcriptional dysregulation is the decreased synthesis of BDNF, a key neurotrophic factor synthesized by cortical neurons and given to striatal neurons as a survival signal (Chiara et al., 2001). Moreover, HTT is implicated in vesicle trafficking by interacting with cytoskeletal and synaptic vesicle proteins, but this interaction is reduced in mHTT, leading to a decrease in transport, so cortical neurons are unable to transport the low amount of synthesised BDNF to synapses, decreasing even more the survival signals sent to the striatal neurons (Schulte & Littleton, 2011; Zheng & Diamond, 2012). Furthermore, since the ability of mHTT to inhibit caspase-3 apoptotic activity is reduced, this may further contribute to the neuronal loss seen in HD.

As in many NDs, mitochondrial dysfunction and oxidative stress are implicated in HD (Ross & Tabrizi, 2011; Schulte & Littleton, 2011). Energy metabolism is impaired in HD patients since mHTT damages mitochondria by several mechanisms:

reduction of energy production and membrane potential, calcium dysregulation, oxidative stress, and inducing caspase-mediated apoptosis (Zheng & Diamond, 2012). Apart from being damaged, mitochondrial transport is impaired in HD, especially in cells with aggregates, leading to a lack of mitochondria at essential subcellular locations, which ultimately causes more stress to the cell (Ross & Tabrizi, 2011; Schulte & Littleton, 2011).

Finally, the kynurenine pathway (KP) of tryptophan degradation is also dysregulated in early-stage HD patients (Cervenka et al., 2017; Green et al., 2012). Although tryptophan is essential to synthesize serotonin, most of it is degraded through the KP into kynurene, which can be synthesized into kynurenic acid (KYNA) by the astrocytes, or into 3-hydroxykynurene (3-HK), which is degraded into quinolinic acid (QUIN), by the microglia. These metabolites have neuroactive effects: QUIN is an NMDA receptor agonist linked to neurotoxicity and apoptosis, and 3-HK is linked to oxidative stress, making both of them neurotoxic. On the other hand, KYNA is an NMDA receptor antagonist and a free-radical scavenger, so it is neuroprotective against the effects of 3-HK and QUIN. Both neurotoxic metabolites are increased in HD patients' brains, while KYNA is decreased, making them a possible therapeutic target of HD, which has been being studied in fruit flies (Breda et al., 2016; Campesan et al., 2011; Green et al., 2012).

1.2.1.6. Genetic modifiers found in previous studies

It has previously been mentioned that the number of CAG repeats of the *HTT* gene correlates with the age of motor onset of HD, nevertheless, there is still some variability in the age of onset between individuals with the same number of CAG repeats (GeM-HD Consortium, 2019; Lee, Jong-Min et al., 2015). This variability is partially inheritable, meaning apart from environmental factors, there are genetic

modifiers of HD involved in altering the age at motor onset that was expected due to the number of CAG repeats of a specific patient. These modifiers are the ones being studied through GWAS.

The first GWAS performed by the GeM-HD consortium was performed in subjects with 40 to 55 glutamines and it was based on the “residual age at motor onset”, the difference between the observed and the predicted age at which each patient developed motor symptoms (Lee et al., 2015). After analysing more than 4000 HD patients, they found polymorphisms in chromosome (chr) 15 (*MTMR10* -inositol-phosphate signalling- and *FAN1* -DNA synthesis-), 8 (*RRM2B* -DNA synthesis and repair, and oxidative stress pathway- and *UBR5* -protein degradation-), and 3 (*MLH1* -mismatch repair-). When studying the pathways involved, they found an enrichment in genes related to DNA repair, mitochondrial fission, and oxidoreductase activity. Both loci at chrs 15 and 8 show significance in the studies done for age at cognitive onset and age at psychiatric onset, however, the locus at chr 3 only shows near significance for the psychiatric onset.

The GeM-HD consortium performed another GWAS in 2019, increasing the sample size to more than 9000 HD patients with 40 to 55 glutamines. The metric used to study the genes involved in HD’s pathogenesis was, again, the difference between the predicted and the observed age at onset of the motor symptoms. Differences in *HTT* haplotypes in both the WT and the mutant alleles, or the number of CAG repeats in the WT allele have no effect on age at onset. This study focused on the sequence encoding the polyQ tail, since glutamine can be encoded by CAG or CAA triplets, it can be an uninterrupted CAG sequence, it can have a CAACAG interruption (+2Q), or a CAACAG-duplication interruption (+4Q). They discovered that, although the duplication adds 4 glutamines to the polyQ tail, individuals with that allele present delayed age at onset compared to individuals with the same polyQ

length but composed only CAG sequences, suggesting that is the uninterrupted CAG repeats and not the total polyQ length is what determines the age at onset. After correcting for the uninterrupted CAG repeats, they looked for other modifiers and were able to validate the ones they discovered in 2015 while finding some new ones in chr 2 (*PMS1*), 5 (*DHFR*, *TCERG1* -pre-messenger RNA (mRNA) splicing and transcriptional elongation regulation-), 7 (*PMS2*), 11 (*CCDC82* -ATM-mediated phosphorylation in response to H₂O₂), and 19 (*LIG1*), a majority of which were involved in DNA repair suggesting that age at onset could be related to somatic expansion of the CAG. Although there was no difference in the age at onset due to sex, some of the modifiers appeared predominantly in women (*MSH3/DHFR*) or men (new loci in chrs 1, 12 and 18). The transcriptome-wide association study (TWAS) indicated that an increase in the expression of *FAN1*, *PMS1* and *ASNSD1* or a decrease in the expression of *MSH3* delayed the age at onset. The presence of these alleles explained between 40 to 87% of the variability due to genetic causes.

1.2.2. Parkinson's Disease

PD (OMIM 168600) was first described by James Parkinson in 1817, although at that time he called it shaking palsy. It was described as a progressive ND that happened during adult life and had a long duration. PD is characterized by its motor symptoms even if these change during the disease progression. In the beginning, patients experience involuntary tremors and lessened muscular power, later the patients' posture changes until they are bent forward, they also develop walking problems and in the latest stages of the disease, patients present swallowing problems and incontinence. Apart from the motor impairment, PD also causes agitation and sleeping problems. However, the senses and the intellect of the patients remain uninjured (Parkinson, 1817). Later, in 1912, Lewy described what is

now known as the histopathological hallmark of PD, the Lewy bodies (LBs). These structures are spherical bodies that appear in the cytoplasm of neurons of PD patients, more specifically in the substantia nigra (Lewy, 1912; Tretiakoff, 1919).

PD is the second most common ND after AD, affecting 1% of the population over 50 years old (Polymeropoulos et al., 1996). The average age of onset of PD is 60 years and the life expectancy after diagnosis is from seven to 20 years (Armstrong & Okun, 2020; Jankovic & Tan, 2020). Although there are familial forms, most PD cases are sporadic, caused by a combination of environmental and genetic risk factors (Jankovic & Tan, 2020; Warner & Schapira, 2003). The environmental risk factors might be the reason why PD has a higher prevalence in men, at a ratio of 1.3 or 2 depending on the study (Ascherio & Schwarzchild, 2016).

Although this disease has been known for two centuries, there is still no cure for PD. So far, there are treatments for the symptoms but none of them modifies the disease progression (Jankovic & Tan, 2020). The most common treatment is levodopa, which is used to treat the dopamine deficiency that leads to the principal motor symptoms, although other drugs are being used for the non-motor symptoms, such as cholinesterase inhibitors and NMDA receptor antagonists for the cognitive function. For moderate to advanced cases of the disease, deep brain stimulation is being used in the thalamus and the globus pallidus. The latest therapeutic advancements are the cell replacement therapies, in which embryonic stem cells or somatic cells are differentiated into dopaminergic midbrain neurons and then transplanted into PD patients (Barker et al., 2013; Barker & Transeuro consortium, 2019). Finally, surgical delivery of gene therapy, in which a viral vector is used to deliver to the putamen the aromatic L-amino acid decarboxylase enzyme – essential for the conversion of levodopa into dopamine and which is lost as the disease progresses - is under clinical trial (Christine et al., 2019).

1.2.2.1. Symptoms of PD

Although PD is widely known for its motor symptoms, 15 to 20 years before the clinical onset of the disease neurodegeneration has already started (Jankovic & Tan, 2020). This neurodegeneration not only affects the neurons of the substantia nigra, but it also affects non-dopaminergic neurons from the vagus dorsal motor nucleus, the locus coeruleus, and the raphe nuclei - regions thought to be related to the non-motor symptoms. Other symptoms that are known to happen before the motor onset are: eye movement sleep behaviour disorder, depression, olfactory dysfunction, and autonomic dysfunction (constipation, orthostatic hypotension).

When half of the neurons from the caudal substantia nigra have been lost, motor symptoms begin to appear (Armstrong & Okun, 2020). Since the causes of PD are varied, the clinical presentation of the disease also has differences between patients, however, the most common motor symptoms are resting tremor, rigidity, and bradykinesia. As the disease progresses, the symptoms worsen and change, patients become unable to stand straight and bent forward, develop gait problems, and in the last stages, they become unable to swallow (Armstrong & Okun, 2020; Parkinson, 1817).

The progression of the disease is evaluated using different methods. The Unified PD Rating Scale is used to evaluate the symptoms, dopamine transporter single-photon emission computed tomography to evaluate the neuronal loss in the substantia nigra, and the protein misfolding amplification method is used to evaluate the type of αSyn aggregates in the cerebrospinal fluid and determine if they correspond to PD or to another synucleinopathy (Armstrong & Okun, 2020; Jankovic & Tan, 2020; Piccini et al., 1997; Shahnawaz et al., 2020).

1.2.2.2. Pathological hallmarks of PD

PD patients are known to have mitochondrial dysfunction due to the impairment of the respiratory chain complex I, impairment of protein degradation via the proteasome system, neuroinflammation and oxidative stress (Jankovic & Tan, 2020). They also present neuronal loss in the substantia nigra pars compacta and the locus coeruleus among others. However, the histopathological hallmarks of PD are the presence of LBs, and the dopamine deficiency caused by the loss of dopaminergic neurons (Laquerriere et al., 1957; Lewy, 1912; Tretiakoff, 1919).

The presence of spherical bodies, another name for LBs, in the cytoplasm of neurons of the substantia nigra of PD patients was described in the 1910s (Lewy, 1912; Tretiakoff, 1919). These LBs are composed of full-length α Syn that aggregates forming 5 nm insoluble straight protofilaments, which combine into 10 nm straight or twisted filaments (Spillantini et al., 1998). These filaments combine to form a dense core surrounded by a less dense region that composes the LB (Duffy & Tennyson, 1965). The α Syn in the LBs is ubiquitinated, meaning it has been marked for protein degradation, but the proteasome has been unable to degrade it (Spillantini et al., 1998). However, a recent study found that LBs are not only formed of α Syn, many of them also include membranes, vesicular structures, and dysmorphic organelles, suggesting that impaired organelle formation or trafficking might be involved in the formation of these aggregates (Shahmoradian et al., 2019). LBs are localized in the brain regions affected by neuronal loss: substantia nigra, locus cerebeleus, nucleus basalis, hypothalamus, and cerebral cortex among others.

1.2.2.3. Aetiology of PD

There is no single cause of PD, there are several genetic, epigenetic -modification of histone methylation- and environmental factors that increase the risk of developing the disease, although age is the most important risk factor (Shahnawaz et al., 2020).

Among the environmental causes of PD are exposure to herbicides and pesticides, heavy metals, organic solvents, toxins in the water and receiving a head injury. Among them, the most important are mitochondrial respiratory complex I inhibitors like the pesticide rotenone and the chemical 1-methyl-4-phenyl-1,2,3,6-tetrahydropyridine (MPTP) which induce parkinsonism by causing the loss of neurons of the substantia nigra (Shahnawaz et al., 2020; Warner & Schapira, 2003). Other environmental factors like smoking, caffeine consumption or hormone levels may also influence the risk level of developing PD (Shahnawaz et al., 2020).

There are many genes involved in PD. A GWAS study found more than 90 loci linked to the disease (Nalls et al., 2019). So far, pathogenic mutations in *SNCA*, *PRKN*, *DJ-1*, *LRRK2*, *PINK1*, *GBA*, *FBXO7*, *VPS35*, *DNAJC6* and *ATP13A2* have been identified in PD families.

1.2.2.3.1. Genes involved in familial forms of PD

SNCA is the gene that encodes α Syn, a small 140 amino acid-long protein involved in vesicle trafficking (axonal transport, docking, priming fusion, and neurotransmitter release) (Jankovic & Tan, 2020). α Syn is mainly expressed in neurons and is thought to be involved in synaptic plasticity (Warner & Schapira, 2003). It is also the main component of LB and Lewy neurites (LN) when it is misfolded and aggregates. It has been hypothesized that PD can spread from cell to cell and travel from the peripheral nervous system to the caudal brainstem via vagus nerves (Breen et al., 2019). Mis-sense mutations in codons 30 and 53 (substitutions A30P and A53T) are known to cause familial forms of PD (Krüger et al., 1998;

Polymeropoulos et al., 1996; Polymeropoulos et al., 1997). Furthermore, multiplications of the SNCA gene or polymorphisms in its regulatory regions that cause an increase in the expression of αSyn are sufficient to cause PD (Farrer et al., 2004; Miller et al., 2004; Singleton et al., 2003).

PRKK, also known as *PARK2*, is the gene that encodes parkin, an E3 ubiquitin ligase involved in proteasomal degradation (Jankovic & Tan, 2020; Warner & Schapira, 2003). It is the most common autosomal recessive PD related gene (50% of the early onset patients). The brains of the patients present a loss of dopaminergic neurons in the substantia nigra pars compacta but LBs are rare.

LRRK2 (*PARK8*) is the most common risk gene identified in sporadic and familial forms of PD (Jankovic & Tan, 2020). The mutation G2019S is present in 1 to 3% of sporadic and 3 to 4% of familial cases, although there are other mutations too. It encodes Dardarin, a large 2527 amino acid protein involved in vesicular trafficking, autophagy, protein synthesis and cytoskeletal function that also interacts with mitochondria. It is highly expressed in medium spiny neurons and microglia, so it has been hypothesized to be involved in the inflammation observed in PD.

The last of the main risk genes is *GBA* (Jankovic & Tan, 2020). It encodes a glucocerebrosidase involved in the lysosomal degradation of sphingolipids. It is the most important genetic risk factor for the general population (mutations in this gene cause a five-fold increase in the risk of developing PD).

Although other genes are known to cause familial forms of PD, they happen very rarely.

1.2.2.3.2. GWAS studies in PD

Contrary to the causative mutations found in familial studies, GWAS are used to find risk factors that contribute to the development of the idiopathic cases of PD

(Chang et al., 2017; Nalls et al., 2014; Nalls et al., 2019). All the studies confirmed several of the genes that had been previously identified in familial cases.

The 2014 GWAS analysed a total of 7.8M SNPs in 14K PD cases and 95K controls (Nalls et al., 2014). 28 independent risk loci were identified, of which six were new (*SIPA1L2*, *INPP5F*, *MIR4697*, *GCH1*, *VPS13C* and *DDRGK1*). The differences in methylation and expression levels in the cortex and the cerebellar tissue related to six of the loci suggested that the risk of PD might not only be caused by the inheritance of the variants but could also be affected by the regulation of the genes. The study found that the decrease in methylation of *NUPL2* caused an increase in its transcription in both brain regions. It also identified a complex interaction in the *NUCKS1-RAB7L1-PM20D1* locus, where *RAB7L1* transcription was increased but the transcription of the other two genes was decreased.

A later study performed by Chang's group in 2017 identified another 17 novel risk loci. They used a sample size of 6.5K cases and 302K controls in which 9.8K SNPs were studied. They discovered that there was an increase in histone H3 acetylation at lysine 27 in the regions of the genome related to PD heritability, which increased the transcription of the genes. This increase in histone acetylation happened in the central nervous system, as well as adrenal and pancreatic cells. As in the other studies, genes that had previously been identified as risk and causative factors of PD were identified (*GBA*, *LRRK2*, *SNCA*, and *MAPT*). Among the genes that were identified in the GWAS, there was an enrichment in those involved in lysosomal, autophagy and mitochondrial biology. Lysosomes are likely involved in the degradation of aggregates, so deficiencies in the pathway would worsen the disease, and therefore, they would likely be risk factors for PD. Five genes were identified, two previously known, *GBA* and *TMEM175*, and three new candidates *CTSB*, *ATP6V0A1*, and *GALC*. Studies show that *Ctsb* in mice can degrade α Syn and that

double-knock out mice for *Ctsb* and *Cts*/present tremors, and cerebral and cerebellar atrophy. Among the mitochondrial genes, the previously known *MCCC1* was identified together with two new candidates *COQ7* and *ALAS1*. Finally, a decrease in *KAT8* was identified as a risk factor since it causes a reduction in autophagy, so proteins and organelles are likely not properly degraded. The new candidate genes that were not involved in the enriched pathways include *SH3GL2*, which is phosphorylated by *LRRK2* and might be involved in clathrin-mediated endocytosis of synaptic vesicles; *ELOVL7* whose dysregulation in mice causes inflammatory astrocytosis and microgliosis, and neuronal degeneration and *SCN3A*, which is associated with enhanced neuronal excitability and is related with epilepsy. Although transcription factors were not included among the enriched pathways, two of them were considered interesting candidates (*SATB1* -development of regulatory T cells-, *ZNF184*, and *TOX3* -neuronal survival-). And lastly, *ITPKB*, a kinase involved in common-variable immunodeficiency, is important because it is a facile drug target.

Finally, in 2019 Nalls' group identified 90 independent genetic risk factors, of which 38 were new. The sample for the study included approximately 37K cases, 18K individuals without the disease but with cases in the family, and 1.4M controls, and a total of 7.8M SNPs were studied for each person. Ten loci containing 22 SNPs in total were identified, nine of the multi-signal loci had been previously identified - they were close to known risk genes such as *GBA*, *NUCKS1/RAB29*, *GAK/TMEM175*, *SNCA* and *LRRK2* (Nalls et al., 2019). Interestingly, the closest gene to the previously unknown multi-signal locus was *GRN*, which had previously been associated with frontotemporal dementia and neuronal ceroid lipofuscinosis. Surprisingly, another two genes related to lysosomal storage disorders were found in the study, *GUSB* and *NEU1*. Among the genes found, there was an enrichment of those that were expressed in the brain, specifically in neurons, and were related to

chemical signalling and stress response pathways, these included four pathways related to vacuolar function, three related to drug targets, the three previously mentioned genes related to lysosomal storage, and two genes involved in endocytosis (*VAMP4* and *NOD2*). Although there seems to be no enrichment in the immune pathways, the P values were close to significant. The polygenic risk score that was used to determine the heritability of PD that was explained by all the variants highlighted during the GWAS determined that they accounted for between 16% and 36% of inheritance depending on the prevalence of the disease in the population, suggesting that the effect of each of the variants is very small.

Apart from genes, four phenotypes that genetically correlated with PD were found (Nalls et al., 2019). There was a positive correlation with putamen volume and with intracranial volume, while there was a negative correlation with tobacco usage and academic qualifications. Among those, putamen and intracranial volumes may be useful as biomarkers of the disease.

1.3. Organisms used to model NDs

NDs are being studied in simple models like *Drosophila melanogaster*, *Caenorhabditis elegans* and *Danio rerio* due to their fast development of pathology and low cost (Dawson et al., 2018; Zheng & Diamond, 2012). These organisms show features of the human disease, including reduced lifespan, protein aggregation/formation of inclusions and progressive neuronal death. As it is mentioned below, several studies begin *in vitro* or with a simple model like yeast and the discoveries are validated in more relevant models like mammalian cells or fruit flies (Bodai et al., 2001; Jackson et al., 1998; Mason et al., 2013). Although these models are good for validation because they are easier to manipulate and present a faster cycle, any discoveries must be validated in higher organisms that permit more

physiologically relevant modelling of neurodegeneration and drug metabolism such as mice or primates (Dawson et al., 2018; Zheng & Diamond, 2012). The more complex models can be genetically engineered to express the causative gene, have the protein inoculated in the brain, or cause disease-like symptoms using chemicals. The more similar to human the model organism, the easier is to translate the findings to human clinical trials.

1.3.1. *Saccharomyces cerevisiae* as a model of NDs

Saccharomyces cerevisiae was the first eukaryotic organism to have its complete genome sequenced (Goffeau et al., 1996). The straightforward culture and fast generation time (1-2 hours), along with the easy genetic manipulation and screening and the considerable availability of molecular and genetic tools, make yeast an important model organism (Miller-Fleming et al., 2008; Tuite, 2019). Furthermore, collections of strains exist with single gene deletions or overexpression (OE) of almost every predicted open reading frame (ORF). In addition, the possibility of maintaining the lines as haploids, crossing them to create diploids, and the facility to study the products of meiosis, make yeast an excellent choice when carrying out genetic research. Another advantage of yeast is that many of the major biological processes and genes are conserved in humans and, even if they are not, it is possible to generate humanized yeast expressing the human genes of interest. However, it must be taken into account that yeast are unicellular organisms, so they lack cellular processes that involve complex interactions between different specialised cell types, and that the results obtained in this model must be validated in higher organisms.

Yeast can be used as models of NDs by expressing the causative gene, usually under the control of an inducible promoter, and tagged with a fluorescent protein so

the expression and the cellular dynamics of the toxic protein can be studied by fluorescent microscopy and flow cytometry (Miller-Fleming et al., 2008; Tuite, 2019). The effect of the protein on yeast health is studied by assessing if there are any defects in its viability -via spotting assays- or on its growth -by generating growth curves and analysing lag, growth speed and maximum growth- (Barton et al., 2018; Miller-Fleming et al., 2008; Tuite, 2019). Moreover, their short life cycle and small genome make it fairly easy to obtain and sequence large populations to perform a QTL analysis (Cubillos et al., 2011; Liti & Louis, 2012). Besides the genetic manipulations, pharmacological testing is also straightforward since yeast live in media and it is simple to include the drug in the recipe (Miller-Fleming et al., 2008; Tuite, 2019).

1.3.1.1. Yeast as a model of HD and PD

Yeast have extensively been used as a model for cellular processes and diseases, including HD and PD, and many of those discoveries have been validated in higher organisms, meaning that yeast can accurately model aspects of the diseases and lead to the identification of promising therapeutic strategies (Giorgini et al., 2005; Mason et al., 2013; Willingham et al., 2003).

Since there are no *HTT* or *SNCA* orthologues in yeast, in order to model the diseases humanized yeast expressing WT and mutant versions of the human protein have been made (Krobitsch & Lindquist, 2000; Lázaro et al., 2014; Meriin et al., 2002; Muchowski et al., 2000; Outeiro & Lindquist, 2003).

HD has been modelled with different constructs that contained the N-terminal fragment of *HTT* - usually exon 1 or a truncated fragment of it - and the polyQ tagged with GFP (Krobitsch & Lindquist, 2000; Meriin et al., 2002; Muchowski et al., 2000). Although all the constructs showed polyQ length-dependent aggregation, only the

one lacking the proline-rich region and containing a FLAG tag was toxic in a polyQ length-dependent manner and only in the presence of the RNQ1 prion (Duennwald et al., 2006; Meriin et al., 2002). It is thought that the acidic nature of the FLAG-tag mimics the SUMOylation that happens in mammalian models, which is necessary for the toxicity (Duennwald et al., 2006; Steffan et al., 2004). Expressing mHTT in yeast leads to aggregation and accumulation of the protein that cause growth impairment (Meriin et al., 2002).

PD is modelled by expressing GFP-tagged full WT SNCA gene, or SNCA with the familial mutations A30P and A53T that are known to cause the disease (Brás et al., 2019; Lázaro et al., 2014; Menezes et al., 2015; Outeiro & Lindquist, 2003). The phenotypes seen in yeast include the accumulation of the protein on the membrane or forming cytoplasmic inclusions, mitochondrial dysfunction, proteasomal impairment and ER stress, problems in vesicular trafficking, and cellular toxicity that induces apoptosis. Other genes that have been related to familial PD are also used to model the disease in yeast: *LRRK2*, *PARKIN*, *PINK1*, *DJ1*, *ATP13A2*, *VPS35*, *UCH-L1*, *EIF4G1* and *GBA* (Brás et al., 2019; Menezes et al., 2015).

High-throughput screens with humanized yeast are a good method to uncover modifier genes and find pathways and possible therapeutic targets for human diseases. A screen with 4850 strains, each of them with a non-essential gene deleted, was assessed for sensitivity to a mHTT fragment and to WT αSyn (Willingham et al., 2003). 52 deletion strains were sensitive to mHTT, with identified genes involved in response to stress, protein folding, and ubiquitin-dependent protein catabolism. In addition, 86 gene deletions were found to enhance WT αSyn toxicity, with roles in lipid metabolism and vesicle-mediated transport. Only one gene deletion was sensitive to both - transcription factor *STP2* - suggesting that the pathogenic mechanisms of both diseases are different.

A different loss of function screen in the same set of strains identified 28 gene deletions that suppressed the toxicity of a mHTT fragment (Giorgini et al., 2005). The suppressors were involved in vesicle transport, vacuolar degradation, transcription, and prion-like aggregation, as well as *BNA4* (kynurenine 3-monoxygenase), involved in the tryptophan degradation pathway, which has been implicated in HD in humans (Beal et al., 1990).

Another high-throughput screen of yeast overexpressing the majority of ORFs transformed with mHTT was tested for suppression of mHTT toxicity (Mason et al., 2013). Out of the more than 5.5K ORFs, only 317 suppressed the toxicity. Among the 172 functionally annotated genes, there was an enrichment in genes involved in mitochondrial import, copper chaperone activity and purine biosynthesis. The most promising genes were *GPX1* and *GPX3*, which encode the GPx antioxidant enzymes. The supplementation of GPx activity was found to be protective in mammalian cell and fruit fly models of HD.

Lastly, a QTL analysis in yeast strains was able to identify *RFU1* and *BUL2* as modifiers of aggregation (Peters et al., 2018). In order to do so, the propensity to form aggregates of mHTT (HTT exon 1 with 75Q tagged with GFP) in 29 *pin*-segregant strains from the cross of a laboratory and a natural yeast strain were evaluated via fluorescence microscopy. Round fluorescence objects with a small diameter (< 2 µm) were considered aggregates. The propensity to form aggregates was used as the parameter for the QTL analysis, in which *RFU1* – an inhibitor of Doa4 deubiquitinase at the late endosome that prevents recycling of ubiquitin in the cell - was uncovered. They validated this experiment by deleting *RFU1* in the parental laboratory strain, which caused a two-fold increase in aggregation. Similar results were obtained when they deleted its orthologue in *C. elegans* and in mammalian cells, proving that the gene is involved in mHTT aggregation. Since there was a SNP

in *BUL2* in the natural strain, and *BUL2* is an adapter of Rsp5 - a ubiquitin ligase involved in the response to proteomic stress that ubiquitinates several of Doa4 targets -, they tested the effects of deleting this gene in the laboratory strain, which caused a 2.6-fold increase in aggregation. Therefore, this study shows that both *RUF1* and *BUL2* are modifiers of mHTT aggregation and that QTL analysis in yeast can be used to identify modifier genes of NDs.

Although high-throughput screens have uncovered interesting therapeutic targets, they have important limitations: not all the genome can be studied since evaluating the effect of deleting essential genes is impossible in haploids, the effect of knocking out or overexpressing a gene can be quite drastic and studying interactions is complicated. Some of these limitations can be overcome by performing a QTL analysis, in which the up and downregulation of the genes are more subtle, and the modifications of several genes are present at the same time.

1.3.2. *Drosophila melanogaster* as a model of neurodegenerative diseases

NDs have been studied in flies in different ways: using mutant flies with shortened lifespan and neurodegeneration, expressing human genes known to cause diseases due to gain of toxic function, downregulating or knocking-down genes related to diseases caused by loss of function, or using drugs to mimic the disease (Maddison et al., 2020; McGurk et al., 2015; Ugur et al., 2016). All these approaches allow researchers to identify the pathways and genes involved in the different stages of the disease progression so new therapeutic targets can be tested. The perks of this organism as a model are its easy maintenance, ten-day life cycle, short lifespan, important level of conservation in both biochemical and developmental pathways, and simple genetics along with the availability of genetic tools and techniques. Fruit flies are an attractive model of NDs because they have a complex nervous system

that shares organization patterns with the human brain, and they exhibit complex behaviours that have been studied to establish behavioural and neurodegeneration assays (McGurk et al., 2015). In addition, drugs can be delivered to the brain easily since the blood-brain barrier is not stringent

The behaviour and health of *D. melanogaster* can be characterized in several ways, which means numerous phenotypes can be studied to assess NDs: neuronal loss (pseudo-pupil assay), movement impairment (locomotor activity test and climbing assay), reduced lifespan (longevity assay), developmental issues (viability assays), memory impairment (olfactory memory test), mitochondrial impairment (respiration assay and electron microscopy), among others (Maddison et al., 2020; McGurk et al., 2015; Ugur et al., 2016).

Drosophila melanogaster has been broadly used in genetic research in recent decades and currently, fruit flies are still being used to study the pathogenesis of NDs and to test drugs. Flies were used to validate the effect of the antioxidant Luteolin in ameliorating HD (Hasan Siddique et al., 2021), to study the progression of the pathology in A β 42 models of AD -mitochondrial fragmentation, calcium import problems, mitochondrial loss, and learning impairment- (Wang & Davis, 2021), to ratify the protective effect of GardeninA -an antioxidant, anti-inflammatory and anti-apoptotic drug - in survival, locomotor activity, and neurodegeneration of paraquat-induced PD flies (Maitra et al., 2021).

1.3.2.1. *GAL4/UAS* system

The *GAL4/UAS* system is a method to directly express a gene in flies based on the expression of GAL4, a transcriptional activator from yeast that only activates the transcription of genes that have a promoter with a GAL4 binding site - the upstream activation sequence (*UAS*) (Brand & Perrimon, 1993; Duffy, 2002). The system is

split between two fly lines, one carrying the *GAL4* gene under the control of an endogenous promotor - it can be tissue-specific or ubiquitous - and the other line carrying the *UAS* element and your favourite gene (*YFG*). The transcription of *YFG* only happens when *GAL4* binds to the *UAS*, and *GAL4* is only expressed in tissues in which the promotor is active, therefore this system allows the control of the

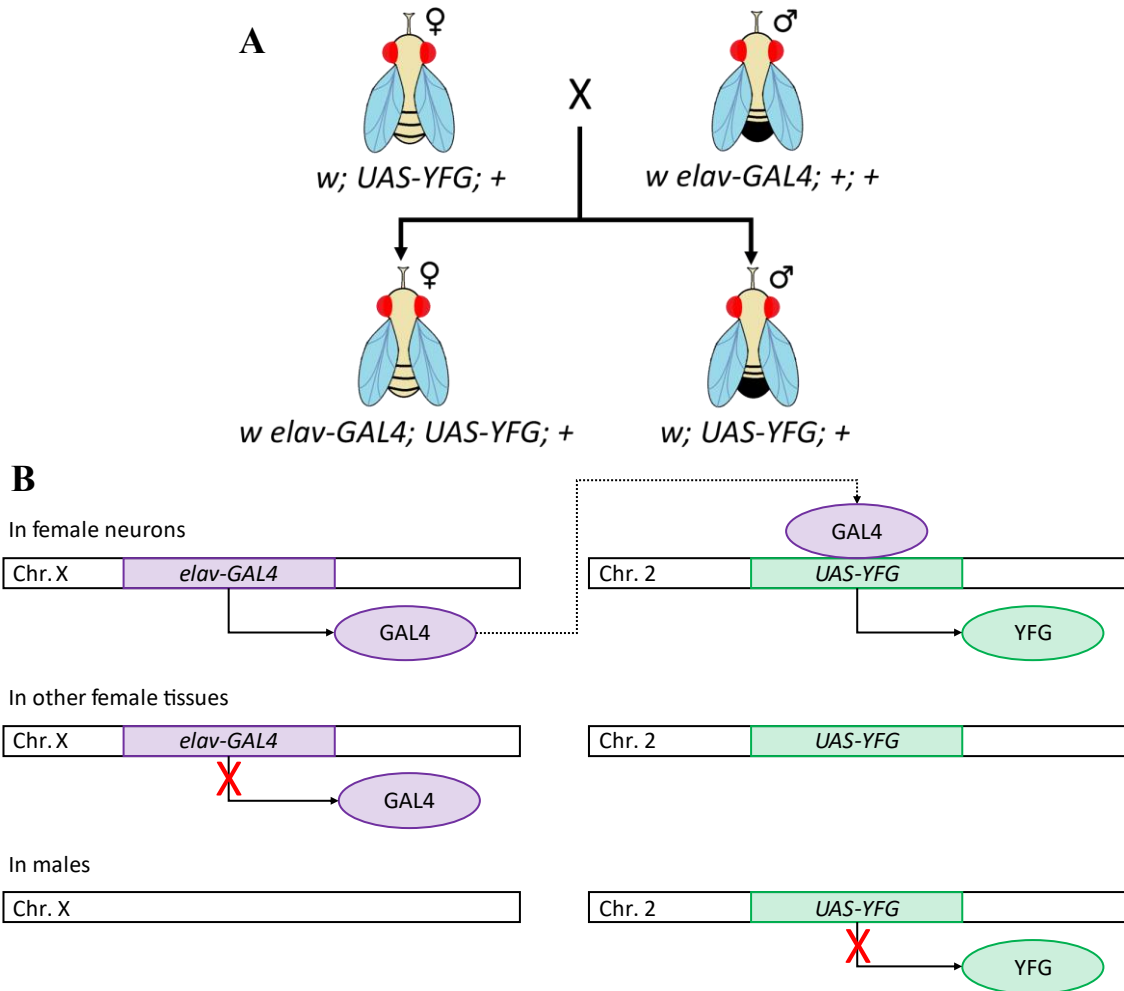


Figure 1.3-1. Crosses for neuronal expression using the *GAL4/UAS* system

A) The desired flies carrying both the *GAL4* and *UAS* elements were obtained by crossing males that carry *elav-GAL4* on the X chromosome with females that carry *UAS-YFG* on the second chromosome. Only the female descendants will carry both parts of the *GAL4/UAS* system, allowing the expression of *YFG*. **B)** In order to express *YFG*, cells must synthesize *GAL4* that will join the *UAS* element and allow the transcription of the gene (Brand & Perrimon, 1993). For this to happen, flies must have both the *elav-GAL4* and the *UAS-YFG* constructs in chromosomes X and 2 respectively. If they lack one of these components, *YFG* will not be expressed. Furthermore, since *GAL4* is under the control of the tissue-specific, pan-neuronal promoter *elav*, *GAL4* will only be synthesised in neurons, so the transcription of *YFG* will only be possible in that cell type (Koushika et al., 1996).

expression of YFG in a tissue-specific manner (Figure 1.3-1; **Error! No se encuentra el origen de la referencia.**). However, the expression of GAL4 is temperature dependant so in order to maintain a stable expression level, the flies must stay at a constant temperature (Duffy, 2002). The minimum expression in flies happens at 16 °C, while 29 °C results in the maximum expression without causing fertility or viability problems due to the high temperatures.

The GAL4 lines were generated by inserting the GAL4 gene close to a characterized promoter or by the enhancer detection technique (Brand & Perrimon, 1993; Duffy, 2002). The enhancer detection technique was used to identify new promoter regions in the *Drosophila* genome. A vector carrying GAL4 inserted downstream to a P-transposase promoter and upstream a *heat shock protein 70* (*hsp70*) terminator was inserted in different genomic regions. Depending on its integration site, it expresses GAL4 in a different pattern, influenced by the endogenous regulatory elements that affect that region -when GAL4 is inserted in the region and transcription direction of a promoter, its expression is induced-. On the other hand, the UAS lines consisted of P-element-based vectors carrying YFG preceded by five GAL4 binding sites and a *hsp70* basal promoter, and followed by the SV40 transcriptional terminator.

The benefits of this system are the creation of stock libraries containing fly lines that are viable even when they carry toxic genes. It also permits the expression of the genes in a specific tissue or developmental stage, as long as a tissue or stage-specific promoter is known (Brand & Perrimon, 1993; Duffy, 2002). Besides overexpressing genes, the GAL4/UAS system also allows the post-transcriptional silencing of genes by RNA-mediated interference (RNAi), which consists of the expression of a short, double-stranded RNA (dsRNA) homologous to the target mRNA that triggers the degradation of both the dsRNA and the mRNA (Giordano et

al., 2002). It also facilitates the experiments, since the same *GAL4* line can be used to induce expression in several *UAS* lines and the other way around, one *UAS* line can be induced in different tissues if crossed with different *GAL4* lines. Finally, the expression of the yeast *GAL80* repressor can block the activity of *GAL4* by binding to the *UAS* element, and its expression can also be tissue-specific, so the expression pattern of *YFG* can be modified - a ubiquitous promoter for *GAL4* would lead to the expression of *YFG* in all the tissues but if there is a neuron-specific promoter for *GAL80* it will repress the expression of *YFG* only in neurons while being expressed in the rest of the fly (Suster et al., 2004).

1.3.2.2. Flies as a model of HD

Although *D. melanogaster* has an endogenous HTT orthologue with ~24% identity and ~50% similarity with the human HTT protein, HD is commonly studied in transgenic fly models expressing human HTT which allows the researcher to control the spatiotemporal expression of the gene and to express mutant versions of the gene (Li et al., 1999). Several studies tested different fragment sizes of HTT with different polyQ lengths and were able to produce an HD-like phenotype in *D. melanogaster*, therefore, fruit flies are considered a good model to study possible drug targets for HD treatment (Green & Giorgini, 2012). The expression of mHTT in flies causes several phenotypes that can be easily assessed: lifespan reduction (eclosion and longevity assays), progressive motor impairment (climbing and locomotor assays), and neurodegeneration (pseudopupil assay).

This approach was validated by the experiments performed by Jackson et al. in 1998, where they modelled HD in flies by expressing a construct that encoded the first 17 amino acids of human HTT attached to a polyQ tail of varying lengths - 2, 75 and 120 - and followed by 125 amino acids of HTT. They expressed these HTT

constructs in the photoreceptor neurons of the eye and determined that the age of onset and the severity of the neurodegeneration depended on the polyQ length. They also noted that the antiapoptotic protein p35 was unable to rescue the polyQ-induced neurodegeneration.

Fruit flies can be used to determine the effect of drugs on diseases. In 2001, it was described that mHTT was able to interact with the acetyltransferase domains of CBP and P/CAF through its polyQ tail *in vitro* leading to a reduction of their acetyltransferase activity, which was verified in cell lines (Bodai et al., 2001). These experiments were then validated in flies expressing the first exon of *HTT* with a 48Q or 93Q tail. HD flies presented high lethality, early adult death and progressive neurodegeneration that were partially restored when the flies were treated with the HDAC inhibitor SAHA, strongly suggesting that HDAC inhibition could be an effective treatment for HD.

Fruit flies have also previously been used to validate the candidate genes uncovered by yeasts genome-wide OE suppressor screens (Mason et al., 2013). As it was mentioned above, GPx were protective against HD in yeasts and mammalian cells, so they then tested it in fruit flies to see the effect in a more complex organism. GPx expression resulted in a 35% neuroprotection, complete locomotor activity restoration, and amelioration of circadian rhythmicity by preventing the degeneration of the circadian lateral ventral neurons. This protection was also obtained when treating the flies with the drug ebselen, which mimics GPx activity, indicating it may be a potential HD pharmacological therapy.

The studies mentioned above are just a few examples that show the important role fruit fly models of HD have when studying disease-related pathways and testing candidate drugs.

1.4. Aims and objectives

In this thesis I aim to identify modifier genes that modulate HTT and αSyn toxicity using QTL mapping, a technology that has been proved useful to uncover the genetic mechanisms underlying the phenotypic variation of complex traits, using yeast as a model (Cubillos et al., 2011; Liti & Louis, 2012). One of the main approaches for identifying QTL is linkage analysis in which individuals with diverged phenotypes are specifically crossed to break down marker linkage by recombination allowing causative loci to segregate together with the nearest genetic marker.

In order to address this question, *mHTT* and *WT SNCA* constructs, under the control of inducible promoters, were transformed into several well-characterized strains containing most of the natural genetic variation of the species (1-2 single SNPs per 100bp). The most resistant and most sensitive strains were intercrossed and used to generate large genetically diverse populations with new combinations of alleles (Cubillos et al., 2011; Liti & Louis, 2012). These descendant strains transformed with the aforementioned plasmids and assessed for differences in growth characteristics caused by both sensitivity and resistance to mHTT and αSyn toxicity. Genomic regions where causal genetic variation was found were assessed for sensitivity and resistance by comparing the frequency of SNP segregation in sensitive/resistant individuals to the whole population. Candidate genes were deleted and overexpressed in yeast. Promising conserved genes were studied using fruit flies in order to identify any potential manipulation of relevant pathways that could be used as a therapeutic approach.

- Characterization and optimization of natural yeast strains (ability to use galactose as source of carbon, phenotypic effects of mHTT and αSyn expression - growth, survival, and cellular distribution of the protein, [PIN+] status).

- Selection of parental strains with extreme phenotypes - most resistant and most sensitive strains to HTT and αSyn expression.
- Intercrosses (generation of a large and diverse population).
- QTL analysis (phenotyping and genotyping of the descendants).
- Validation of the modifier genes in yeast (deletion and OE in HD and PD yeast models).
- Characterization of HD fly models (eclosion, lifespan, neurodegeneration, locomotor skills).
- Validation of the modifier genes in flies (effect of the downregulation of selected genes in mHTT toxicity).

2. Materials and methods

2.1. *Saccharomyces cerevisiae* strains

Fourteen *S. cerevisiae* natural isolates from our yeast library containing most of the genetic variability of the species (1-2 SNPs per 100 bp) were assessed in these experiments (Figure 2.1-1, Table 2.1-1). Ten of these strains were isolated in China (Duan et al., 2018), while the other four are derived from the North American (NA), wine European (WE), sake (SA) and west African (WA) strains (Louvel et al., 2013).

Table 2.1-1. Yeast strains information

Strain	Mating type	Origin	Ecology
SX1	<i>MATa, ho::KanMX4</i>	Qinling Mountain, China	Bark, <i>Fagaceae</i> plant
SX3	Diploid	Qinling Mountain, China	Bark, <i>Carya</i> sp.
BJ6	<i>MATa, ho::KanMX4</i>	Changping, China	Persimmon
BJ20	<i>MATa, ho::KanMX4</i>	Dongling Mountain, China	Bark, <i>Quercus wutaishanica</i>
HN6	<i>MATa, ho::KanMX4</i> <i>MATa, ho::KanMX4</i>	Bawangling Mountain, China	Rotten wood
HN10	<i>MATa, ho::KanMX4</i> <i>MATa, ho::KanMX4</i>	Wuzhi Mountain, China	Rotten wood
HN15	<i>MATa, ho::KanMX4</i>	Wuzhi Mountain, China	Rotten wood
HN16	<i>MATa, ho::KanMX4</i>	Wuzhi Mountain, China	Soil
HN19	Diploid	Wuzhi Mountain, China	Bark, <i>Fagaceae</i> plant
FJ7	<i>MATa, ho::KanMX4</i> <i>MATa, ho::KanMX4</i>	Wuzhi Mountain, China	Bark, <i>Hovenia acerva</i>
NCYC3597	<i>MATa, ho::HYG</i>	DBVPG6765 (WE) derivate	Unknown
NCYC3600	<i>MATa, ho::HYG</i>	DBVPG6044 (WA) derivate	Unknown
NCYC3607	<i>MATa, ho::HYG</i>	YPS128 (NA) derivate	Unknown
NCYC3605	<i>MATa, ho::HYG</i>	Y12 (SA) derivate	Unknown
BY4741	<i>MATa, ho::HYG</i>	Derived from S288C	Laboratory

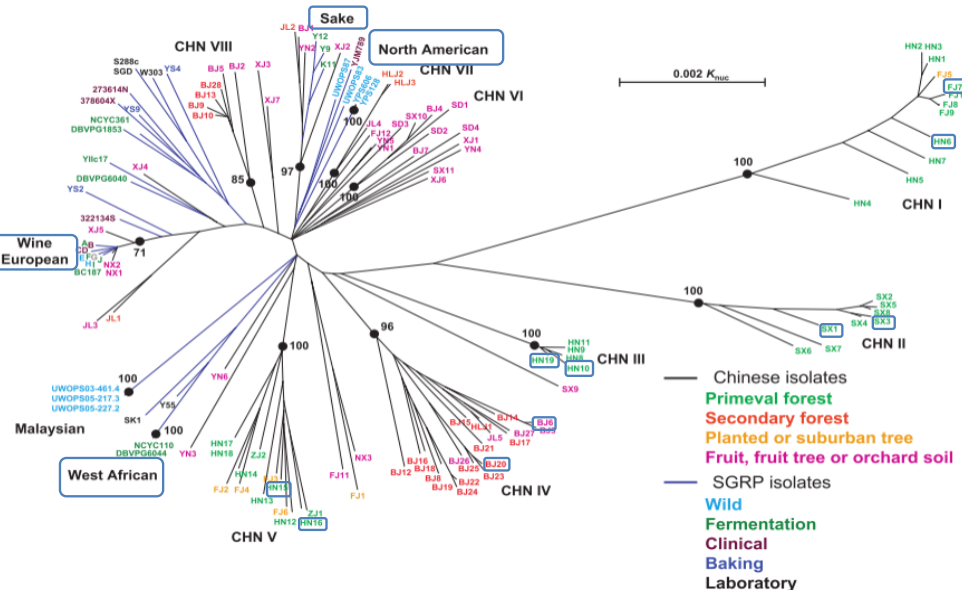


Figure 2.1-1. Phylogenetic diversity of the natural yeast strain isolates

Neighbour-joining tree proposed by (Wang et al., 2012). The scale bar represents 0.002 substitutions per nucleotide position. Strains evaluated in this project are squared in blue.

2.1.1. Yeast Maintenance

2.1.1.1. Media for yeast

All media types were prepared using deionized water (dH_2O). Unless stated otherwise, the pH was adjusted between 6.0 and 6.5, usually 6.3, using either 1 M HCl or 2.5 M NaOH before the addition of the agar.

Before sterilization, the media was placed in glass bottles with 20% of their volume free to avoid the spillage of the contents. The bottles were marked with autoclaving thermosensitive tape and introduced into a steam autoclave to be sterilized at 20 psi, 121 °C for 20 minutes. Heat sensitive components were added after autoclaving when the media had cooled down to approximately 60 °C.

A plate of each batch of selective media was tested to confirm that the preparation was correct. All media types were stored at 4 °C inside plastic bags.

All the recipes include the amount of each component needed to prepare 800 mL of said type of media. To prepare liquid media, the agar was not included.

2.1.1.1.1. Types of plates and tubes

Petri dishes (90 mm): were filled with 25 mL of media and took approximately 10 minutes to dry. If the plates were going to be used for tetrad dissection, they were poured and dried on top of a levelled table, so the surface of the media was flat.

PlusPlates (Singer instruments #PLU-003): were rectangular plates used for PHENOS. They were filled with 40 mL of hard media or 80 mL of soft media and took 30 to 45 minutes to dry. PHENOS plates were always poured on top of a levelled table to avoid problems with the printing of yeasts and with the FLUOstar Omega plate reader (BMG Labtech).

50 mL tubes: transparent tubes used for the liquid cultures. A maximum of 5 mL of media were added to allow proper oxygenation.

2.1.1.1.2. Yeast extract peptone dextrose (YPD) and yeast extract peptone galactose (YPGal) media

8 g of yeast extract (Scientific Lab Supplies LTD #212750)

16 g of bacto-peptone (Scientific Lab Supplies LTD #211677)

16 g of D-glucose (Fisher Scientific #10385940)

8 mL of 0.5% adenine (0.5% adenine, 5% HCl in dH₂O, filter-sterilized)

16 g of agar (BioGene #400-050) only included in the solid media.

The composition of the YPGal media is the same except the D-glucose is replaced with high purity galactose (\geq 99%. Sigma #G0750). Since galactose should not be autoclaved, a 20% galactose solution was prepared and filter-sterilized. As with YPD, YPGal has a final 2% concentration of the sugar so, for a final media volume of 800 mL, the other solutes were diluted to a total volume of 720 mL and 80 mL of 20% galactose were added after autoclaving and cooling down the media.

2.1.1.1.3. Synthetic defined (SD) complete (SC) and dropout (SD-aa) media

5.4 g of yeast nitrogen base without amino acids (YNB. Sigma Aldrich #Y0626)

16 g of D-glucose

0.7 g of complete or dropout powder

16 g of agar in the solid media.

The SD-aa media had the same composition as the SC except for the complete powder, which had all the essential amino acids, and was replaced with the dropout powder that lacked one or more amino acids (Sherman, 2002). The SD media was also made with galactose, substituting the 16 g of D-glucose for 80 mL of 20% galactose as explained in the YPGal media. When SD media was used for the soft PHENOS plates, the 16 g of agar were replaced with 5.2 g of bacto-agar (Scientific Lab Supplies LTD #214010), and the pH was set precisely at 6.3.

2.1.1.1.4. Complete powder and dropout powders

The amino acids (Sigma Aldrich) were mixed in the quantities stated in Table 2.1-2 to make complete powder (Sherman, 2002).

Table 2.1-2. Amino acid composition of the complete powder

Amino acid	Weight (g)
Adenine	0.8
Arginine	0.8
Aspartic acid	4
Histidine	0.8
Leucine	0.8
Lysine	1.2
Methionine	0.8
Phenylalanine	2
Threonine	8
Tryptophan	0.8
Tyrosine	1.2
Uracil	0.8

2.1.1.1.5. FoA (5-Fluoroorotic acid) media for *ura3Δ0* selection

5.4 g of YNB

16 g of D-glucose

0.7 g of uracil dropout powder

0.04 g of uracil

0.8 g of FoA

16 g of agar

FoA is heat-sensitive, so it was added after the sterilization of the media when it had cooled down.

2.1.1.1.6. Potassium acetate (KAc) media for sporulation

16 g of KAc

16 g of D-glucose

0.7 g of complete powder

1.76 g of yeast extract

16 g of agar

The pH of the final media was set to 7.

2.1.1.1.7. Minimal media

5.4 g of YNB

16 g of D-glucose

16 g of agar

2.1.1.2. Growth, storage, and recovery of yeast strains

2.1.1.2.1. Growth conditions

The optimal growth temperature for the yeasts used during these experiments was 30 °C. When using solid media, the plates were positioned upside down on the incubators to avoid the formation of condensation drops on the lid that might fall into

the media and mix the samples. Alternatively, liquid cultures were grown on a shaking incubator at 250 rpm. The samples were placed in transparent sterile 50 mL tubes, using a maximum of 5 mL of media to allow proper oxygenation.

2.1.1.2.2. Storage conditions and sample recovery

For short term storage, the plates were kept upside down at 4 °C. Plates were stored in these conditions for a maximum of a month, before needing to replica plate them on fresh media. For long term storage, yeasts were kept in a -80 °C freezer. In order to freeze the yeast, a large patch of at least a quarter of a petri dish was incubated until fully grown, then it was collected from the plate and inoculated into a sterile cryotube with 1 mL of 25% glycerol. After being frozen, stored yeasts were recovered by scraping some of the ice, spreading it on a YPD plate, and growing them for one or two days. If the yeast had any auxotrophic markers, they were tested on selective media plates for confirmation.

2.1.1.2.3. Obtaining single colonies

A few yeast were scraped from a plate with a wooden stick and a line was drawn in the top part of a new plate of the desired media. With a clean stick, a new line was drawn crossing the first one to take a small number of yeasts. This process was repeated again, and then, with a clean stick, a zig-zagging line was drawn from the last line to the bottom of the plate, diluting the number of yeasts until single cells were separated. The plates were grown at 30 °C for three days to allow the colonies to grow.

2.1.2. Plasmids and deletion cassettes

2.1.2.1. Maintenance of *Escherichia coli*

2.1.2.1.1. Media for bacteria

Both, solid and liquid Luria Broth (LBr) media were supplied by the departmental technicians. The composition of 800 mL of this media was:

4 g of yeast extract

8 g of tryptone

4 g of NaCl

16 g of agar for the solid media

When LBr media with ampicillin (LBr-Amp) was needed, 1 µL of 100 mg/mL ampicillin per mL of LBr media was added after the sterilization, when the media cooled down but had not solidified yet. The only type of plates used for LBr media were Petri dishes. All the LBr-Amp and the LBr plates were stored at 4 °C, while the liquid LBr was stored at room temperature.

2.1.2.1.2. Growth, storage, and recovery of *E. coli*

Bacteria liquid cultures and plates were grown at 37 °C in LBr media overnight. Like the yeast plates, bacteria were stored for up to a month in a fridge at 4 °C. For long term storage bacteria were grown on LBr liquid media overnight, 500 µL of the culture was mixed with 500 µL of 50% sterile glycerol in a 1 mL cryotube that was then stored in a freezer at -80 °C.

The recovery of the bacteria was done by scraping some ice from the frozen stock and spreading it into an LBr plate. If the bacteria carried a plasmid with ampicillin resistance, after incubating the plate overnight, the bacteria were passed to a LBr-Amp plate and the colonies that grew were used for the experiments.

2.1.2.2. Gene cloning and bacterial transformation

2.1.2.2.1. PCR amplification of candidate genes

Gene cloning was performed by amplifying the gene by PCR from one of the plasmids and inserting it into a vector with the desired selection marker using restriction enzymes (RE). The first step was to extract the plasmid DNA using the E.Z.N.A plasmid DNA mini kit I (OMEGA bio-Tek #D6943) following the spin protocol. The bacteria were cultured overnight at 37 °C in 5 mL LBr-Amp, centrifuged, and treated with RNase I and other chemicals to lyse the cell, prevent DNA degradation and help the DNA bind to the column. The DNA was washed and eluted in a clean tube. The concentration of plasmid DNA was quantified using a Nanodrop.

The primers for the amplification of the desired gene were designed using ApE 2.0.49 software (Davis, 2004). The primers' sequences were homologous to the flanking regions of the gene but also had a target sequence for a RE at the end (marked in red in Table 2.1-3). The RE selected had a unique cutting site in the target plasmid while not having any cutting sites inside the gene.

After the plasmid extraction, the PCR was performed with the Q5 High-fidelity DNA polymerase (New England Biolabs #M0491) adding the following amounts per sample: 5 µL of Q5 reaction buffer, 0.5 µL 10 mM dNTPs, 1.25 µL of both 10 µM primers, 0.25 µL of Q5 polymerase, 10 ng of template DNA and dH₂O to a final volume of 25 µL. The thermocycler was set to denaturalize the DNA at 98 °C for 30 seconds and then cycle 30 times denaturalizing at 98 °C for 10 seconds, annealing at the desired temperature for 30 seconds and amplifying at 72 °C for 45 seconds, followed by a final 2-minute amplification. The thermocycler conditions were maintained between genes, except for the annealing temperature (Ta), which was changed depending on the primers that were being used as seen in Table 2.1-3;**Error! No se encuentra el origen de la referencia..**

Table 2.1-3. Primers and Ta for gene cloning

Gene-RE	Primer	Ta (°c)
GFP-Spel	gatc <u>ACTAGT</u> ATGGTGAGCAAGGGCGAGGAGCTG	65
GFP-Sall	gatc <u>GTCGAC</u> TTACTTGTACAGCTCGTCCATGCC	65
SNCA-Sall	gatc <u>GTCGAC</u> TAGTACGGATTAGAAGCCGCCGAG	65

2.1.2.2.2. Transformation of the gene into an intermediate vector for easier digestion

The PCR product was quantified with the nanodrop and ligated to pJET1.2 blunt Cloning Vector (Thermo scientific #K1232) – blunt refers to the ends of a DNA fragment in which there are no unpaired bases - in a 3:1 molar ratio, following the manufacturer's instructions: 0.15 pmol of the PCR product and 0.05 pmol of the plasmid were mixed on ice with 1 µL T4 DNA ligase, 10 µL reaction buffer, and dH₂O to a total volume of 20 µL. The ligation mix was thoroughly mixed using a vortex and incubated at room temperature for five minutes.

The ligation product was used to transform *E. coli* in order to recover the cloned plasmid. 150 µL of the competent bacteria were thawed on ice, mixed gently with 10 µL of ligation mix from the previous step, and incubated on ice for 30 minutes before a two-minute heat shock at 40 °C. After the heat shock, the bacteria were placed on ice for three minutes, before adding 1 mL of LBr media at 37 °C and incubating them for 90 minutes at 37 °C while shaking. 150 µL were plated in a LBr-Amp plate while the rest of the mix was centrifuged, the supernatant discarded, and the pellet resuspended and plated in another LBr- Amp plate. Both plates were incubated at 37 °C overnight. For the cases where no colonies were on the plate the next day, the PCR product was purified before a second ligation attempt and the molar ratio for the ligation was changed to 5:1.

2.1.2.2.3. RE digestion and integration into the final vector

Several colonies from the transformation plate were incubated overnight at 37 °C in LBr-Amp liquid media, and the plasmids were extracted with the E.Z.N.A plasmid DNA mini kit I, following the spin protocol. Finally, both the pJet and the target plasmids were digested with the corresponding REs: 1 µg of DNA, 5 µL of buffer and 1 µL of RE, and dH₂O to a total volume of 50 µL were mixed, incubated at 37 °C for 15 minutes and inactivated at 65 °C or 80 °C depending on the enzyme (see Table 2.1-4). The digestion product was run on a 1% agarose gel with ethidium bromide (EtBr. 5 µL per 100 mL 1xTBE) and the bands corresponding to the cut target plasmid and the genes were purified using the Zymoclean Gel DNA Recovery Kit (Zymo research #D4008). To extract the DNA, the band was cut out of the gel, placed inside a clean 1.5 mL tube, and weighed. Three volumes of ADB were added and the mix was incubated at 55 °C until the gel was dissolved. The liquid was passed through a column and washed, and the DNA was recovered in a new clean tube.

Finally, the gene and the plasmid were mixed at a 3:1 molar ratio, on ice, with 2 µL of ligation buffer and 1 µL of T4 DNA ligase (New England Biolabs # M0202) and dH₂O up to 20 µL. The ligation mix was incubated at room temperature for 15 minutes and then 10 µL were used to transform bacteria as previously described.

To confirm that the insert was in the correct orientation, the plasmid was digested with XbaI, following the manufacturer's instructions (Table 2.1-4). The plasmids were sent to be sequenced at Source Bioscience to confirm there were no mutations or deletions caused during the cloning process. To sequence the whole gene, primers homologous to the vector were used for the sequencing. T7F (TAATACGACTCACTATAGGG) and M13R (AGCGGATAACAATTTCACACAGGA) were used for pRS327 and GDPF (GGTCCTTCTTGAGTTGTAAC) and CYC1R (GCGTGAATGTAAGCGTGAC) for pJet. Lastly, since all the constructs expressed

GFP, the plasmids were used to transform yeast, incubated in selective media with galactose and observed under the fluorescence microscope to confirm that the proteins were being expressed.

Table 2.1-4. RE digestion protocol

RE	Digestion	Inactivation	NEB #
Spel	37 °C, 15 min	80 °C, 20 min	R0133
Sall	37 °C, 15 min	65 °C, 20 min	R0138
XbaI	37 °C, 15 min	65 °C, 20 min	R0145

2.1.2.3. Amplification of DNA cassettes for gene deletion by homologous recombination

2.1.2.3.1. Cassette for the deletion of the *URA3* gene (*ura3Δ0*)

The DNA of a *ura3Δ0* strain was extracted by resuspending a fresh colony - less than ten days old - in 20 µL of 0.02M NaOH, incubating it at room temperature for five minutes and thoroughly mixing it with a vortex. After centrifuging the sample, the supernatant was used as a template for the PCR. The template was amplified using primers flanking the *URA3* gene:

URA3 Forward: 5' CTGTGGTTTCAGGGTCCATA

URA3 Reverse: 5' TGGAGTTCAATGCGTCCATC

The PCR master mix was made with BIOTAQ DNA polymerase (Bioline # BIO-21040): 2 µL NH4 buffer, 0.6 µL Mg²⁺, 0.8 µL 10 mM dNTPs, 1 µL each primer, 0.2 µL polymerase, 1 µL DNA cassette and H₂O to a total volume of 20 µL. The thermocycler was set to denaturalize the DNA at 95 °C for 1 minute and then cycle 30 times denaturalizing at 95 °C for 30 seconds, annealing at 50 °C for 30 seconds and amplifying at 72 °C for 90 seconds, followed by a final 10-minute amplification.

The PCR products were run on a 1% agarose gel to confirm that they were the expected size (300 bp), and then extracted from the gel and purified using the Zymoclean Gel DNA Recovery Kit as mentioned above.

2.1.2.3.2. Cassette for the substitution of the gene with *LEU2* (*gene::LEU2*)

The genomic DNA of the yeast was extracted using the E.Z.N.A. Yeast DNA extraction kit (OMEGA bio-Tek #D3370) according to the manufacturer's instructions. 5 mL of YPD media were inoculated with a yeast colony and grown overnight at 30 °C with shaking. The yeast were centrifuged, the supernatant discarded, and the pelleted yeast were treated with β-mercaptoethanol and lyticase to break the cell walls and denaturalize the proteins, lysed with glass beads, treated with Proteinase K and then with RNase A, washed with ethanol and finally passed through a column to obtain pure genomic DNA.

Primers were designed with 18-20 bp of homology with the flanking regions of *LEU2* (sequence underlined) and 42 bp or more homology with the flanking regions of the gene that was to be substituted (Table 2.1-5). These primers were used to amplify *LEU2* from a WT strain with the Q5 High-fidelity DNA polymerase, following the same protocol mentioned during the gene cloning protocol. The thermocycler was set to denaturalize the DNA at 98 °C for 30 seconds and then cycle 30 times denaturalizing at 98 °C for 10 seconds, annealing at 56 °C for 30 seconds and amplifying at 72 °C for 45 seconds, followed by a final 2-minute amplification. The PCR products were run on a 1% agarose gel to confirm that they were the expected size (~1780 bps), and then extracted from the gel and purified following the Zymoclean Gel DNA Recovery Kit protocol as mentioned above.

Table 2.1-5. Primers for the amplification of the deletion cassettes

Gene del	Primer
<i>lys2</i> Fw	atgactaacgaaaaggctggatagagaagttggataatccaactct <u>ggaaatactcaggatcg</u>
<i>lys2</i> Rv	ttaagctgctgcggagctccacgagcaccgcacgtgaagcaacc <u>cacgttqagccattagtatc</u>
<i>far10</i> Fw	tgtcgttgttatatttgaagctatagatataatcgaatcc <u>ggaaatactcaggatcg</u>
<i>far10</i> Rv	ctgacgtgaaaagcggatcggtgtcttacgt <u>cacgttqagccattagtatc</u>
<i>taf2</i> Fw	tggacagtgaagagggtgacaacaggataaaataggtgacttc <u>ggaaatactcaggatcg</u>
<i>taf2</i> Rv	ttgttgctgagtcgttagtaatatcatatttatacaaata <u>cacgttqagccattagtatc</u>
<i>gsy2</i> Fw	aactgtgattgaagtttactaccctcagagaaaaatttga <u>ggaaatactcaggatcg</u>
<i>gsy2</i> Rv	tatggtaagattttaatactgtttatcatccataggat <u>cacgttqagccattagtatc</u>
<i>dss4</i> Fw	ttcaattaaaaggctggaaaaatggggaaataacagagaac <u>ggaaatactcaggatcg</u>
<i>dss4</i> Rv	ttctggtggcggcaacctatttgttctagtgctaccaaa <u>cacgttqagccattagtatc</u>
<i>tif6</i> Fw	tttggacaagagcataattcaactaactctagaaaacaata <u>ggaaatactcaggatcg</u>
<i>tif6</i> Rv	gacttgaggaaggagggaatcccctcaggagtacgtacat <u>cacgttqagccattagtatc</u>
<i>ppm1</i> Fw	actccgcataaaactagatgataaagagtacaacaactcgcc <u>ggaaatactcaggatcg</u>
<i>ppm1</i> Rv	taagcatattaagatcaaatttttagtgaggctgtaaataaaaa <u>cacgttqagccattagtatc</u>
<i>mrx21</i> Fw	atagtattgacttcaaatttttaatcggttattcgtaac <u>ggaaatactcaggatcg</u>
<i>mrx21</i> Rv	tcattacttggtttcgtgacccaaggctgtcacctcaac <u>cacgttqagccattagtatc</u>
<i>rpa135</i> Fw	aagaatattgacaataaacgtagaattacgcatttttgtag <u>ggaaatactcaggatcg</u>
<i>rpa135</i> Rv	tcatttaccattctatatcaatttggaaagaagggtatttct <u>cacgttqagccattagtatc</u>

After the transformation, the DNA was extracted following the NaOH DNA extraction protocol mentioned above for the amplification of the *ura3Δ0* fragment, and the gene deletions were checked by PCR with the BioClassic Taq polymerase (PCR BIO #PB10.15-01) following the manufacturer's instructions: 5 µL buffer, 1 µL 10 mM dNTPs, 2 µL of each primer, 5 µL DNA, 1 µL Taq, and dH₂O up to 50 µL. The primers used for checking the deletions are listed in Table 2.1-6. The primer named as the corresponding gene was combined with *LEU2* during the deletion-check PCR. The thermocycler was set to denaturalize the DNA at 95 °C for 1 minute and then cycle 30 times denaturalizing at 95 °C for 30 seconds, annealing at the 47 °C for 30 seconds and amplifying at 72 °C for 90 seconds, followed by a final 10-minute amplification. The PCR products were run on a 1% agarose TBE gel, and the fragment size compared to the expected size shown in Table 2.1-6.

Table 2.1-6. Primers and fragment sizes for the deletion-check PCR

Gene	Primer	Size del (bp)
<i>far10</i>	GGCAAGAGTGACAAAGTAAC	1995
<i>taf2</i>	TTGGACAGTGAAGAGGTGAC	1865
<i>gys2</i>	TTAAGGTTCCCTGCCTTCC	1916
<i>dss4</i>	TCTTCGTAAGGCTGACTGG	1963
<i>tif6</i>	ATCCCTCGTTGGTCTTATAG	1858
<i>ppm1</i>	AAAGAAGATGGGTCAAGGGTC	1993
<i>mrx21</i>	ATACCAAGTTGCTCGTTCC	1890
<i>rpa135</i>	TGAGATTACTCTTGCAGTG	2130
<i>LEU2</i>	CACGTTGAGGCCATTAGTATC	N/A

2.1.2.4. List of plasmids and DNA cassettes

During these experiments, three auxotrophic genes were deleted, human disease-related genes were overexpressed, and possible modifier genes were deleted and overexpressed (Table 2.1-7). All the plasmids used in these experiments were 2-micron plasmids with ampicillin resistance.

Table 2.1-7. List of plasmids and DNA cassettes

Auxotrophic Markers				
Gene	Marker (media)	Tag	Vector (promotor)	Source
<i>ura3</i>	No (FoA)	No	DNA cassette	Giorgini Lab
<i>leu2</i>	URA3	No	pEL9	(Louis & Haber, 1989)
<i>lys2</i>	LEU2	No	DNA cassette	Giorgini Lab
Disease Plasmids				
<i>HTT25Q</i>	<i>URA3/LYS2</i>	GFP & FLAG	pRS426 / 327 (GAL1)	(Meriin et al., 2002)
<i>HTT103Q</i>	<i>URA3/LYS2</i>	GFP & FLAG	pRS426 / 327 (GAL1)	(Meriin et al., 2002)
<i>GFP</i>	<i>URA3/LYS2</i>	GFP	pRS426 / 327 (GAL1)	Giorgini Lab
<i>SNCA WT</i>	<i>URA3/LYS2</i>	GFP	pRS426 / 327 (GAL1)	(Lázaro et al., 2014) / Giorgini Lab
<i>SNCA A30P</i>	<i>URA3</i>	GFP	pRS426 (GAL1)	(Lázaro et al., 2014)
<i>SNCA A53T</i>	<i>URA3</i>	GFP	pRS426 (GAL1)	(Lázaro et al., 2014)

OE Plasmids

RNQ1	<i>URA3</i>	GFP	pAG246 (GDP)	Prof. Tuite (University of Kent)
FAR10	<i>URA3</i>	No	pGB1805 (GAL)	Horizon
TIF6	<i>URA3</i>	No	pGB1805 (GAL)	Horizon
PPM1	<i>URA3</i>	No	pGB1805 (GAL)	Horizon
MRX21	<i>URA3</i>	No	pGB1805 (GAL)	Horizon
RPA135	<i>URA3</i>	No	pGB1805 (GAL)	Horizon
TAF2	<i>URA3</i>	No	pGB1805 (GAL)	Horizon

Deletion Cassettes

taf2	<i>LEU2</i>	No	DNA cassette	Giorgini Lab
gsy2	<i>LEU2</i>	No	DNA cassette	Giorgini Lab
dss4	<i>LEU2</i>	No	DNA cassette	Giorgini Lab
tif6	<i>LEU2</i>	No	DNA cassette	Giorgini Lab
ppm1	<i>LEU2</i>	No	DNA cassette	Giorgini Lab
mrx21	<i>LEU2</i>	No	DNA cassette	Giorgini Lab

2.1.2.4.1. Auxotrophic markers

As mentioned above, *URA3* deletion was performed with a small DNA fragment homologous to the flanking regions of the gene (Figure 2.1-2 A). After the transformation, the transformed colonies were selected using FoA media and checked by PCR using the primers used for the amplification of the plasmid.

The *LEU2* gene was deleted using the pEL9 plasmid (Louis & Haber, 1989) (Figure 2.1-2 B). This plasmid contains a *LEU2* gene that has been disrupted by the insertion of *URA3* (*leu2::URA3*). To prepare the plasmid for the transformation, pEL9 was linearized using Sall (New England Biolabs #R0138) following the manufacturer's instructions; it was incubated at 37 °C for one hour and inactivated at 65 °C for 20 minutes. The product was run on a gel and the linear DNA was cut out and purified using the Zymoclean Gel DNA Recovery Kit. This plasmid was used to transform *ura3Δ0* colonies, the transformants were selected in SD-URA media. The colonies were then passed to SC, so they lose the *URA3*, and later replica plated into FoA. The colonies that grew on FoA were tested in SD-URA and SD-LEU to confirm both deletions.

The last auxotrophic marker to be deleted was *LYS2*. This deletion was performed in *leu2Δ0* strains because the template had *LEU2* as a marker (Figure 2.1-2 C). The transformation was performed with the *lys2::LEU2* DNA fragment mentioned above, the extremes of which were homologous to the flanking regions of *LYS2* while the central region encoded *LEU2*. After the transformation, the colonies were selected in SD-LEU, and the colonies that grew were tested in SD-LYS.

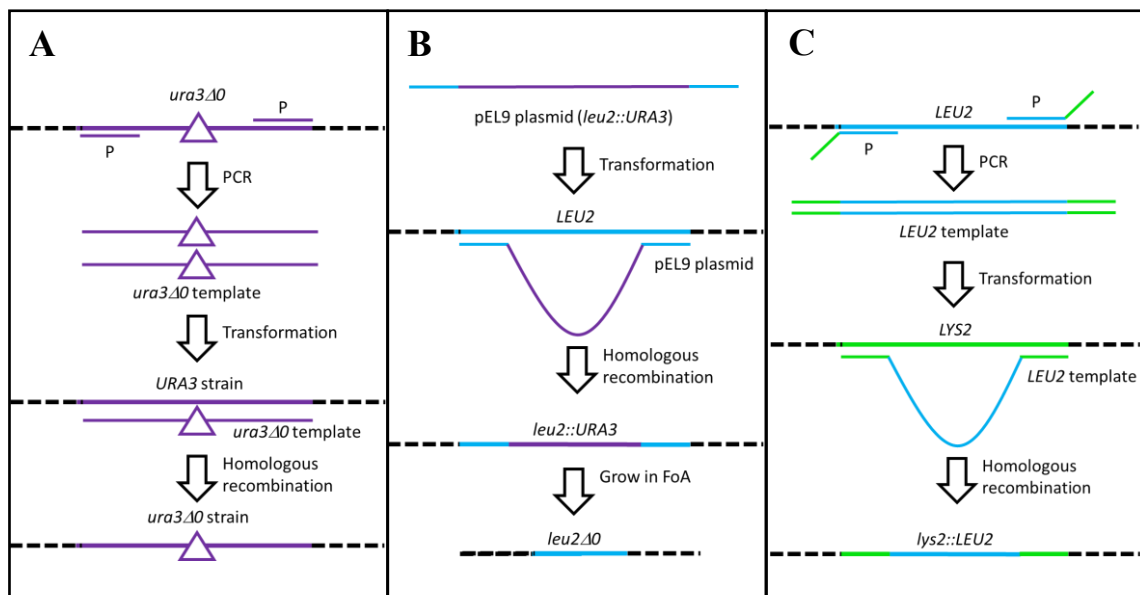


Figure 2.1-2. Auxotrophic markers deletion protocol

The deletion of auxotrophic markers was performed in three different ways. **A)** To delete *URA3*, primers flanking the gene were used to amplify that region in a strain that was already *ura3Δ0*. That DNA was used as a deletion cassette for the transformation. The strains that underwent homologous recombination with the cassette became *ura3Δ0* and were able to grow in FoA media. **B)** *LEU2* was deleted using the pEL9 plasmid, which contain the *LEU2* gene interrupted by *URA3*. The plasmid was linearized and used for the transformation. The yeast that recombined became *leu2Δ0* and *URA3*, they were selected in SD-URA, then passed to SC, and finally grown on FoA so they lose the *URA3*. Colonies that grew on FoA were *ura3Δ0* and *leu2Δ0*. **C)** Deletion of *LYS2*, was performed with a DNA cassette created by amplifying the *LEU2* gene with primers that were homologous to the flanking regions of *LYS2*. The resulting DNA cassette was used to transform the *leu2Δ0* yeasts. Those that underwent homologous recombination with the fragment became *lys2::LEU2*. This method was also used to generate the DNA cassettes and delete the possible modifier genes.

2.1.2.4.2. Plasmids

HD was modelled in yeast transforming them with a plasmid encoding the first 17 amino acids of the human *HTT* gene attached to a tail of 25 (WT) or 103 (mutant) CAG repeats, intercalated with CAA triplets for stability purposes, under the control of the *GAL1* promoter, so the expression was repressed in the presence of glucose and induced by galactose (Meriin et al., 2002). This gene was tagged with *FLAG* to mimic the SUMOylation of the protein that happens in humans, and with *GFP* to track the protein. There were two plasmid vectors with *URA3* (pRS426) and *LYS2* (pRS327) as markers, so transformants were selected in SD-URA and SD-LYS respectively.

PD was modelled by expressing the whole *αSyn* protein. There were three different constructs, one carrying the WT gene, and two carrying the gene with the mutations found in familial forms of PD: A53T and A30P (Lázaro et al., 2014). Like *HTT*, *αSyn* was *GFP*-tagged and under the control of the *GAL1* promoter. The *GFP* tag was cloned into the same *URA3* empty vector (pRS426) to be used as a control. Both the *GFP* and the WT *SNCA* were cloned into a *LYS2* vector (pRS327).

The *RNQ1* plasmid was obtained from Professor Mick F. Tuite (University of Kent). *RNQ1* was inserted into the pAG246 vector, so the expression is under the control of the constitutive promoter *GPD*, and it has *URA3* as an auxotrophic marker. Like *HTT* and *αSyn*, *RNQ1* is also *GFP* tagged.

The OE plasmids for *FAR10*, *TIF6*, *PPM1*, *MRX21*, *RPA135* and *TAF2* were obtained from the OE collection (Perkin Elmer, Horizon Yeast ORF collection). The plasmids were extracted from the yeasts of the collection, transformed into bacteria for replication, and then extracted from the bacteria for the transformations. All these plasmids had *URA3* as a marker and were under the control of the *GAL* promoter.

2.1.2.4.3. Deletion of possible modifier genes

The possible modifier genes were (*TAF2*, *GSY2*, *DSS4*, *TIF6*, *PPM1* and *MRX21*) deleted using the same mechanism as with *LYS2* (Figure 2.1-2 C). The *LEU2* gene was amplified with primers that had a region of homology to the modifier gene so they could recombine. The transformation was performed in *leu2Δ0* strains, and SD-LEU plates were used as selective media.

2.1.3. Transformation of yeast strains

2.1.3.1. Lithium Acetate (LiAc) transformation protocol

This LiAc transformation protocol is based on the protocol described by Gietz and Schiestl in 2007. First, a fresh single colony was resuspended in 5 mL of YPD media and incubated overnight at 30 °C while shaking at 250 rpm until they reached the stationary phase. The optic density at 600 nm (OD600) of the culture was measured with the spectrophotometer and diluted to 0.2. Then the dilution was allowed to grow for three hours in the same conditions as before until it reached the logarithmic phase (OD600 of approximately 1). The yeasts were pelleted, washed with 1 mL of dH₂O, then washed with 1 mL of 100 mM LiAc, and the supernatant was discarded. The transformation mix was added following this order: 240 µL 50% polyethylene glycol (PEG), 36 µL 1M LiAc, 40 µL single-stranded carrier DNA (ssDNA. 2mg/mL in 1x TE buffer), 0.5-1 µg DNA, dH₂O to a total volume of 360 µL. The mix was pipetted to mix the reagents and then vortexed to resuspend the yeast, followed by a 30-minute incubation at 30 °C, and a 30-minute heat shock at 42 °C in a water bath. Finally, the yeast cultures were centrifuged at 6000 rpm for 15 seconds, resuspended in 500 µL of dH₂O, and 100 µL were plated in selective media, spreading a lawn using glass beads and incubated at 30 °C for three days. The isolated colonies were streaked

for singles. All the materials and reagents were sterile, and the experiments were performed in a sterile environment to avoid contamination.

Since the efficiency of the transformations with DNA cassettes for recombination was quite low, the protocol was modified again for those specific cases. One colony was cultured, diluted, and grown until it was in the logarithmic growth phase. The sample was centrifuged, and the pellet was directly resuspended in 240 µL 50% PEG, 36 µL 1M LiAc, 40 µL 2mg/mL ssDNA, 1 µg template DNA, and dH₂O to a total volume of 360 µL. The sample was directly incubated at 42 °C for 30 to 60 minutes in a water bath, mixing every 15 minutes. The sample was centrifuged, resuspended in 100 µL of dH₂O, and all the cells were plated in selective media.

2.1.3.2. High-throughput transformation protocol

The high-throughput transformation protocol performed during these experiments was described by Giorgini and Muchowski (2006). A colony was resuspended in 100 µL of YPD in each well of a 96-well microtiter plate. The yeasts were grown at 30 °C overnight, or until they reached the stationary phase (OD₆₀₀ ≥ 5). The plate was centrifuged, the supernatant discarded, and the cells washed with dH₂O. For each plate, 2 mL of the transformation mix (0.2 M LiAc, 40% PEG, 100 mM dithiothreitol) were mixed with 100 µL ssDNA (10 mg/mL) and 20 µg of plasmid. The yeasts were resuspended in 20 µL of the mix per well and then heat shocked at 42 °C for 30 minutes. Finally, 5 µL of cells per well were spotted into a selective media plate and allowed to grow at 30 °C for three days. The new colonies were streaked for singles in selective media.

2.1.4. Phenotyping yeast strains

2.1.4.1. Spotting assay

Spotting assays were performed following the protocol described by Giorgini and Muchowski in 2006. A fresh single colony was inoculated in 5 mL of selective media and grown at 30 °C in a shaking incubator for one or two days, until it reached the stationary phase. The OD600 was adjusted to 0.4 and the yeast were incubated again at 30 °C for between 30 minutes to three hours. After the incubation, 1 in 5 serial dilutions were performed and 5 µL of cells were spotted in selective media with galactose. The plates were dried for 30 minutes until all the liquid was absorbed and then incubated at 30 °C for at least three days (Figure 2.1-3). Representative images of the colonies were taken after 3 days.

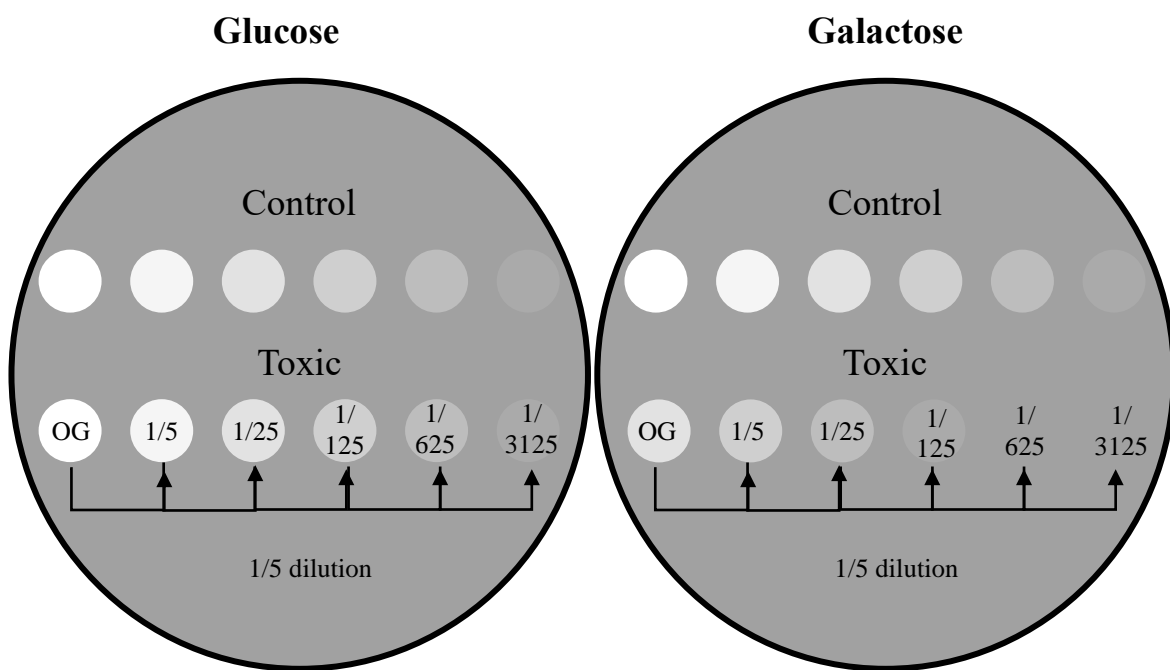


Figure 2.1-3. Spotting assay protocol

The yeasts are grown until stationary phase, diluted so all of them start from a similar cell density, and incubated so they begin to grow again. Then 1/5 serial dilutions are performed and spotted in a control (glucose) and experimental (galactose) plates. After the yeast have grown, if there are no differences in the number of colonies in the glucose plate, any difference in the number of colonies between the toxic and the control transformants in the galactose plate represents a reduction in survival.

2.1.4.2. Phenotyping in solid media (PHENOS)

A fresh single colony was resuspended in 100 µL of 25% glycerol in each well of a 96-well microtiter plate. The Rotor HDA Colony Manipulation Robot (Singer Instruments) was loaded with disposable plastic repads (Singer instruments #REP-001 and #REP-003) and used to mix the content of the wells and plate a drop of the cell suspension into a rectangular plate containing hard media, creating the stock plate (Table 2.1-8 Stock). This plate can be in a 96-well plate format, or in a 384-well plate format, in which each sample has four technical replicas. The stock plate was incubated at 30 °C for up to 48 hours, until the colonies were grown. Then, the rotor was used to pass those yeast to the surface of the soft plate (Table 2.1-8 Soft), where they were grown overnight at 30 °C, before using the rotor again to pin through the colonies and the agar, taking a small amount of yeast on the tip of each pin of the repad, and printing it into the experimental plate (Table 2.1-8 Experiment, Figure 2.1-4).

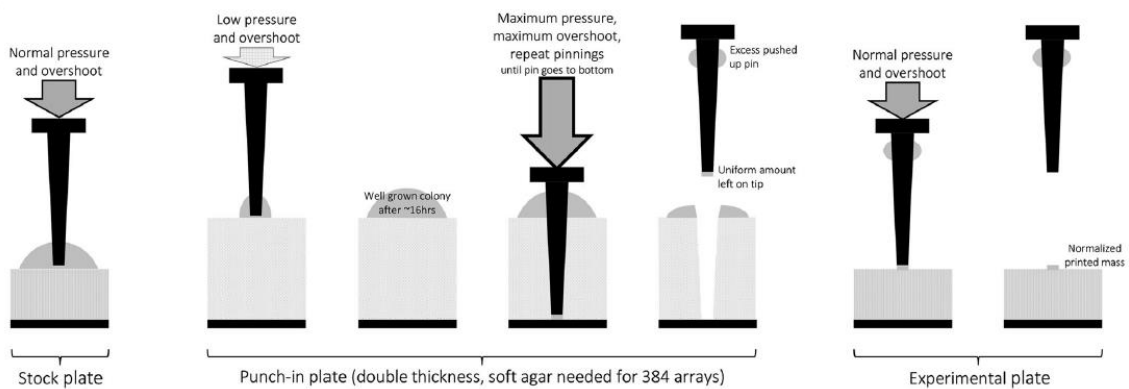


Figure 2.1-4. Punch-in method to normalize mass for PHENOS experiments

Long 384-repads are used to transfer the yeast from the stock plate to the soft agar plate, where they are grown overnight. The same type of repads are used to pin through the soft agar, taking a small amount of yeast on the tip of each pin, and printing approximately the same mass of all the samples in the experimental plate. Image source: Barton *et al*, 2018.

Table 2.1-8. Rotor protocols for PHENOS

Protocol	Repad pins	Mix	Pressure source	Pressure target	Wells original	Wells target	Repeat pin
Stock	96	Original	N/A	70%	96	384	Original
Soft	384	No	70%	≤ 20%	384	384	No
Experiment	384	No	100%	70%	384	384	Original
Glycerol	96	Both	70%	N/A	96	96	No

In order to create the growth curves, a plate reader was used to measure the OD600 of each colony. The first measurement was taken just before the yeast were printed in order to have a blank measurement of the OD600 of the agar plate itself. After the printing, OD600 measurements were taken every 20 minutes for three days. The temperature of the plate reader was kept constant at 30 °C throughout the length of the experiment.

When the readings were over, the data from the plate reader were introduced in the PHENOS software. PHENOS was used to name the samples, identify the plates as control or treatment, generate the growth curves, and compare the growth of the control and treatment plates -each control yeast was compared only with the treatment yeast located in the same position of the plate- (Figure 2.1-5). The software provided a file for each plate containing: the name and position of the samples, the blank measurement, the initial printed mass, the final mass, the maximum slope of the curve -maximum growth speed of the yeast on the logarithmic phase-, the duration of the lag phase -time between the printing and the beginning of the logarithmic phase-, the maximum change -difference in OD600 between the original printed mass and the final mass-, and OD600 measurements of each sample taken during the experiment. Also, after comparing a control and a treatment plate, PHENOS generated another file with the difference in growth, in maximum slope and in lag phase duration, which was used for the QTL analysis.

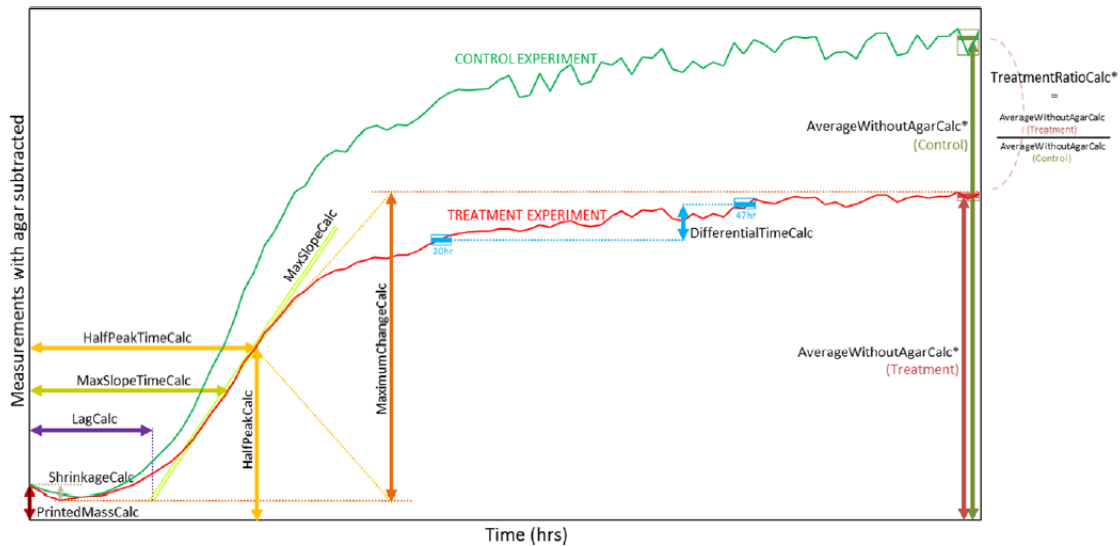


Figure 2.1-5. Illustration of the growth curves provided by PHENOS with all the parameters analysed by the software

PHENOS uses the data from the plate reader to generate growth graphs and analyses the different parameters of the curves: printed mass, lag phase duration, maximum slope, maximum growth, and maximum change. It can also compare the three main parameters (lag, slope, and maximum growth) between control and treatment plates. Image source: Barton *et al*, 2018.

Prior to the experiments, the rotor was sterilized using the inbuilt UV light for 20 to 45 minutes to avoid contamination. During the experiments, the yeast were separated depending on their mating type to avoid any possible interference caused by the mating signals.

2.1.4.3. Aggregation assessment

2.1.4.3.1. Fluorescence microscopy

Fluorescence studies were performed in freshly transformed yeast -transformed less than ten days before the experiment-. For the quantification of the number of aggregates in HTT and α Syn transformed yeasts, three fresh single colonies of each transformant were grown at 30 °C in a shaking incubator for 16 hours in selective liquid media with galactose to induce gene expression. 135 μ L of the culture were mixed with 15 μ L of 37% formaldehyde (Sigma #252549) to obtain a final concentration of 3.7% formaldehyde in the culture. The mix was incubated at room

temperature in a dark place for ten minutes, centrifuged at 8000 rpm for five minutes, and resuspended in 100 μ L of 0.1 M potassium phosphate buffer. The potassium phosphate buffer was made by mixing 8.34 mL of 1M K_2HPO_4 with 1.6 mL of 1M KH_2PO_4 , in a final volume of 500 mL. Both original solutions needed to be filter-sterilized, and the pH of the final buffer was adjusted to 7.5.

Lastly, 3 μ L of fixed cells were set on a slide, dried for one minute, and a coverslip was placed and sealed with nail polish on the edges to avoid evaporation. An Olympus FV1000 confocal microscope at 40x magnification, Kalman 4, was used to visualize the GFP-tagged proteins. Ten images were taken of each of the three replicas. The number of GFP foci was counted in all the cells expressing GFP. Cells were grouped based on the number of foci they had: 0, 1-2, 3-4, or more than 4. The percentage of cells included in each of the groups was assessed for all the strains, and the differences between strains were studied using a Two-way ANOVA corrected by Tukey's multiple comparisons test.

RNQ1 expression was constant since the transformation with the plasmid because it was expressed from a constitutive promoter, so induction was unnecessary. Single colonies were taken from the transformation plate, resuspended in 135 μ L dH₂O and fixed with formaldehyde and visualized as explained above. The presence of aggregates was determined, but not the number of aggregates per cell.

2.1.4.3.2. Filter trap

Protein extraction

A freshly transformed colony was resuspended in 5 mL of selective media with galactose to induce the expression from the plasmid. The yeasts were incubated at 30 °C in a shaking incubator for 16 hours to keep the results consistent with those obtained from the fluorescence microscopy experiments. The cells were harvested at 4 °C and resuspended in 250 μ L of ice-cold breaking buffer (1x PBS, 50 mM

ethylenediaminetetraacetic acid (EDTA), protease inhibitor cocktail) and 250 mg of glass beads. The yeasts were lysed for 90 seconds using a bead beater, placed on ice to settle, and the supernatant transferred to a clean tube.

Protein quantification

The protein concentration was determined using the Bradford assay. Samples were diluted 1/10 and 1/100, BSA was used to create a standard curve, and an equal volume of QuickStart Bradford Dye Reagent (Bio-Rad #500-0201) was added to each sample. After incubating it for five minutes in a dark place, the samples were measured in a plate reader with the absorption set at 595 nm.

Filtering

The protein lysates were run through a nitrocellulose membrane (NC) with a pore size of 0.45 µm (Whatman #10401197) to detect total levels of the protein, and through a cellulose acetate membrane (CelAc) with a pore size of 0.22 µm (GVS #1224211) to detect sodium dodecyl sulphate (SDS)-insoluble aggregates.

10 µg of protein were mixed with PBS with SDS -2% (CelAc) or 0.05 (NC)- at a final volume of 200 µL. The samples were boiled for five minutes and later left to cool down at room temperature to avoid SDS's precipitation. The membranes were equilibrated in PBS with SDS -0.1% (CelAc) or 0.05 (NC)- before assembling the filtering apparatus. Two sheets of 3MM paper soaked in the corresponding SDS-PBS solution were placed under the equilibrated membrane without leaving bubbles, and the apparatus was screwed maintaining equal pressure on all sides.

The membrane was washed twice with 100 µL of SDS-PBS solution, the samples were mixed well and filtered at low pressure, and the membrane was washed twice again before disassembling the apparatus.

Immunodetection

After taking the membranes from the apparatus, they were rinsed for five minutes in 1x TBS with 0.05% tween (TBS-Tween), then blocked for one hour with TBS-Tween with 3% milk, and finally incubated overnight at 4 °C with the primary antibody. The next day, the primary antibody was removed, the membrane washed with PBS, and incubated with the secondary antibody for one hour at room temperature. Finally, the membrane was washed twice with TBS-Tween, dried gently, and revealed with the Westar Supernova Chemiluminescent substrate for western blotting (Cyanagen XLS-3,0020) following the manufacturer's instructions. The images were taken after 5 minutes of incubation and visualized with the GeneSys software.

The primary antibody used to detect the HTT protein was an anti-FLAG mouse monoclonal IgG that was diluted 1:1000 in TBS-Tween with 3% milk (OctA probe H-5, anti-FLAG. Santa Cruz Biotechnology #sc166355). This antibody was detected by the secondary horse anti-mouse IgG that carried horseradish peroxidase (Peroxidase anti-mouse IgG. Vector Laboratories #PI-2000).

2.1.4.4. Flow Cytometry

The expression of the fluorescent proteins from the plasmids was induced for 16 hours to keep the results consistent with those from fluorescent microscopy and filter trap. A single colony from a freshly transformed plate was inoculated into selective liquid media with glucose and grown overnight at 30 °C while shaking. The next day, the cells were washed with PBS, and separated into two tubes -one with selective media with glucose and the other one with galactose-, at a final OD600 of 0.2. The yeasts were grown for 16 hours while shaking. Then, 100 µL of culture were diluted in 900 µL of dH₂O and thoroughly mixed, 10 µL were placed into the counting grid of a hemacytometer, and a coverslip was placed. After a few minutes to allow the cells

to settle, the number of cells in the large grid squares was counted under the microscope with a 10x lens. The number of cells in the sample was calculated following this formula:

$$\text{Total cells/mL} = \frac{\text{Total cells counted}}{\text{Number of squares counted}} * \text{Dilution factor} * 10000$$

The culture was diluted to obtain a final concentration of 10^7 . The yeast were fixed for 10 minutes with 3.7% formaldehyde while being kept in a dark place. Finally, the samples were diluted 1/10 in H₂O and briefly sonicated in a water bath before being run in the flow cytometer.

An Accuri C6 Plus flow cytometer (BD Biosciences) was used for the experiments. Since the protein used was GFP, the FITC filter was used (excitation was set at 488 nm and emission at 530/30 nm). The samples were run with a slow or medium flow speed. To allow around 100 cells to pass per second. Between 5000 to 10000 cells were allowed to run through the cytometer. For each strain, a negative control (samples grown on media with glucose) was run to use as a blank.

Lastly, the flow cytometry data were analysed using the FCS Express 7 software. First, the negative controls were used to determine the basal level of green emission of the cells. Then, a gate was set to only select cells with a green emission higher than that level in the galactose samples, so only the cells expressing GFP were selected. Finally, the average intensity of the GFP signal was calculated and compared between the three parental strains using a two-way ANOVA corrected by Tukey's multiple comparison test. A difference in the intensity of the GFP signal between the strains transformed with the same plasmid would mean that the plasmid expression is different between strains, which could be the reason for the different toxicity phenotypes.

2.1.5. Intercrosses of yeast strains

2.1.5.1. Yeast crossing protocol

The first step to cross two yeast strains (one **a** and one **α**) was to resuspend a colony of each of them in 100 µL of H₂O, mix it, spread it on a YPD plate using glass beads, and incubate it overnight at 30 °C (Figure 2.1-6). The resulting colonies were replica plated onto SD-LEU and LYS to select for diploids, grown overnight, and replica plated onto sporulation media (KAc media) and incubated for two days, until they reached 90% sporulation efficiency. The cells were collected from the plate, resuspended in 50% ether and vortexed for five minutes to kill the non-sporulated yeasts. After being washed four times, the cells were resuspended in 900 µL dissection buffer and 100 µL zymolase (10 mg/mL), and incubated at 37 °C for 30 minutes, mixing every ten minutes, to release the gametes. After washing it, part of the solution was stored at -80 °C as first generation (F1), while the rest was spread on a YPD plate and grown overnight to allow the matting of the gametes, the cells were collected, and the same steps as before were followed until the 12th generation (F12) was reached.

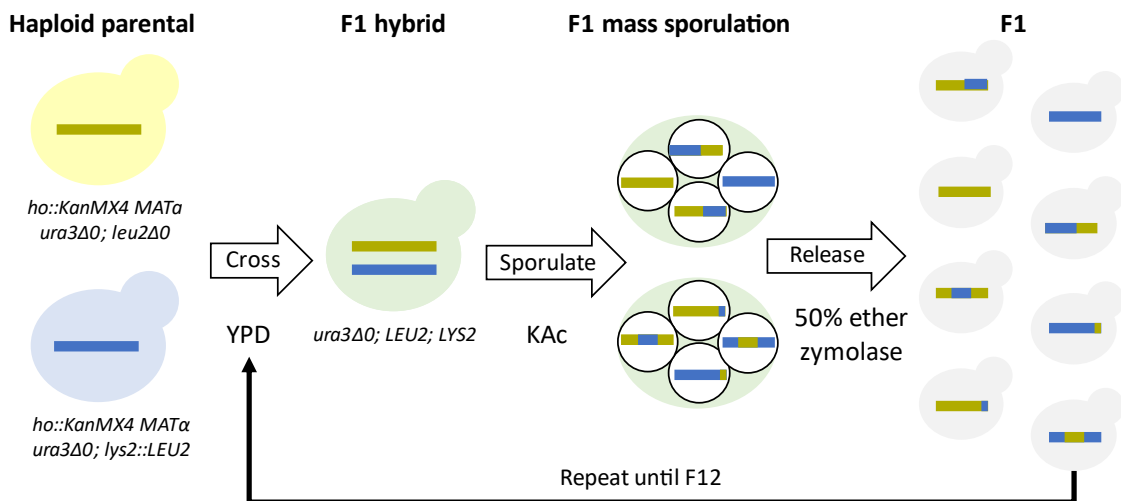


Figure 2.1-6. Yeast crossing protocol to generate the F12

Two parental strains with different mating types and different selection markers (*leu2Δ0* and *lys2::LEU2*) were crossed in YPD, passed to SC -LYS -LEU to select only the diploids. Then they were replica plated into sporulation media, and when the spores were formed (2-3 days later), they were treated with 50% ether to kill the non-sporulated yeast, and with zymolase to release the spores. The spores were grown and allowed to mate in YPD, and the process was repeated until the F12 was reached.

2.1.5.2. Tetrad dissection

The product of the last cross was plated into a YPD plate using glass beads and grown overnight at 30 °C. Later, it was replica plated using a velvet into KAc media, which lacks nutrients, so the yeasts starve and generate spores. The plates were incubated at 30 °C for two days. Some of the cells were collected and resuspended in 95 µL of dissection buffer (1 M sorbitol, 10 mM EDTA, 10 µM sodium-phosphate buffer pH 7.2) and 5 µL of zymolase (10 mg/mL). The mix was incubated at 37 °C for 12 minutes, and 400 µL of dissection buffer were added to terminate the digestion. In the waiting time, two parallel lines were cut in the centre of a levelled YPD plate, separated by approximately one centimetre, with a sterile scalpel. 6 to 8 µL of the digest were poured forming a line parallel to the cuts, avoiding touching the agar (Figure 2.1-7 A). The plate was left to dry for ten minutes or until the digestion solution was absorbed by the plate. Then the tetrads were dissected using an inverted microscope with a glass needle. A tetrad was taken with the needle from the central channel and carefully dropped at the edge, it was poked until one of the spores

separated and the other three were moved one position closer to the channel, dropped there, and the actions were repeated until all four spores were split forming a line on the plate. Then, the needle was cleaned by punching through the agar a few times before dissecting the next tetrad. When the plate was full, the central channel was taken away so the yeast there would not overgrow and spread on the plate, and the yeast were incubated at 30°C for at least three days, until the spores grew (Figure 2.1-7 B). Only the tetrads in which all the four spores grew were used.

For each cross, a F12 formed by 96 descendants coming from 24 tetrads was generated.

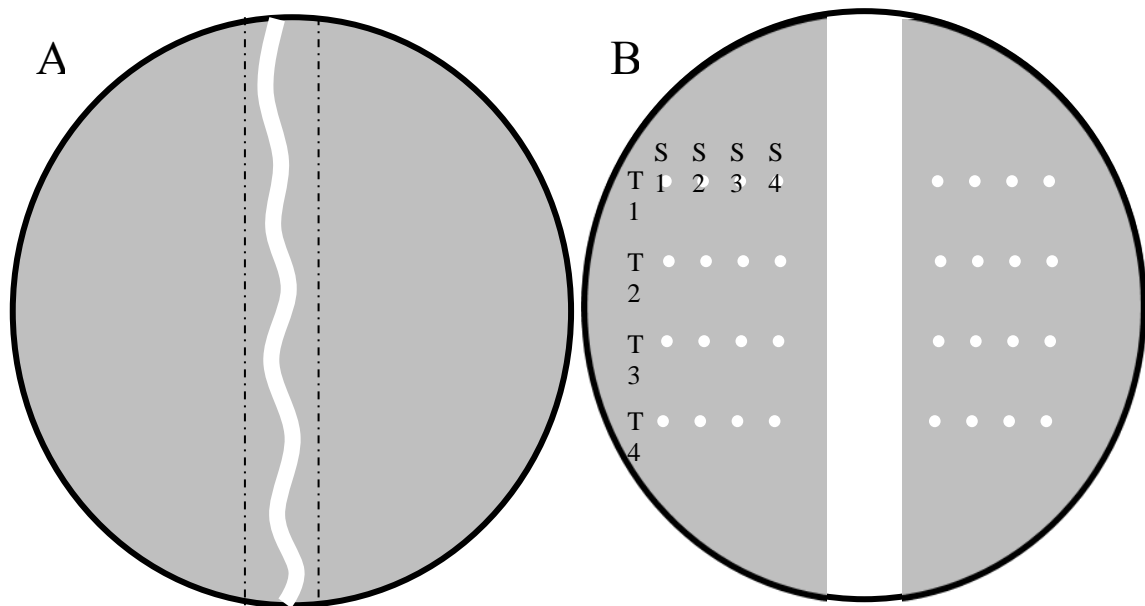


Figure 2.1-7. Dissection YPD plates

A) The position of the cuts is indicated by dashed lines and the location where the yeast should be positioned before the tetrad dissection is performed. **B)** A representation of the plate after three days of incubation, when the central channel has been removed and the spores (S) of each tetrad (T) have grown.

2.1.5.3. Mating type test

A plate with several separate spots of yeast with an unknown mating type was replica plated in two YPD plates. Later, a plate with a lawn of a known α -mator was replica plated on top of one of the YPD plates, and a plate with an α -mator on the other. They were allowed to grow at 30 °C overnight before replica plating them to

minimal media and grown for one or two days at 30 °C. The yeasts that grew were the opposite mating type that the mator of that plate.

2.1.6. Genotyping yeast strains

2.1.6.1. Genomic DNA extraction

As before, the genomic DNA of the yeast was extracted using the E.Z.N.A. Yeast DNA extraction kit (OMEGA bio-Tek #D3370) according to the manufacturer's instructions. YPD media was inoculated with a yeast colony and grown overnight at 30 °C while shaking. The yeasts were treated with β-mercaptoethanol and lyticase to break the cell walls and denaturalize the proteins, lysed with glass beads, treated with Proteinase K and then with RNase A, washed with ethanol and finally passed through a column to obtain pure genomic DNA.

2.1.6.2. DNA quantification

The DNA quantification was performed with the QuantiFluor dsDNA system (Promega #E2671) following the manufacturer's instructions. First, a 1x TE dilution was made and 50 µL of QuantiFluor dye were added per 20 mL. A standard curve was generated using the provided λ DNA (100 µg/µL). The curve started in 200 µg and it was formed by serial 1 in 4 dilutions (50, 12.5, 3.1, 0.78, 0.2, 0.05 µg/ µL). In the end, 200 µL of the diluted dye were added to each well, and 1 µL of the samples and 2 µL of the standards were loaded in duplicate on the black 96-well fluorescent plate. Lastly, the plate was run on a plate reader setting the emission at 520 nm and the excitation at 485 nm, and the concentration of DNA was calculated.

The purity of the DNA was determined using a Nanodrop. The samples were required to have a 260/280 absorbance ratio between 1.8 and 2.0 and 260/230 ratio between 1.8 and 2.4, indicating that there was no protein or salt contamination.

2.1.6.3. Sequencing

The DNA samples were sent to the Earlham Institute for whole-genome Illumina sequencing. FastQC reports were created for each sample to evaluate the quality of the sequencing (base sequence quality, read depth and GC content and level of sequence duplication). The FASTQ sequencing files were aligned to the *S. cerevisiae* reference strain genome S288C.

2.1.7. Bioinformatics

2.1.7.1. QTL analysis

Shmootl script was based on an R/qtl interval mapping developed for QTL interval analysis that contained the necessary pipelines to perform the QTL analysis in yeast (Broman, 2003; Broman, 2015). This software was optimized for analysing yeast populations by the bioinformatician Dr Yue Hu (2020) and other developers at the GitHub site (<https://github.com/gact/shmootl>). Shmootl is based on the R scan-one tool, which scanned one marker at a time and therefore did not provide information about interactions between genes.

To perform the QTL analysis, the whole genome sequences of the F12 populations were aligned with the reference genome of the S288C strain for variant calling. The linkage between the polymorphisms present in each strain and its growth characteristics during the PHENOS assay was studied via the logarithm of the odds (LOD), which estimated the probability of the markers to be responsible for that particular phenotype -for example, a LOD of 2 meant that the polymorphism was 100 times more likely to be responsible for the phenotype than not-. The threshold value of the LOD for the population was calculated following the method of Churchill & Doerge (1994). First, each dataset was permuted 1000 times to remove the association between the trait value and the polymorphisms of that individual. This

was done by changing the trait value of an individual to another one with a different genetic background, in order to generate a population that considered the genetic variability present in all the samples but in which there was no association between the genetic markers of the QTL and the phenotype. After the permutations, the critical value was calculated with this formula: $100(1 - \alpha)$, in which α is the false discovery rate (FDR). Finally, the QTL effect of the permuted data were ordered by their value, and the critical value was used to calculate the percentile -the FDR was set at 0.05, so the percentile during these experiments was 95-. The LOD value of the sample corresponding to the 95 percentile was selected as the experiment-wise threshold. The polymorphisms with a LOD significantly higher than the threshold were considered as possible QTL.

The file provided by PHENOS included the comparison between the control and the disease transformants for the three main phenotypes (maximum speed, lag, and maximum growth), however, since the differences were mainly seen in the maximum growth, the linkage study was performed based on that phenotype.

2.1.7.2. Study of the interactome and the pathways enriched in the QTL

The interaction networks and KEGG pathway enrichment analysis of the genes that were in each QTL interval were performed using the online tools STRING (<https://string-db.org/>) and DAVID 6.8 (<https://david.ncifcrf.gov/>) respectively. These analyses were performed with the human orthologues of the genes and only included those that had only one human orthologue. The analysis included the results from the three crosses but was done separately for the mHTT and the α Syn QTL.

The analysis done with String showed the physical and functional associations between the query proteins, the confidence of the analysis was set at the highest possible (0.9), and the evidence used was obtained through experiments and

databases. The only genes included in the network figures were those that were connected to at least another gene from the list. Lastly, the colouring of the nodes was used to highlight the KEGG pathways that were enriched in both the String and the DAVID analysis.

The DAVID software was used to study if there was an enrichment in genes involved in specific pathways. The analysis was performed with the standard parameters count (minimum number of genes) of two, EASE (maximum score for the enrichment analysis) of 0.05, and Benjamini correction.

2.1.7.3. Other bioinformatic tools

The reported function of the genes and the existence of fly and human orthologues were screened using the Saccharomyces Genome Database (SGD) YeastMine (<https://yeastmine.yeastgenome.org/yeastmine/bag.do>).

The function and the expression of those genes in the brains of flies were examined using FlyBase (<http://flybase.org/>). And the involvement of the human orthologues with pathologies was screened using Alliance of Genome Resources (<https://www.alliancegenome.org/>) and National Centre for Biotechnology Information (NCBI. <https://www.ncbi.nlm.nih.gov/>).

2.2. *Drosophila melanogaster*

2.2.1. Fly lines

All the fruit fly lines were obtained from the Vienna and Bloomington stock centres or were crossed with other lines to obtain the desired genotypes (Table 2.2-1).

Table 2.2-1. Fly lines

Name	Genotype	Location	Provider ID
HTTEx1	w; UAS-HTT _{EX1} 25Q; +	2R:15054298	BDSC #68408
mHTT Ex1	w; UAS-HTT _{EX1} 120Q; +	2R:15054298	BDSC #68414
mHTT 108	w; UAS-HTT ₁₀₈ 120Q; +	2R:15054298	BDSC #68430
Strat	w; UAS-Strat RNAi; +	2L:22019296	VDRC #105730
eIF6	w; UAS-eIF6 RNAi; +	2L:22019296	VDRC #108094
DPCoAC	w; UAS-DPCoAC RNAi; +	2L:22019296	VDRC #101378
3M	w; pKC26(+); +	2L:22019296	VDRC #60100
elav	w elav-GAL4; +; +	X:523350	BDSC #458
3M-HTT	w; UAS-3M, UAS-HTT _{EX1} 25Q; +	2L:22019296 2R:15054298	Giorgini Lab
3M-mHTT	w; UAS-3M, UAS-HTT _{EX1} 120Q; +	2L:22019296 2R:15054298	Giorgini Lab
Strat-mHTT	w; UAS-Strat, UAS-HTT _{EX1} 120Q; +	2L:22019296 2R:15054298	Giorgini Lab
eIF6-mHTT	w; UAS-eIF6, UAS-HTT _{EX1} 120Q; +	2L:22019296 2R:15054298	Giorgini Lab

HD was modelled using three fly lines described by Barbaro et al. (2015) with different naturally occurring human *HTT* fragments integrated into the same region of the right arm of the second chr. These *HTT* fragments are under the control of 5 *UAS* elements and consist of: the first exon with a 25Q tail, the first exon with a 120Q tail, and the first 108 amino acids with a 120Q tail.

The downregulation lines of the possible HD modifier genes (*eIF6*, *Strat* and *DPCoAC*) were part of the phiC31 RNAi library (KK), which used the phiC31 integrase system to insert the constructs into the VIE-260B landing site, on the left arm of the second chr (Keleman et al., 2009). The inserted transgenes consisted of inverted repeats of the gene -short hairpin RNA (shRNA)-. The control line for the lines of the RNAi library, *3M*, contained the empty VDRC pKC26 cloning vector inserted as well at the VIE-260B landing site.

2.2.2. Maintenance of fruit flies

Fruit flies are kept in transparent plastic tubes closed with cotton flugs, with 5 mL of maize-based medium at the bottom (Table 2.2-2). The flies were kept in temperature and light controlled rooms. The lights were set on a 12-hour day / 12-hour night cycle, and the temperature was 18 °C in the stock room and 25 °C in the experimental room. Stock flies were kept in the same tubes for a maximum of four weeks, while the experimental flies and the ones that were being expanded were changed to new food once or twice a week.

Table 2.2-2. Fly food recipe

Component	Amount	Company (ID)
Maize meal	72 g	SLS #FLY1076
Glucose	79.3 g	Fisher #10385940
Brewer's yeast	50 g	MP Biomedicals #903312
Agar	8.5 g	BIO GENE #400-050
Propionic acid	3 mL	Fisher #10193190
20% nipagin in ethanol	10 mL	SLS #H5501
H ₂ O	1 L	

2.2.3. Fly crosses

The conditions for the fly crosses were always the same. Female virgin flies from one genotype were crossed with males from a different one and they were kept in a room at 25 °C, with 12 hours of light and 12 hours of darkness, for seven days before removing the parents from the tube so they would not be mistaken with the descendants. The descendants began to hatch at day ten and were collected for only nine days to avoid collecting flies that came out of the cross between the descendants.

The crosses between the *elav-GAL4* and the *UAS-YFG* lines to obtain the experimental flies were always performed with the same number of flies in order to

keep the experiments consistent - ten tubes with four female virgin *UAS-YFG* flies were crossed with four *elav-GAL4* male flies for each genotype.

2.2.3.1. Cross to express HTT in neurons

The three different lines of homozygous female virgin flies carrying *UAS-HTT* on the second chr (*HTT Ex1*, *mHTT Ex1*, and *mHTT 108*) were crossed to male flies carrying *elav-GAL4* on the X chr. Female virgin descendants from each cross were collected and used for the experiments since they had one copy of *UAS-HTT* and also one copy of *elav-GAL4*, completing the *GAL4/UAS* system (Figure 2.2-1). Since male flies inherited the Y chr from their parents, they did not inherit the *elav-GAL4*, which meant that they were not expressing *HTT*, so they were used as a control for the viability assay (Figure 1.3-1 B).

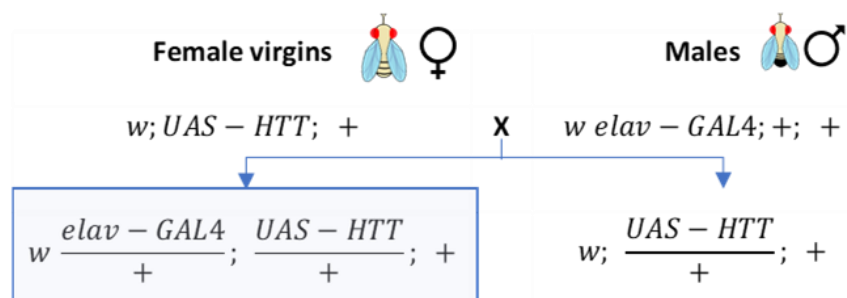


Figure 2.2-1. Crossing scheme to obtain flies that express the HTT constructs in neurons

Female virgin flies from the *HTT* lines (*HTT Ex1*, *mHTT Ex1*, and *mHTT 108*) were crossed with males carrying *elav-GAL4* to obtain a progeny that expressed both the *HTT* in neurons. Female virgins from the last cross (blue square) were used to perform the experiments.

2.2.3.2. Cross to downregulate the expression of the modifier genes in neurons

Homozygous female virgin flies from the three *UAS-RNAi* lines (*Strat*, *eIF6* and *DPCoAC*) plus the empty vector control (3M) were collected and crossed with *elav-GAL4* males (Figure 2.2-2). Similar to the *HTT* cross, only the female descendants from these crosses carry both transgenes, so they were used as experimental flies while the males were used as the control for the viability assay. The phenotypes seen on the *elav-GAL4; 3M* flies were used as a control for all the experiments.

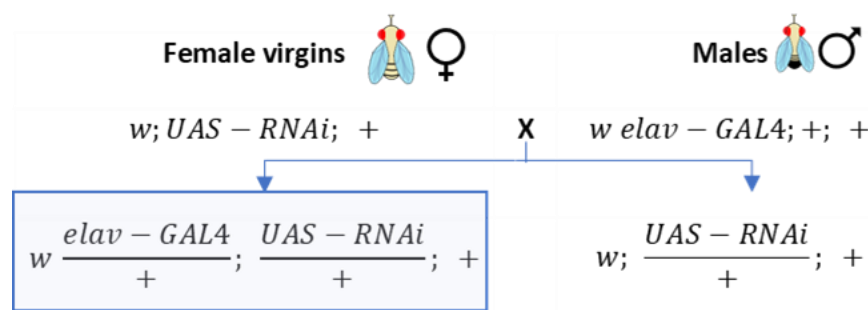


Figure 2.2-2. Crossing scheme to obtain flies that express the different *RNAi* in neurons

Female virgin flies from the *RNAi* lines (*Strat-RNAi*, *eIF6-RNAi*, and *DPCoAC-RNAi*) and the control 3M line were crossed with males carrying *elav-GAL4* to obtain a progeny in which the females expressed the *RNAi* in neurons. Female virgins from the cross (blue square) were used to perform the experiments.

2.2.3.3. Cross to express HTT and downregulate the modifiers in neurons

Four crosses were needed to obtain experimental flies that expressed *mHTT Ex1* and the shRNA that downregulated the expression of the modifier genes (*Strat* and *eIF6*) in neurons (Figure 2.2-3). As a control, the 3M line was crossed with both *HTT Ex1* and *mHTT Ex1* following the same crossing scheme.

The first step was to cross the *RNAi* with the *HTT UAS* lines. From those crosses, heterozygous female virgin flies carrying both transgenes were collected and crossed with *Cy0*, the second chr balancer line, that prevented further recombination and carried a dominant curly wing marker. Females and males with curly wings were

collected and crossed, separating each pair in a tube. After seven days, the parents were collected, their DNA was extracted, and a PCR was performed to determine if they carried both *UAS* transgenes. From the crosses in which both parents were recombinants, the female descendants without curly wings were homozygous for both *UAS* constructs and thus, those flies were crossed to the *elav-GAL4* males to generate the experimental flies that were heterozygous for *elav-GAL4* in the X chr and for *UAS-RNAi*, *UAS-HTT* in the second.

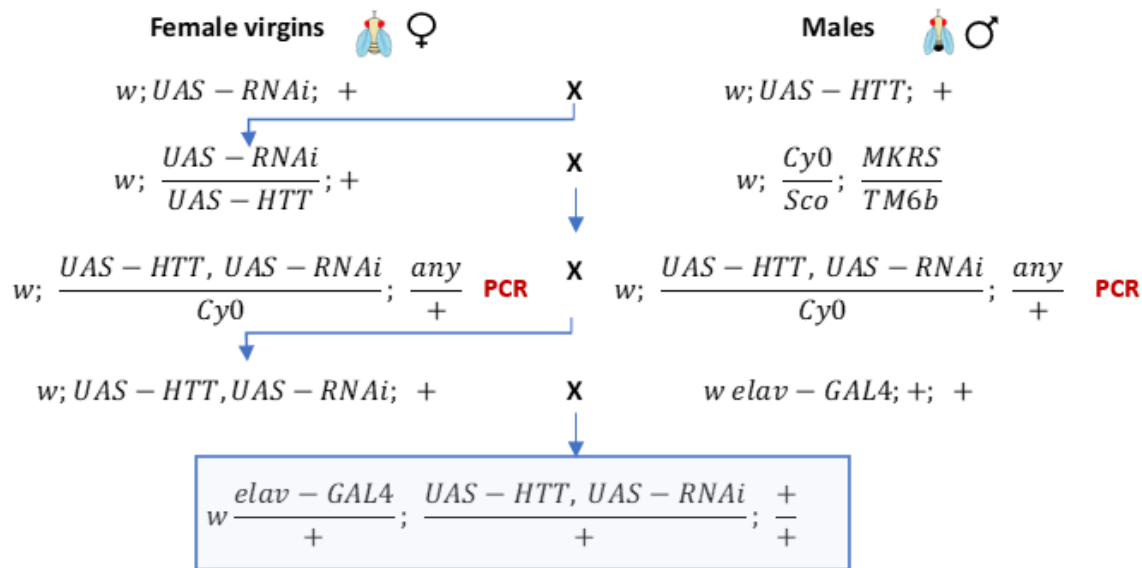


Figure 2.2-3. Crossing scheme to obtain the flies that express both the RNAi construct and HTT in the neurons

Female virgin flies from the two RNAi lines (*Strat* and *eIF6*) and from the 3M control line carrying the empty vector were crossed to the *mHTT* line. The 3M control line was also crossed with the control *HTT*. The descendants from the cross were balanced and crossed together to obtain homozygotes with both the RNAi and the *HTT*. After PCR-based genotyping, they were crossed with males carrying *elav-GAL4* to obtain progeny that expressed both the shRNA and *HTT* in neurons. Female virgins from the last cross (blue square) were used to perform the experiments.

2.2.3.3.1. Genotyping of the HTT and modifier recombinants

In order to genotype the flies, they were knocked out using CO₂ and each fly was transferred to a separate tube that was placed on ice to keep the fly slept. 50 µL of ice-cold squishing buffer and 1 µL of proteinase K (10 mg/mL) were added to each sample. The squishing buffer was made of 9.8 mL of dH₂O, 100 µL of 1 M Tris (pH

8), 20 µL of 0.5 M EDTA, and 50 µL of 5 M NaCl. The flies were squished with the help of a plastic tip and incubated at 37 °C for 30 minutes followed by two minutes at 95 °C to inactivate the proteinase K. The tubes were centrifuged to send the debris to the bottom, and the supernatant was transferred to a clean tube. The fly DNA extract was stored at -20 °C until used for the PCR.

The PCR for the amplification of the *3M* empty vector, and the *eIF6* and *Strat* shRNAs was performed with the PCR Bio Classic Taq polymerase following the manufacturer's instructions (5 µL buffer, 1 µL dNTPs, 2 µL each primer, 5 µL fly DNA, 1 µL Taq, 34 dH₂O). The thermocycler was set to denaturalize the DNA at 95 °C for 1 minute and then cycle 30 times denaturalizing at 95 °C for 30 seconds, annealing at the Ta mentioned in Table 2.2-3 for 30 seconds and amplifying at 72 °C for 90 seconds, followed by a final 10-minute amplification.

Table 2.2-3. Primers for genotyping the recombinant flies

Gene	Primer sequence	Ta (with UAS)
<i>UAS</i>	ACCACTGCTCCCATTCA	N/A
<i>HTT</i>	CCCTGGAAAAGCTGATGAAG	60 °C
<i>eIF6</i>	TCTGGCAGGCTGTTACGCAGGTG	63 °C
<i>Strat</i>	ACCATGATCTGAGCACCCGCCAC	63 °C
<i>3M</i>	TGTAAAACGACGGCCAGT	55 °C

However, *HTT* was amplified using that polymerase but with a buffer made in the laboratory: 501 µL of 2M Tris HCl (pH 8.8), 249 µL of 1M ammonium sulphate, 100.5 µL of 1M MgCl₂, 10.8 µL of β-mercaptoethanol, 10.2 µL of 10 mM EDTA (pH 8), 225 µL of each of the dNTPs (100 mM), 51 µL of BSA (50 mg/mL) and 204 µL of dH₂O.

The PCR master mix for the HTT gene had 1.8 µL buffer, 0.4 µL each primer, 0.4 µL Taq, 0.25 µL 1M Tris HCl, 5 µL fly DNA, and 11.75 µL dH₂O. The thermocycler was set to denaturalize the protein at 95 °C for 30 seconds, cycle 30 times (10 seconds denaturalization at 95 °C, 30 seconds annealing at 60 °C, 90 seconds extension at 72 °C), followed by 10 minutes of extension at 72 °C.

All the PCRs were performed using a forward primer specific for the construct (*HTT*, *3M*, *eIF6* or *Strat*) and the reverse primer of the *UAS* region.

2.2.4. Phenotyping of flies

2.2.4.1. Viability assay

The viability assay began by setting up a ten-tube cross, each of them with four *elav-GAL4* male flies and four *UAS-YFG* female virgin flies. The parental flies were kept at 25 °C for seven days before removing them from the tubes. The tubes were kept at the same temperature and the pupae began to hatch three days later. The number of flies of each sex that hatched from each tube was counted every day for nine days, and all the female virgin flies were collected and later used for the other phenotyping experiments.

The data analysis was performed using GraphPad Prism 7. The percentage of female flies from each tube was calculated and used to calculate the average percentage of female flies of each genotype. The differences between genotypes were studied by performing a one-way ANOVA corrected by Tukey's multiple comparisons test.

2.2.4.2. Survival assay

The survival experiments used female virgin flies. Ten tubes with ten flies each were set up for each genotype. All the flies were kept at 25 °C and were changed to new food twice a week without using CO₂ to immobilise them. The number of flies that were alive was counted from the day they emerged (day 0) until the day all the flies died. When YFG was highly toxic, the number of flies was counted daily, while for milder phenotypes, it was counted twice a week.

The data analysis was performed using GraphPad Prism 7. The Mantel-Cox test (also known as log-rank) was performed to determine if there was a difference in the survival curves of the overall populations.

2.2.4.3. Pseudopupil assay

The pseudopupil assay was performed to score the number of rhabdomeres per ommatidium in female virgin flies of the same age. Before the experiment, flies were kept in tubes with food at 25 °C and pushed to fresh food twice a week until they reached the desired age. On the day of the experiment, the flies were immobilised with CO₂, the heads were cut, mounted on a glass slide with nail polish -carefully placing them to avoid touching the eyes-, and observed at 50x magnification using the ECLIPSE Ci-L microscope (KODAK), and representative images were taken with the NIS-Elements L camera control software. For each fly, the number of rhabdomeres was counted in at least 50 ommatidia. The sample size of each genotype and time point varies slightly due to the death of the flies while being aged.

The data analysis was performed using GraphPad Prism 7. First, the average number of rhabdomere per ommatidia was calculated for each fly. Then, the average per genotype at each time point was calculated. Finally, a two-way ANOVA corrected by Tukey's multiple comparisons test was performed to compare the differences between genotypes at each time point.

The percentage of neuroprotection of the flies able to rescue the mHTT phenotype was calculated following this formula:

$$\% \text{ Neuroprotection} = \frac{\text{Total amount of neurodegeneration}}{\text{Rescue}} \times 100$$

In which 'Total amount of neurodegeneration' is the result of subtracting the rhabdomere number in the 3M-mHTT flies from the rhabdomere number in the 3M-HTT control flies (thus the average number of rhabdomeres lost), and 'Rescue' is the

subtraction of the rhabdomere number from the *3M-mHTT* flies from the rhabdomere number of the *RNAi-mHTT* (average number of rhabdomeres gained from rescue).

2.2.4.4. Locomotor activity assay

Female virgin flies that had not been anaesthetized in the last 24 hours at least were used for the experiments. More than 50 flies of each genotype were evaluated with the counter current climbing apparatus on days three and ten. First, a group of 10 to 20 flies was loaded in tube 0, the tube was connected to the apparatus, and the flies were given five minutes to acclimatize (Figure 2.2-4). Then, the apparatus was tapped three times to send the flies to the bottom of the tube, set still on the table for ten seconds so the flies could climb, and then the top part was slid to the right to separate the flies that climbed from those that did not. Lastly, the flies were tapped down, the top part went back to its original position, and the flies were allowed to climb for ten seconds again. This process was repeated for a total of five climbing trials. In the end, the number of flies on each tube was counted (Andreazza et al., 2019; Benzer, 1967).

After all the flies were evaluated, a score was given to each tube - tube 0 was 0% climbing, 1 was 20%, 2 was 40%, until 5 which was 100% climbing (Andreazza et al., 2019). GraphPad Prism 7 was used to calculate the average climbing performance of each genotype each day, and a two-way ANOVA corrected by Tukey's multiple comparisons test was performed to compare the differences between genotypes at each time point.

The experiments were performed at the same time of the day, at least one hour after lights were switched on, and the apparatus was cleaned between experiments to minimize the effect of external variables.

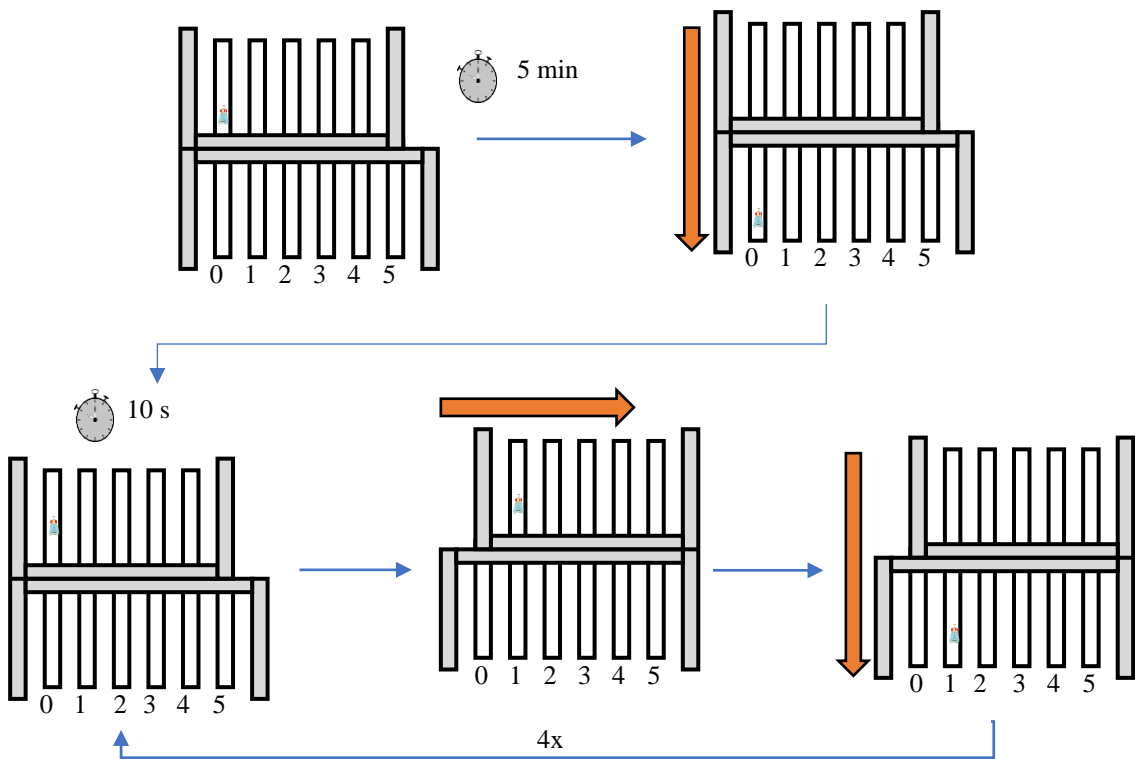


Figure 2.2-4. Counter current climbing apparatus protocol

Flies are loaded in tube 0 and let to acclimate for five minutes. Then, they are tapped to the bottom of the tube and allowed ten seconds to climb. The top part of the apparatus slides to the right, passing all the flies that climbed above the threshold to the next tube. The flies are tapped down again, the top part slides back to its original position, and the flies are allowed to climb again. This process is repeated for a total of five climbing trials.

3. Selection of parental strains for QTL analysis

The aim of this thesis is to find the genetic modifiers responsible for the variability in HD and PD, by performing a QTL analysis in yeast. Large, genetically diverse populations are necessary for the QTL analysis since these studies are based on LD and many recombination events are required to break the linkage groups into small regions so that each marker highlights only a few genes (Londin et al., 2013; Plomin et al., 2009; Visscher et al., 2012). Hence, the first step was to select the parental strains that would be crossed to generate the aforementioned population. Therefore, in this chapter we assessed the effect of mHTT and α Syn on 14 natural yeast isolates containing most of the genetic variation of the species by assessing their growth by using PHENOS, their survival via spotting assay, and the distribution of the toxic proteins inside the cells using fluorescence microscopy.

3.1. Results

Fourteen *S. cerevisiae* strains from our natural yeast library were assessed in this experiment (Table 2.1-1). In order to choose the most appropriate parental strains for the population of the QTL analysis, the selection criteria for the parental strains were the ability to grow using galactose as carbon source, the possibility to delete key auxotrophic genes to allow for plasmid selection (*URA3*, *LEU2* and *LYS2*), and the presence of an extreme phenotype when expressing mHTT and α Syn.

3.1.1. Selection of strains able to use galactose as a source of carbon

Firstly, strains able to grow using galactose as source of carbon (GAL+) were necessary. Since all the *HTT* and *SNCA* plasmids were under the control of the *GAL1*

promoter for expression, strains with strongly impaired growth on galactose would be of no use for these experiments.

To determine which of our strains were GAL+, spotting assays were performed to assess the viability of yeast by plating drops of serial dilutions in two types of media (YPD and YPGal) and determining if there was any difference between them in the number of colonies present. Yeast were grown on YPD - a complete media for yeast

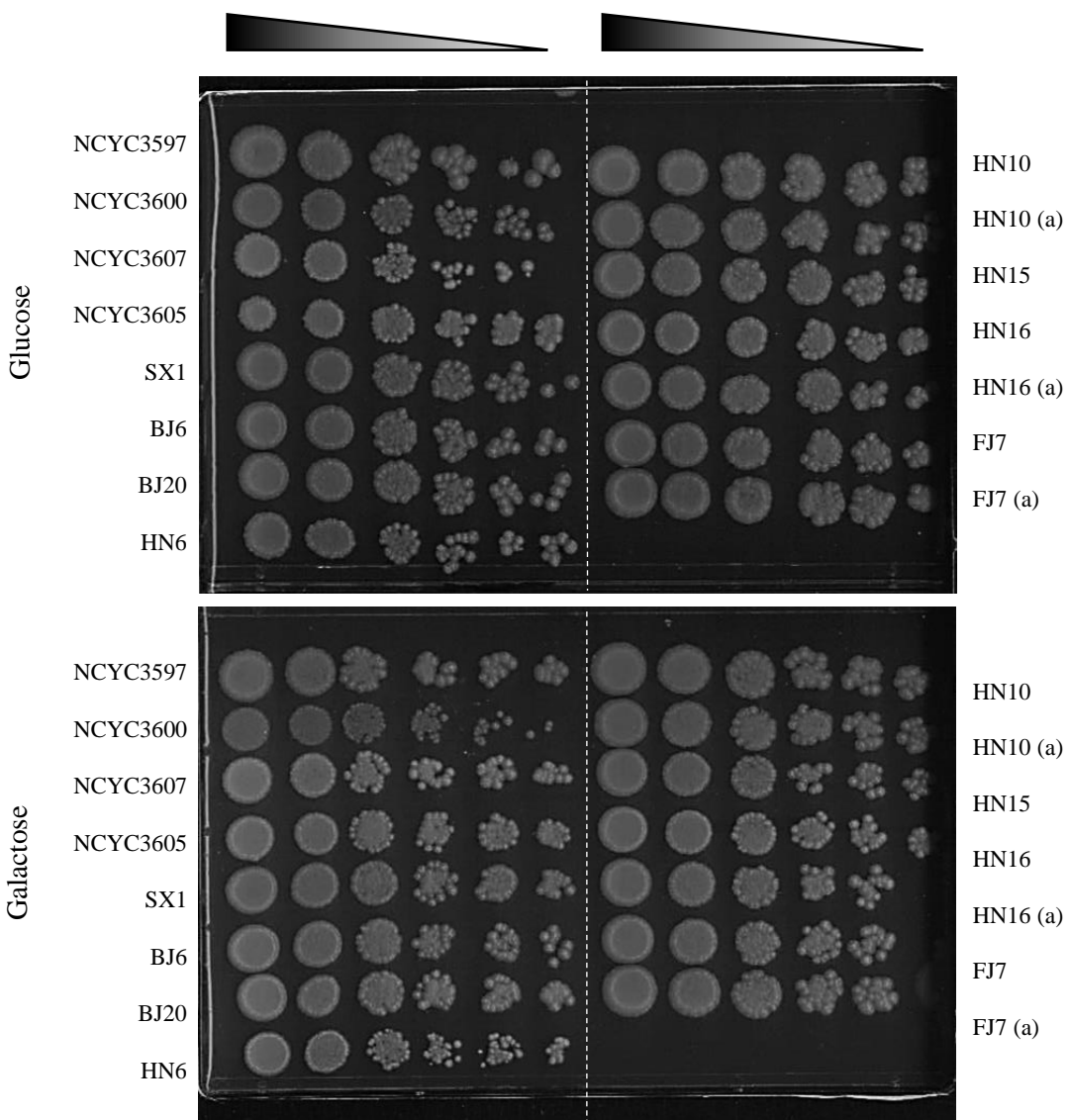


Figure 3.1-1. Not all yeast strains have the ability to use galactose as source of carbon.

Spotting assay of the yeast natural isolates after three days of growth on YPD (top) and YPGal media (bottom). Serial dilutions of each strain were grown from higher (left) to lower concentration (right). For those strains of which both mating types were available, a matters are marked as (a). A decrease in the size and number of colonies was seen in NYCY3600 when growing in media with galactose.

growth with 2% glucose - as the control plate and in YPGal - same composition but with 2% galactose instead of glucose - as the experimental plate. After a three-day incubation period, images were taken to compare the growth of the strains in both types of media. As can be seen in Figure 3.1-1, most of the strains grew well on both types of media. However, NCYC3600 had fewer and smaller colonies in galactose than in glucose in the three replicates and, although the difference was not so dramatic as to make the strain completely unusable, we decided to exclude it from the study since we had several other strains to choose from.

This experiment proved to be also useful to verify that there was no difference in growth between α and α maters of the same strain, since HN10, HN16 and FJ7 grew equally well in both glucose and galactose regardless of their mating type.

3.1.2. Deletion of *URA3* in the GAL+ strains

Secondly, in order to transform the GAL+ yeast with the plasmids, the deletion of *URA3* was necessary since that was the auxotrophic marker of all our plasmids. This was achieved by amplifying the deleted *URA3* sequence from a *ura3Δ0* strain by PCR, performing a LiAc transformation with the *ura3Δ0* DNA fragment and growing the cells in FoA selective media as explained in Chapter 2 (Figure 2.1-2 A).

To verify that the gene was properly deleted in the strains and that the growth of the colonies was unrelated to an unexpected resistance to FoA, the deletion of *URA3* was confirmed by amplifying the fragment by PCR with the same primers and running the PCR product on a 1% agarose electrophoresis gel. The results confirmed that all the colonies growing on FoA media were *ura3Δ0* due to the difference in size between the DNA fragments amplified from the deleted and WT gen (300 bp and 1.5k bp respectively).

3.1.3. Effect of mHTT expression in yeast

Thirdly, the effect of mHTT expression on growth, viability and cellular distribution of the protein was studied to determine the most interesting strains to use as parentals for the population that would be used during the QTL analysis. In order to do so, all *ura3Δ0* strains were transformed separately with the *HTT* plasmids using the same LiAc transformation protocol. After the transformation, cells were grown on SD -URA media to select those colonies that had been transformed, which were later used for the viability (spotting assay) and growth assays (PHENOS) as well as for the cellular distribution of HTT (confocal fluorescence microscopy and filter trap).

It is known that the 103Q tract in the *mHTT* construct is long enough to aggregate and induce toxicity in the presence of a FLAG-tag, however, there are no toxic effects related to the 25Q in the *HTT* construct, which makes it a reliable control for mHTT toxicity (Mason & Giorgini, 2011).

3.1.3.1. The effect of mHTT on viability is affected by the genotype

The effect mHTT had on the viability of the strains was evaluated by a spotting assay following the same protocol as before but changing the media to SD -URA galactose to induce the expression of the plasmid. SD -URA with glucose was used as a control for the accuracy of the dilutions. Besides, the laboratory strain BY4741 which has been previously characterized as sensitive to mHTT expression in several studies was used to establish that the plasmids were being expressed and the degree of viability of the strains (Mason & Giorgini, 2011; Meriin et al., 2002). Any strain with higher viability than BY4741 was considered resistant and with less viability was considered sensitive. As can be seen in the spotting assays in Figure 3.1-2, different strains exhibit different degrees of viability when expressing mHTT. On the one hand, there is no decrease in the growth of mHTT transformants in the

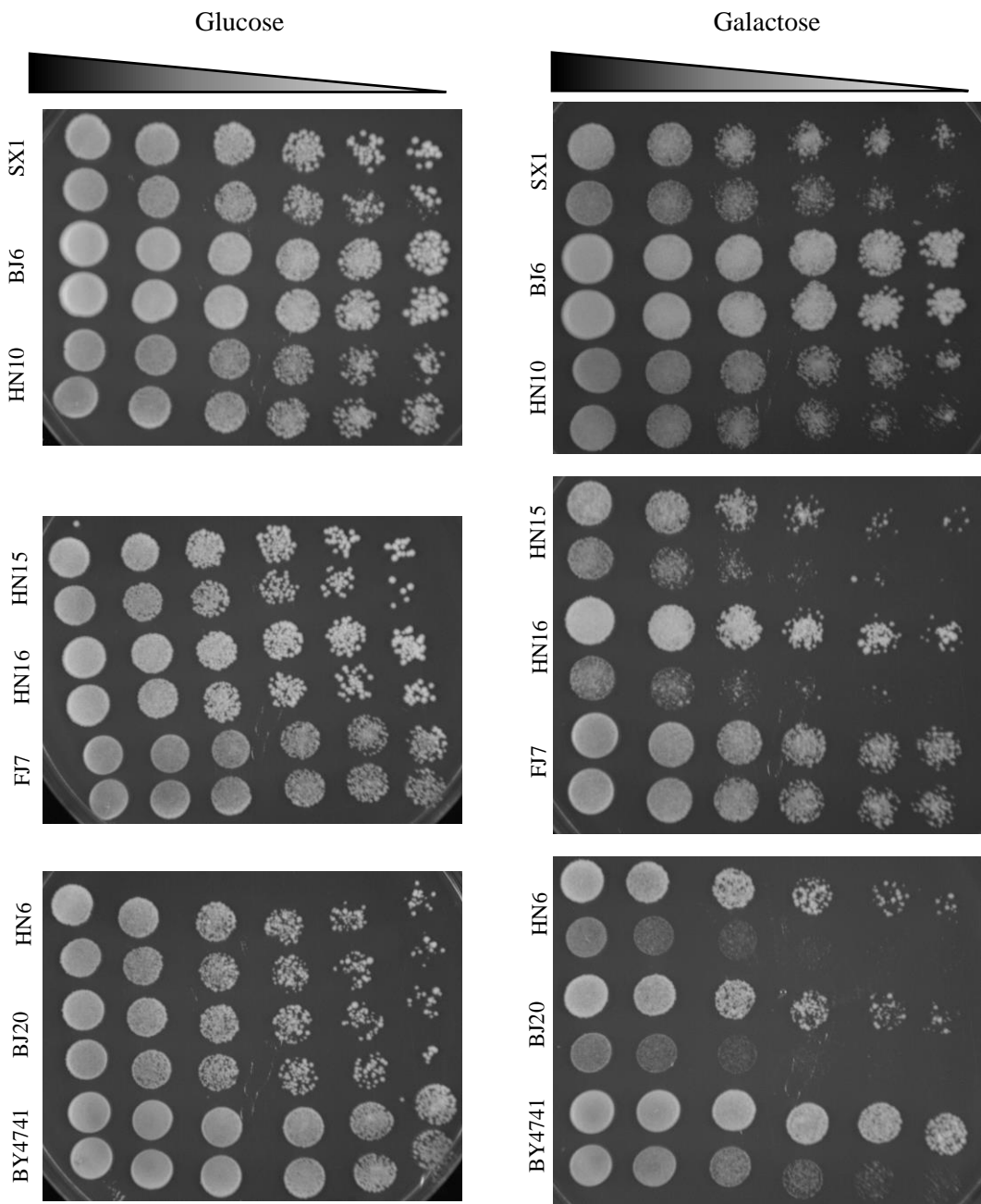


Figure 3.1-2. Yeast strains present a wide range of viability phenotypes while expressing mHTT.

Image of a spot assay in SD -URA media with glucose (left) or galactose (right) after three days of growth at 30°C of the HTT transformants (HTT top, mHTT bottom of each strain). There were no differences in viability between the HTT and mHTT transformants when expression was repressed by glucose. BY4741 is a laboratory strain sensitive to mHTT: higher viability than BY4741 was considered resistant and similar or lower was considered sensitive. Strains SX1, BJ6, HN10 and FJ7 showed slight to no decrease in the number of colonies when expressing mHTT, so they were considered resistant. While HN15, HN16, HN6 and BJ20's viability was lower than BY4741's, so they were classified as sensitive.

SX1, BJ6, HN10 and FJ7 strains, so they were considered resistant. On the other hand, HN15, HN16, HN6 and BJ20 showed a dramatic decrease in viability even when compared to the sensitive BY4741, being especially striking in the case of HN6 and BJ20.

3.1.3.2. The effect on growth of mHTT is affected by the genotype

The effect of mHTT toxicity on growth was evaluated using PHENOS, a high-throughput tool which facilitates QTL analysis using yeast by comparing the growth parameters of each strain in different conditions during an extended period. For this experiment, four replicas of each strain were grown on SD -URA media with galactose, at 30°C, for three days, inside a plate reader programmed to measure the OD600 of each sample every 20 minutes. Data obtained from the plate reader was analysed with PHENOS software and the graphs were plotted using GraphPad (Prism).

The *ura3Δ0* strains that were transformed with the *HTT* plasmids and used for the spotting assay were also assessed by using this method. Among all of them, SX1, HN6 and BJ20 showed the most promising phenotypes (Figure 3.1-3). SX1, one of the resistant strains according to the spotting assay, did not suffer growth impairment due to mHTT. In contrast, the two strains that had shown a dramatic decrease in their viability in the spotting assay (BJ20 and HN6) showed again a significant decrease in their growth - both in maximum growth (MG) and maximum slope (MS) -. Surprisingly, the control strain BY4741 showed only a slight decrease in MG while expressing mHTT, however, it was not significant. This could be explained by the growth speed of the strain. While taking images for the spotting assay, it was obvious that BY4741 grew faster than the rest of the strains. A faster growth rate and a milder reduction in the viability compared with the other sensitive strains allowed BY4741

to reach the stationary phase in three days so the difference in MG between HTT and mHTT transformants was not significant. However, looking at the MS, which indicates the growth speed, it can be seen that the mHTT transformant grows significantly slower.

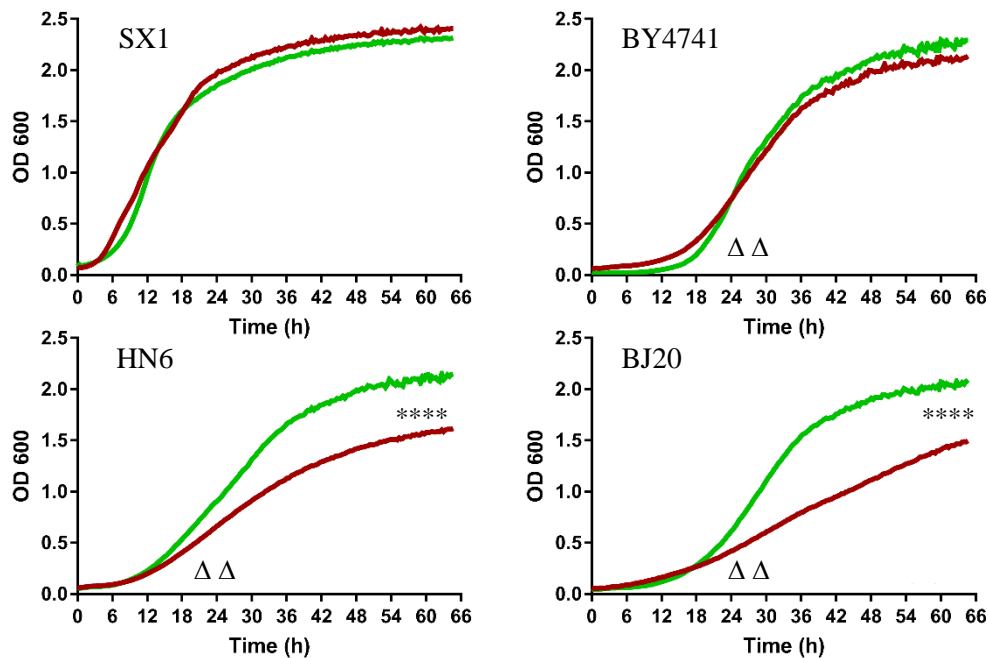


Figure 3.1-3. Differences in growth due to mHTT toxicity can be assessed using PHENOS.

Yeast were grown on a plate reader at 30°C for three days while measuring the growth (OD₆₀₀) every 20 minutes. Data from the plate reader was analysed using PHENOS. Differences in maximum growth between HTT (green) and mHTT (red) were seen in HN6 and BJ20, and in maximum slope in HN6, BJ20 and BY4741. Two-way ANOVA corrected by Tukey's multiple comparisons test. ** P < 0.01; **** P < 0.0001.

MG's significance is shown with stars (*) while MS' is shown with triangles (Δ).

3.1.3.3. Cellular distribution and kinetics of mHTT are affected by the genotype

It has been reported that mHTT has the ability to aggregate in patients' neurons and this phenotype is also present in yeast (Mason & Giorgini, 2011; Meriin et al., 2002). To determine if our yeast strains form inclusions, we used the GFP-tag of the

HTT protein to analyse how they behave in the different yeast strains by visualizing them using confocal fluorescence microscopy.

The expression of HTT was induced for 16 hours before fixing and visualizing the yeast with an Olympus FV1000 confocal microscope at 40x magnification. In each strain, the cellular distribution of HTT and mHTT were assessed and the number of cells with aggregates and the number of aggregates per cell were compared. For the aggregate quantification, approximately 100 yeast expressing HTT were analysed per sample, and each strain had three replicates, as explained in Chapter 2. Figure 3.1-4 A shows representative images of the cellular distribution of both HTT and mHTT thanks to the GFP-tag. HTT was dispersed through the cytoplasm while mHTT appeared in the form of small foci in all the strains regardless of them being sensitive (HN6 and BJ20) or resistant (SX1) to mHTT toxicity. Nevertheless, the percentage of cells with foci and the number of foci per cell varied widely between strains (Figure 3.1-4 B). SX1 had a significantly higher number of cells without foci compared to the other two ($P < 0.0001$) -although the image shows a high number of cells with foci since it was chosen to illustrate the number of aggregates per cell in the cells that presented foci so it could be compared between strains-. HN6 had a higher number of cells without foci than BJ20 ($P = 0.0168$), and a higher number of cells with only one or two foci than SX1 ($P < 0.0001$). BJ20 also had more cells with one or two foci than SX1 ($P < 0.0001$), and it had a higher number of cells with three or four foci compared to SX1 and HN6 ($P = 0.0465$ and 0.0028 respectively). There was no significant difference in the number of cells with more than four foci. These data show that the genetic background of the strains influences the aggregation pattern of mHTT.

In order to determine the nature of the foci, a filter trap assay was performed as explained in Chapter 2. In short, after inducing the synthesis of HTT for 16 hours, the

protein was extracted, quantified, diluted in different concentrations of detergent, and denaturalized by heat. After that, the same amount of protein was filtered through two different types of membranes separately. The NC membrane had small enough pores to trap all the protein, so it was used to assess the total amount of protein, whereas the CelAc membrane had bigger pores, so only aggregated protein stayed. Finally, the membranes were incubated with anti-FLAG antibodies to determine if HTT was present in the sample.

The presence of antibody signal in the CelAc membrane indicated that the foci in the microscopy images were aggregates since they couldn't be solubilized with a detergent. Surprisingly, the filter trap showed that mHTT formed aggregates in all the strains (Figure 3.1-4 C). This means that there were aggregates in our strains regardless of them being sensitive or resistant, contradicting what was previously described by Meriin *et al.* in 2002, whose study said that mHTT aggregation correlates with toxicity. However, it is true that our resistant strain had a higher percentage of cells without aggregates than both sensitive strains, but the characterization of more resistant and sensitive strains would be needed to determine if a higher percentage of cells without aggregates correlates with resistance.

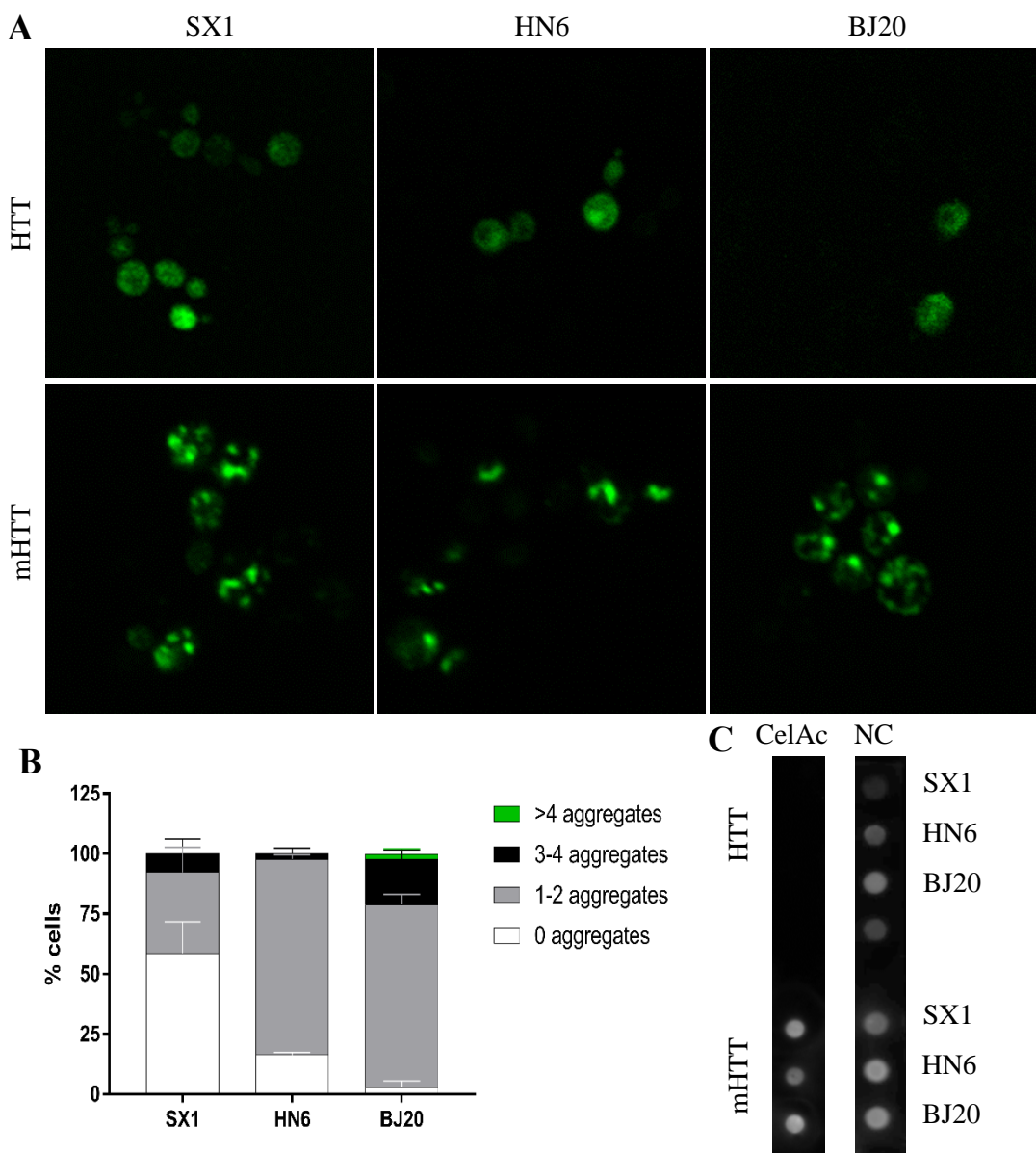


Figure 3.1-4. There are differences in the aggregation dynamics of the strains.

A) Confocal microscopy images taken after 16 hours of galactose induction. The HTT-GFP signal is dispersed in the cytoplasm of the cell while mHTT-GFP signal forms foci in all the strains. **B)** The quantification of the number of foci per cell in the mHTT transformants shows that it varies between strains, being SX1 the one with less cells with foci and BJ20 the one with more cells with foci and with more foci per cell. **C)** The nature of these foci was determined by filter trap performed in triplicate. Anti-FLAG signal was detected in the NC membrane in all the strains, confirming that they were expressing HTT and mHTT as expected. Furthermore, anti-FLAG signal was only detected in the mHTT transformants in the CelAc membrane, indicating that, while mHTT forms aggregates in all the strains, HTT forms them in none.

3.1.4. Effect of alpha-synuclein expression in the parental strains

The same procedure was followed for the yeast PD model in order to determine if the yeast strains showed similar phenotypes when expressing α Syn, since it is also known to appear in the form of aggregates (LBs) in patients' brains (Lewy, 1912; Tretiakoff, 1919).

Plasmids containing the WT *SNCA* gene or the gene with mutations responsible for familial PD (A53T and A30P) were employed. Since WT α Syn is toxic and aggregates in yeast, it was impossible to use it as control as was done in the HTT experiments. The empty vector pRS426 could have been enough, however, to ascertain that the phenotypes were caused by α Syn and not by the GFP-tag, it was decided to clone *GFP* into the empty vector and use it as a control.

As it was explained in Chapter 2, to clone *GFP* into the empty vector, primers complementary to the plasmid sequence flanking the gene were designed. These primers also had target sequences for the REs Spel and HindIII to be able to digest them and insert them in the same place *SNCA* was. After amplifying the gene with a high-fidelity polymerase, the PCR product was cloned into a pJET plasmid and transformed into bacteria to amplify it and to facilitate the digestion by the REs (Figure 3.1-5 A). Finally, *GFP* was cut out from pJET and ligated into the empty vector pRS426 (Figure 3.1-5 B). Confirmation of the ligation was performed by extracting the plasmid DNA from random colonies, digesting it with the previously mentioned enzymes and running it in a gel (Figure 3.1-5 C). All the *SNCA* plasmids as well as the *GFP* control were sent to be sequenced before the experiments began.

In order to determine the effect of α Syn, the *ura3Δ0* yeast were transformed with all the *SNCA* and the *GFP* control plasmids, and then analysed via spotting assay, PHENOS and fluorescence microscopy.

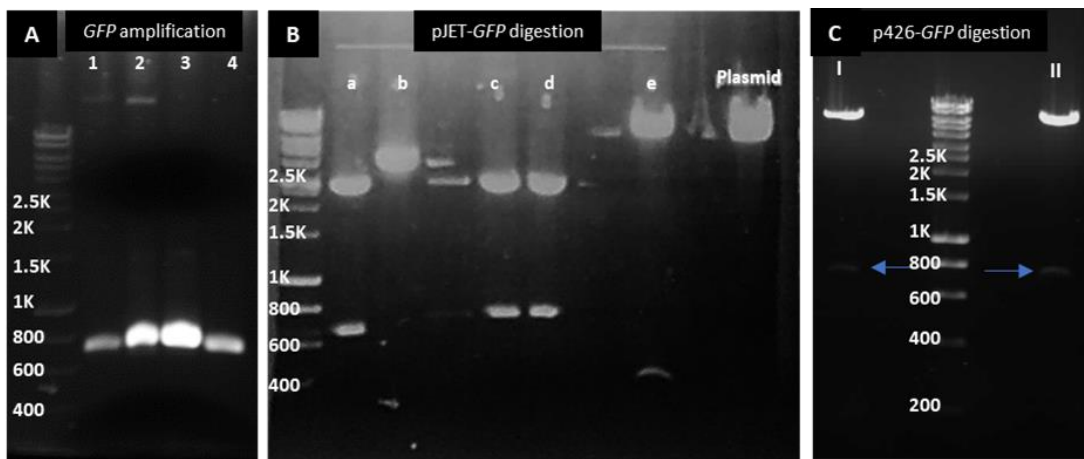


Figure 3.1-5. Agarose electrophoresis gels of the amplification and integration of GFP into pRS426.

A) Product of the high-fidelity PCR amplification of *GFP* from the WT SNCA plasmid. The ~720 bp band corresponds to *GFP* while the upper band corresponds to the plasmid template DNA. The ~720 bp band of lines **2** and **3** was cut from the gel, purified and ligated into the pJET plasmid. Recovery of *GFP* from pJET and linearization of pRS426 was performed with the restriction enzymes Spel and HindIII.
B) Digested pRS426 was ran to confirm linearization (Plasmid). The pJet-GFP digestion lines **a** and **e** show bands of an unexpected size while **b** does not present a band that could correspond with *GFP*. The expected ~720 bp band is present in lines **c** and **d**. DNA was purified from **c**, **d** and **plasmid**, *GFP* was sequenced and ligated into the linearized pRS426. The integration of *GFP* into pRS426 was confirmed by digestion with the same enzymes **C)** The two colonies that were checked had the expected ~720 bp band (arrows pointing at **I** and **II**). Images taken with GeneGnome XRC imaging system (Syngene).

3.1.4.1. The effect of αSyn on viability is affected by the genotype

The viability assay showed similar results to the one previously done with HTT, although there was greater variability among strains since the sensitivity to different types of αSyn changed between strains (Figure 3.1-6). As it was seen in HTT, BJ20 and HN6 that were sensitive to mHTT were also sensitive to WT and A53T αSyn, but resistant to A30P. The only strain that seems to be somewhat sensitive to A30P was HN15. On the other hand, SX1 appeared to be resistant although it showed some sensitivity to A53T. However, the SX1 WT αSyn transformant seemed to be overgrown on both glucose and galactose, so the experiment was repeated (Figure 3.1-7). Although SX1's resistance was confirmed, WT αSyn transformant grew at a

more normal rate, which could indicate that there was a problem with the original OD600 measurement of that sample.

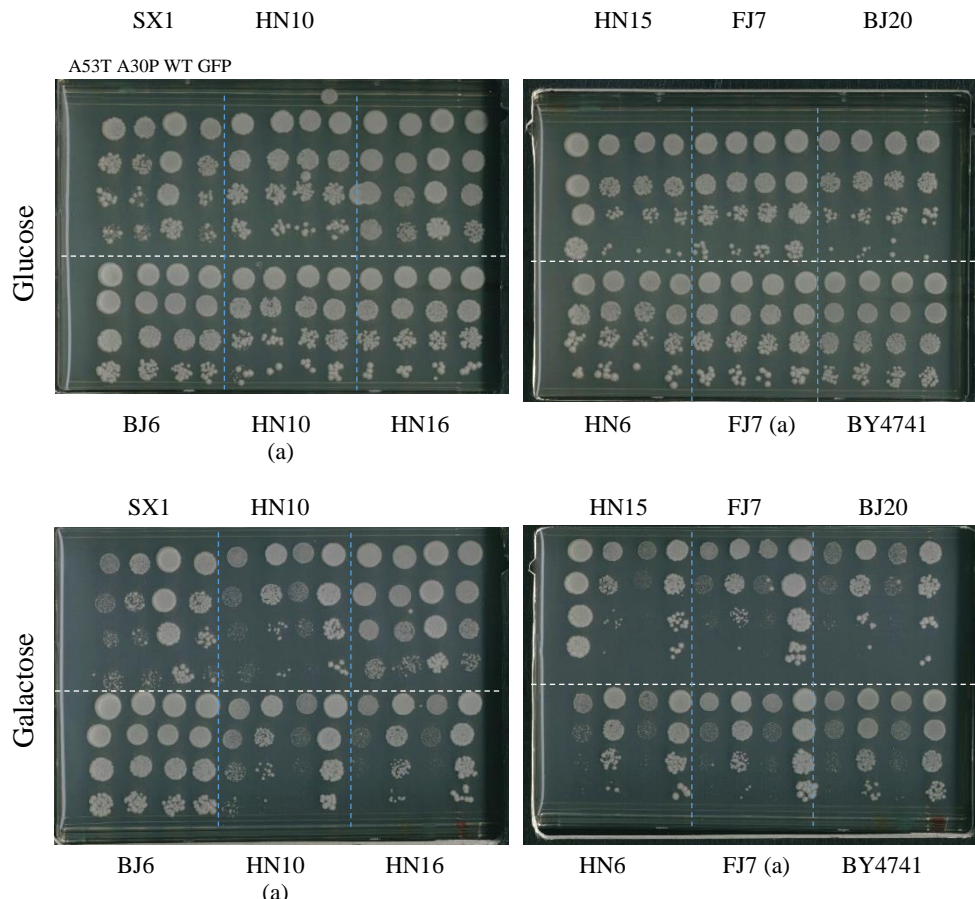


Figure 3.1-6. Yeast strains present a wide range of viability phenotypes while expressing αSyn.

Image of a spot assay in SD -URA media with glucose (top) or galactose (bottom) after three days of growth at 30°C of the SNCA transformants (from left to right of each transformant: A53T, A30P, WT, GFP). There were no differences in viability between the *GFP* and *SNCA* transformants when expression was repressed by glucose. BY4741 is a laboratory strain sensitive to αSyn: higher viability than BY4741 was considered resistant and lower was considered sensitive. Strain BJ6 showed slight to no decrease in the number of colonies when expressing any type of αSyn, so it was considered resistant. SX1 seemed to be resistant too, although there was some sensitivity to A53T. While HN15, HN16, HN6 and BJ20's viability was lower than BY4741's, so they were classified as sensitive.

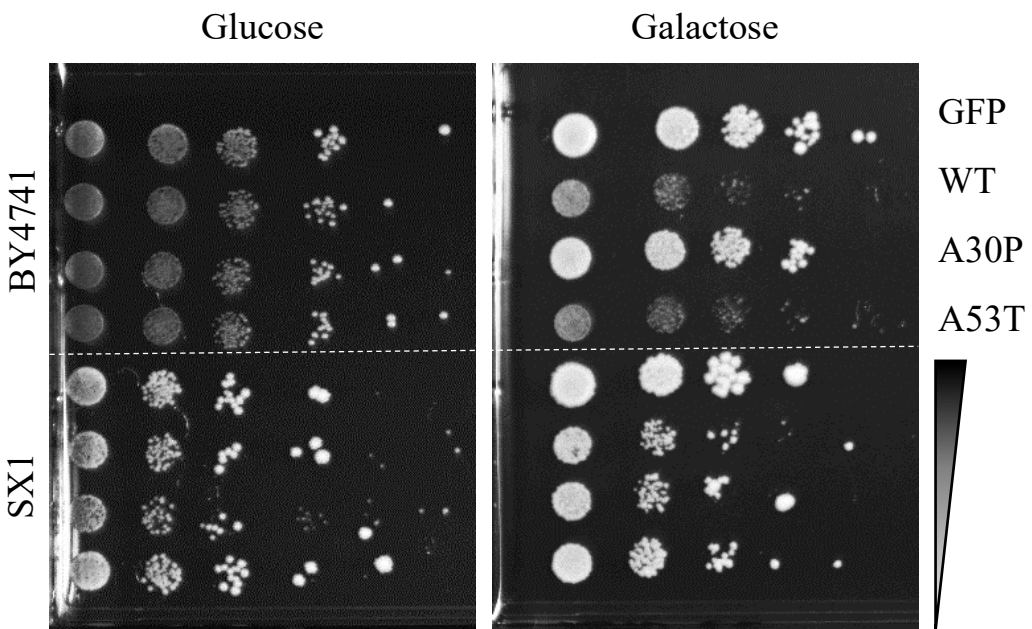


Figure 3.1-7. SX1 is resistant to αSyn expression.

Image of a spot assay in SD -URA media with glucose (left) or galactose (right) after three days of growth at 30°C of the SNCA transformants (from top to bottom of each transformant: GFP, WT αSyn, A30P, A53T). The laboratory strain BY4741 displayed a reduced viability of WT and A53T αSyn transformants. Similar to the previous experiment, SX1's viability was not notably reduced while expressing any of the SNCA constructs, and WT αSyn was not overgrown.

3.1.4.2. The effect on growth of αSyn is affected by the genotype

Following what was done for HTT, the PHENOS assay was used to determine the effect of αSyn expression on growth in all the strains (Figure 3.1-8). In accordance with the spotting assay results, MG was significantly reduced due to A53T and WT αSyn compared to the GFP control in BJ20 ($P < 0.0001$), while only WT αSyn caused a significant decrease in HN6 ($P < 0.0001$) and BY4741 ($P = 0.0011$). Surprisingly, the MG of WT αSyn was higher than the GFP in SX1, however, this difference was not significant. Unlike with the spotting assay, validation with fresh transformants showed the same increase in growth rate due to WT αSyn expression but it was never significant.

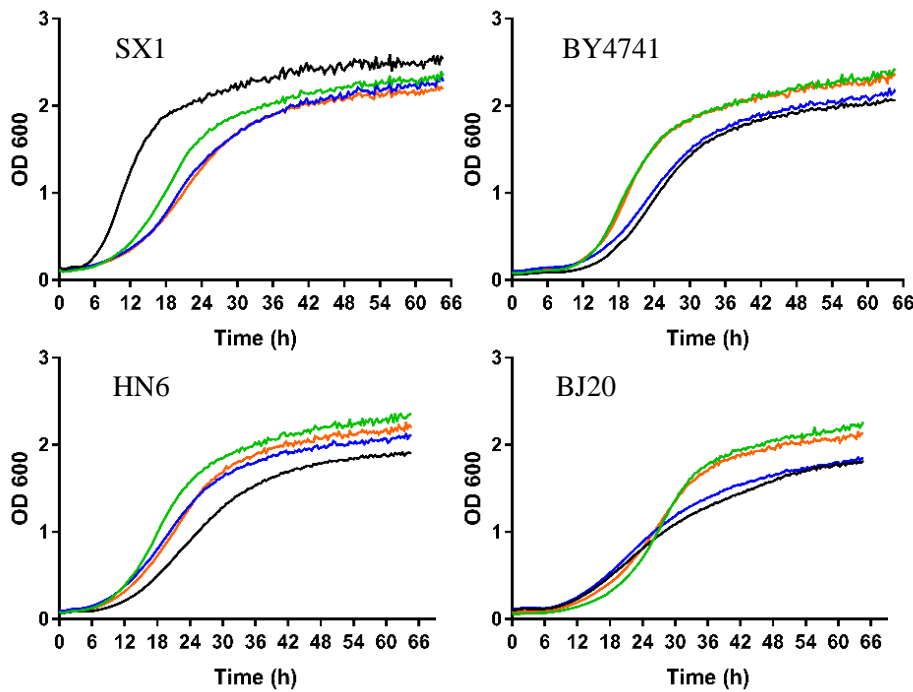


Figure 3.1-8. Differences in growth due to α Syn toxicity can be assessed using PHENOS.

Yeast were grown on a plate reader at 30°C for three days while measuring the growth (OD600) every 20 minutes. Data from the plate reader was analysed using PHENOS. Differences in MG between GFP (green) and α Syn transformants (WT - black, A30P – blue, A53T - orange) were seen in all the strains. There were no significant growth differences among the SX1 while WT and A30P α Syn were toxic for HN6, BJ20 and BY4741.

Two-way ANOVA corrected by Tukey's multiple comparisons test.

3.1.4.3. Cellular distribution and kinetics of α Syn are similar between genotypes

The aggregation experiments with α Syn were performed only with the WT protein, since it was the one causing more severe growth defects. In order to be consistent between experiments, the cells were induced for 16 hours with galactose media before the visualization. The cells present a diffuse signal when expressing GFP alone but presented three different phenotypes - diffuse signal, foci, and peripheral signal – when expressing α Syn (Figure 3.1-9 A). The quantification was performed in the same way as it was done for the HTT transformants and it showed no significant differences between the strains in any of the parameters (Figure 3.1-9 B).

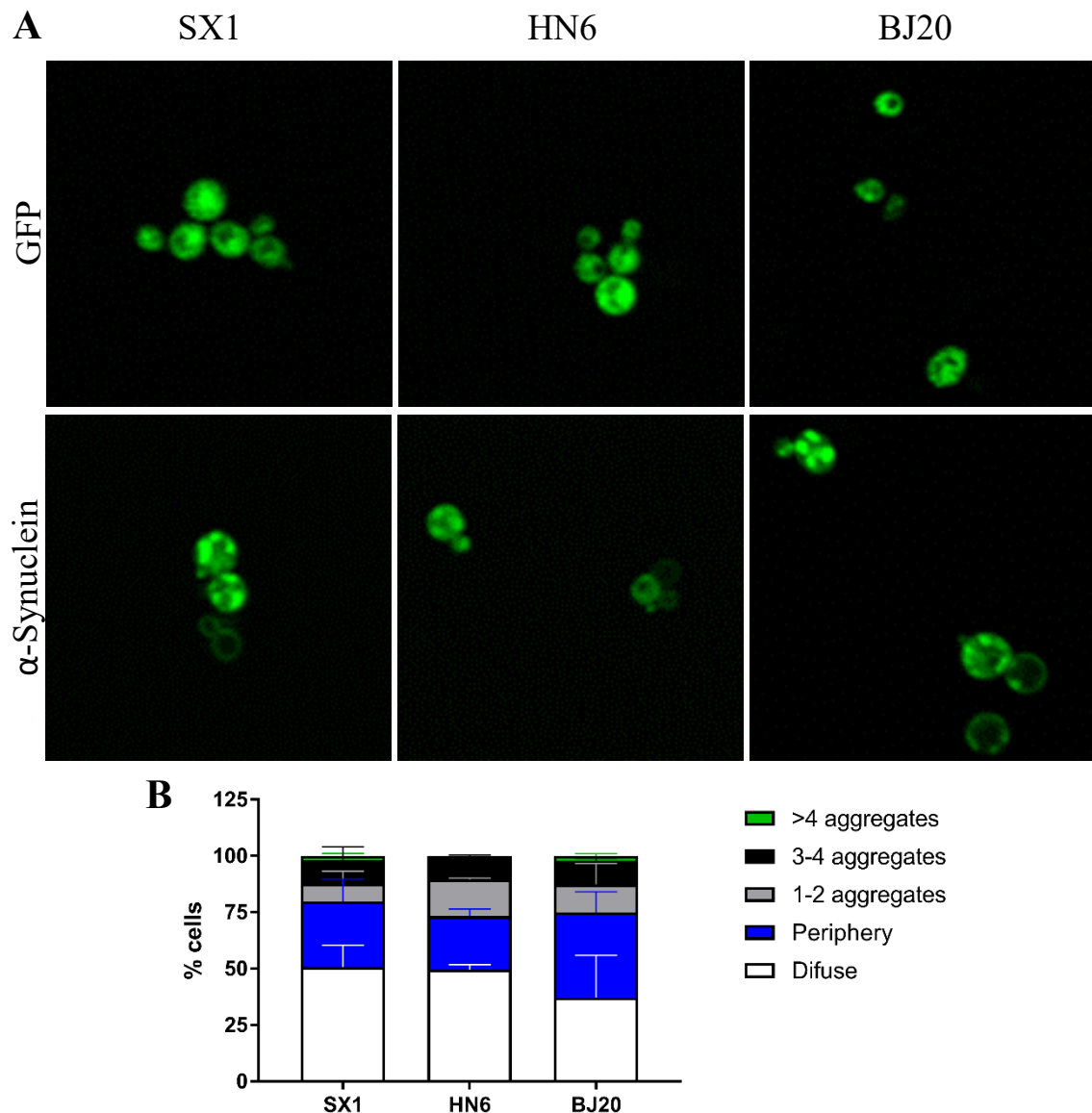


Figure 3.1-9. There are no differences in the aggregation dynamics of WT α Syn in the parental strains.

A) Confocal microscopy images taken after 16 hours of induction. The GFP signal is dispersed in the cytoplasm of the cell while α Syn-GFP signal forms foci or stays in the periphery of the cell in all the strains. **B)** The quantification shows no difference in the percentage of cells without foci, in the number of foci per cell, nor in the cells in which the protein is in the periphery.

Two-way ANOVA corrected by Tuckey's multiple comparisons test.

3.1.5. Further characterization of the selected parental strains

SX1, HN6 and BJ20 were selected as the parental strains due to their extreme growth phenotypes – SX1 was one of the most resistant strains to both mHTT and

α Syn, while HN6 and BJ20 were the most sensitive ones -. Therefore, it was necessary to characterize them further than the other strains.

3.1.5.1. The parental strains carry the [PIN+] prion

Firstly, it was necessary to verify they carried the [PIN+] prion, since it is involved in the aggregation of mHTT (Meriin et al., 2002). As explained in Chapter 2, the confocal fluorescence microscopy images were taken three days after the transformation with the *RNQ1-GFP* plasmid since induction was unnecessary because the protein was expressed from a constitutive promoter. It is known that native RNQ1 does not aggregate, so the GFP signal would be diffuse in the absence of [PIN+], but it would appear as foci in the presence of the prion since it causes the aggregation of the protein (Meriin et al., 2002). Due to the results obtained from the microscopy and filter trap assays, it was assumed they did carry the prion, and the images confirmed it (Figure 3.1-10).

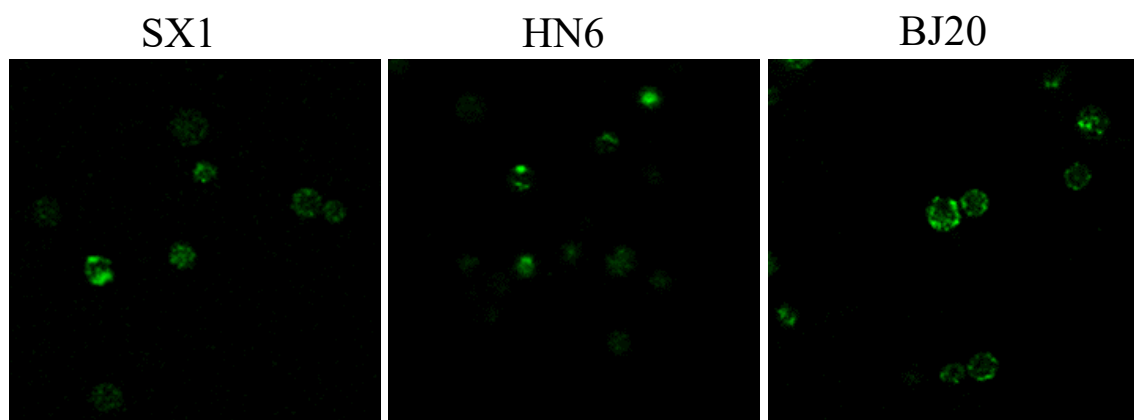


Figure 3.1-10. All the parental strains are [PIN+].

Confocal microscopy images show foci in all the parental strains when expressing RNQ1-GFP for 72 hours. The fact that RNQ1 aggregates indicates that there is presence of the [PIN+] prion, which makes the RNQ1 protein misfold and aggregate.

3.1.5.2. The expression levels from pRS426 and pRS327 are unrelated to the decrease in toxicity

The other parameter that was assessed was the level of expression from the *HTT* and *SNCA* plasmids in the parental strains. This was done to ensure that the toxicity seen in the sensitive strains was not caused by an increase in the expression of the toxic protein when compared to the resistant strains.

The expression levels in the parental strains were measured in the transformants carrying the pRS426 plasmid with the *HTT* and the *GFP* constructs and the pRS327 plasmid with *HTT* that will be used later. The toxic proteins were not used because the intensity of the signal might vary depending on the presence and number of aggregates in each cell. The expression of the proteins was induced except in the control sample, and they were analysed by flow cytometry. The data was plotted and the samples with a higher green signal than the control – those that were expressing GFP - were selected for the data analysis as can be seen in Figure 3.1-11 A. The intensity of the signal was compared between strains transformed with the same plasmid (Figure 3.1-11 B). There was no significant difference in the intensity of the green signal between the strains when expressing HTT from pRS327 and GFP from pRS426, which means the expression level is similar in all the strains and therefore the different phenotypes seen when expressing the toxic proteins are unrelated to the level of expression. Surprisingly, the expression level of HTT from pRS426 was higher in the resistant strain SX1 than in the sensitive strains HN6 and BJ20 and there was no difference in expression between the sensitive strains. However, an increase in mHTT expression is unlikely to be the cause of the resistance seen in that strain.

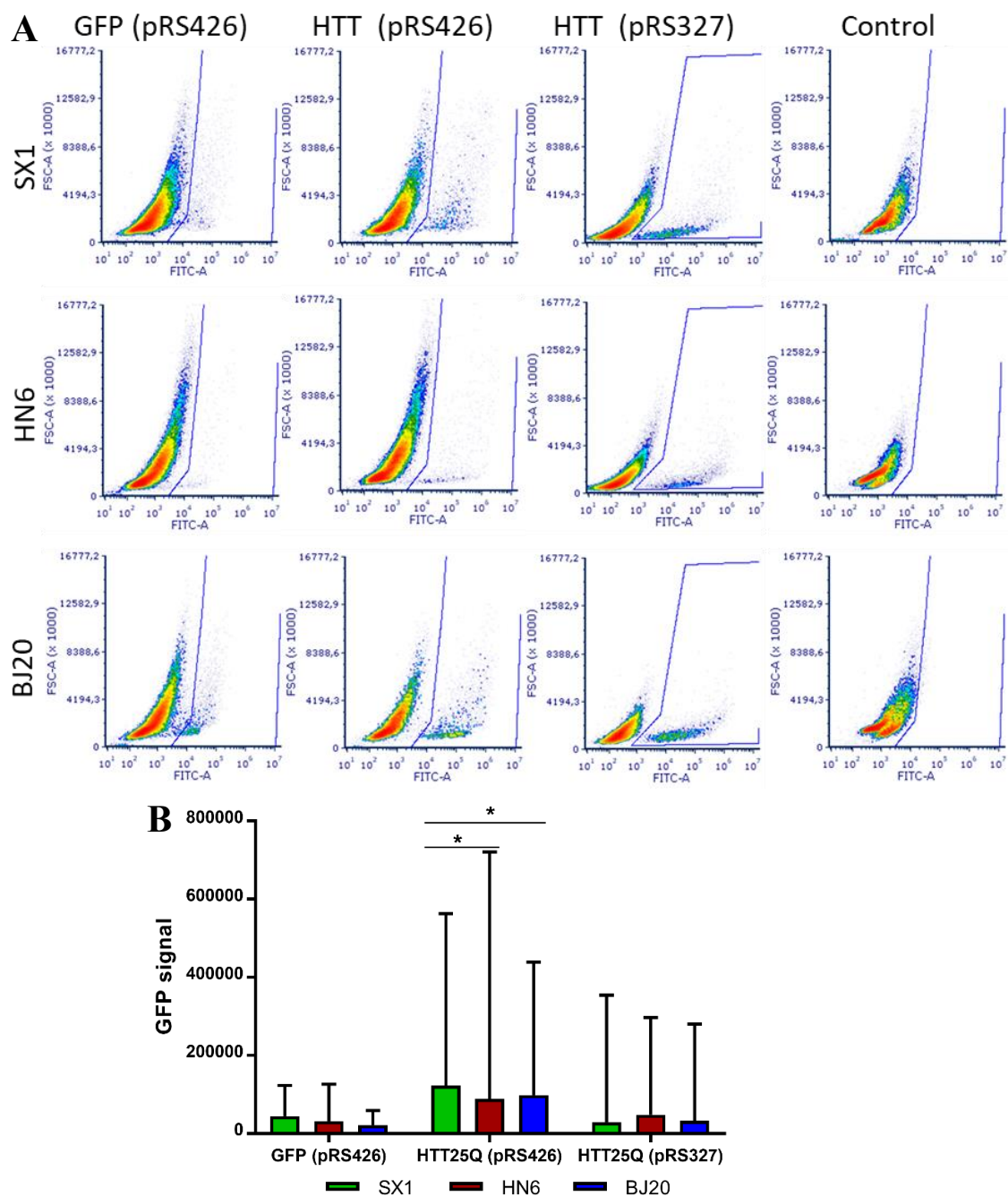


Figure 3.1-11. Comparison of the level of expression from pRS426 and pRS327 plasmids on the parental strains.

A) Flow cytometry plots showing the size (FSC-A) and GFP signal intensity (FITC-A) of the parental strains when expressing HTT-GFP from pRS426 and pRS327 and GFP from pRS426 after 72 hours of galactose induction. The uninduced strain was used as a control for the background green signal. **B)** Graphic showing the differences in GFP signal among the parental strains. There is a significant increase in intensity in SX1 HTT-GFP pRS426 when compared to the other parental strains transformed with the same construct.

Two-way ANOVA corrected by Tukey's multiple comparisons test. * P < 0.05.

3.2. Discussion

In order to choose the most appropriate parental strains for the population of the QTL analysis, we wanted to select strains showing an extreme phenotype when expressing mHTT and αSyn. Since PHENOS was going to be used for the QTL analysis, the first step was selecting the parameter that would be used to evaluate the sensitivity of the strains. As mentioned in Chapter 2, PHENOS provides three parameters: maximum OD600, MS, and lag. Although no significant difference was found in the MG of the sensitive strain BY4741 due to its fast growth speed, there was no problem assessing any of the experimental strains. Since both lag and growth speed presented a higher variability between replicas, we determined that MG was more reliable.

From the results of the spotting assays and PHENOS, the sensitive strains were easy to select since the dramatic decrease in growth and viability of HN6 and BJ20 when expressing mHTT and WT αSyn was far beyond what was seen in any other strain. Likewise, the strains BJ6 and SX1 were the most promising resistant strains. However, there was no HTT-GFP signal from BJ6 although it was certain that *URA3* was deleted, and it was growing on SD -URA after the transformation. Since the possibility of the yeast losing the plasmid exists and BJ6 was the only strain in which that happened, it was decided against using that strain. Interestingly, SX1 presented an increase in growth while expressing WT αSyn during the PHENOS assay, probably due to the reduction of the lag phase - although the reasons why the expression of WT αSyn would decrease the lag phase remain unclear -. Since A30P and A53T seemed to have a lesser effect on growth than WT αSyn, the WT construct was chosen for the phenotyping required for QTL analysis, while A30P would be the next in line since it shows higher toxicity than A53T.

Regarding aggregation, the presence of mHTT aggregates was detected by microscopy and confirmed with the filter trap in resistant and sensitive strains, which made these strains interesting since aggregation had been linked to toxicity in other strains (Meriin et al., 2002). However, in our strains that was not the case, since mHTT formed aggregates in the resistant strain SX1, which made it an interesting candidate for the QTL analysis. However, this difference in aggregation was not seen in the α Syn transformants, where the percentage of cells without aggregates, with the protein signal in the periphery of the cell, and the number of aggregates per cell were similar in the three parental strains.

Finally, the expression of the control proteins from the plasmids was studied using flow cytometry to determine that the expression levels were similar between strains. Two of the plasmids (*HTT* pRS327 and *GFP* pRS426) showed no difference between strains and the remaining one (*HTT* pRS426) presented an increase in expression in the resistant strain SX1. Since it is unlikely for an increase in toxic protein to cause resistance and the size of some cells seemed to be higher than in the other transformants of the same strain, it is likely that two cells were analysed at once and caused an increase in both size and green signal or that the cell contained more plasmids since they are two-micron plasmids.

Based on these results, we chose the resistant strain SX1 and the most sensitive strains HN6 and BJ20 as our parental strains. Since there were three strains, it was decided to perform three parallel crosses between them to generate the QTL population since a huge genetically diverse population is required. To achieve this, in the next chapter we will explain how we performed 12 rounds of intercrosses that broke the linkage groups, increasing the genetic diversity among the descendants, which allowed us to find the genetic mechanism underlying the differences in mHTT and α Syn toxicity resistance between strains by performing a QTL analysis.

4. Intercrosses and QTL analysis

The previous chapter described the selection of the three parental strains to be used for the intercrosses and QTL analyses. These included SX1, a strain that did not present growth or survival deficits when expressing either mHTT or WT α Syn, and HN6 and BJ20, the most sensitive strains to mHTT and α Syn toxicity. However, QTL analysis requires a large and diverse population in order to map the genes involved in the phenotypic variation present in these strains (Londin et al., 2013). This chapter describes the procedure to prepare the parental strains for the cross, the intercross, and the QTL analysis.

4.1. Results

4.1.1. Parental strain preparation and intercrosses

In order to generate that population, it was necessary to delete the *LEU2* and *LYS2* genes in order to have auxotrophic markers to be able to select the descendants from the cross. *LEU2* deletion was performed using the LiAc transformation protocol with the pEL9 plasmid, the yeasts were grown on SD -URA to select the transformants that were *leu2::URA3*, then passed to SC to allow them to lose the *URA3*, and finally grown on FoA media to select the transformants that have lost *URA3* and are *leu2Δ0* (Louis & Haber, 1989). These transformants were then used for the deletion of *LYS2* by performing a LiAc transformation with the *lys2::LEU2* DNA cassette. The transformants were selected in SD -LEU. Then, three pairwise crosses were performed. The resistant strain SX1 (*MAT a, leu2Δ0*) was crossed with the sensitive strains HN6 and BJ20 (*MAT α, lys2::LEU2*) separately, and both sensitive strains HN6 (*MAT a, leu2Δ0*) and BJ20 (*MAT α, lys2::LEU2*) were crossed together. For each cross, the parental strains were mixed in YPD to generate

diploids that carried both *LEU2* and *LYS2* (F1 hybrids), and later they were plated into SD -LEU -LYS media to select for those diploids. The F1 hybrids were sporulated in KAc media, the non-sporulated cells were killed with ether, and the gametes were released with zymolase. The gametes from the F1 were crossed between themselves until the F12 generation was obtained, as explained in Chapter 2. The F12 descendants were sporulated and dissected until 96 spores coming from 24 tetrads were obtained from each cross. Finally, the mating type of the F12 strains was determined by crossing each strain with known α and α maters and verifying with which they were able to mate.

These three sets of 96 spores compose a relatively large population that underwent recombination numerous times so the linkage groups became small, allowing a more precise mapping and making it advantageous for the QTL analysis.

4.1.2. PHENOS of F12 strains

All the spores from each of the three crosses were transformed with the *HTT*, *mHTT*, *GFP* and *SNCA URA3* constructs following the high-throughput transformation protocol. This method was unable to introduce the construct in some strains, so the remaining strains were then transformed following the LiAc transformation protocol. The transformants were arrayed in 96-spots PlusPlates with SD -URA media using the rotor. Each plate contained strains with the same construct and mating type to avoid any possible interference mating signals could have in the growth of the strains. The position of the strains in the plates was the same for all the constructs to allow PHENOS to perform the growth comparison.

As explained in Chapter 2, in order to perform the PHENOS growth assay, the transformants were arrayed in a 384-spot format, with four replicas of each of the 96 strains, and grown inside a plate reader at 30 °C for three days in SD -URA plates

with galactose. The data was transferred to the PHENOS software to generate growth curves and the difference in those growth curves between the controls (HTT and GFP) and their respective toxic transformants (mHTT and αSyn). The ratio of MG between the toxic and the control transformants was used to determine the toxic effect of the protein's expression, which was the phenotype used for the QTL analysis where the polymorphisms present in the most resistant strains and in the most sensitive strains (included in Figure 4.1-1) were compared to those of the general population to determine which genes were related to the disease.

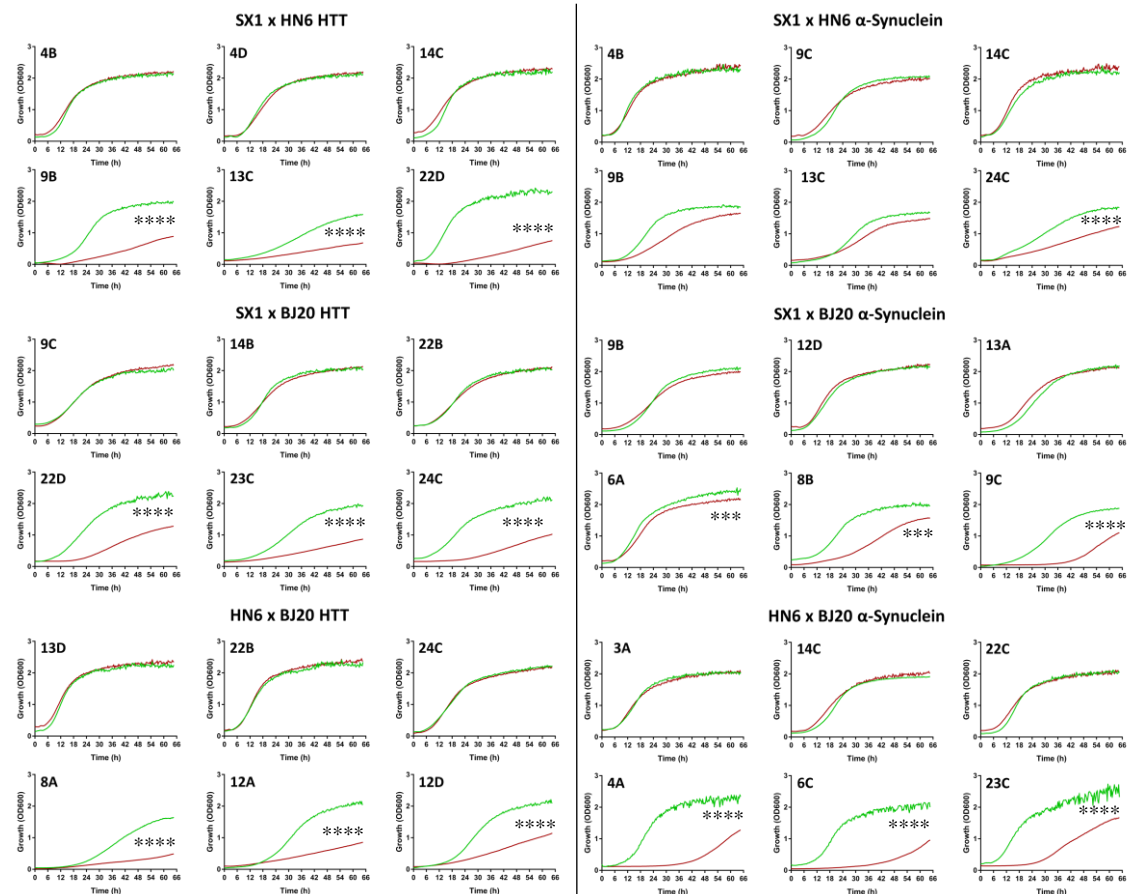


Figure 4.1-1. αSyn and mHTT toxicity is variable among the F12 strains of the three intercrosses

Growth curves of the most resistant and most sensitive strains of each cross. HTT and GFP (green) were used as controls for mHTT and αSyn (red) respectively. The resistant strains 4B and 14C, and the sensitive strains 9B and 13C from the SX1 x HN6 cross displayed the same phenotype to both mHTT and αSyn expression, although αSyn toxicity had a less noticeable effect. On the contrary, 9C from SX1 x BJ20 was resistant to mHTT but sensitive to αSyn.

Two-way ANOVA corrected by Tukey's test (**P < 0.001; ***P < 0.0001).

4.1.3. Aggregation of mHTT is unrelated to growth or survival

As explained in Chapter 3, there is no relationship between mHTT aggregation and toxicity in our parental strains, both the sensitive (HN6 and BJ20) and resistant (SX1) strains had aggregates that were captured in the filter trap, although there were differences in the number of aggregates between the strains as seen in the fluorescence microscope – possibly caused by differences in the efficacy of the chaperone and the protein degradation systems -. To establish if mHTT aggregation occurred in all our strains regardless of toxicity, a filter trap was performed in duplicate for several F12 strains and compared with the difference in growth between the HTT and mHTT transformants (Figure 4.1-2). This experiment was performed in different strains from the ones shown in the most resistant and most sensitive strains since a gradient of growth phenotypes was needed.

There were aggregates in both sensitive (16B – SX1 x HN6) and resistant strains (23B – HN6 x BJ20). However, there were also sensitive (18B – SX1 x HN6) and resistant (24B – HN6 x BJ20) strains with low signal in the CelAc membrane. These results suggest that there is no relationship between mHTT toxicity and aggregation.

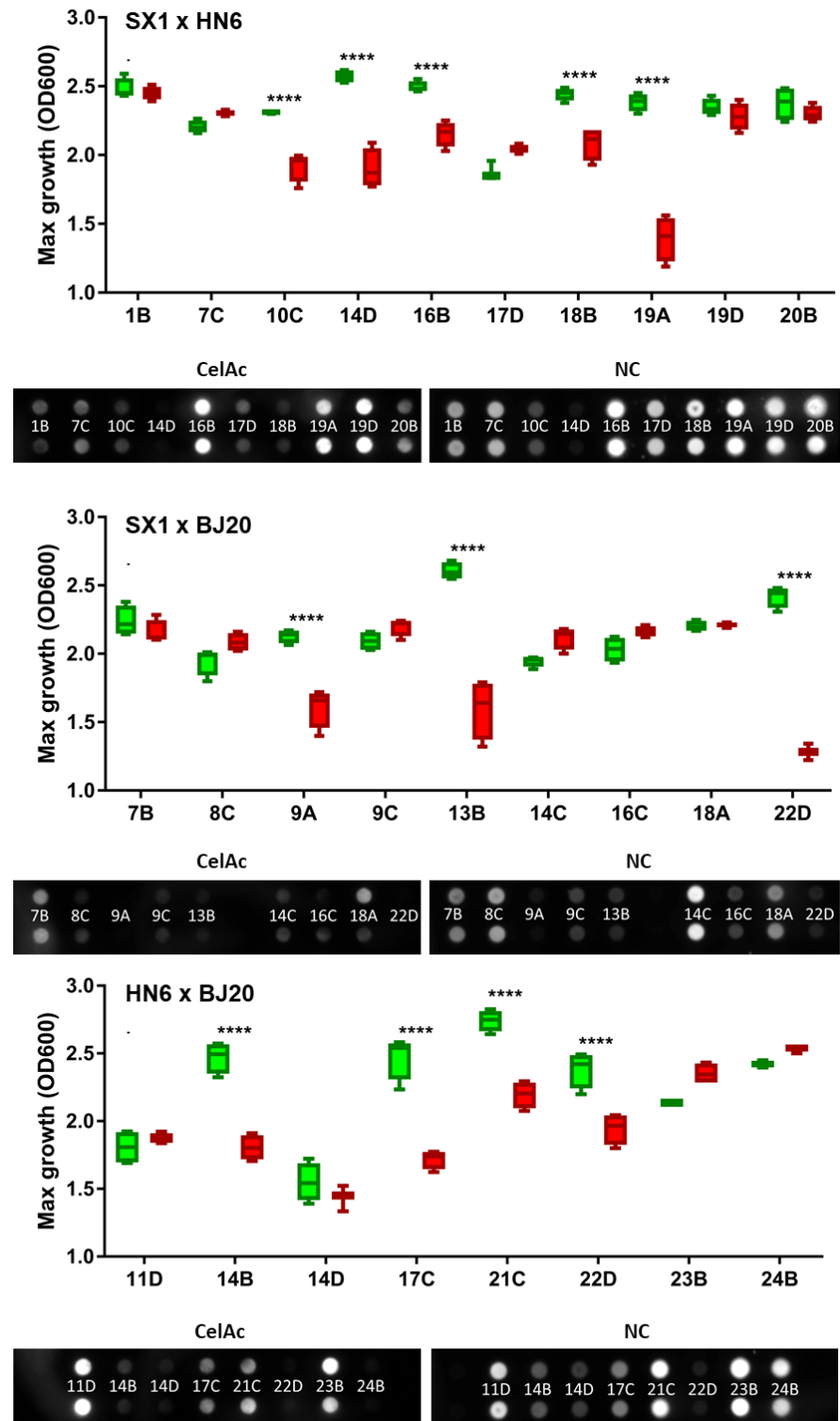


Figure 4.1-2. Aggregation of mHTT is unrelated to its toxicity

Strains with different growth phenotypes were selected for the filter blot to clarify the role of aggregation in toxicity. The boxplots show the maximum growth of the HTT (green) and mHTT transformants (red). Two-way ANOVA corrected by Tukey's multiple comparisons test (****P < 0.0001). The filter trap shows that not all the mHTT transformants present aggregates captured in the CelAc membrane, and there is variability in the amount of mHTT captured by the NC membrane. There are both resistant strains with both high (SX1 x HN6 16B) and low signal (SX1 x HN6 18B) in the CelAc membrane, meaning mHTT aggregation is unrelated to toxicity.

4.1.4. QTL analysis

QTL analysis was performed by comparing SNP segregation frequencies of resistant and sensitive strains with the SNP frequencies of the whole population. Any differences found in the segregation of SNPs in resistant or sensitive strains will indicate the location of a possible modifier gene. As it was explained in Chapter 2, in order to do that, the genomic DNA of all the strains was obtained using the E.Z.N.A. Yeast DNA extraction kit and sequenced at the Earlham Institute, and the phenotypic data used was the ratio of MG between the toxic and the control transformants of each strain. A different number of QTL was identified for each cross and each disease, most of them being polygenic, meaning that the region highlighted during the QTL analysis contained at least two genes (Table 4.1-1).

Table 4.1-1. Number of loci and genes identified during the QTL analysis

QTL analysis results for HTT		
Cross	Number of loci	Number of genes
SX1 x HN6	36	658
SX1 x BJ20	23	170
HN6 x BJ20	75	566

QTL analysis results for αSyn		
Cross	Number of loci	Number of genes
SX1 x HN6	1	18
SX1 x BJ20	6	64
HN6 x BJ20	113	740

4.1.4.1. mHTT QTL analysis

The QTL analysis of the HD yeast strains shows that one QTL in chr 16 with five genes appears in all the HD crosses (*COX10*, *MRPL40*, *NIP100*, *SPT14* and *TRE1*), one of which appeared among the deletion suppressors of mHTT toxicity previously identified (*MRPL40*) (Giorgini et al., 2005). Apart from the QTL that is in all three sets, several QTL were present in two of the crosses. 23 genes grouped in five QTL appeared in both SX1 x BJ20 and HN6 x BJ20 crosses. Among those genes, two of them, *RAD16* on chr 2 and *CSC1* on chr 12, were among the deletion suppressors

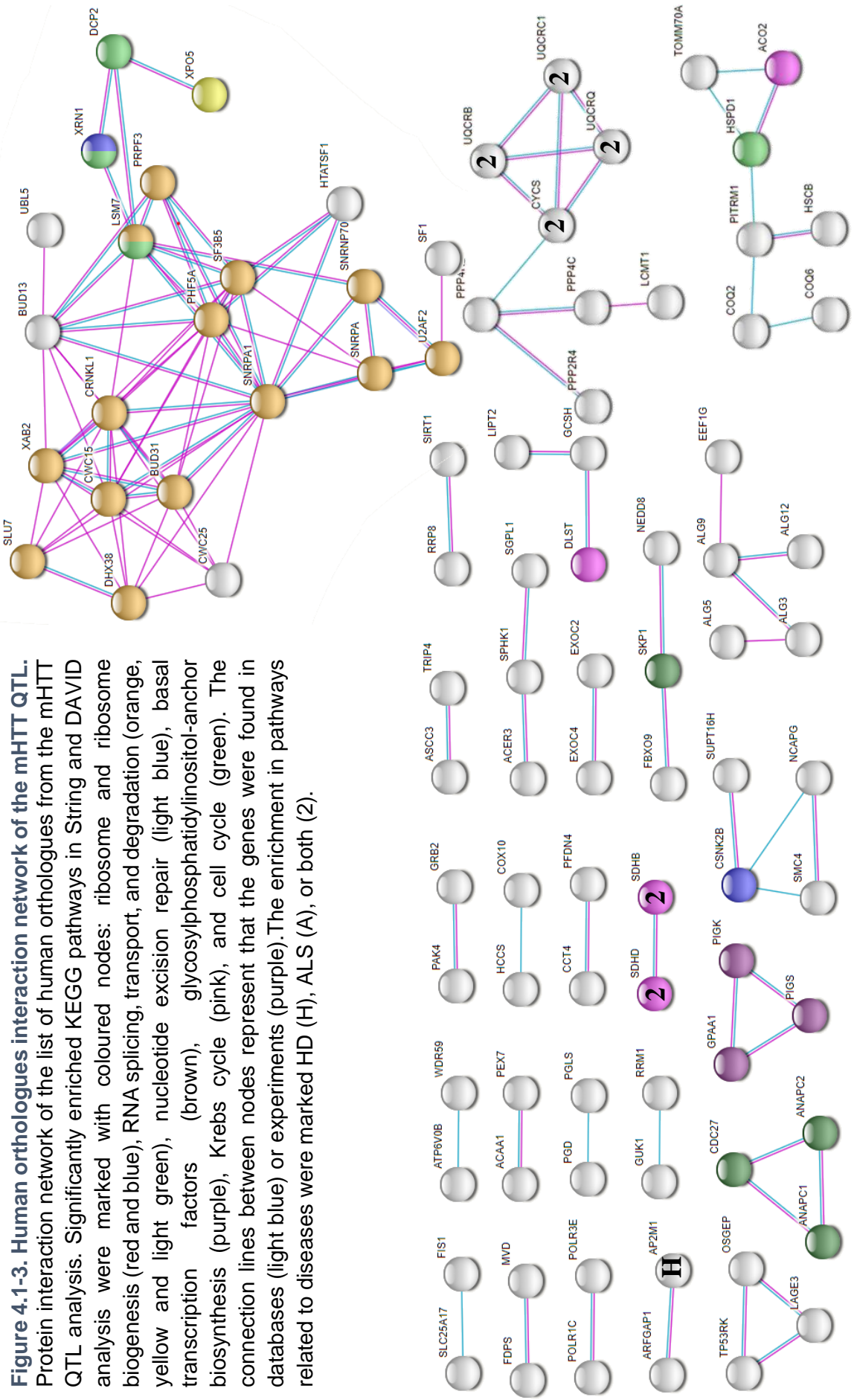
(Giorgini et al., 2005) and one, *YDR154C* in chr 4, was identified as an ORF overexpression (OE) suppressor of mHTT toxicity (Mason et al., 2013). There were 44 genes in ten QTL in common between SX1 x HN6 and HN6 x BJ20 crosses. Among them, one QTL on chr 7 had two genes that were highlighted in previous studies, one of them appeared on the deletion suppressor list (*PNC1*) and another one among previously identified deletion enhancers of mHTT toxicity (*OCH1*) (Giorgini et al., 2005; Willingham et al., 2003). And another QTL in chr 11 had three genes, *YET1*, *YNK1* and *YKL069W*, that were differentially expressed in yeast expressing mHTT versus HTT in a previous study (Tauber et al., 2011). Some of the genes that were highlighted in the QTL analysis have human orthologues that previous studies have associated with HD: *HDAC1* (Bodai et al., 2001; Thomas et al., 2008), *IDH1* (Gruber-Bzura et al., 2017), *TIMELESS* (Faragó et al., 2019), *GRB2* (Baksi et al., 2013) and *SIRT1* (Baldo et al., 2019; Jiang et al., 2011).

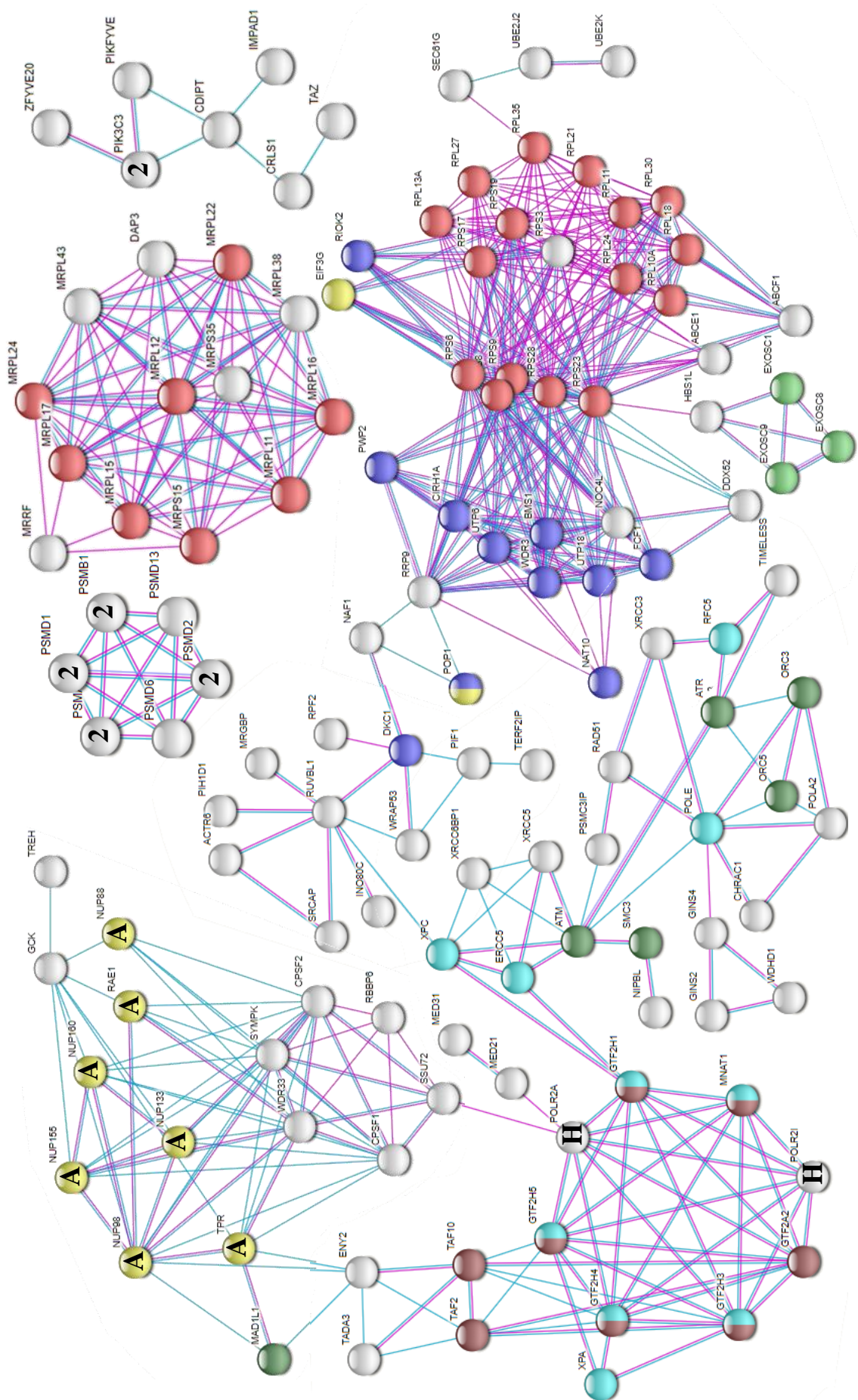
Table 4.1-2. Pathways enriched in the mHTT QTL list

Pathway	Genes	P-value
Ribosome	25	< 0.0001
Metabolic pathways	69	< 0.0001
Nucleotide excision repair	10	< 0.0001
Ribosome biosynthesis in eucaryotes	13	< 0.0001
Spliceosome	16	< 0.0001
Basal transcription factors	8	0.00062
GPI-anchor biosynthesis	6	0.0012
Biosynthesis of antibiotics	15	0.011
RNA transport	13	0.012
Proteasome	6	0.015
Citrate cycle	5	0.016
Cell cycle	10	0.022
RNA degradation	7	0.042

Among the 1318 yeast genes that appeared in the HD QTL analysis, 440 of them had a one-to-one orthologue in humans. DAVID's KEGG pathways analysis

determined there was an enrichment in several pathways, including ribosome synthesis, DNA repair, transcription factors, RNA metabolism, GPI-anchor biosynthesis, protein degradation, energy synthesis, and cell cycle (Table 4.1-2). String included those pathways and also highlighted an increase in genes related to two diseases: HD and ALS (Figure 4.1-3).





4.1.4.2. αSyn QTL analysis

Unlike in the HD study, there were no QTL that appear in the three crosses on the PD QTL analysis, however, there were two QTL that appear in both SX1 x BJ20 and HN6 x BJ20. One of these one located on chr 6 contained eight genes (*KEG1*, *IRC6*, *DUG1*, *MRX20*, *CNN1*, *BNA6*, *RMD8* and *YMR31*). Interestingly, all those genes appear in the HD QTL list and two of them (*DUG1* and *RMD8*) were in the deletion enhancer list (Willingham et al., 2003). The remaining QTL was on chr 16 and was composed of three genes (*SWI1*, *IRC15* and *CTF19*). One of the genes that was highlighted in the QTL analysis, the vacuolar protein sorting 13C (*VPS13*) gene, had a human orthologue (*VPS13A* and *VPS13C*) which had previously been associated with autosomal-recessive early-onset parkinsonism with rapid and severe progression, and early cognitive decline (Lesage et al., 2016).

Among the 797 genes in the PD QTL analysis, 257 had one-to-one human orthologues. DAVID KEGG pathways analysis determined there was an increase in several pathways, with the most significant being: ribosome synthesis, RNA metabolism, protein degradation, and energy synthesis (Table 4.1-3, Figure 4.1-4).

Table 4.1-3. Pathways enriched in the αSyn QTL list

Pathway	Genes	P-value
Ribosome biogenesis in eukaryotes	11	< 0.0001
Ribosome	11	0.00036
RNA transport	11	0.0022
RNA degradation	7	0.0042
DNA replication	5	0.0054
Proteasome	5	0.011
Citrate cycle	4	0.021
Carbon metabolism	7	0.029

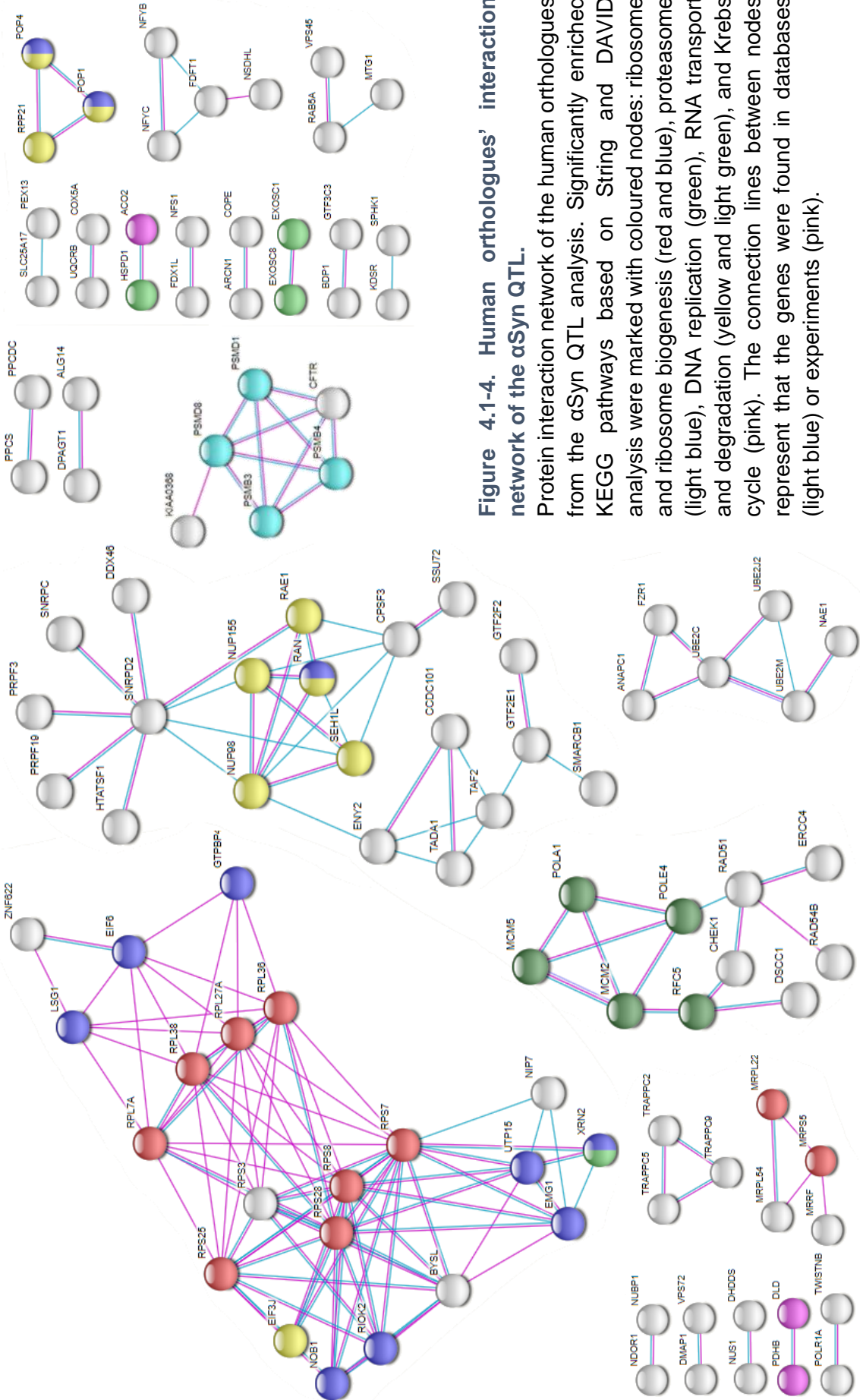


Figure 4.1-4. Human orthologues' interaction network of the α Syn QTL.

Protein interaction network of the human orthologues from the α Syn QTL analysis. Significantly enriched KEGG pathways based on String and DAVID analysis were marked with coloured nodes: ribosome and ribosome biogenesis (red and blue), proteasome (light blue), DNA replication (green), RNA transport and degradation (yellow and light green), and Krebs cycle (pink). The connection lines between nodes represent that the genes were found in databases (light blue) or experiments (pink).

Lastly, among all the genes identified during the QTL analysis, 217 genes grouped in 30 QTL were listed in both the HD and the PD studies. 65 of those genes had a one-to-one human orthologue and were used for the ontology analysis using DAVID, in which an enrichment on the ribosome synthesis (four genes, $P = 0.031$) and RNA degradation (four genes, $P = 0.0068$) was found.

4.2. Discussion

Despite yeast being a simple organism, they have been a useful model for the study of NDs (Miller-Fleming et al., 2008; Tuite, 2019). Quantitative traits involved in NDs have been studied in yeast mainly by performing high-throughput studies with OE and knock-out collections (Miller-Fleming et al., 2008; Tuite, 2019). Although valuable, this approach has the disadvantage of not being able to study the effect of downregulating essential genes, and the effects of completely deleting or strongly overexpressing a gene can have drastic effects. However, these caveats can be avoided by using natural isolates to perform a QTL analysis, since the genotypic variability present in those strains occurs in nature, so there are no problems with the level of expression of the genes, which allows the study of the whole genome, including the essential genes.

The results from these experiments show that yeast orthologues of human genes known to be implicated in HD and PD are highlighted during the QTL analysis. Among those genes there are *HDAC1*, whose inhibition ameliorates the transcription impairment present in HD and prevents neurodegeneration (Bodai et al., 2001; Thomas et al., 2008), *IDH1*, which is involved in energy metabolism and is decreased in HD patients (Gruber-Bzura et al., 2017), *TIMELESS*, which is part of the circadian clock and which expression pattern is altered in HD causing sleep disorders (Faragó et al., 2019), *GRB2*, which OE facilitates the clearance of mHTT aggregates through

the autophagolysosome (Baksi et al., 2013), *SIRT1*, which is increased in the brains of HD patients and is responsible for metabolic symptoms (Baldo et al., 2019; Jiang et al., 2011), and *VPS13C*, which has previously been associated with autosomal-recessive early-onset parkinsonism with rapid and severe progression, and early cognitive decline caused by mitochondrial dysfunction (Lesage et al., 2016). Furthermore, several genes had also previously been identified as HD modifiers in yeast studies performed with deletion and OE collections (Giorgini et al., 2005; Mason et al., 2013; Willingham et al., 2003), and some had their expression altered due to mHTT (Tauber et al., 2011). These results indicate that QTL analysis in yeast is likely a valuable tool to uncover genetic modifiers of NDs.

The QTL analysis provided a list of more than a hundred loci for each disease model, and the ontology analysis of the human orthologues showed enrichment in the genes of some pathways that were common to both diseases. Those pathways were involved in ribosome synthesis, RNA transport and degradation, and energy synthesis. The ribosome synthesis and the RNA degradation pathways were also highlighted when studying the pathways enriched among the genes that appeared in both HD and PD QTL analysis. Some of these pathways - protein catabolism (Willingham et al., 2003) and transcription (Giorgini et al., 2005)- were also enriched in previous yeast studies. These results suggest that, although both diseases act through different processes, they have some common mechanisms.

In order to choose the genes for validation, those in the QTL that were found in both diseases were selected. Among them, the known modifier genes and those that appeared in previous yeast studies were discarded, and from the rest, only those that were closest to the QTL's peak - the central point of the region highlighted during the analysis – and had human and fly orthologues that were expressed in the brain were selected. In the end, *FAR10*, *GSY2*, *DSS4*, *TIF6*, *PPM1*, *MRX21*, *RPA135* and

TAF2 were selected for validation.

4.2.1. *SLMAP (FAR10)*

SLMAP is the human orthologue of *FAR10*. It encodes a tail-anchored membrane protein involved in docking and membrane fusion process via protein-protein interactions (Hwang & Pallas, 2014). It is involved in vesicular trafficking, endocytosis, and exocytosis (Hwang & Pallas, 2014); *SLMAP* plays a role in the exocytosis of the insulin-dependent glucose transporter GLUT4 in mice adipose tissue and might be involved in diabetes (Chen & Ding, 2011). Interestingly, GLUT4 colocalizes with GLUT3 in rat neurons and it is thought to provide an extra intake of glucose in the presence of insulin (Apelt et al., 1999). Furthermore, studies show that HD patients present brain glucose hypometabolism - especially in the frontal and temporal lobes, the cortex, and the striatum - that precedes the clinical onset of the disease, and that an increase in the level of the glucose transporter GLUT3 is able to delay the onset of HD (Ciarmiello et al., 2006; Vittori et al., 2014). In total, this suggests that a decrease in glucose intake in the neurons caused by a transport impairment that prevents the exocytosis of GLUT4 to the membrane would lead to an earlier onset of HD. Therefore, an increase in *SLMAP*, the protein responsible for the exocytosis of GLUT4, might be able to delay the onset of HD.

Another role of *SLMAP* is location targeting for both the yeast FAR complex and its human orthologue the STRIPAK complex, which is implicated in cell growth and survival by negatively regulating the JNK apoptotic pathway and positively regulating the ERK survival pathway (Hwang & Pallas, 2014). Notably, it is implicated in circadian rhythms by dephosphorylating CLOCK via PP2A so it can be active in the evenings (Andreazza et al., 2015; Hwang & Pallas, 2014). The STRIPAK complex has been related to several diseases like cancer, autism, and cardiovascular

diseases. Interestingly, this complex is also a negative regulator of the Hippo pathway that is involved in transcriptional regulation, which is altered in HD (Bae et al., 2017; Hwang & Pallas, 2014; Mueller et al., 2018). When the Hippo pathway is active, MST2 is phosphorylated (pMST2) and is able to phosphorylate YAP, which then is unable to translocate to the nucleus and is degraded in the cytoplasm (Bae et al., 2017). On the other hand, the Hippo pathway becomes inactive when STRIPAK interacts with pMST2 via SLMAP and then dephosphorylates it via PP2A. Inactive MST2 is unable to phosphorylate YAP, so YAP translocates to the nucleus, binds to transcription factors, and promotes cell survival. Interestingly, YAP levels are decreased in HD patients' cortex due to an increase in the levels of pMST1 and 2, which leads to transcriptional dysregulation and cell death (Mueller et al., 2018). Since SLMAP is responsible for the interaction of PP2A and pMST2, and pMST2 is upregulated in HD leading to the degradation of YAP, which causes transcriptional dysregulation and apoptosis, upregulating SLMAP might ameliorate the transcriptional problems.

4.2.2. *LCMT1 (PPM1)*

Interestingly, although the methyltransferase LCMT1 is not a component of the STRIPAK complex, it is also related to it since LCMT1 is responsible for PP2A activation by methylating it (mPP2A) (Javadpour et al., 2019; Sontag & Sontag, 2014). Active PP2A stays in the cytoplasm rather than in the nucleus and is involved in metabolism, neural development, transcription, cell cycle, proliferation, and apoptosis. PP2A also interacts with proteins that have been related to AD (NMDAR, APOE4, GLUTR5, GSK3 β , CDK5, ERK and JNK). Decreased levels of mPP2A lead to the activation of ERK and JNK which can cause tau hyperphosphorylation, and to an increase in the formation of A β aggregates, which can disrupt long term

potentiation and neuronal transport. PP2A inhibitors are upregulated, leading to the tau kinases being upregulated in the brains of AD patients.

Similarly, LCMT1 is downregulated in PD while PP2A inactivator PME1 is upregulated, causing a decrease in active PP2A that leads to the increase in phosphorylation of α -synuclein at Ser129, and therefore to the formation of aggregates (Javadpour et al., 2019). Interestingly, the OE of α Syn has been related to the inactivation of LCMT1 and the activation of PME1.

Lastly, PP2A and PP1 have been related to increased excitotoxicity due to mHTT (Metzler et al., 2010). An increase in the NMDAR signal leads to excitotoxicity in HD due to a decrease in the phosphorylation of mHTT at Ser421 due to PP1 and PP2A, which causes trafficking defects. Downregulation of PP1 and PP2A prevents NMDAR-related cell death in mouse models. However, the role of PP2A in mHTT dephosphorylation is small compared to the role of PP1, which is responsible for more than 80% of this dephosphorylation.

Taking these studies into account, it is highly likely that LCMT1 plays a role in HD and PD. As explained before, mPP2A plays a role in transcription, cell survival, and circadian rhythms (Andreazza et al., 2015; Bae et al., 2017; Hwang & Pallas, 2014; Mueller et al., 2018). Since PP2A activation seems to be protective against AD and PD related phenotypes and is probably beneficial in HD models - although it might slightly increase excitotoxicity - upregulating LCMT1 is likely beneficial in all the diseases.

4.2.3. RABIF (DSS4)

RABIF was initially considered a GEF (guanine exchange factor) responsible for activating a specific set of Rab GTPases. However, later studies showed that it binds to a different region of the Rab protein, causes a conformational change in order to

release the GDP, and allows the Rab to stay nucleotide-free and not be degraded by the proteasome, leading to RABIF being considered a Rab-stabilizing holdase chaperone that promotes the nucleotide exchange and has a low GEF catalytic activity for some Rabs rather than a GEF itself (Gulbranson et al., 2017; Itzen et al., 2006; Nuoffer et al., 1997). Rab GTPases are proteins involved in different steps of vesicular trafficking (Goody et al., 2017). They are inactive when bound to GDP and become active when a GEF exchanges that GDP for GTP. Rabs interact with motor proteins and with proteins involved in fusing membranes. After the membrane fusion, a GTP activating protein (GAP) inactivates the Rab by hydrolysing the GTP. However, their function is known to be compromised in several NDs, including but not limited to AD, PD, and HD (Kiral et al., 2018).

In normal conditions, HTT interacts with Rabs from various compartments in different ways, therefore, a reduction in HTT leads to several changes in vesicle trafficking: reduction of bi-directional motility of Rab19 (endosomal recycling) and Rab3 (synaptic vesicles), reduction in retrograde movement of Rab7 (late endosomes), increase in anterograde movement of Rab2 (ER-Golgi), and altered subcellular location of Rab8 (ER-Golgi) (White et al., 2015). Similar to what happens when HTT is lowered, in HD, HTT loses its function and becomes unable to interact properly with the Rabs, causing the mislocalization of Rab8 that leads to the impairment of the Golgi-lysosome trafficking, and problems in endosome motility and recycling due to Rab5 and Rab11. Several studies show that these impairments can be overcome by overexpressing some of the impaired Rabs: the OE of Rab8 in HD model flies led to the improvement in neurodegeneration, eclosion, lifespan and circadian rhythms, and also to an increase in the number of insoluble mHTT aggregates (Delfino et al., 2020), while the OE of Rab11 in primary cell cultures from mice and fly models also lead to an improvement in neurodegeneration, synaptic

loss, and behaviour (Richards et al., 2011; Steinert et al., 2012). Rab11 is able to rescue neurodegeneration because of its involvement in the transport and fusion of the multivesicular body and the autophagosome during the process of protein clearance in cell cultures from HD mice (Richards et al., 2011). It is also involved in the exocytosis of vesicles originating in the ER and its impairment would lead to a reduction in dendrites.

Unsurprisingly, RABIF also interacts with Rabs that have not yet been directly related to HD, such as Rab1, Rab10 and Rab13 (Gulbranson et al., 2017; Nuoffer et al., 1997). Among them, Rab10 is particularly interesting since it is necessary for the insulin-stimulated exocytosis of the glucose transporter GLUT4 (Gulbranson et al., 2017). Downregulation of RABIF leads to faster degradation of Rab10, which causes defects in exocytosis of GLUT4 and a decrease in glucose intake, which, as mentioned above, could lead to an earlier onset of HD. Taking this into account, the presence of RABIF stabilizing and preventing the degradation of Rab10 seems important for delaying the onset of HD.

Unsurprisingly, Rabs are also impaired in PD (Homma et al., 2021). The kinase LRRK2, which is strongly associated with familial and idiopathic forms of PD, phosphorylates several Rabs, including Rab3 (A to D), Rab 5 (A to C), Rab8 (A and B), Rab10, Rab12, Rab29, Rab35 and Rab43 (Steger et al., 2016; Steger et al., 2017). Among them, Rab8A and Rab10 are especially interesting since they are involved in cilia formation, necessary for the sonic hedgehog (Shh) signalling pathway, which is neuroprotective against toxins that cause PD-like symptoms (Dhekne et al., 2018; Steger et al., 2017). In the presence of pathogenic LRRK2, Rab10 becomes phosphorylated and blocks the formation of cilia (Dhekne et al., 2018). This is thought to cause the cholinergic neurons of the striatum to become unable to receive the Shh signal from the dopaminergic neurons, and therefore not

release the neuroprotective GDNF, leading to the known selective loss of dopaminergic neurons in PD. Another protein from this family, Rab8A, is phosphorylated by pathogenic LRRK2 leading to problems in the position and cohesion of the centrosome (Madero-Pérez et al., 2018). Two other RABIF substrates, Rab8A and Rab3A, are neuroprotective against α -synuclein in nematode and rat neuronal cultures (Gitler et al., 2008).

As it has been mentioned before, RABIF allows the release of the GDP from the Rabs, but it does not act as a GEF, so the proteins remain inactive. An increase in inactive Rab10 might mitigate the deleterious effects of the pathogenic LRRK2. Also, preventing the degradation of Rab3A and Rab8A might have a neuroprotective effect. Therefore, overexpressing RABIF may be neuroprotective against PD.

4.2.4. EIF6 (TIF6)

EIF6 is a translation initiation factor regulated by insulin (Brina et al., 2015; Miluzio et al., 2016). In normal conditions, EIF6 binds to the 60S ribosome competing with the mRNA and preventing translation, however, in the presence of insulin, EIF6 gets phosphorylated and is released from the ribosomal subunit, allowing the formation of the active 80S complex, and increasing the translation efficiency, especially that of transcriptional factors involved in lipid synthesis and glycolysis. These lipids and glycolytic enzymes are involved in the cell cycle, cholesterol and lipid biosynthesis, glycolysis, and DNA packaging. Therefore, the downregulation of EIF6 would lead to a decrease in translation, deficits in 60S maturation and ribosome assembly, and to histone hyperacetylation that can be prevented by inhibiting HDACs (Brina et al., 2011; Brina et al., 2015; Miluzio et al., 2016). It has been reported that Interestingly, the expression of EIF6 is reduced in the brains of mice models of HD (Morton, A. J. et al., 2018; Morton, A. Jennifer et al., 2005; Rouillard et al., 2016), however, HD

patients present a decrease in histone acetylation rather than hyperacetylation (Peña-Altamira et al., 2013), suggesting that EIF6 is not the main factor responsible for the deacetylation in HD. Seeing as genes involved in ribosomal biosynthesis were highlighted in both the HD and the PD QTL analysis, the potential role of EIF6 in these diseases is most likely related to its involvement in transcription, so the upregulation of EIF6 might be protective.

4.2.5. *POLR1B* (*RPA135*)

RPA135 is an essential gene in yeast; it is part of the RNA polymerase I (RNA Pol I), which is responsible for the synthesis of ribosomal RNA (rRNA) and the maintenance of the nucleolar structure (Kobayashi et al., 1998). The deletion of this gene leads to a decrease in the number of genes for rRNA (rDNA) from 150 copies to approximately one half of the WT number, although this reduction does not affect the rate of rRNA synthesis – these experiments were performed in a *rpa135::LEU2* strain with a helper plasmid containing the 35S rRNA coding region to avoid lethality -. Considering that the loss of *RPA135* is lethal although it has no effect on the synthesis of rRNA, the essential role of *RPA135* may be the maintenance of the nucleolar structure by preserving the appropriate number of rDNA since the structure of the nucleolus is altered in the deletion strain and the number of rDNA repeats is maintained in the WT strains. The *RPA135* orthologue in humans, *POLR1B*, also forms the RNA Pol I (Werner et al., 2015). RNA Pol I is responsible for the synthesis of rRNA and may be involved in the early cellular differentiation of pluripotent stem cells into neurons by interacting with the ribosome modification enzymes through the TCOF1-NOLC1 complex and changing the translational program. Interestingly, nucleolar stress has been associated with several NDS including AD, PD and HD (Parlato & Kreiner, 2013; Parlato & Liss, 2014).

For example, downregulating the initiation transcription factors can cause HD-like phenotypes (Kreiner et al., 2013; Lee, J. et al., 2011; Lee, J. et al., 2014). The RNA Pol I transcription initiation factor UBF1 is downregulated in the striatum of HD mice, leading to deficits in ribosomal transcription (Lee et al., 2011; Lee et al., 2014). The decrease in UBF1 activity can be reverted with histone deacetylase inhibitors (trichostatin A), ameliorating the phenotype. Furthermore, knocking-down RRN3 - a RNA Pol I initiation transcription factor necessary for efficient transcription - in medium spiny neurons of mice causes a perturbation in nucleolar function that leads to the progressive loss of those neurons and HD-like motor symptoms (Kreiner et al., 2013). The nucleolar function impairment leads to the release of ribosomal proteins to the nucleoplasm, disrupting the activity of MDM2, ubiquitin ligase responsible for degrading p53, causing an increase in the level of p53, and therefore apoptosis (Kreiner et al., 2013; Parlato et al., 2008; Yuan et al., 2005).

Similarly, nucleolar stress causes an increase in p53 in MPTP mice models of PD (Rieker et al., 2011). This increase in p53 leads to downregulation of mTOR, mitochondrial dysfunction, increased oxidative stress and finally to the degeneration of the dopaminergic neurons. Remarkably, the ribosomal transcription disruption can also be linked to mitochondrial impairment in HD (Jesse et al., 2017). PGC-1 α is an inducer of mitochondrial biogenesis responsive to energy demand that associates with rDNA when active and recruits RNA Pol I and UBF1 under stress conditions in healthy individuals. However, this process is disrupted in HD patients since mHTT represses the transcription of many genes, including PGC-1 α , which leads to the disruption of ribosomal biogenesis and therefore to a reduction in the synthesis of proteins needed for ATP production.

Finally, rat models mimicking the dopaminergic loss of PD with intrastriatal injections of 6-hydroxydopamine develop alterations similar to those caused by PD -

nucleolar morphology alterations, decrease in nucleolar and cellular volume and cell death (Healy-Stoffel et al., 2013). Therefore, the upregulation of RNA Pol1 might be beneficial in both diseases.

4.2.6. *TAF2* (*TAF2*)

TAF2 is a scaffold protein that is part of the TFIID complex, which promotes transcription mediated by the RNA Polymerase II (RNA Pol II) (Kumar et al., 2014). In HD its function is impaired since mHTT interacts with the transcription machinery, modifies the chromatin structure by altering the histone post-translational modifications, and interacting with the DNA. Another component of TFIID, TAF1, is downregulated in HD and rescuing it to normal levels ameliorates the pathology (Hernández et al., 2020). However, this rescue might be unrelated to its role in transcription since TAF1 is also able to regulate apoptosis mediated by p53.

There is a decrease in nucleic acids in the cytoplasm of the neurons in the areas of the brain affected by neurodegeneration in PD patients (Zhang et al., 1999). This is caused by the accumulation of ROS, which causes oxidative stress and by an increase in 8-OHG, which can be introduced in the RNA instead of guanosine by RNA Pol II, causing the oxidation of the RNA (Abe et al., 2003; Nunomura et al., 2006; Zhang et al., 1999). Oxidative RNA damage begins in the early stages of NDs, and it can be detected by the increased levels of 8-OHG in the CSF of the patients. The oxidation of the nucleic acids leads to the inhibition of mitochondrial function due to the damage in mitochondrial DNA and the reduction of protein synthesis due to the damage in rRNA (Nunomura et al., 2006; Zhang et al., 1999).

4.2.7. *GYS1* and *GYS2* (*GYS2*)

GYS2 is a glycogen synthase that has two human orthologues, GYS1 and GYS2.

However, only *GSY1* has been reported to be expressed in the brain (Duran et al., 2013; Raben et al., 2001). This is interesting because neurons are a cell type that does not accumulate glycogen in normal conditions, but accumulations of glycogen in neurons of patients have been reported for several NDs (AD, PD, ALS and Lafora syndrome) (Inoue et al., 2006). The accumulation of glycogen is thought to be protective against ER stress. In mouse models of HD, the expression of mHTT in neurons causes proteasomal and oxidative stress, which increases the amount of active GYS1, increasing the level of glycogen and reducing cytotoxicity (Rai et al., 2018). Furthermore, glycogen delays the aggregation of mHTT in cells and the accumulated glycogen colocalizes with the mHTT aggregates *in vivo* and induces autophagy, which improves the clearance of mHTT aggregates. Therefore, the upregulation of *GSY1* may be able to delay the onset of both HD and PD.

4.2.8. *SLC25A42 (MRX21)*

Although *SLC25A42* is the most similar human gene to *MRX21*, they are both mitochondrial carriers but only share a 29% identity and 41% similarity, so the spectrum of molecules they transport may be different (Fiermonte et al., 2009). *SLC25A42* is a mitochondrial carrier expressed in neurons able to transport coenzyme A (CoA), dephospho-CoA, deoxy-adenine nucleotides, and adenosine 3', 5' -diphosphate (PAP), with its main role being the import of CoA in exchange for PAP (Fiermonte et al., 2009; Haitina et al., 2006). Since CoA is synthesised in the cytosol, it is necessary to import it into the mitochondria so the Krebs cycle can proceed. However, CoA is also involved in the urea cycle, β-oxidation, heme biosynthesis, branched-chain amino acid oxidation and protein acetylation.

Notably, the downregulation of this gene has been related to mitochondrial myopathy with muscle weakness, lactic acidosis, encephalopathy, developmental

regression, and epilepsy (Shamseldin et al., 2016). Both HD and PD present mitochondrial impairment, therefore the downregulation of SCL25A42 would likely worsen disease phenotypes.

In conclusion, these six genes were selected for validation because of their involvement in pathways and mechanisms that are known to be altered in HD and PD. Therefore, in the following chapters the effect of the downregulation and OE of the genes in the parental yeast strains, as well as the downregulation of *RAB1F*, *EIF6* and *SLC25A42* in fruit flies, will be assessed.

5. QTL validation in *Saccharomyces cerevisiae*

The genes that were selected as possible modifiers of mHTT and αSyn toxicity in the previous chapter must be validated in order to ascertain potential functional relevance. In order to determine their effect on the toxicity phenotype, these genes were overexpressed and deleted in the parental strains to test if there was any suppression or enhancement of the toxicity.

5.1. Results

5.1.1. Effect of the deletion of the modifier gene candidates on mHTT and αSyn toxicity in the parental strains

The knock-out strains were obtained by deleting the genes by substituting the gene with *LEU2*. Since the strains were haploid, it was only possible to delete the non-essential genes from the modifiers list: *DSS4*, *GYS2*, *PPM1*, *TAF2*, *TIF6* and *MRX21*. First of all, it was necessary to design primers that had sequences of homology with the *LEU2* gene, so it could be amplified and used as a marker for the transformation, and with the gene that was being deleted, so that sequence could be used for the homologous recombination during the transformation. As was the case for the primers used for the deletion of *LYS2* in the parental strains, the primers were designed with sequences homologous to the flanking regions of *LEU2*, and sequences that were complementary to the flanking regions of the gene that was going to be deleted (Table 2.1-5). Next, these primers along with genomic DNA from the WT laboratory strain were used to amplify the *LEU2* gene by PCR and the PCR product was used to transform the parental *ura3Δ0; leu2Δ0* strains. The transformants were selected on SD-LEU media since the *LEU2* gene should have been inserted interrupting the gene we desired to knock down (*gene::LEU2*). To

verify the gene was interrupted, a PCR with one primer homologous to the flanking region of the gene and the other one to *LEU2* was performed, so there was amplification only in the strains where *LEU2* was inserted interrupting the gene (Table 2.1-6, Figure 5.1-1). The recombination was successful for most targeted genes, but not achieved for *DSS4* and *TIF6* in the strain SX1, and for *TIF6* in BJ20. Finally, these deletion strains were transformed with both *HTT* constructs, and with the *SNCA* and *GFP* plasmids that had *URA3* as a marker. The transformants were selected in SD -URA -LEU to confirm they carried the deletion and the plasmid before being used for the PHENOS assay.

The strains were arrayed in two plates, one with the controls (*ura3Δ0* parental

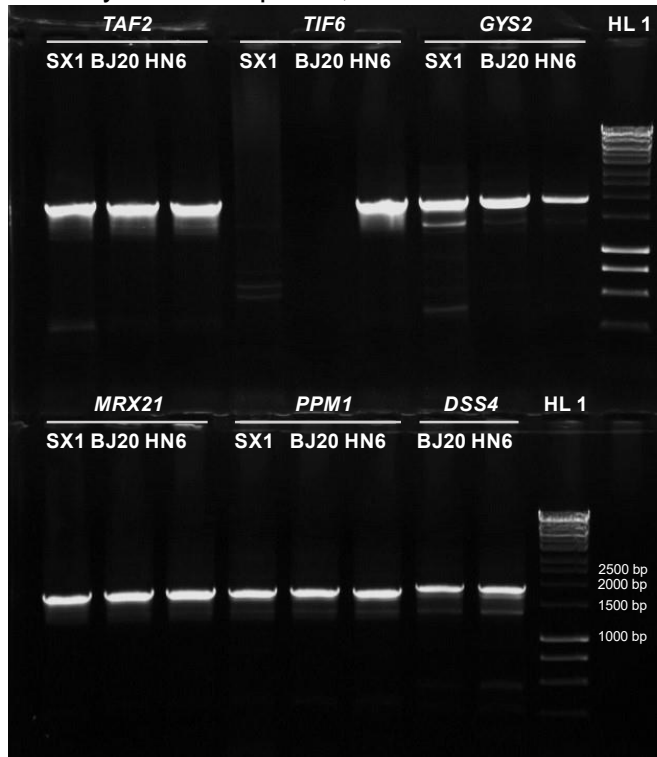


Figure 5.1-1. Most of the non-essential genes were deleted in all the strains using the homologous recombination transformation protocol.

Image of the agarose gel containing the PCR products for the validation of the parental strains' *gene::LEU2* transformants. The PCR was performed using one primer complementary to the flanking region of the gene and another one to the *LEU2* gene so only transformants in which *LEU2* was inserted would be amplified. The expected fragment size was between 1865 and 2130 bp depending on the gene that was deleted (Table 2.1-6), which corresponds to the size seen on the gel when compared to Hyper ladder 1 (HL 1). This gel shows that *TAF2*, *GYS2*, *MRX21* and *PPM1* were deleted in all the parental strains, *DSS4* was deleted in HN6 and BJ20, and *TIF6* was deleted only in HN6.

strains with *GFP*, parental and deletion strains with *HTT* and with *GFP*) and the second with the experimental strains (deletion strains with *GFP*, and parental and deletion strains with *mHTT* and *SNCA*). The parentals and deletion strains were transformed with *GFP* because they were *ura3Δ0* and therefore, unable to grow in SD-URA media without the plasmid. Since PHENOS only compares strains that are in the same position, it was necessary to have the deletion-GFP strains in the control plate to compare it against the *αSyn* transformants to determine the effect of *αSyn* toxicity, and also in the experimental plate to compare it against the parentals to determine if the deletion had any deleterious effects. None of the parental strains presented severe growth deficits due to the deletions, so it was possible to use them for the validation experiments (data not shown). The effect on growth due to the toxic proteins on each strain was determined based on the difference in maximum growth (dMG) and in maximum speed (dMS) between the toxic and the control transformants. This provides an indication of the difference in growth due to the toxic protein. Then, the effect of the deletion on the toxicity of *mHTT* and *αSyn* was calculated by comparing the dMG and dMS of the gene deletion strains to the control parental using a one-way ANOVA.

In the resistant strain SX1, only the deletions of *GYS2*, *PPM1*, *TAF2* and *MRX21* were studied (Figure 5.1-2, Table 5.1-1). There was no significant difference in dMG nor in dMS between the controls - *HTT* and *GFP* - and their corresponding toxic transformants - *mHTT* and *αSyn* - of the parental SX1 strain. This resistance was also present in the *MRX21* deletion strain, suggesting that the gene is not involved in the suppression of *mHTT* and *αSyn* toxicity in the SX1 background. On the other hand, the deletions of the remaining three genes caused growth deficits. The deletion of *PPM1* was the least damaging, it did not affect MG, but it significantly slowed growth in the *mHTT* model (37% dMS). This dMS was significantly different from *HTT*

SX1, meaning that the deletion enhanced mHTT toxicity. However, it had a worse effect in the PD model, where both the MG and the MS were significantly affected (9% dMG and 41% dMS). Again, the dMS was significantly different from the control, meaning it also increased αSyn toxicity. The deletions of *GYS2* and *TAF2* were more harmful, causing a significant decrease in both MG (14% and 22% in HD, and 14% and 13% in PD respectively) and in MS (54% and 60% in HD, and 45% and 39% in PD respectively). Both deletions significantly increased dMG and DMS compared to the HD SX1 control, and also increased dMS in the PD control, suggesting that both deletions enhance toxicity.

Table 5.1-1. Effect of the deletion of the possible modifier genes on mHTT and αSyn toxicity in the parental strains.

Deletions			WT	<i>dss4</i>	<i>gys2</i>	<i>ppm1</i>	<i>taf2</i>	<i>tif6</i>	<i>mrx21</i>
SX1	HD	dMG	-5	-	14 * ₃	2	22 * ₄	-	1
		dMS	5	-	54 * ₃	37 * ₁	60 * ₄	-	14
	PD	dMG	6	-	14	9	13	-	5
		dMS	-8	-	45 * ₃	41 * ₂	39 * ₂	-	14
HN6	HD	dMG	29	22	14 * ₂	14 * ₁	18	10 * ₂	20
		dMS	59	47	46	43 * ₁	47	37 * ₂	39 * ₂
	PD	dMG	14	8	9	10	19	8	16
		dMS	20	28	30	32 * ₁	30	29	24
BJ20	HD	dMG	29	8 * ₃	4 * ₄	9 * ₃	5 * ₄	-	3 * ₄
		dMS	66	29 * ₃	1 * ₄	21 * ₄	-8 * ₄	-	1 * ₄
	PD	dMG	18	3	7	36 * ₂	8	-	3 * ₁
		dMS	32	7 * ₁	-8 * ₃	67 * ₃	-10 * ₃	-	-14 * ₄

dMG = 100 - [(max growth toxic / max growth control) x 100].

dMS = 100 - [(max slope toxic / max slope control) x 100].

One-way ANOVA corrected by Tukey's test. *₁ P < 0.05; *₂ P < 0.01; *₃ P < 0.001; *₄ P < 0.001.

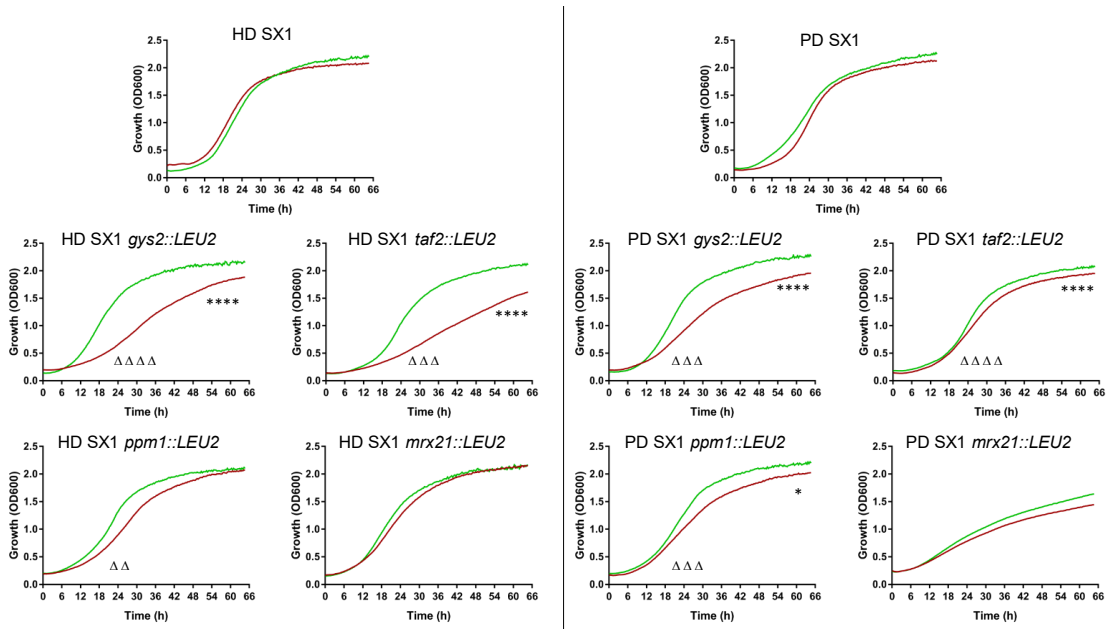


Figure 5.1-2. The deletion of *GYS2*, *TAF2* and *PPM1* in the resistant strain SX1 enhances toxicity of mHTT and α Syn.

PHENOS growth curves of HD (left) and PD (right) yeast models showing the effect of the deletion of *GYS2*, *TAF2*, *PPM1* and *MRX21* on the toxicity of mHTT and α Syn. There is no significant difference in MG or MS when expressing the control (HTT and GFP; green) and the toxic proteins (mHTT and α Syn; red) in the parental strain SX1, nor when *MRX21* is deleted. The deletion of *GYS2* and *TAF2* cause a significant decrease in MG and MS due to both mHTT and α Syn, while the deletion of *PPM1* enhances the effect of α Syn, decreasing MG and MS, and of mHTT, decreasing only MS.

Two-way ANOVA corrected by Tukey's multiple comparisons test. * P < 0.05; ** P < 0.01; *** P < 0.001; **** P < 0.0001. MG significance is shown with stars (*) while MS significance is shown with triangles (Δ).

The sensitive strain HN6 showed significant differences in MG and MS between the control and the toxic protein in both the HD and the PD models (Figure 5.1-3, Table 5.1-1) compared to the HD SX1 control. When modelling HD, the MG in HN6 was 29% lower in the mHTT transformant than in the HTT one, and the MS was 59% lower in the α Syn than in the GFP transformant. All six gene deletions were partially protective against mHTT toxicity, however, there was still a significant dMG and dMS between the control and the toxic transformants in all the deletion strains. Among them, the strongest rescue was due to deletion of *TIF6*, where dMG was only 10% and dMS 37%, both significantly higher than in the parental HN6 strain. The rescue

due to *GYS2* and *PPM1* deletion was slightly lower, both of which presented a 14% dMG due to mHTT, and a 46% and 43% dMS respectively. The MG rescue was significant in both cases, but the MS rescue was only significant with the *PPM1* deletion. The HN6 model of PD showed a 14% dMG and a 20% dMS due to αSyn toxicity. Contrary to the results of the HD model, none of the deletions significantly

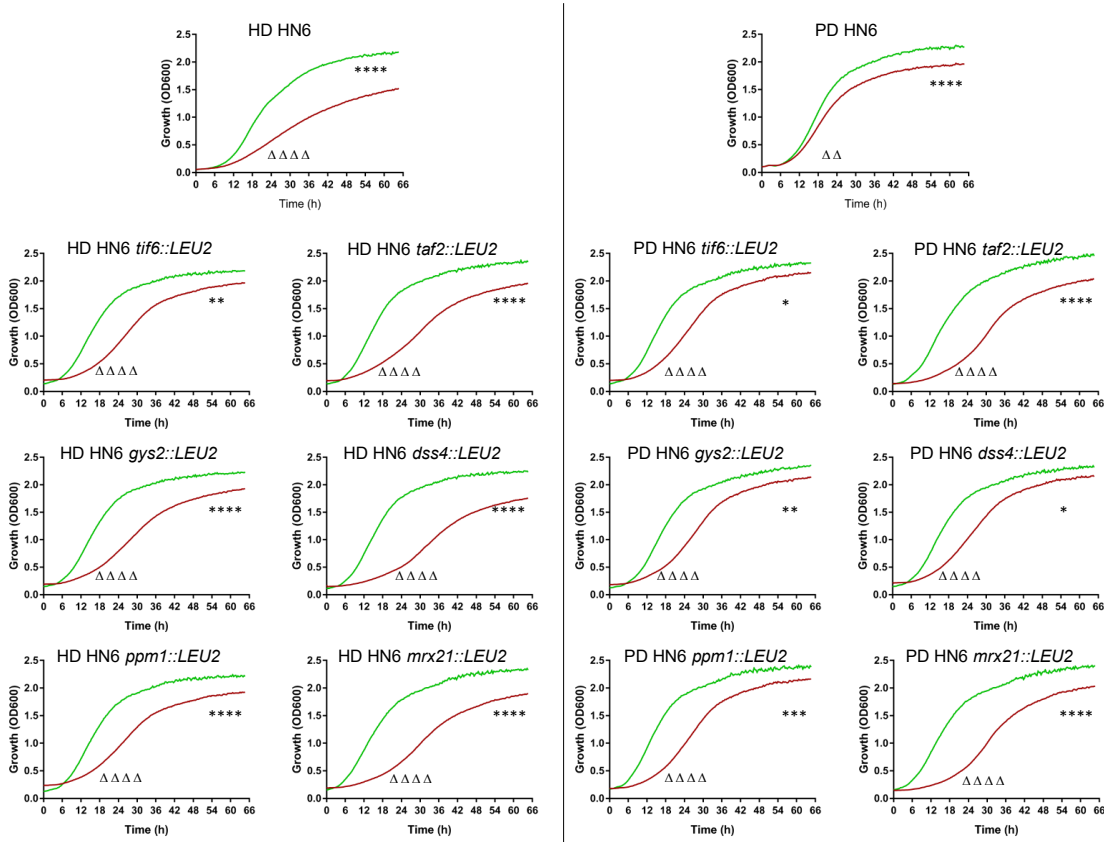


Figure 5.1-3. The deletion of *TIF6*, *PPM1* and *GYS2* reduces toxicity of mHTT, and the deletion of *TIF6* and *DSS4* reduces the toxicity of αSyn in the sensitive strain HN6.

PHENOS growth curves of HD (left) and PD (right) yeast models showing the effect of the deletion of *TIF6*, *GYS2*, *DSS4*, *TAF2*, *PPM1* and *MRX21* on the toxicity of mHTT and αSyn; HTT and GFP (green), mHTT and αSyn (red). There is a significant decrease in MG and MS between the control and the toxic transformants of the strain HN6. There is a partial rescue in HD when deleting *TIF6*, and a smaller rescue when deleting *PPM1* and *GYS2*, although the decrease in MG and MS caused by mHTT and αSyn is still significant. The deletion of *DSS4* and *MRX21* had almost no effect in ameliorating the growth deficits caused by mHTT. In PD there is a partial rescue in MG when deleting *TIF6* and *DSS4*, but it worsens the MS. The deletion of *TAF2* and *MRX21* slightly enhance αSyn toxicity.

Two-way ANOVA corrected by Tukey's multiple comparisons test. * P < 0.05; ** P < 0.01; *** P < 0.001; **** P < 0.0001. MG significance is shown with stars (*) while MS significance is shown with triangles (Δ).

rescued α Syn toxicity compared to the HN6 parental strain. Even though the protection was not significant, the deletions of *DSS4* and *TIF6* achieved the greatest rescue, both of them presented a dMG of only 8% compared to the 14% of the WT parental, but their growth was slower at 28% and 29% dMS, respectively, compared to the 20% of the WT parental. The only deletion that enhanced α Syn toxicity was *PPM1*, in which dMS was 32%.

The remaining sensitive strain BJ20 showed significant deficits in MG (29%) and MS (66%) due to the expression of mHTT (Figure 5.1-4, Table 5.1-1). The five gene deletions were significantly protective against mHTT toxicity, with only *DSS4* presenting a significantly slower growth when expressing mHTT (29% dMS) and *PPM1* a significant decrease in MG (9%). The other three deletions - *GYS2*, *TAF2* and *MRX21* - rescued the phenotype to HTT levels. When modelling PD, BJ20 showed a significant 18% decrease in MG and 32% in MS. Four out of the five deletions showed a smaller decrease in MG and MS. The strongest rescue was achieved with the deletion of *MRX21* (3% dMG and 14% dMS) which was the only strain to significantly rescue MG. On the contrary, the deletion of *PPM1* significantly enhanced α Syn toxicity, causing a significant decrease in MG (36%) and MS (67%) that doubled those shown by the WT parental.

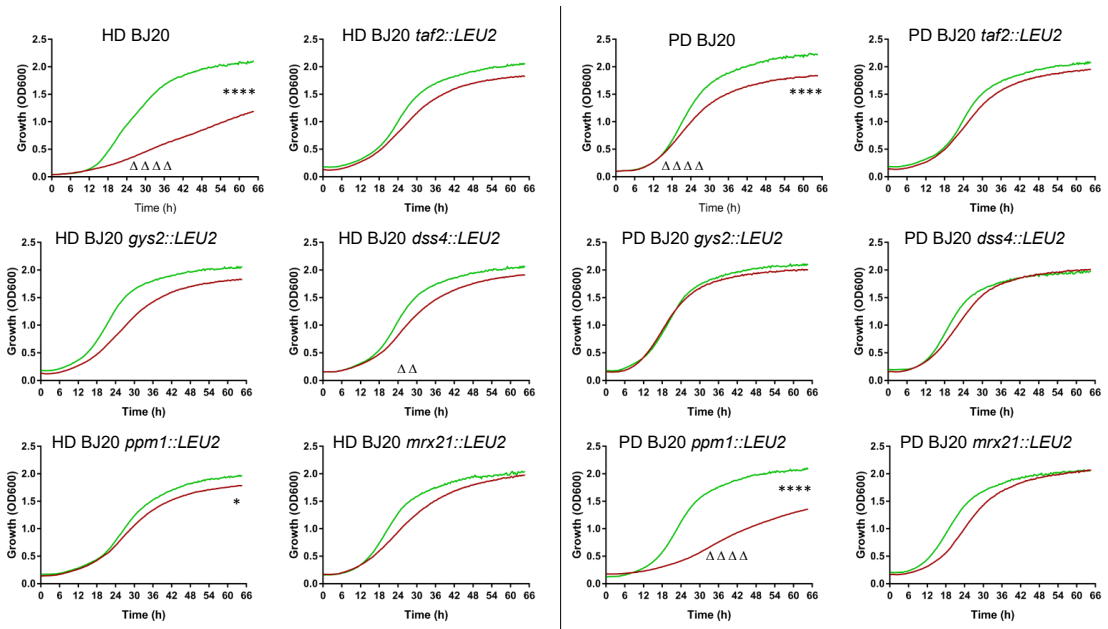


Figure 5.1-4. The deletions of *TAF2*, *GYS2*, *DSS4*, *PPM1* and *MRX21* in the sensitive strain BJ20 decrease toxicity of mHTT, and all except *PPM1* decrease α Syn toxicity.

PHENOS growth curves of HD (left) and PD (right) yeast models showing the effect of the deletion of *GYS2*, *DSS4*, *TAF2*, *PPM1* and *MRX21* in the toxicity of mHTT and α Syn; HTT and GFP (green), mHTT and α Syn (red). There is a significant decrease in MG and MS between the control and the toxic transformants of the strain BJ20. There is a partial rescue in mHTT toxicity when deleting *PPM1* (MG increase) and *DSS4* (MS increase) and an almost complete rescue when deleting *TAF2*, *GYS2* and *MRX21*. In the PD model, there is an almost complete rescue when deleting *TAF2*, *GYS2*, *DSS4* and *MRX21*, but there is an enhancement of α Syn toxicity when deleting *PPM1* (reduction of MG and MS).

Two-way ANOVA corrected by Tukey's multiple comparisons test. * $P < 0.05$; ** $P < 0.01$; **** $P < 0.0001$. MG significance is shown with stars (*) while MS significance is shown with triangles (Δ).

5.1.2. Effect of the OE of the modifier gene candidates on mHTT and α Syn toxicity in the parental strains

The OE strains were obtained by transforming the *ura3Δ0*; *lys2::LEU2* parental strains with the corresponding OE plasmid from the Yeast ORF collection (Horizon) and the *HTT* and *SNCA* plasmids. Since the plasmids from the Yeast ORF collection had *URA3* as a marker, it was necessary to generate *SNCA* and *GFP* constructs that had a different auxotrophic marker. Given that we had *HTT* plasmids with *LYS2* as a

marker, the *SNCA* and *GFP* constructs were cloned into the pRS426 plasmid, the same 2-micron plasmid with a *GAL1* promoter and *LYS2* as marker used for the *HTT* constructs. This was achieved by amplifying the gene by PCR with a high-fidelity polymerase to avoid errors and primers that were homologous to the flanking regions of the gene and had a RE digestion target at the end. The PCR product was cloned into a pJet vector and transformed into bacteria in order to increase the amount of plasmid. This was necessary because the REs were unable to recognise their targets in the PCR product since it was too close to the edge of the DNA fragment, so cloning the sequence into the plasmid solved this problem. Both the pRS426 and the pJet plasmids carrying *GFP* and *SNCA* were digested with Sall, the digestion product was run on an agarose gel, and the linearized plasmid and the fragments corresponding to the size of the genes were purified, ligated, and transformed into bacteria to keep as stock. Both plasmids were sequenced to confirm there were no mutations or deletions in the sequences of the genes due to the cloning process. The last step consisted of transforming parental strains with the plasmids, inducing the gene expression with galactose, and observing the samples under the fluorescent microscope to confirm they were being expressed. As can be seen in Figure 5.1-5, all the parental strains were able to express GFP and αSyn from the new plasmids, presenting a diffuse cytoplasmic signal due to GFP and inclusions or ring-like signal due to αSyn. Finally, the parental strains transformed with the *LYS2* vectors carrying *HTT*, *SNCA* and *GFP* were transformed with the OE plasmids, and the transformants were selected in SD -URA -LYS to confirm they were carrying both plasmids before being used for the PHENOS assay.

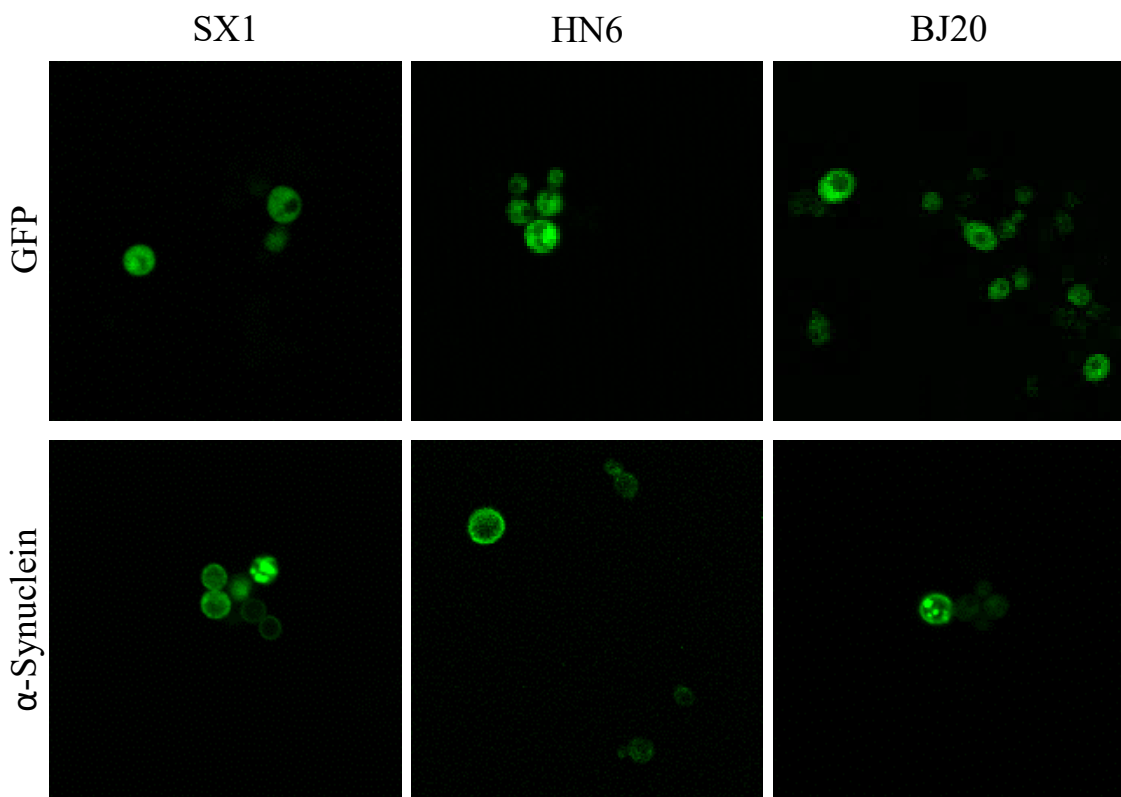


Figure 5.1-5. There is expression of GFP and α Syn to confirm the cloning of those genes into the pRS426 LYS2 plasmids in the parental strains.

Confocal fluorescence images of the parental strains transformed with the *GFP* and *SNCA* pRS426 plasmids after 16 hours of induction with galactose. The presence of signal from both the *GFP* and the *SNCA* plasmids indicates that the genes were properly cloned into the plasmid. As with the original *URA3* plasmid, the *GFP* transformants of all the parental strains show a diffuse signal throughout the cytoplasm, while the α Syn stays close to the cellular membrane forming a ring-like signal or forms intracellular aggregates.

From the original list of eight possible phenotype modifier genes, only four were available in the OE collection: *DSS4*, *TAF2*, *TIF6* and *MRX21*. After transforming the parental strains, they were arrayed in two plates, one with the controls (*ura3Δ0*; *lys2::LEU2* parental strains with *GFP*, parental and OE strains with *HTT* and with *GFP*) and the second with the experimental strains (OE strains with *GFP*, and WT and deletion strains with *mHTT* and *SNCA*). The OE-GFP strains were present in the control plate to compare them against the α Syn transformants to determine the effect of α Syn toxicity, and also in the experimental plate to compare them against the parents-GFP to determine if the OE of the genes had any deleterious effects. None

of the parental strains presented severe growth deficits due to the OE of any gene, so they were used for the validation experiments (data not shown). As in the deletion experiment, the effect of the toxic proteins in growth on each strain was determined based on the dMG and the dMS between the toxic and the control transformants. Then, the effect of the gene OE on the toxicity of mHTT and αSyn was calculated by comparing the dMG and dMS of the deletion strains to the control parental using a one-way ANOVA.

As expected, the resistant strain SX1 showed no significant differences in growth due to the expression of the toxic proteins (Figure 5.1-6, Table 5.1-2). In the HD model, the *TIF6* and *DSS4* OE strains presented resistant phenotypes resembling the WT parental. On the contrary, the OE of *TAF2* led to a 9% decrease in MG due to mHTT expression, and more noticeably, the OE of *MRX21* caused a significant decrease in both MG (21%) and MS (28%). The OE of those genes significantly increased mHTT toxicity compared to the SX1 control. Interestingly, in the PD model, *TAF2* and *TIF6* OE strains showed resistant phenotypes, while the OE of *DSS4* and *MRX21* had no significant effect on αSyn toxicity.

Table 5.1-2. Effect of the OE of the possible modifier genes on mHTT and αSyn toxicity in the parental strains.

OE			WT	<i>DSS4</i>	<i>TAF2</i>	<i>TIF6</i>	<i>MRX21</i>
SX1	HD	dMG	-6	1	9 * ₄	-7	21 * ₄
		dMS	-2	4	8	-20	28 * ₁
	PD	dMG	1	7	-2	-11 * ₃	9
		dMS	11	10	-13 * ₁	-33 * ₂	4
HN6	HD	dMG	15	-2 * ₄	-1 * ₄	3 * ₄	-4 * ₄
		dMS	24	-3 * ₄	3 * ₃	25	-4 * ₄
	PD	dMG	67	72	66	59 * ₁	66
		dMS	75	72	60 * ₂	56 * ₄	64 * ₁
BJ20	HD	dMG	16	19	19	12	27
		dMS	39	39	14 * ₁	14 * ₁	40
	PD	dMG	5	4	17	-	-5 * ₁
		dMS	3	-5	31 * ₂	-	-10 * ₁

dMG = 100 – [(max growth toxic / max growth control) x 100].

dMS = 100 – [(max slope toxic / max slope control) x 100].

One-way ANOVA corrected by Tukey's test. *₁ P < 0.05; *₂ P < 0.01; *₃ P < 0.001; *₄ P < 0.0001.

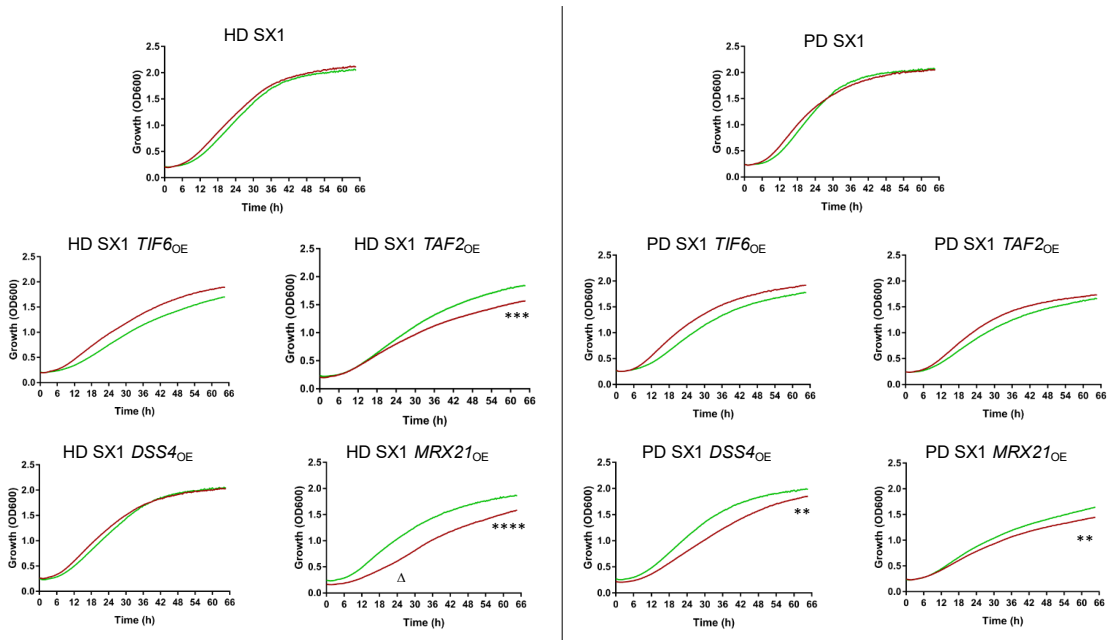


Figure 5.1-6. The OE of *TAF2* and *MRX21* in the resistant strain SX1 enhances toxicity of mHTT, and the OE of *DSS4* and *MRX21* of α Syn.

PHENOS growth curves of HD (left) and PD (right) yeast models showing the effect of the OE of *TIF6*, *TAF2*, *DSS4* and *MRX21* on the toxicity of mHTT and α Syn. There is no significant difference in MG or MS when expressing the control (HTT and GFP, green) and the toxic proteins (mHTT and α Syn, red) in the strain SX1, nor when *TIF6* is overexpressed. There is no significant effect when *DSS4* is overexpressed in the HD model, but there is a reduction in MG in the PD model. The OE of *TAF2* has no effect on α Syn toxicity but enhances mHTT toxicity causing a decrease in MG. *MRX21* OE enhances toxicity of both mHTT and α Syn.

Two-way ANOVA corrected by Tukey's multiple comparisons test. * P < 0.05; ** P < 0.01; *** P < 0.001; **** P < 0.0001. MG significance is shown with stars (*) while MS significance is shown with triangles (Δ).

The sensitive strain HN6 showed a milder sensitivity to mHTT (15% MG and 24% MS decrease) and a stronger sensitivity to α Syn toxicity (67% MG and 75% MS decrease) when expressed from the *LYS2* plasmid than from the *URA3* one (Figure 5.1-7, Table 5.1-2). Surprisingly, the OE of *DSS4*, *TAF2* and *MRX21* rescued MG and MS in the mHTT strain to WT levels, while the OE of *TIF6* rescued MG but had no effect on MS (25% decrease due to mHTT expression). On the contrary, none of the OE strains was able to rescue the growth defects caused by α Syn. There was significant rescue due to *TIF6* OE (59% MG and 56% MS decrease), but the growth was still severely impaired. There was also a significant rescue in MS when

overexpressing *TAF2* and *MRX21*, but it was barely noticeable.

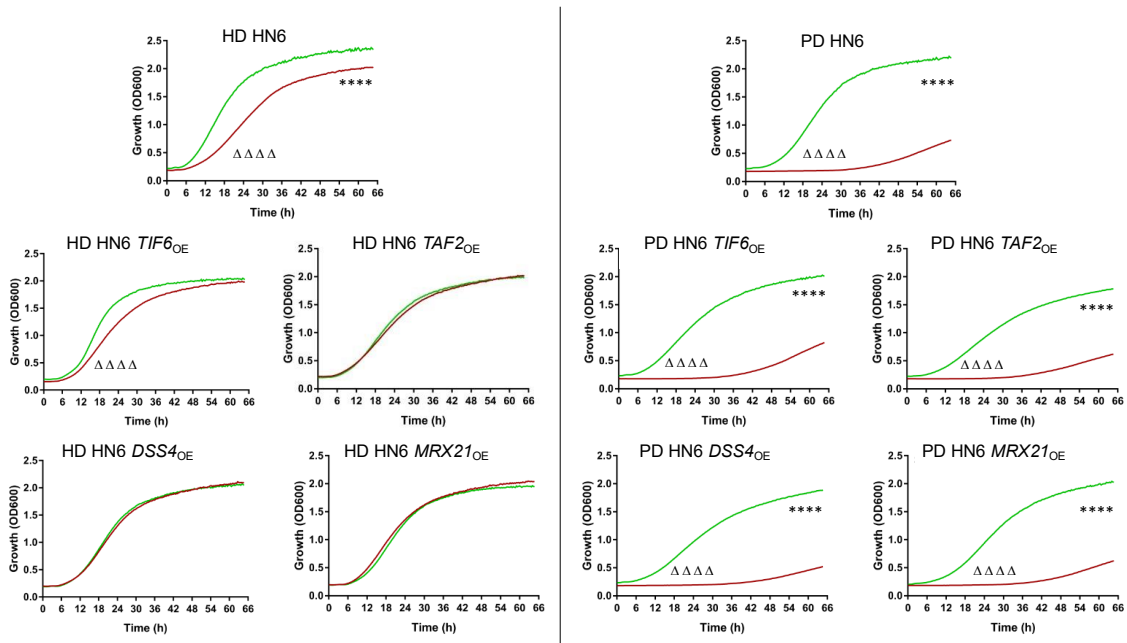


Figure 5.1-7. The OE of *TIF6*, *TAF2*, *DSS4* and *MRX21* is protective against mHTT toxicity in the sensitive strain HN6.

PHENOS growth curves of HD (left) and PD (right) yeast models showing the effect of the OE of *TIF6*, *TAF2*, *DSS4* and *MRX21* in the toxicity of mHTT and α Syn -HTT and GFP (green), mHTT and α Syn (red)-. There is a significant decrease in MG and MS between the control and the toxic transformants of the strain HN6. In the HD model, there is a total rescue of mHTT toxicity when overexpressing *DSS4*, *TAF2* and *MRX21*, and a partial rescue when overexpressing *TIF6* (significant MS decrease). In the PD model, there is a small rescue of α Syn toxicity due to *TIF6* OE, but the MG and MS when expressing mHTT were less than half than when expressing HTT. The other gene OE strains had barely any effect on improving growth.

Two-way ANOVA corrected by Tukey's multiple comparisons test. * P < 0.05; ** P < 0.01; *** P < 0.001; **** P < 0.0001. MG significance is shown with stars (*) while MS significance is shown with triangles (Δ).

Interestingly, both the HD and PD models of BJ20 present milder phenotypes when expressing the proteins from the *LYS2* plasmids than from the *URA3* (Figure 5.1-8, Table 5.1-2). The expression of mHTT in BJ20 causes a reduction in MG of 16% and in MS of 39% compared to the control HTT. The OE of *TIF6* in this strain slightly improves MG (12% dMG) and partially rescues the defects in MS (14% dMS). Both *TAF2* and *DSS4* OE slightly worsen the defects in MG (19% dMG), but while *DSS4* has no effect on MS, *TAF2* improves it (14% dMS). The last OE strain, *MRX21*,

worsens MG and slightly worsens MS (27% and 40% decrease respectively) although the effect on mHTT toxicity is not significant. Interestingly, there are no significant growth impairments associated with the expression of α Syn in the WT BJ20 strain, and this resistance is also present when overexpressing *DSS4* and *MRX21*. On the contrary, *TAF2* OE enhances α Syn toxicity causing a 17% dMG and a 31% dMS compared to those of the GFP transformant, however only the decrease in MS is significant. The transformation of the *TIF6* OE strain with *GFP* and *SNCA* did not work.

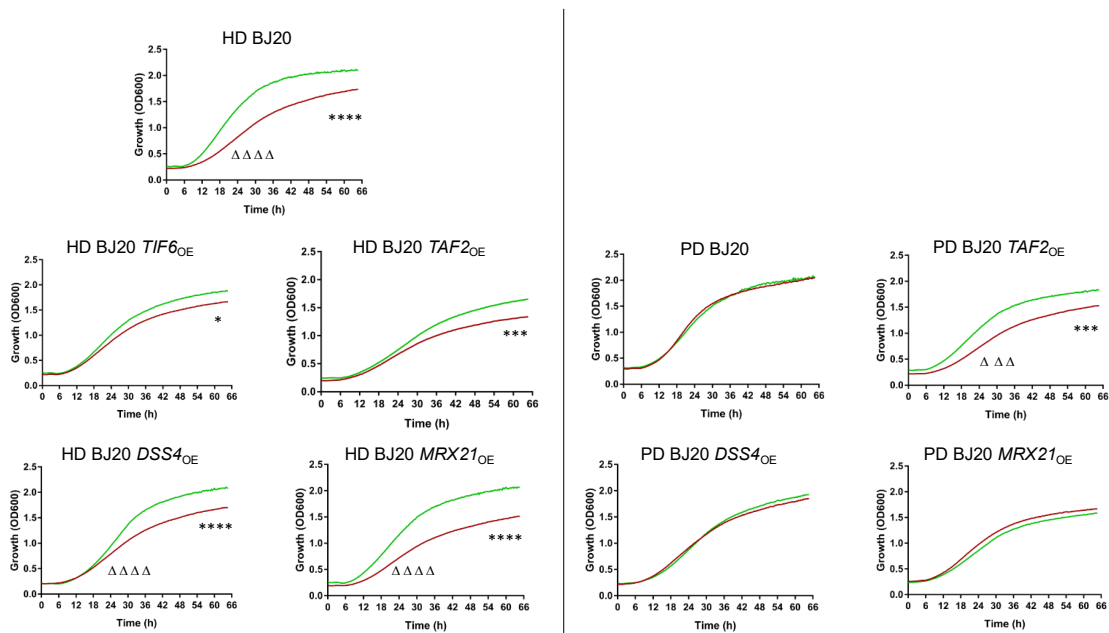


Figure 5.1-8. OE of *TIF6* in the sensitive strain BJ20 decreases toxicity of mHTT. PHENOS growth curves of HD (left) and PD (right) yeast models showing the effect of the OE of *TIF6*, *TAF2*, *DSS4* and *MRX21* on the toxicity of mHTT and α Syn; HTT and GFP (green), mHTT and α Syn (red). There is a significant decrease in MG and MS between the HTT and the mHTT transformants of the strain BJ20 while there is no significant difference between the GFP and α Syn transformants. In the HD model, the OE of *TIF6* is slightly protective, while the OE of *MRX21* is detrimental. *TAF2* and *DSS4* OE strains have no effect on improving growth. In the PD model, the OE of *DSS4* and *MRX21* do not enhance the toxicity of α Syn, while the OE of *TAF2* leads to a significant decrease in MG and MS due to α Syn toxicity. The transformation for the OE of *TIF6* did not work for the PD model.

Two-way ANOVA corrected by Tukey's multiple comparisons test. * P < 0.05; *** P < 0.001; **** P < 0.0001. MG's significance is shown with stars (*) while MS' is shown with triangles (Δ).

5.1.3. Effect of the deletion of other possible modifier genes on mHTT and αSyn toxicity in BY4741

Lastly, nine other candidate genes that were present on both the HD and PD QTL lists were studied. These genes were present in polygenic QTL with four or fewer genes and were non-essential. Six of the genes appeared in pairs within three QTL: *RPD3* and *PEX6*, *YCR043C* and *PER1*, and *SNT1* and *ELO2*. The remaining three were in different QTL and were the only gene from their respective QTL that was present on both HD and PD lists: *GIN4*, *PPZ2* and *BPH1*. These strains were obtained from the Stanford Genome Technology Centre's Yeast Knock-Out collection, which used kanamycin (KanMX) cassettes to replace the ORF in the laboratory strain BY4741 (Chu & Davis, 2008). These strains had *URA3* deleted as a marker, so the *URA3* plasmids were used for the experiments. The original BY4741 as well as the deletion strains were transformed with the *HTT*, *mHTT*, *GFP* and *SNCA* constructs. As it was done with the parental deletion strains, the controls and the toxic transformants were arrayed in different plates to compare the differences in growth between the HTT and mHTT transformants, the GFP and αSyn transformants, and the control and deletion strains. As in the previous experiments, the effect in growth of the toxic proteins on each strain was determined based on the dMG and the dMS between the toxic and the control transformants. Then, the effect of the deletion on the toxicity of mHTT and αSyn was calculated by comparing the dMG and dMS of the gene deletion strains to the control BY4741 using a one-way ANOVA.

Although none of the genes were essential and therefore none of the deletions were lethal, the deletion of *GIN4* and *PEX6* caused a vast extension of the lag phase that delayed the beginning of the logarithmic phase to 43 and 52 hours respectively. Since the experiments measured the optic density of the plates for only 66 hours, those two strains were unable to reach the stationary phase and therefore the MG

and MS used for the calculations shown in Table 5.1-3 are probably inaccurate.

The strain BY4741 is sensitive to mHTT and α Syn toxicity, and their expression caused a significant delay in growth (28% and 41% dMS respectively), although they had no significant effect on MG (Figure 5.1-9, Table 5.1-3). Interestingly, the expression of the toxic constructs caused a significant decrease in MS in all the deletion strains too, however only the deletion of *PER1* and *GIN4* enhanced α Syn toxicity enough to increase the dMS. Furthermore, *GIN4* deletion also increased α Syn toxicity enough to affect dMG. *SNT1* deletion was the only one with a lower dMS (21% in both HD and PD) and also presented a smaller dMG than the control in both disease models, but the protective effect was not significant when compared to the control BY4741. Among the other deletion strains, several presented differences in MG between the control and the toxic transformants. *BPH1* and *ELO2* presented significant differences between HTT and mHTT (14% and 15% dMG respectively), while *PER1* and *PPZ2* presented differences between GFP and α Syn (38% and 24% dMG), and *YCR043C* presented differences in both (24% dMG HD and 14% in PD) but none of these caused significant changes in the phenotype.

Table 5.1-3. Effect of the deletion of possible modifier genes in mHTT and αSyn toxicity in the laboratory strain BY4741.

Deletion	HD		PD	
	MG	MS	MG	MS
WT	11	28	12	41
bph1	14	51	7	50
snt1	-2	21	4	21
elo2	15	49	12	50
ycr043c	24	50	14	47
per1	8	51	38	67 *1
ppz2	12	50	24	59
gin4	28	46	60 *2	72 *3
pex6	41	87 *4	22	72 *1
rpd3	10	46	9	58

dMG = 100 – [(max growth toxic / max growth control) x 100].

dMS = 100 – [(max slope toxic / max slope control) x 100].

One-way ANOVA corrected by Tukey's test. *1 p < 0.05; *2 p < 0.01; *3 p < 0.001; *4 p < 0.001.

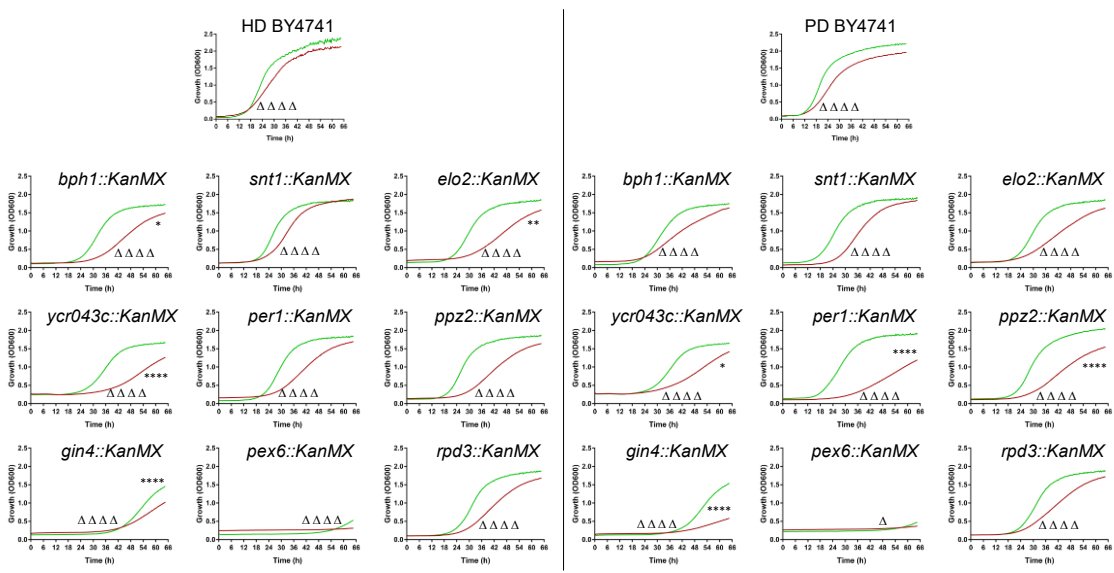


Figure 5.1-9. The deletion of *SNT1* is protective against mHTT and α Syn toxicity in the laboratory strain BY4741.

PHENOS growth curves of HD (left) and PD (right) yeast models showing the effect of the deletion of *BPH1*, *SNT1*, *ELO2*, *YCR043C*, *PER1*, *PPZ2*, *GIN4*, *PEX6* and *RPD3* in the laboratory strain BY4741 on the toxicity of mHTT and α Syn (HTT and GFP, green; mHTT and α Syn, red). There is a small reduction of MG and a significant decrease in MS between the control and the toxic transformants of the strain BY4741. In the HD model, the deletion of *SNT1* improves both MG and MS, while the deletion of *BPH1*, *ELO2*, *YCR043C* and *GIN4* enhance the toxicity of mHTT and decrease MG. The deletion of *PER1*, *PPZ2* and *RPD3* have no effect in MG but slow MS. In the PD model, the deletion of *SNT1* also improves both MG and MS, while the deletions of *YCR043C*, *PER1*, *PPZ2* and *GIN4* enhance the toxicity of α Syn. *BPH1*, *ELO2* and *YNK330W* deletions have no significant effect on MG but decrease MS. The deletion of both *PEX6* and *GIN4* increase the lag phase considerably.

Two-way ANOVA corrected by Tukey's multiple comparisons test. * $P < 0.05$; ** $P < 0.01$; **** $P < 0.0001$. MG significance is shown with stars (*) while MS significance is shown with triangles (Δ).

5.2. Discussion

Previous research demonstrates that it is possible to uncover phenotype modifier genes of mHTT and α Syn by expressing the causative proteins in ORF knock-out and OE yeast collections (Giorgini et al., 2005; Mason et al., 2013; Willingham et al., 2003). Therefore, a similar approach can be used to validate the possible modifier genes that were discovered during the QTL analysis. In the previous chapter, eight

genes that might be involved in the sensitivity to mHTT and αSyn toxicity were selected for validation: *FAR10*, *GSY2*, *DSS4*, *TIF6*, *PPM1*, *MRX21*, *RPA135* and *TAF2*. These genes were identified in the QTL analysis of both disease models, were not already known modifier genes, nor appeared as toxicity enhancers or suppressors in previous yeast studies (Giorgini et al., 2005; Mason et al., 2013), and had human and fly orthologues that were expressed in the brain. Among them, two were essential genes and therefore could not be deleted in the haploid parental strains. In future studies it would be possible to study the effect of deleting the two essential genes, *FAR10* and *RPA135*, by generating hemizygote diploid strains that had only one allele deleted, meaning they would still have a WT allele of the essential gene available. However, it would be necessary to characterize the effect of the toxic proteins in the diploid parental strains since it might differ from the effect in the haploids.

In order to see if these genes affected the susceptibility to mHTT and αSyn toxicity, they were deleted and overexpressed in the parental strains. Performing the experiment in three strains with different susceptibility levels to the toxicity of the proteins allows a better characterization of the effect of these modifications: a subtle toxicity enhancement might be easier to appreciate in a resistant strain than in a sensitive strain, and while the suppression of toxicity can only be studied in sensitive strains, it might have a different effect depending on the genetic background. The deletion experiments were performed by replacing the desired gene with *LEU2*. Since the strains employed were haploid, only the six non-essential genes from the previous list were studied (*GSY2*, *DSS4*, *TIF6*, *PPM1*, *MRX21* and *TAF2*). Since the gene deletion was performed via homologous recombination with a DNA fragment, and that type of transformation has low efficiency, the deletion of *TIF6* only worked in the HN6 strain and the deletion of *DSS4* in SX1 failed.

Among the deletions, that of *PPM1* yielded the most noticeable phenotypic modulation. The deletion of *PPM1* enhanced αSyn toxicity in the three parental strains, especially in BJ20 in which it doubled the dMG and the dMS. This enhancement of αSyn toxicity correlated with the literature, since the human orthologue of *PPM1*, *LCMT1*, is known to be downregulated in PD (Javadpour et al., 2019). This downregulation causes a decrease in the amount of active PP2A, a protein involved in metabolism, neural development, transcription, the cell cycle, proliferation and apoptosis, and whose downregulation has been related to the increase in phosphorylation of αSyn Ser129 and the formation of aggregates (Javadpour et al., 2019; Sontag & Sontag, 2014)

As mentioned before, in humans the Hippo pathway, which is involved in transcription is altered in HD (Bae et al., 2017; Hwang & Pallas, 2014; Mueller et al., 2018). PP2A is involved in this pathway, it inactivates pMST2, making it unable to phosphorylate YAP, which translocates to the nucleus and promotes transcription of cell survival factors. Low levels of *PPM1* lead to a decrease in active PP2A and to the degradation of YAP. Interestingly, low YAP levels due to an increase in pMST2 have been described in the brains of HD patients and are known to cause transcriptional dysregulation and cell death (Mueller et al., 2018). Although the Hippo pathway is not present in yeast and there is no YAP orthologue, the FEAR/MEN pathways are thought to be their precursor (Marston, 2014). In them, PP2A plays an important role in regulating the activation of the transcription factor Cdc14, which is involved in the cell cycle, proliferation, and apoptosis. This could explain why *PPM1* deletion led to the enhancement of mHTT toxicity in SX1.

Unexpectedly, the deletion of *PPM1* was protective against mHTT toxicity in both sensitive strains. On one hand, it could be caused by a compensatory effect in which the cell increases the synthesis of other PP2A activators to prevent transcriptional

dysregulation and cell death. On the other hand, this protection is only seen in two of the strains and it affects mHTT toxicity but not αSyn, this suggests that a different modifier related to the FEAR/MEN pathway might be involved. The reason for this hypothesis is that *FAR10* - *SLMAP* in humans - was one of the genes uncovered during the QTL analysis. SLMAP is responsible for the interaction between PP2A and pMST2 but is not involved in the interaction between PP2A and αSyn, so the presence of a polymorphism that increases SLMAP affinity to pMST2 in those two strains might partially compensate for the effects of a decrease in active PP2A (Bae et al., 2017; Mueller et al., 2018). However, PP2A is also related to the TOR and ceramide signalling pathways in yeast, which are involved in stress response, cell cycle regulation, calcium homeostasis and vesicle trafficking (Zabrocki et al., 2002), so the modulation of these pathways might be responsible for the protection. Therefore, further experiments are necessary to determine the underlying cause of this protection, including the OE of *PPM1* to establish if it can suppress the toxicity of both mHTT and αSyn, and the OE of *FAR10* in SX1 - or the cloning of *FAR10* from HN6 and BJ20 to replace the gene in SX1 - to determine if that is, in fact, the mechanism behind the protection. Finally, if both *PPM1* and *FAR10* are involved in the protection, overexpressing of both genes in the same strain would be interesting to see if they present a synergistic protective effect that leads to a higher rescue.

The OE experiments were only performed for four out of the eight genes on the list since the OE plasmids were not available in the collection. The effect of the OE of *DSS4*, *TAF2*, *TIF6* and *MRX21* on mHTT and αSyn phenotypes was also studied in the three parental strains.

The OE of *TIF6* was protective against mHTT and αSyn toxicity in both sensitive strains - although the effect on αSyn toxicity in HN6 was small - and had no negative effects in the resistant strain. In yeast, TIF6 is involved in the maturation of rRNA,

and its downregulation leads to an impairment in protein synthesis (Basu et al., 2001). Therefore, knowing that there is a decrease in rRNA due to the oxidation of nucleic acids in PD and other NDs as a result of the accumulation of ROS (Abe et al., 2003; Nunomura et al., 2006; Zhang et al., 1999), the OE of TIF6, a protein that is necessary for the adequate maturation of the 60S subunit (Basu et al., 2001), would be beneficial to prevent the impairment in protein synthesis: if there is less rRNA available, it is necessary that it matures correctly and becomes part of the ribosome.

The results from the other genes were inconclusive. *DSS4* deletion was protective against mHTT and αSyn toxicity in BJ20, but its OE was protective against mHTT in HN6 and had no effect in SX1. *MRX21* OE was protective against mHTT toxicity in HN6 but it enhanced the toxicity in SX1, and its deletion was protective in BJ20. Lastly, *TAF2* OE and deletion enhanced mHTT toxicity in SX1, although the deletion was protective in BJ20 and the OE in HN6. The apparent unpredictability of these results might be caused by the method employed during the experiments, since both the deletion of the gene and their OE from a galactose promoter produce massive changes in the amount of protein available. Therefore, milder changes in the amount of protein caused by the downregulation of the proteins instead of the deletion of the gene, and by the OE of the gene from a weaker promotor might produce more coherent results. Another option would be identifying the polymorphism associated with the resistance or sensitivity in the F12 strains used for the QTL analysis and cloning it into the parental strains to see if the effects were maintained. However, it is also possible that the different response to the modifier was caused by the genetic differences between the strains, which would cause this variability to be maintained regardless of the method employed to modify the gene.

The last experiment of this chapter consisted of studying the effect on mHTT and

α Syn toxicity of nine different genes (*RPD3*, *PEX6*, *YCR043C*, *PER1*, and *GIN4*, *PPZ2*, *BPH1*, *SNT1* and *ELO2*) using the deletions available in the Stanford Genome Technology Centre's Yeast Knock-Out collection in the laboratory strain BY4741. These were non-essential genes, present in both the HD and PD model QTL analysis, that appeared in polygenic QTL with four or fewer genes.

Interestingly, none of the deletions had a significant effect enhancing or suppressing mHTT toxicity in this strain. This is particularly surprising since *RPD3* is orthologous to human histone deacetylases (*HDAC1* and *HDAC2*) and studies show that HD patients present a decrease in histone acetylation (Peña-Altamira et al., 2013), and that the inhibition of HDAC1 ameliorates the transcription impairment and prevents neurodegeneration in HD (Bodai et al., 2001; Thomas et al., 2008). A possible explanation is that the complete deletion of this gene, which is involved in maintaining the proper histone acetylation levels, leads to defects in transcription (Zhou et al., 2009). This, together with the transcriptional dysregulation caused by mHTT, nullifies the protection the decrease in RPD3 should accomplish. Interestingly, there is another gene in the list involved in the same process. NCOR1, SNT1's human orthologue, represses transcription in two different ways: through chromatin condensation by recruiting HDAC1 and HDAC2 via mSin3, and by directly interacting with some basal transcription factors (Boutell et al., 1999). The fact that mHTT is able to interact with NCOR1 in a polyQ length-dependent manner and the location of NCOR1 is altered in the cortical and caudate neurons of HD patients - being present only in the cytoplasm instead of in the cytoplasm and the nucleus-, could explain the transcriptional problems associated to HD (Boutell et al., 1999). Taking this into account, it is understandable that the deletion of this gene does not enhance mHTT toxicity -its deletion does not affect growth in the control, so other proteins are able to regulate transcription in its absence, and since it is not present

it can not interact with mHTT and alter transcription-.

Excitingly, two of the gene deletions had a significant effect on α Syn toxicity. *PER1* and *GIN4* deletion enhanced the toxicity of α Syn. *GIN4* is a protein kinase involved in cell bud growth, in mitotic checkpoint signalling and in the formation of the septin ring. It also is one of the kinases responsible for the phosphorylation of ubiquitin at Ser57, which plays a role in oxidative and proteotoxic stress (Hepowit et al., 2020). However, since there are other kinases involved in the process that could compensate for the loss of *GIN4*, the toxicity enhancement of α Syn in the *GIN4* deletion strain might not be related to this mechanism. *GIN4* is orthologous to *BRSK1* and *BRSK2* - two human genes encoding BR serine/threonine kinases - which have similar functions to the yeast gene: mitotic G2 DNA damage checkpoint signalling and protein phosphorylation. Interestingly, both genes are expressed in neurons: *BRSK1* is involved in neurotransmitter release by phosphorylating RIM1 -possibly during docking or vesicle priming (Inoue et al., 2006)-, while *BRSK2* is involved in axonal development and polarization of cortical neurons, and mutations in this gene have been related to developmental delay and intellectual disability (Hiatt et al., 2019). Besides that, it is known that in response to ER stress caused by the accumulation of misfolded proteins, the cells trigger the unfolded protein response (UPR), which consists of the transcriptional up-regulation of specific proteins (e.g., molecular chaperones and folding enzymes), the global inhibition of protein synthesis and the activation of apoptotic pathways (Wang et al., 2012). One of the upregulated proteins is *BRSK2* which also translocates from the nuclear periphery to the ER, meaning its function probably changes during the UPR. Furthermore, researchers have found that knocking down *BRSK2* increases apoptosis during ER stress in tumoral cells while its OE prevents it (Wang et al., 2012). Although the diseases are different, the UPR is also triggered during PD, so this same mechanism might be

responsible for the increase in α Syn toxicity due to the deletion of *GIN4*.

PER1 encodes a protein of the ER involved in the remodelling of the GPI anchor by GPI-phospholipase A2 for the association of GPI-anchored proteins (GPI-AP) to lipid rafts. This post-translational membrane anchoring is thought to be necessary for proper protein sorting and trafficking (Fujita et al., 2006). Interestingly, although the deletion of this gene did not have a significant effect on mHTT toxicity, there was an enrichment of genes involved in the GPI-anchor biosynthesis pathway during the HD QTL analysis. Mutations in *PGAP3* (post-GPI attachment to proteins phospholipase 3), the human ortholog of *PER1*, lead to deficits in the formation of GPI-anchored proteins and have been associated with neurologic hyperphosphatasia with cognitive disability (Howard et al., 2014; Knaus et al., 2016). In relationship to PD, a deficit in the formation of GPI-APs could be harmful, especially for the downregulation of GFR α 1, which is part of the GDNF family receptor, necessary for the detection of the glial cell line-derived neurotrophic factor (GDNF) - a molecule able to prevent the degeneration of nigrostriatal neurons and reverse the functional deficits in primate models of PD (Howard et al., 2014). Considering the deficits in protein trafficking associated with the deletion of *PER1*, the protein misfolding associated with the OE of α Syn, and the loss of the GDNF family receptor-a, the enhancement of α Syn toxicity due to the deletion of *PER1* is reasonable. This data also implies that the OE of this gene may suppress the toxicity of α Syn and ameliorate associated phenotypes.

6. QTL validation in *Drosophila melanogaster*

The aim of this chapter is to validate three of the genes identified during the QTL analysis in yeast: *DSS4* (*Strat* in flies), *TIF6* (*eIF6*) and *MRX21* (*DPCoAc*). In order to do so, first, it was necessary to characterize a fly model of HD. The model from Barbaro et al., (2015) was chosen since it has a control *HTT* and several *mHTT* with different levels of toxicity. Then, the effect of the downregulation of the candidate modifier genes was studied with shRNA lines and using the line carrying the empty vector (3M) as a control. The aim of these experiments is to determine if the downregulation of the selected genes causes any phenotypic modulation of the flies independent of *HTT* expression. This information is essential since the *mHTT* flies are severely sick, so any modification that causes further impairment would most likely only cause more damage instead of improvement. Finally, the effect of the downregulation of the modifiers in the *mHTT* toxicity was studied. If the downregulation of the protein is protective against *mHTT*, drugs that inhibit it can be studied as a potential treatment. On the other hand, if the downregulation enhances *mHTT* toxicity, the OE of the gene can be studied as a therapeutic target.

6.1. Results

6.1.1. Characterization of the HTT lines

The characterization of the effect of the expression of human *HTT*, both WT and mutant, in fruit flies was essential for these experiments since it was necessary to validate that there is a toxic effect caused by *mHTT* in order to be able to use these flies as a model of the disease. These fly lines were established and characterized by Barbaro et al., (2015) to study the effect of several *HTT* fragments that occur naturally in HD patients. They analysed the lifespan, locomotor activity,

neurodegeneration and viability of the flies, and aggregation of mHTT while expressing it in neurons. The two shortest fragments, exon 1 – caused by aberrant splicing (Sathasivam et al., 2013)- and 108 aa – cleaved by an endopeptidase (Lunkes et al., 2002)-, were chosen since they are present in the aggregates found in the brain of mice and patients (DiFiglia et al., 1977; Landles et al., 2010; Lunkes et al., 2002; Sathasivam et al., 2013). These fragments were also the most toxic, Ex1 significantly impaired all the metrics mentioned above and was the fastest to form aggregates while 108 impaired motor function and longevity to a lesser extent and formed aggregates slower (Barbaro et al., 2015).

6.1.1.1. Cross to obtain the flies that express HTT in the neurons

Due to the toxicity of mHTT, the *UAS-GAL4* system was used for a tissue-specific expression of the protein. Therefore, homozygous female virgin flies carrying *UAS-HTT* on chr 2 were crossed with male flies carrying *elav-GAL4* on chr X. Female virgin descendants from the cross were collected and used for the experiments since they had one copy of *UAS-HTT* and also one copy of *elav-GAL4*, completing the *GAL4/UAS* system that allowed the expression of *HTT* in the neurons (Brand & Perrimon, 1993; Koushika et al., 1996). Since male flies inherit chr Y from their parents, they do not inherit the *elav-GAL4*, which means that they are not expressing *HTT*, so they can be used as a control for the viability assay (Figure 2.2-1). The expression of *HTT* was limited to the neurons using the *elav-GAL4* driver since ubiquitous expression of the mutant versions causes a developmental impairment so severe that none of the flies reaches adulthood (Barbaro et al., 2015).

6.1.1.2. Expression of mHTT Ex1 in neurons reduces the viability of flies

Viability was assessed by comparing the percentage of female versus male flies that eclose from the pupal case after the above cross. If the expression of the gene was innocuous, the expected ratio of females and males would be 1:1, however, if the gene has a toxic effect (as is the case with mHTT), the number of female flies that make it to adulthood would be reduced while the number of males would stay the same since they do not express the gene.

To assess if there was any difference, the number of male and female flies that hatched from each tube was counted daily for 9 days. The percentage of females was calculated for the ten tubes, and the average percentage of adult female flies was compared between genotypes (Figure 6.1-1). No significant difference in the percentage of females was observed between the control HTT Ex1 and the mHTT 108 (53.1% and 52.3% respectively), but both were significantly higher than with mHTT Ex1, which only had 31.3% females. This reduction in the percentage of females shows that mHTT Ex1 causes a toxic effect that prevents flies from reaching adulthood and corroborates the results obtained by Barbaro et al. (2015).

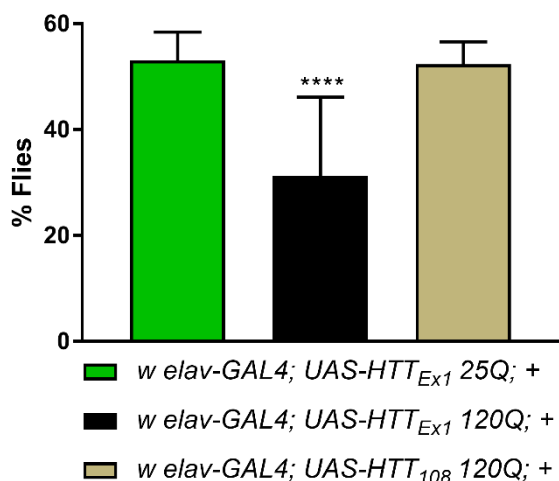


Figure 6.1-1. Expression of mHTT Ex1 causes a reduction in the number of flies that make it to adulthood.

Graph showing the percentage of total flies that are female which make it to adulthood of each genotype. There is no significant difference between the control HTT Ex1 and mHTT 108, but mHTT Ex1 significantly decreases the number of female flies compared to the other two genotypes.

One-way ANOVA corrected by Tukey's multiple comparisons test.
**** P < 0.0001.

6.1.1.3. Expression of mHTT in neurons reduces the lifespan of flies

Longevity was next assessed in the above fly genotypes. The lifespan of the flies was significantly reduced when they express any of the mHTT fragments compared to the control (Figure 6.1-2). The maximum survival of the three lines was quite different, with mHTT Ex1 flies being the first to die (ten days), followed by mHTT 108 (34 days), and then by the control line HTT Ex1 that had the longest lifespan (77 days). Surprisingly, there was only a slight difference in the average 50% survival of the strains (mHTT Ex1 - 4 days, mHTT 108 - 6 days, and HTT Ex1 - 12 days) since there was an unexpectedly high number of deaths in the control line during the first few days.

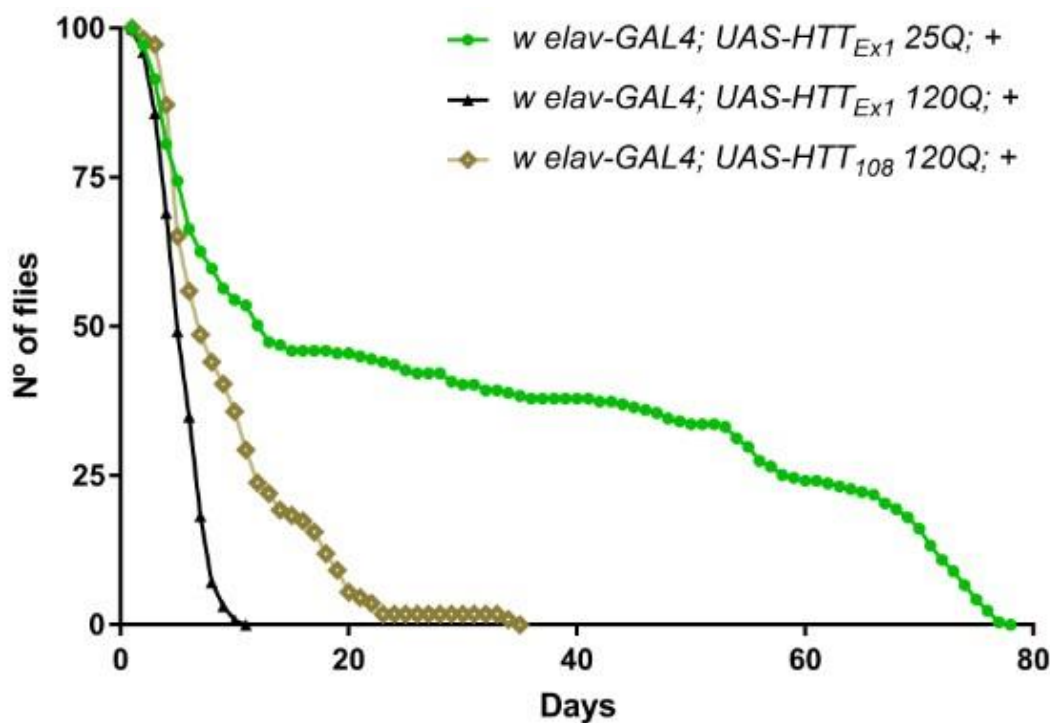


Figure 6.1-2. Expression of mHTT causes a significant reduction in the lifespan of the flies.

Graph showing the difference in lifespan of the HTT genotypes. There is a slight difference in the average 50% survival of the strains (mHTT Ex1 - 4 days, mHTT 108 - 6 days, and HTT Ex1 - 12 days). There is a significant difference between the survival of the mHTT lines (mHTT Ex1 - 10 days, and mHTT 108 - 34 days) compared to the control HTT Ex1 (77 days).

Log-rank Mantel-Cox test. P < 0.0001.

6.1.1.4. Expression of mHTT Ex1 in neurons causes neurodegeneration from day one

Neurodegeneration caused by mHTT was assessed by comparing the average number of rhabdomeres per ommatidia in the compound eyes of the flies. A normal fly has eight rhabdomeres per ommatidium, seven of which are visible by microscopy, so the presence of fewer than this number indicates that the expression of mHTT leads to neuronal loss. The average number of rhabdomeres per ommatidium was calculated for each fly and used to calculate the average per genotype at each age. As can be seen in Figure 6.1-3, both the control HTT and mHTT 108 had an average of approximately seven rhabdomeres per ommatidium even at day 15 (6.994 and 6.990 respectively). On the other hand, flies expressing mHTT Ex1 exhibited significant rhabdomere loss from day one (6.348) compared with the other genotypes, which worsened on day three (5.918). There is no data on the mHTT Ex1 flies at day 15 because, as seen in the longevity experiment, they did not survive that long. This experiment shows that mHTT Ex1 causes neurodegeneration in the flies from day one that worsens with time.

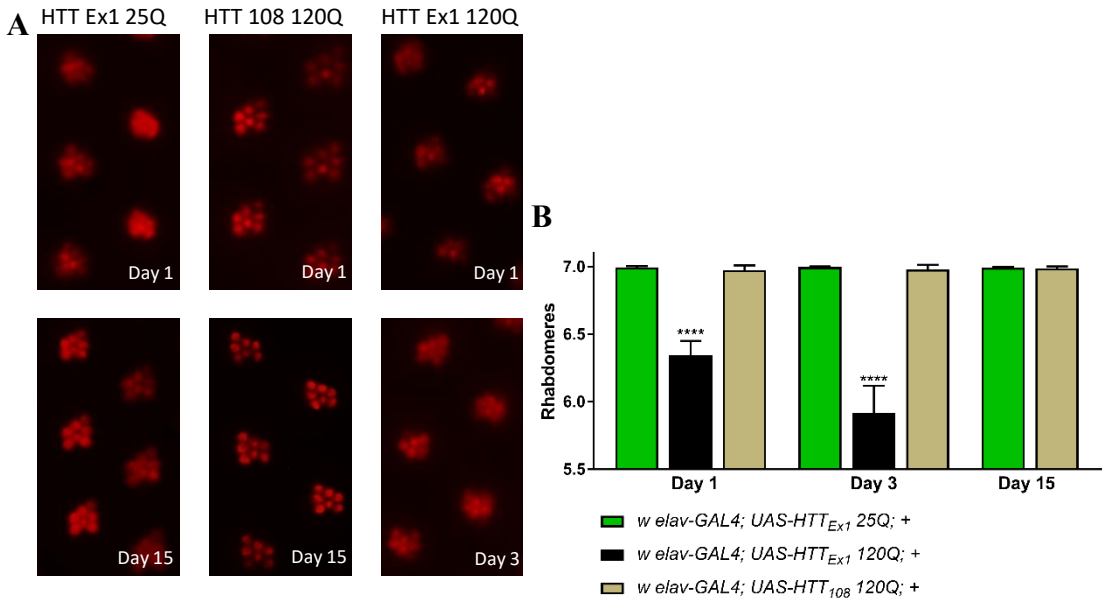


Figure 6.1-3. The expression of mHTT Ex1 causes neurodegeneration from day one.

A) Microscopy images at 50x magnification showing the rhabdomeres of several ommatidia in the eyes of 1-, 3- and 15-day-old female virgin flies. Neurodegeneration is present in mHTT Ex1 flies from day one. **B)** Average rhabdomere count of 1-, 3- and 15-day-old female virgin flies. There is a significant decrease in the mean number of rhabdomeres per ommatidium at day one and at day three between mHTT Ex1 (6.348, n = 14; and 5.918, n = 8 respectively) and the control HTT Ex1 (6.997, n = 15; and 6.998, n = 16). These data indicate that the expression of mHTT Ex1 causes neurodegeneration from day one. There is no significant difference in the average rhabdomere count between the control and the mHTT 108 flies at any of the timepoints (6.990, n = 17, and 6.994, n = 17 at day 1 and day 15 respectively).

Two-way ANOVA corrected by Tukey's multiple comparisons test. ***P < 0.0001.

6.1.1.5. Expression of mHTT in neurons causes locomotor impairment

Movement impairment was assessed with the counter current climbing apparatus, which is based on the principle that flies present negative geotaxis and therefore if placed inside a tube, they would try to climb to the top (McEwen, 1918). Therefore, as described in Chapter 2, to evaluate locomotor activity the flies were placed inside a tube, allowed to climb for a few seconds, and separated between those that passed the threshold and those that did not. To establish if there was any difference between genotypes, the average number of tubes climbed by the flies of each genotype was compared. As it can be seen in Figure 6.1-4, mHTT 108 caused a slight movement

impairment (63.6%) while mHTT Ex1 rendered the flies almost unable to climb (1.9%). Both of these deficiencies in movement were statistically significant when compared to the control HTT Ex1 flies (89.1%). *Elav-GAL4* flies (74.6%) were used as a negative control and the comparison shows that the pan-neuronal expression of HTT Ex1 did not cause any movement impairment.

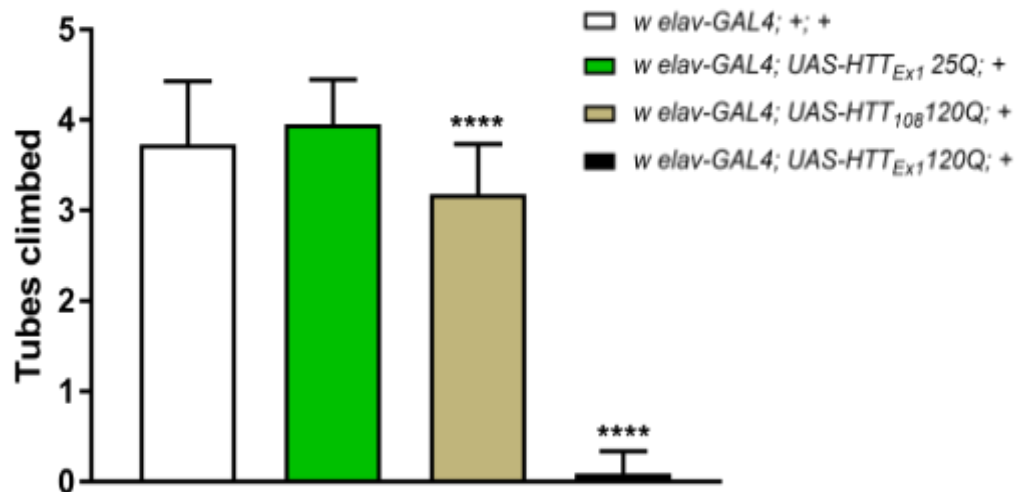


Figure 6.1-4. Expression of mHTT causes movement impairment in flies.

Graph showing the average number of times that the flies from each genotype are able to climb to the top tube of the climbing apparatus in ten seconds. There is a slight movement impairment due to the expression of mHTT 108 compared to the control HTT (63.6%, n = 125; and 79.1%, n = 234; respectively). Whereas flies expressing mHTT Ex1 are almost unable to climb even once (1.9%, n = 151). *Elav-GAL4* flies (74.6% n = 30) were used as climbing control to determine if HTT Ex1 caused movement impairment, but there is no difference between the two genotypes.

One-way ANOVA corrected by Tukey's multiple comparisons test. ****P < 0.0001.

6.1.2. Characterization of the modifier lines

The modifier genes *Strat*, *eIF6* and *DPCoAC* were selected among the QTL list provided by the yeast experiments because they were expressed in the brain of the flies and because downregulation lines with the construct inserted in the same place on the second chr were available, reducing potential position effects when comparing modifiers. This downregulation was performed by RNAi in neurons thanks to the

expression of shRNA via the *GAL4/UAS* system. The 3M line, which carried the empty cloning vector inserted in the same location, was used as control.

6.1.2.1. Cross to obtain the flies that express the different shRNA in neurons

The downregulation lines were obtained crossing female virgin flies carrying the *UAS-RNAi* sequence (*Strat*, *eIF6* or *DPCoAC*) or the empty vector (3M) with male flies carrying the *elav-GAL4* driver Figure 2.2-2; **Error! No se encuentra el origen de la referencia..** The expression of the shRNA was limited to the neurons to be consistent with the HTT experiments. As mentioned above, only the female descendants carry both the *GAL4* and *UAS* construct, so female virgins were used for the experiments.

6.1.2.2. The downregulation of *DPCoAC* in neurons reduces the viability of flies

The viability assay was performed as in the HTT experiment to keep it consistent. The number of adult male and female flies that hatched from each genotype was counted, the average percentage of female flies was calculated and then compared between genotypes. Figure 6.1-5 shows approximately 50% of the flies were female in all the genotypes except for *DPCoAC-RNAi*, which is expected when there is no toxic effect due to the modification and there are no developmental problems. However, the downregulation of *DPCoAC* significantly decreased the percentage of female flies to 30.1%, meaning that there were developmental problems and that its downregulation was deleterious for the flies.

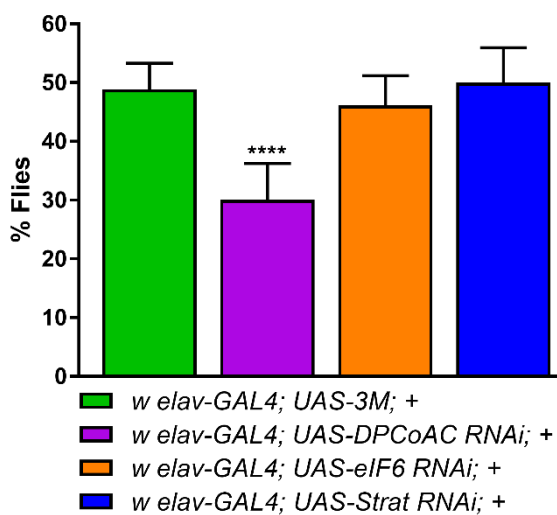


Figure 6.1-5. Downregulation of DPCoAC causes a reduction in the number of flies that make it to adulthood.

Graph of the percentage of female flies that make it to adulthood in each genotype. There is no significant difference between the control 3M (48.9%) and the downregulation of *Strat* and *eIF6* (50.0% and 46.1% respectively), but the downregulation of *DPCoAC* is significantly different from 3M (30.1%).

One-way ANOVA corrected by Tukey's multiple comparisons test. ****P < 0.0001.

6.1.2.3. The downregulation of *DPCoAC* in neurons reduces the lifespan of flies

The lifespan of the RNAi modifier flies was studied by keeping 100 flies of each genotype in fresh food and scoring their lifespan. Due to the high death rate of the *DPCoAC*-RNAi flies, the number of flies was counted daily in the beginning and twice a week later, since the other genotypes present a much lower death rate.

Figure 6.1-6 shows that *DPCoAC*-RNAi caused a significant reduction in the lifespan of the flies (maximum lifespan of 6 days). Meanwhile, *Strat*-RNAi and *eIF6*-RNAi lines did not show a significant difference in survival compared to the control 3M line (84, 88 and 84 days, respectively).

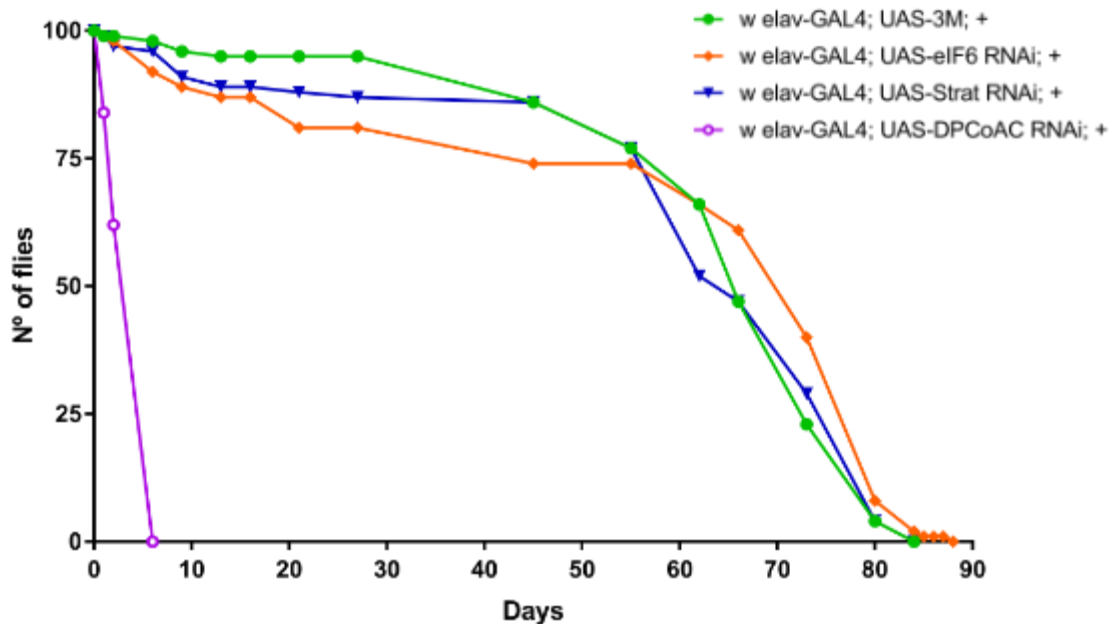


Figure 6.1-6. Downregulation of *DPCoAC* causes a significant reduction in the lifespan of the flies.

Graph showing the difference in lifespan of the RNAi lines. There was no significant difference in longevity between the *Strat*-RNAi and *eIF6*-RNAi lines when compared to the control 3M line (84, 88 and 84 days respectively). However, *DPCoAC*-RNAi causes a dramatic reduction in the number of flies early in the experiment (maximum lifespan of 6 days. $P < 0.0001$).

Log-rank Mantel-Cox test.

6.1.2.4. There is no neuronal loss caused by the downregulation of the genes in flies

The average number of rhabdomeres per ommatidia per fly was used to determine if the downregulation of any of the modifier genes caused neurodegeneration in the flies. Both the microscopy images and the graph in Figure 6.1-7 show that there is no rhabdomere loss after 30 days due to the downregulation of either *Strat* (6.996) or *eIF6* (7) compared to 3M control flies (7). Due to the short lifespan of the *DPCoAC* flies, rhabdomeres were only counted at day one, however, there was no sign of neuronal loss in those flies either (7) compared to 3M at the same age (7).

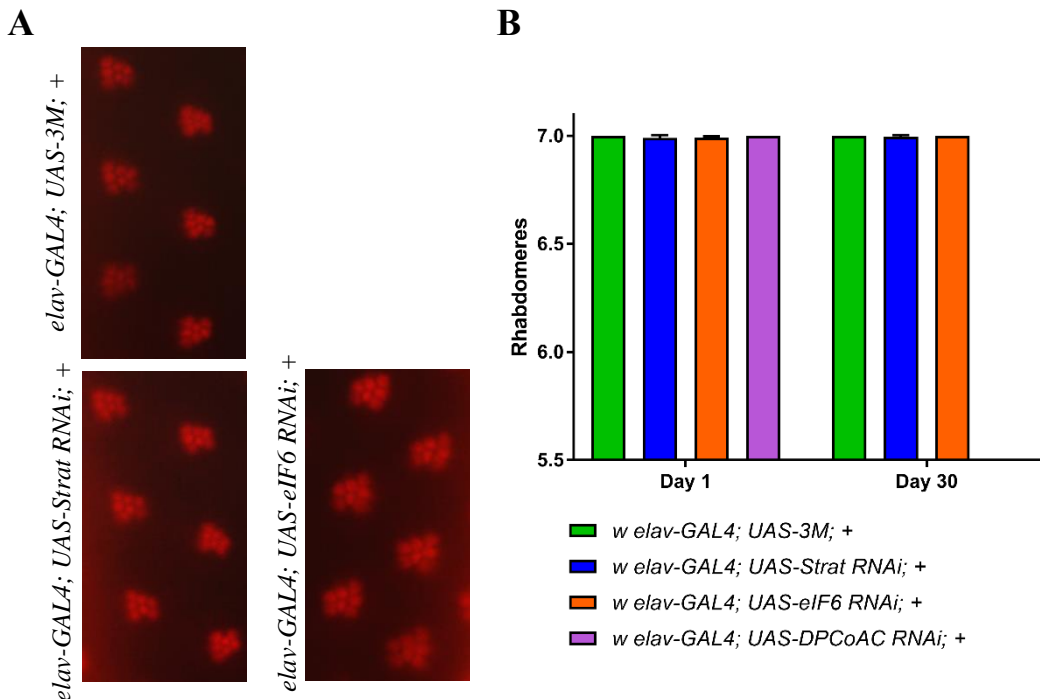


Figure 6.1-7. Downregulating the expression of *Strat*, *DPCoAC* or *eIF6* has no neurodegenerative effects in the fly eye.

A) Microscopy images at 50x magnification showing the rhabdomeres of several ommatidia in the eyes of 30-day-old female virgin flies, with no neurodegeneration exhibited in any of the lines. **B)** Average rhabdomere count of 1- and 30-day-old female virgin flies. There is no statistically significant difference in the mean number of rhabdomeres per ommatidium at day 30 between the *Strat* and *eIF6* downregulation lines (6.996, n = 8; and 7, n = 8, respectively) and the control 3M line (7, n = 8). This indicates that the downregulation of *Strat* or *eIF6* has no neurodegenerative effects in flies at day 30. There are no results for *DPCoAC* downregulation at day 30 since the flies died prior to the experiment, but there were no signs of neurodegeneration when examined at day one when compared to the 3M control (7, n = 6 and 7, n = 5). Two-way ANOVA corrected by Tukey's multiple comparisons test.

6.1.3. Effect of the downregulation of the modifier genes on the toxicity of HTT

The previous experiments show that the downregulation of *DPCoAC* causes an important impairment in both the viability and the survival of the flies although it did not cause neurodegeneration. However, this impairment was enough for it to be discarded from the study as a modifier of mHTT toxicity. Therefore, only downregulation of *eIF6* and *Strat* was assessed for modification of mHTT toxicity. In these experiments, only the short fragment of the mHTT was used since the longer

fragment did not cause a phenotype in several of the parameters that were assessed above.

6.1.3.1. Cross to obtain the flies that express HTT and the shRNA in neurons

In order to assess the effect of the downregulation of the genes on mHTT toxicity, it was necessary to generate flies that carried both the *UAS-RNAi* and *UAS-HTT* transgenes and then cross them to the *elav-GAL4* driver line to have descendants that express both UAS constructs in the neurons. However, since both UAS constructs were on the second chr, it was necessary to cross them in order to find recombinant flies that carry both *UAS* on the same chr.

As it is shown in Figure 2.2-3, this process consisted of four crosses before obtaining the experimental flies. The first step was to cross both *UAS* lines, from there heterozygous female virgin flies were collected and crossed with the second chr *Cy0* balancer line that prevents further recombination and carries a dominant curly wing marker. Females and males with curly wings were collected and crossed separating each pair in a tube. After seven days, the parents were collected, their DNA was extracted, and a PCR was performed to determine if they carried both *UAS* constructs (Figure 6.1-8). The female descendants without curly wings from the cross in which both parents are recombinants were homozygous for both *UAS* constructs and thus, these flies were crossed to the *elav-GAL4* males to generate the experimental flies that were heterozygous for *elav-GAL4* in the first chr and *UAS-RNAi, UAS-HTT* in the second.

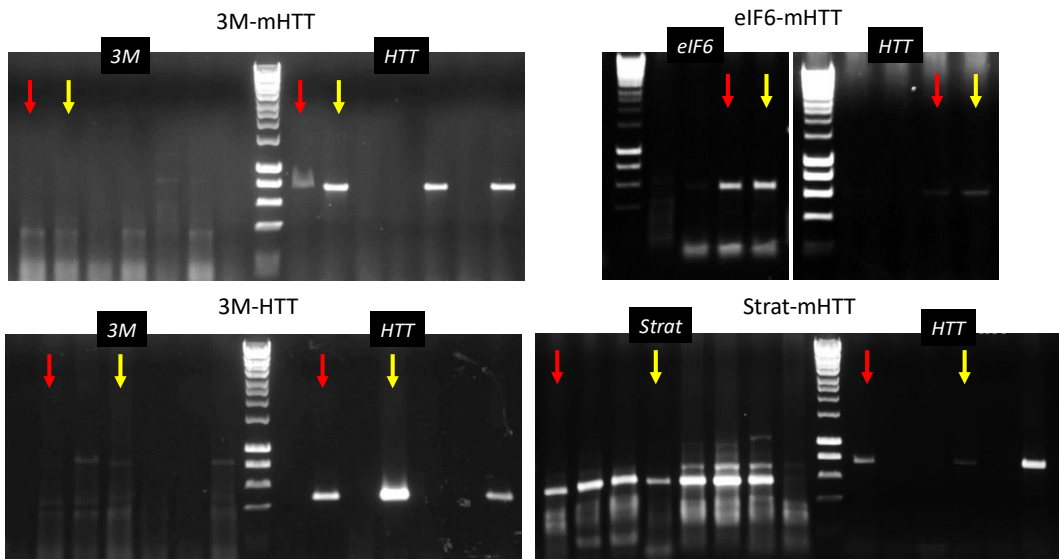


Figure 6.1-8. Agarose electrophoresis gels of the recombination PCR.

PCR product from the males and females used for the cross to obtain RNAi-HTT flies. In each genotype, the same-coloured arrows point at the PCR product coming from the same fly.

6.1.3.2. Downregulation of *Strat* and *eIF6* does not modulate the viability of mHTT flies

Consistently with the previous experiments, viability was assessed using the average percentage of adult female flies that made it to adulthood. The percentage of female flies from 3M-mHTT and 3M-HTT was compared to confirm there was a difference due to the expression of the toxic protein. Then, 3M-mHTT was compared to the RNAi-HTT lines to see if there was any effect on viability due to the RNAi in the mHTT background. Figure 6.1-9 shows that there was still a notable decrease in the percentage of female flies when expressing 3M-mHTT (13.2%) compared to 3M-HTT (52.2%). It is also shown that there was no significant difference between Strat-mHTT and eIF6-mHTT (12.9% and 10.4% respectively) when compared to 3M-mHTT. Thus, the downregulation of *Strat* and *eIF6* does not modulate the viability of mHTT flies.

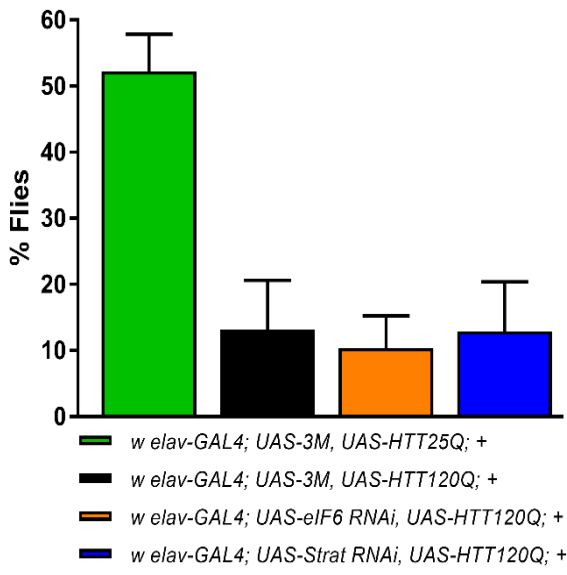


Figure 6.1-9. There is no rescue in the percentage of flies that make it to adulthood when downregulating *Strat* or *eIF6*.

Graph of the percentage of female flies that make it to adulthood in each genotype. There is no significant difference between the control 3M-mHTT (13.2%) and the downregulation of Strat-mHTT and eIF6-mHTT (12.9% and 10.4% respectively), but all three genotypes are significantly different from 3M-HTT (52.2%. P < 0.0001).

One-way ANOVA corrected by Tukey's multiple comparisons test.

6.1.3.3. Downregulation of *Strat* and *eIF6* does not modulate the lifespan of mHTT flies

The lifespan was also studied following the same protocol (Figure 6.1-10). As was seen in the first experiment in this chapter, there is a drastic reduction in the lifespan of the flies when expressing mHTT compared to HTT (57 and 78 days respectively). This shortened lifespan was also present while downregulating either *Strat* or *eIF6* (57 and 43 days). There was no significant difference in the survival of the flies due to the modifiers, however, there seemed to be a slight increase in the number of flies that were alive after 15 days when downregulating *Strat* (Strat-mHTT 16, 3M-mHTT 6) although this difference was no longer visible at day 45.

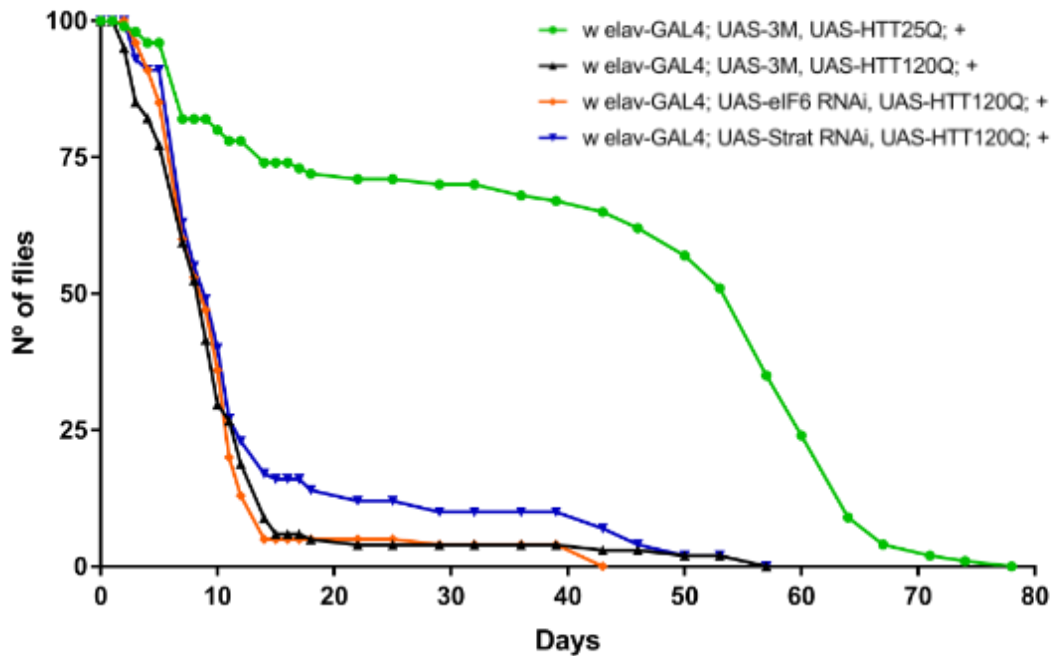


Figure 6.1-10. No significant rescue in longevity was found due to the downregulation of *Strat* or *eIF6*.

Graph showing the survival of the RNAi-HTT lines. There is a dramatic reduction in the lifespan of 3M-mHTT when compared to 3M-HTT (57 and 78 days respectively. $P < 0.0001$). There is no significant difference between the RNAi-mHTT and the 3M-mHTT lines. There is an increase in survival in 15-to-45-day-old flies when downregulating *Strat*, but not an increase in lifespan (57 days).

Log-rank Mantel-Cox test.

6.1.3.4. Downregulation of *Strat* partially rescues the neurodegeneration caused by mHTT

As in the previous sections, neurodegeneration was evaluated using the pseudopupil assay. Microscopy images show that there was neurodegeneration in all the mHTT lines while the 3M-HTT flies still presented all the rhabdomeres in each ommatidium on day seven (Figure 6.1-11 A). There was a significant decrease in the average number of rhabdomeres in 3M-mHTT (6.472), Strat-mHTT (6.526), and eIF6-mHTT flies (6.502) when compared to 3M-HTT flies (6.994) from day one ($P < 0.0001$. Figure 6.1-11 B). However, by day seven there was a significant reduction in the neurodegeneration when downregulating *Strat* as compared to 3M-mHTT flies (6.027 and 5.740 respectively. $P < 0.001$), which represents a level of

neuroprotection of 22.9%. There was also a slight increase in the rhabdomere number of the eIF6-mHTT flies (5.828), but it was not statistically significant.

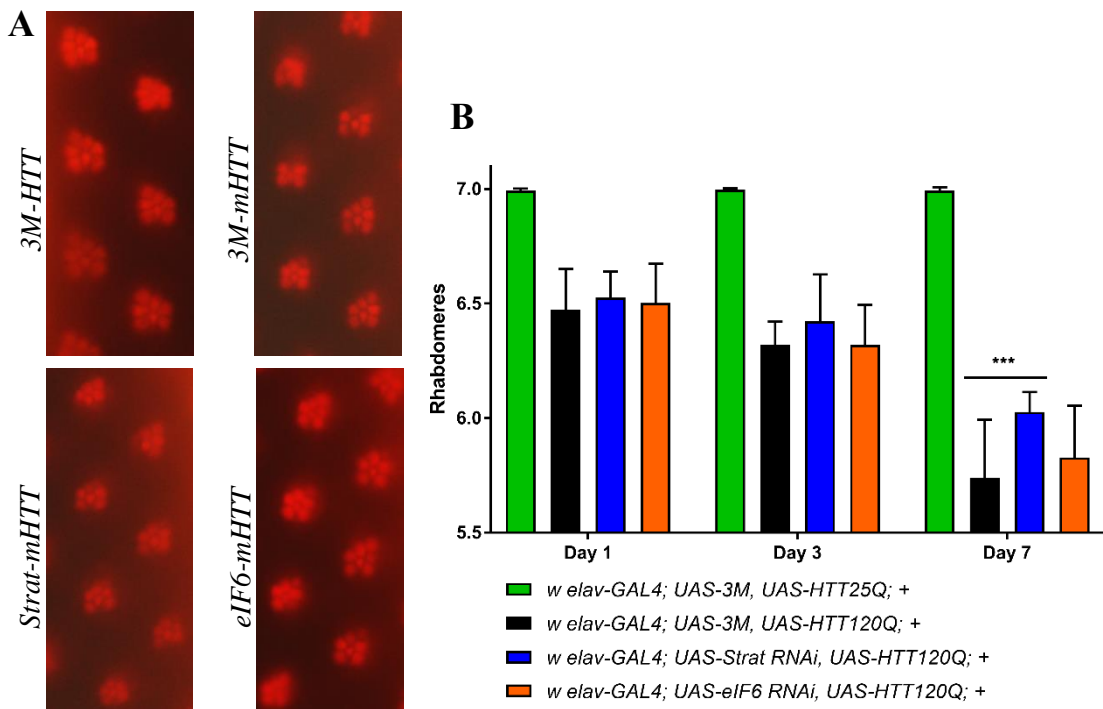


Figure 6.1-11. Downregulating the expression of *Strat* partially rescues the neurodegeneration caused by mHTT.

A) Microscopy images at 50x magnification showing the rhabdomeres of several ommatidia in the eyes of 7-day-old female virgin flies, with neurodegeneration in all the mHTT lines. **B)** Average rhabdomere count of 1-, 3- and 7-day-old female virgin flies. There is a statistically significant difference in the mean number of rhabdomeres per ommatidia at day 7 between the Strat-mHTT line (6.027; n = 8) and the toxic control 3M-mHTT (5.740; n = 8) ($P < 0.001$). There is a statistically significant difference between the Strat-mHTT line and the 3M-HTT control line (6.992; n = 10. $P < 0.0001$), meaning the downregulation of *Strat* offers modest protection against mHTT toxicity (22.9% neuroprotection).

Two-way ANOVA corrected by Tukey's multiple comparisons test. *** $P < 0.0001$.

6.2. Discussion

The aim of this chapter was to validate in flies the results obtained by the downregulation of *DSS4* (*Strat*), *TIF6* (eIF6) and *MRX21* (*DPCoAC*) in the yeast model of HD. The first experiments presented in this chapter were designed to establish that our results were in concordance with those obtained by Barbaro et al.,

(2015) when they researched the toxic effects of naturally occurring HTT fragments. They discovered that the shortest fragments were the most toxic. Similarly, our results indicate that both mHTT fragments have a deleterious effect when expressed in the neurons of the flies. However, although both fragments are toxic, mHTT Ex1 had a significantly stronger phenotype. While mHTT 108 shortened the lifespan and modestly impaired movement by 15.5%, mHTT Ex1 shortened the lifespan more dramatically, caused a more profound movement impairment that prevented flies from climbing (77.2% reduction), led to neurodegeneration from day one (0.65 rhabdomeres lost at day one and 1.08 at day three), and decreased the number of flies that made it to adulthood. Taking this into account, it was decided to use mHTT Ex1 for the following experiments since it presented a wider range of phenotypes and, due to its stronger toxicity, any modification in the phenotype for better or for worse would suggest that the up or downregulation of the gene involved could be a strong candidate as a therapeutic target. Movement impairment experiments were determined unnecessary unless there was a strong rescue in the other parameters since the climbing phenotype was extremely strong when expressing mHTT Ex1 and only a dramatic improvement would likely ameliorate it.

After selecting the mHTT line for the experiments, it was necessary to choose the modifiers. The candidate genes were selected from the modifiers that were validated in the parental yeast strains in Chapter 5. Among them, we selected those that had downregulation lines available – RNAi KK lines -, and in particular those which had the transgene inserted in the same location to avoid any variation due to the place of insertion of the construct. In the end, the *DPCoAC*, *Strat* and *eIF6* RNAi lines were selected for analysis, with the 3M line as a control. All the shRNA constructs are inserted in the same region of chr 2. After selecting the candidate genes, it was necessary to assess if their downregulation caused any deleterious effect on the

flies. As described above, the downregulation of *DPCoAC* caused a dramatic reduction in the number of flies that made it to adulthood and early death, so it was deemed unfit and was taken out of the study. On the other hand, the *Strat* and *eIF6* knockdown flies were as healthy as the 3M control flies in all the parameters observed (neurodegeneration, longevity, and viability), and so they were chosen for the validation procedure.

The validation of *Strat* and *eIF6* as modifiers of mHTT in flies was studied by downregulating the genes by co-expressing the respective shRNAs with mHTT. 3M-HTT flies were used as healthy controls while 3M-mHTT flies were used as disease controls for all the validation experiments. As seen above, the downregulation of *eIF6* did not lead to any improvement in mHTT phenotypes, however, the downregulation of *Strat* yielded 22.9% neuroprotection by day seven in the pseudopupil assay, and slightly increased the number of flies that survived more than 15 days in the longevity assay although it had no effect in the total lifespan nor in the viability of the flies.

These results are consistent with those seen in yeast, where the deletion of *DSS4* and *TIF6* had a slight protective effect in the sensitive strains, probably caused by a compensatory effect, but their OE caused a more significant rescue. Taking this into account, it would be worth it to study the effect of the OE of these genes in HD and PD fly models.

As has been mentioned before, *EIF6*, the human orthologue of *eIF6*, is a translation initiation factor regulated by insulin (Brina et al., 2015; Miluzio et al., 2016). It binds to the 60S ribosomal subunit and prevents translation, however, in the presence of insulin, it gets phosphorylated and releases the subunit, allowing the formation of the 80S complex. This causes an increase in the translation of transcription factors involved in the cell cycle, cholesterol and lipid biosynthesis, glycolysis, and DNA packaging. The downregulation of EIF6 leads to a decrease in

translation since there are deficits in the maturation of the 60S subunit and in the formation of the 80S ribosomal complex (Brina et al., 2011; Brina et al., 2015; Miluzio et al., 2016). This, together with the decrease in rRNA due to the oxidation of nucleic acids in NDs as a result of the accumulation of ROS (Abe et al., 2003; Nunomura et al., 2006; Zhang et al., 1999), explains why the downregulation of this gene in flies had no beneficial effects.

On the other hand, the slight protection obtained by the downregulation of *Strat*, *RABIF* in humans, can be explained by a compensatory effect. As was explained before, RABIF is a Rab-stabilizing holdase chaperone for several Rabs, including Rab8 and Rab10 (Delfino et al., 2020; Gulbranson et al., 2017; Itzen et al., 2006). Previous studies have shown that the OE of Rab8 was protective against mHTT toxicity in flies - improved neurodegeneration, eclosion, lifespan and circadian rhythms, and also increased the number of insoluble mHTT aggregates (Delfino et al., 2020) -. Interestingly, the downregulation of RABIF also caused an increase in the degradation of Rab10, which is involved in the exocytosis of the glucose transporter GLUT4 (Gulbranson et al., 2017). As it was mentioned before, defects in the exocytosis of this receptor lead to a decrease in glucose intake (Apelt et al., 1999), which can contribute to the glucose hypometabolism seen in the brain of HD patients and to an earlier onset of the disease (Ciarmiello et al., 2006; Vittori et al., 2014). Therefore, as mentioned above, the protection caused by the downregulation of Strat would be due to a compensatory effect. The downregulation of Strat causes an increase in the degradation of Rabs because they become unstable, therefore, to maintain the appropriate protein levels, the cell increases the synthesis of those same Rabs and, if the speed of this synthesis is faster than the degradation, the level of Rabs increases, which can cause the protection seen during the experiments.

Taking this into account, it would be interesting to see the effect of the OE of those genes in the HD model flies.

7. Discussion and future directions

Through this work, we have shown that QTL analysis is a highly valuable tool to uncover genes involved in the inheritance of non-Mendelian traits - such as those potentially involved in the age at onset and in the risk to suffer from NDs. Indeed, yeast are a good model for QTL analysis as they share major biological processes and conserved genes with humans, their genome has been completely sequenced and is thoroughly annotated, and it is easy to obtain large and diverse populations through intercrosses to break linkage groups. The QTL analysis in Chapter 4 identified several genes that previous studies had associated with HD and PD-like syndromes, therefore suggesting that it is possible to find phenotype modifier genes of NDs using yeast as a model. The disease-related genes consisted of six genes where human orthologues had been related to HD - *HDAC1* (Bodai et al., 2001; Thomas et al., 2008), *IDH1* (Gruber-Bzura et al., 2017), *TIMELESS* (Faragó et al., 2019), *GRB2* (Baksi et al., 2013) and *SIRT1* (Baldo et al., 2019; Jiang et al., 2011)- and one related to Parkinsonism - *VPS13C* (Lesage et al., 2016). Furthermore, these experiments also validated the results from previous studies modelling HD in yeast since the QTL analysis performed in the mHTT transformants also identified as candidates genes some that were highlighted in the deletion study [5 genes which deletion suppressed toxicity and two which enhanced toxicity (Willingham et al., 2003)], the OE study [60 which when overexpressed suppressed toxicity (Mason et al., 2013)], and the differential expression study [84 genes were differentially expressed in the HTT and the mHTT transformants (Tauber et al., 2011)]. Therefore, assessing the differences in MG of humanized yeast expressing mHTT and αSyn is a quick and simple method to study the genes and pathways involved in HD and PD.

Considering this, other parameters could be used for the QTL analysis, for example, aggregation. In Chapter 3 we established that all three parental strains,

resistant or sensitive, show aggregation of mHTT and α Syn, albeit with some differences in the number of aggregates. Together with the results seen in Chapter 4, in which the F12 strains display the presence or absence of mHTT aggregates regardless of their sensitivity to the protein's toxicity, these results lead us to the conclusion that aggregation in itself does not correlate with toxicity in yeast. Nevertheless, aggregation is a process present in multiple NDs, and expanding our knowledge of the routes and genes underlying this process could lead to the discovery of new therapeutic targets. Therefore, in future experiments it would be worth performing a QTL analysis on aggregation; this could be done via filter trap, comparing the intensity of the signal between the CelAc and NC membranes to establish how much protein is aggregated in each strain, or using fluorescence microscopy to determine the percentage of cells with aggregates and the number of aggregates per cell. Another possibility is to study the aggregation dynamics of mHTT in live cells, using a recording system like the Livecyte 2 (Phasefocus). This microscopy system can be set to maintain a certain temperature and to image the samples using light and fluorescence microscopy every couple of minutes, providing a substantial amount of data but reducing phototoxicity. This data could be used to determine how long the cell takes to generate a certain quantity of protein, how much protein is present before it begins to aggregate, how long does it take for the aggregates to form, if the aggregates are being cleared, and if it is possible for the cells to inherit the aggregates from their progenitors. Furthermore, these parameters could also be used for the QTL analysis since it would be especially interesting to find which genes make the strains resistant and also allow them to clear mHTT before or after it forms aggregates.

The results from the QTL analysis were especially interesting since they uncovered an enrichment in genes related to ribosome synthesis, RNA metabolism,

protein degradation and energy metabolism in both HD and PD models. Beside those pathways, an enrichment in genes related to DNA repair, transcription, glycosylphosphatidylinositol-anchor biosynthesis, and cell cycle was found in the HD model. Some of these pathways- protein catabolism (Willingham et al., 2003) and transcription (Giorgini et al., 2005)- were also enriched in previous yeast studies.

Regarding the selection of the possible modifier genes, it was impossible to verify the complete list so, in order to reduce the number of genes to validate, I needed them to follow certain criteria: be in both the mHTT and the α Syn QTL lists, be the closest gene to the peak (the central point of the region highlighted during the analysis), have human and fly orthologues that were expressed in the brain and not being an already known modifier of the disease. These requirements reduced the list from hundreds of genes to the eight main genes that were to be studied in the parental strains: *FAR10*, *GSY2*, *DSS4*, *TIF6*, *PPM1*, *MRX21*, *RPA135*, and *TAF2*. An easy way to determine the effect these genes had on the toxicity caused by mHTT and α Syn was to delete and to overexpress them in the parental strain - to ascertain in the resistant SX1 if they enhanced the toxicity, and in the sensitive strains HN6 and BJ20 if they were deleterious or protective. Due to their status as essential genes, the deletions of *FAR10* and *RPA135* were impossible in the parental strains since they were haploids, therefore as a follow-up experiment, it would be valuable to generate diploids of the parental strains and delete those two genes in hemizygosity to discern if it confers some protection, although, as it was mentioned in Chapter 4, due to their function it seems very unlikely their deletions would have a protective effect.

On one hand, *RPA135* and its human orthologue *POLR1B* encode a subunit of the RNA Pol I responsible for the synthesis of rRNA and the maintenance of the nucleolar structure (Kobayashi et al., 1998), and its downregulation would cause

defects in transcription and nucleolar stress, which has been associated with NDs including HD and PD (Parlato & Kreiner, 2013; Parlato & Liss, 2014). Previous studies have shown that downregulating initiation transcription factors associated with RNA Pol I cause HD and PD-like phenotypes in mice such as defects in rDNA transcription (Lee et al., 2011; Lee et al., 2014), mitochondrial impairment (Jesse et al., 2017; Rieker et al., 2011) and perturbation of the nucleolar function that can lead to apoptosis (Kreiner et al., 2013; Parlato et al., 2008; Rieker et al., 2011; Yuan et al., 2005). Therefore, it is reasonable to expect the downregulation of *RPA135* to be detrimental, however, its OE might be protective.

On the other hand, *FAR10* and its orthologue *SLMAP*, encode a protein involved in docking and membrane fusion during vesicle trafficking and exocytosis (Hwang & Pallas, 2014). It is involved in the exocytosis of GLUT4, an insulin-dependent glucose transporter that colocalizes with GLUT3 to provide an extra intake of glucose in neurons (Apelt et al., 1999; Chen & Ding, 2011). This is important since HD patients display glucose hypometabolism in the brain that precedes the onset of the disease and the increase of GLUT3 is able to delay the onset of the disease (Ciarmiello et al., 2006; Vittori et al., 2014). Therefore, the deletion of this gene being protective is highly improbable since, alongside the glucose hypometabolism of the patients, it would also cause a decrease in glucose intake in the neurons caused by a transport impairment that prevents the exocytosis of GLUT4 to the membrane, which may lead to an earlier onset of HD. *SLMAP* is also part of the STRIPAK complex, and for that reason, it is implicated in several processes (Hwang & Pallas, 2014). Among them, the role of PP2A, another component of the STRIPAK complex, in dephosphorylating CLOCK so it can be active during the evenings is especially interesting, since circadian rhythms are altered in HD and PD (Andreazza et al., 2015; Hwang & Pallas, 2014; Jankovic & Tan, 2020; Morton, A. Jennifer, Wood et al., 2005). However, the

most interesting role of STRIPAK in relation to survival is the negative regulation of the Hippo pathway. Indeed, YAP levels are decreased in the brains of HD patients due to an increase in pMST1 and pMST2, causing transcriptional dysregulation and cell death (Bae et al., 2017; Hwang & Pallas, 2014; Mueller et al., 2018). The function of STRIPAK also suggests that the OE of *FAR10* is more expected to have beneficial effects than its deletion. However, only the precursor of this pathway, the FEAR/MEN pathway, exists in yeast so more experiments are needed (Marston, 2014; Zabrocki et al., 2002).

Apart from *RPA135* and *FAR10*, it was possible to delete the other six genes in at least one of the parental strains and test their effect on mHTT and α Syn toxicity by PHENOS. The results from this experiment served to identify the deletion of *PPM1* as an enhancer of α Syn toxicity in all three parental strains and of mHTT toxicity in the resistant strain. LCMT1, the human orthologue of *PPM1*, is the methyltransferase responsible for the activation of PP2A (Javadpour et al, 2019; Sontag and Sontag, 2014). Therefore, LCMT1 is involved in circadian rhythms and the Hippo pathway (FEAR/MEN in yeast) via PP2A, so its upregulation is expected to be more beneficial than its deletion (Andreazza et al., 2015; Bae et al., 2017; Hwang & Pallas, 2014; Mueller et al., 2018). This deletion is particularly interesting since *LCMT1* is downregulated in PD, causing a decrease in active PP2A, which is related to the increase in the phosphorylation of α Syn and its aggregation (Javadpour et al., 2019).

The deletion of *GYS2* has curious effects - it worsens both mHTT and α Syn toxicity in SX1 while improving them in BJ20, and it improves mHTT toxicity but not α Syn in HN6. These results contradict what has been previously described: there is an accumulation of glycogen in neurones in several NDs and glycogen is thought to be protective against ER stress (Inoue et al., 2006). There are also studies showing that

mHTT causes proteasomal and oxidative stress that led to an increase in active GYS1 - the human orthologue of GYS2, increasing the accumulation of glycogen (Rai et al., 2018). Furthermore, the accumulated glycogen was found to colocalize with mHTT aggregates and induce autophagy, improving the clearance of the aggregates and reducing mHTT toxicity. Taking this into consideration, it would be interesting to study if there are differences in glycogen accumulation between the resistant and the sensitive strains when expressing the toxic proteins and, if there are, it would be nice to perform a study of the accumulation of glycogen and the clearance of the aggregates fixing cells at different times and staining them with PAS to visualize the aggregates under the light microscope. It would also be worth it to determine if the OE of *GYS2* is protective against mHTT and αSyn in the parental strains.

The OE of four of the genes (*DSS4*, *TAF2*, *TIF6* and *MRX21*) was performed in the parental strains. The results from this experiment showed that the OE of *TIF6* suppressed mHTT and αSyn toxicity in both sensitive strains and had no effect in the resistant one, which could suggest the resistance strain is resistant because TIF6 is naturally upregulated. Although there was also a small rescue when deleting the gene in yeast, the downregulation of *eIF6*, its orthologue in flies, showed no protective effect in any of the parameters studied. Therefore, as it was mentioned in the discussion of Chapter 5, the protection seen when overexpressing TIF6 is likely associated with the fact that oxidative stress is a common trait of NDs and the accumulation of ROS can cause the oxidation of nucleic acids, causing a decrease in rRNA and thus an impairment in transcription (Abe et al., 2003; Nunomura et al., 2006; Zhang et al., 1999). Since *TIF6*, and its human orthologue *EIF6*, are involved in the maturation of rRNA (Basu et al., 2001), it is reasonable that an increase in this

protein ameliorates the transcriptional deficits caused by the oxidative stress. As a future experiment, it would be interesting to test the protective effects of overexpressing this gene in fly models of HD and PD.

The results from the deletion and OE of the other genes in the parental strains were inconclusive since their effect varied between strains. *DSS4* is one of those genes, its OE was protective against mHTT in the sensitive strain HN6 and had no effect in the resistant strain SX1 nor the sensitive strain BJ20, while its deletion was protective against mHTT in BJ20 but had no effect in HN6. Interestingly, a rather small neuroprotective effect also appeared when downregulating *Strat*, the fly orthologue of *DSS4*. Although it might seem like both the downregulation and the OE of this gene have protective effects, given the function of the protein, it is more likely that the protection caused by its downregulation is due to compensatory effects. *RABIF* (the human orthologue of *Strat* in flies and *DSS4* in yeast) is a Rab-stabilizing holdase chaperone that promotes the release of GDP from Rab GTPases by causing a conformational exchange and allows Rab to stay nucleotide-free without being degraded; it has a low GEF catalytic activity for some Rabs, but its main role is the stabilization of Rabs- (Gulbranson et al., 2017; Itzen et al., 2006; Nuoffer et al., 1997). Since Rab GTPases are impaired in multiple NDs, including HD and PD, causing problems in vesicular trafficking (Kiral et al., 2018), it is reasonable to think that RABIF could play a role in ameliorating this process. Studies have shown that the OE of either Rab8, which is involved in Golgi-lysosome trafficking and becomes impaired when HTT is reduced (White et al., 2015), or Rab11, which is involved in endosome motility and recycling, is enough to rescue neurodegeneration in HD models (Delfino et al., 2020; Richards et al., 2011; Steinert et al., 2012). Both proteins, Rab8 and Rab11, are substrates of RABIF (Gulbranson et al., 2017; Nuoffer et al., 1997). Another of the RABIF interactors, Rab10, could be involved in HD since,

although it does not interact with HTT, is involved in the exocytosis of GLUT4 (Gulbranson et al., 2017). The downregulation of RAB1F leads to faster degradation of Rab10, causing defects in GLUT4 exocytosis and a decrease in glucose intake. In HD patients, there is already a glucose hypometabolism seen in the brain, so a deficit in the exocytosis of the transporter would further worsen the disease and could bring forward its onset (Ciarmiello et al., 2006; Vittori et al., 2014). Taking this into account, we suggest that the protective effects of overexpressing *RAB1F* are due to its role as a Rab-stabilizer, while the protection seen when it is deleted or downregulated is due to a compensatory effect in which the cells are producing more Rabs to compensate for those that are being degraded. Indeed, if this production is faster than the degradation, it would lead to a small OE of Rabs and, as we have mentioned before, the OE of some of them is neuroprotective against mHTT. Taking this into account, it would be interesting to test the OE of *Strat* in a fly model of HD.

In relation to the second set of genes that were in both QTL lists, nine genes were verified in the laboratory strain BY4741 (*RPD3*, *PEX6*, *YCR043C*, *PER1*, and *GIN4*, *PPZ2*, *BPH1*, *SNT1* and *ELO2*). Only two of them had any significant effect on the disease phenotypes - enhancing αSyn toxicity (*PER1* and *GIN4*), although a longer PHENOS experiment that allows the study of the growth curves until the stationary phase would be necessary for the deletion of *PEX6* and *GIN4*.

The human orthologue of *GIN4*, *BRSK2*, is one of the genes upregulated during the UPR response caused by ER stress (Wang et al., 2012). During stress conditions, BRSK2 migrates from the periphery of the nucleus to the ER, and it is involved in preventing apoptosis - since its deletion increases apoptosis in tumoral cells during ER stress while its OE prevents it (Wang et al., 2012). As the UPR response is also triggered in PD, this mechanism might be responsible for the

enhancement of α Syn toxicity due to the deletion of *G/N4*. Therefore, future research should include the OE of this gene in the parental strains.

The deletion of *PER1* causes an enhancement in α Syn toxicity. *PER1* and its human orthologue PGAP3 are involved in the post-translational membrane anchoring of GPI-APs (Fujita et al., 2006). One of these GPI-APs is GFR α 1, which is part of the GDNF family receptor-a, necessary for the detection of GDNF, which is able to prevent neurodegeneration and reverse functional deficits in PD models (Howard et al., 2014). Therefore, it is reasonable that the loss of this GDNF receptor caused by the deletion of *PER1* enhances α Syn toxicity. It also suggests that the OE of this gene might improve the PD associated phenotypes.

It is interesting that neither the deletion of *RPD3* nor *SNT1* had any effect on mHTT toxicity since their human orthologues (HDAC1 and 2, and NCOR1 and 2 respectively) have been related to HD (Boutell et al., 1999; Peña-Altamira et al., 2013). In the case of HDAC1, its inhibition ameliorates transcriptional impairment and prevents neurodegeneration (Bodai et al., 2001; Thomas et al., 2008), but its deletion causes a dysregulation in histone acetylation levels (Zhou et al., 2009), which could worsen the transcriptional impairment caused by mHTT and nullify the beneficial effects that its inhibition should have. In the case of NCOR1, it is likely that the deleterious effects it causes in transcription are related to its mislocalisation when it interacts with mHTT, and since its deletion would prevent this interaction, those transcriptional problems should not happen (Boutell et al., 1999). However, since it is an important transcriptional regulator, its deletion does not cause beneficial effects either.

In summary, it is possible to identify potential modifier genes by performing a QTL analysis in yeast using the differences in MG as the defining phenotype. The main

advantages are that a large population can be obtained and analysed easily, several diseases can be studied in the same population, and the results are easy to validate in the same or in more complex models like fruit flies. During this thesis, we established that aggregation of mHTT and αSyn does not correlate with toxicity in yeast, and identified four modifier genes. The deletion of *PPM1* enhances both mHTT and αSyn toxicity in yeast, the deletion of *PER1* and *GIN4* enhances αSyn toxicity, and the OE of *TIF6* suppresses mHTT and αSyn toxicity. In conclusion, these four genes, specially *TIF6*, are interesting therapeutic targets for HD and PD although further study is needed.

8. Bibliography

Abe, T., Isobe, C., Murata, T., Sato, C., Tohgi, H., 2003. Alteration of 8-hydroxyguanosine concentrations in the cerebrospinal fluid and serum from patients with Parkinson's disease. *Neuroscience Letters*. **336**, 105-108.

Anderson, K. & Marder, K., 2001. An overview of psychiatric symptoms in Huntington's disease. *Current Psychiatry Reports*. **3**, 379-388.

Andreazza, S., Bouleau, S., Martin, B., Lamouroux, A., Ponien, P., Papin, C., Chélot, E., Jacquet, E., Rouyer, F., 2015. Daytime CLOCK Dephosphorylation Is Controlled by STRIPAK Complexes in Drosophila. *Cell Reports (Cambridge)*. **11**, 1266-1279.

Andreazza, S., et al, 2019. Mitochondrially-targeted APOBEC1 is a potent mtDNA mutator affecting mitochondrial function and organismal fitness in Drosophila. Springer Science and Business Media LLC.

Apelt, J., Mehlhorn, G., Schliebs, R., 1999. Insulin-sensitive GLUT4 glucose transporters are colocalized with GLUT3-expressing cells and demonstrate a chemically distinct neuron-specific localization in rat brain. *Journal of Neuroscience Research*. **57**, 693-705.

Armstrong, M.J. & Okun, M.S., 2020. Diagnosis and Treatment of Parkinson Disease: A Review. *JAMA : The Journal of the American Medical Association*. **323**, 548-560.

Ascherio, A. and Schwarzschild, M.A., 2016. The epidemiology of Parkinson's disease: risk factors and prevention. Elsevier BV.

Bae, S.J., Ni, L., Osinski, A., Tomchick, D.R., Brautigam, C.A., Luo, X., 2017. SAV1 promotes Hippo kinase activation through antagonizing the PP2A phosphatase STRIPAK. *eLife*. **6**.

Baksi, S., Jana, N.R., Bhattacharyya, N.P., Mukhopadhyay, D., 2013. Grb2 Is Regulated by Foxd3 and Has Roles in Preventing Accumulation and Aggregation of Mutant Huntingtin. *PLoS One*. **8**, e76792.

Baldo, B., Gabery, S., Soylu-Kucharz, R., Cheong, R.Y., Henningsen, J.B., Englund, E., McLean, C., Kirik, D., Halliday, G., Petersén, Å, 2019. SIRT1 is increased in affected brain regions and hypothalamic metabolic pathways are altered in Huntington disease. *Neuropathology and Applied Neurobiology*. **45**, 361-379.

Barbaro, B.A., Lukacsovich, T., Agrawal, N., Burke, J., Bornemann, D.J., Purcell, J.M., Worthge, S.A., Caricasole, A., Weiss, A., Song, W., Morozova, O.A., Colby, D.W., Marsh, J.L., 2015. Comparative study of naturally occurring huntingtin fragments in Drosophila points to exon 1 as the most pathogenic species in Huntington's disease. *Human Molecular Genetics*. **24**, 913-925.

Barker, R.A., Barrett, J., Mason, S.L., Björklund, A., 2013. Fetal dopaminergic transplantation trials and the future of neural grafting in Parkinson's disease. *Lancet Neurology*. **12**, 84-91.

Barker, R.A. & Transeuro consortium, 2019. Designing stem-cell-based dopamine cell replacement trials for Parkinson's disease. *Nature Medicine*. **25**, 1445-1453.

Barton, D.B.H., Georghiou, D., Dave, N., Alghamdi, M., Walsh, T.A., Louis, E.J., Foster, S.S., 2018. PHENOS: a high-throughput and flexible tool for microorganism growth phenotyping on solid media. *BMC Microbiology*. **18**, 9.

Basu, U., Si, K., Warner, J.R., Maitra, U., 2001. The *Saccharomyces cerevisiae* TIF6 Gene Encoding Translation Initiation Factor 6 Is Required for 60S Ribosomal Subunit Biogenesis. *Molecular and Cellular Biology*. **21**, 1453-1462.

Beal, M.F., Matson, W.R., Swartz, K.J., Gamache, P.H., Bird, E.D., 1990. Kynurenone Pathway Measurements in Huntington's Disease Striatum: Evidence for Reduced Formation of Kynurenic Acid. *Journal of Neurochemistry*. **55**, 1327-1339.

Benzer, S., 1967. Behavioral Mutants of *Drosophila* Isolated by Countercurrent Distribution. *Proceedings of the National Academy of Sciences - PNAS*. **58**, 1112-1119.

Bodai, L., Apostol, B.L., Jackson, G.R., Zhu, Y., Kazantsev, A., Thompson, L.M., Kurokawa, R., Schmidt, E., McCampbell, A., Marsh, J.L., Housman, D.E., Poelman, M., Steffan, J.S., Pallos, J., Greenwald, M., 2001. Histone deacetylase inhibitors arrest polyglutamine-dependent neurodegeneration in *Drosophila*. *Nature (London)*. **413**, 739-743.

Bonelli, R.M. & Beal, M.F., 2013. Huntington's disease. In Schlaepfer, T. E. & Nemeroff, C. B., eds, *Handbook of Clinical Neurology*. 3rd ed. Philadelphia: Elsevier.

Boutell, J.M., Thomas, P., Neal, J.W., Weston, V.J., Duce, J., Harper, P.S., Lesley Jones, A., 1999. Aberrant Interactions of Transcriptional Repressor Proteins with the Huntington's Disease Gene Product, Huntingtin. *Human Molecular Genetics*. **8**, 1647-1655.

Brand, A.H. & Perrimon, N., 1993. Targeted gene expression as a means of altering cell fates and generating dominant phenotypes. *Development*. **118**, 401-415.

Brás, I.C., Popova, B., Braus, G.H. and Outeiro, T.F., 2019. Yeast-Based Screens to Target Alpha-Synuclein Toxicity. In Bartels, T., ed, *Alpha-synuclein. Methods and protocols*. New York: Humana Press. 145-156.

Breda, C., Sathyasaikumar, K.V., Sograte Idrissi, S., Notarangelo, F.M., Estranero, J.G., Moore, G.G.L., Green, E.W., Kyriacou, C.P., Schwarcz, R., Giorgini, F., 2016. Tryptophan-2,3-dioxygenase (TDO) inhibition ameliorates neurodegeneration by modulation of kynurenone pathway metabolites. *Proceedings of the National Academy of Sciences - PNAS*. **113**, 5435-5440.

Breen, D.P., Halliday, G.M., Lang, A.E., 2019. Gut–brain axis and the spread of α-synuclein pathology: Vagal highway or dead end? *Movement Disorders*. **34**, 307-316.

Brina, D., Grosso, S., Miluzio, A., Biffo, S., 2011. Translational control by 80S formation and 60S availability: The central role of eIF6, a rate limiting factor in cell cycle progression and tumorigenesis. *Cell Cycle*. **10**, 3441-3446.

Brina, D., Miluzio, A., Ricciardi, S., Clarke, K., Davidsen, P.K., Viero, G., Tebaldi, T., Offenhäuser, N., Rozman, J., Rathkolb, B., Neschen, S., Klingenspor, M., Wolf, E., Gailus-Durner, V., Fuchs, H., Hrabe De Angelis, M., Quattrone, A., Falciani, F., Biffo, S., 2015. eIF6 coordinates insulin sensitivity and lipid metabolism by coupling translation to transcription. *Nature Communications*. **6**.

Broman, K.W., 2015. R/qtlcharts: Interactive Graphics for Quantitative Trait Locus Mapping. *Genetics (Austin)*. **199**, 359-361.

Broman, K.W., 2003. Mapping Quantitative Trait Loci in the Case of a Spike in the Phenotype Distribution. *Genetics (Austin)*. **163**, 1169-1175.

Budworth, H. & McMurray, C.T., 2013. A Brief History of Triplet Repeat Diseases. *Trinucleotide Repeat Protocols*. Totowa, NJ: Humana Press. 3-17.

Campesan, S., Green, E., Breda, C., Sathyasaikumar, K., Muchowski, P., Schwarcz, R., Kyriacou, C., Giorgini, F., 2011. The Kynurenone Pathway Modulates Neurodegeneration in a Drosophila Model of Huntington's Disease. *Current Biology*. **21**, 961-966.

Cervenka, I., Agudelo, L.Z., Ruas, J.L., 2017. Kynurenines: Tryptophan's metabolites in exercise, inflammation, and mental health. *Science*. **357**.

Chang, D., Nalls, M.A., Hallgrímsdóttir, I.B., Hunkapiller, J., Van Der Brug, M., Cai, F., Kerchner, G.A., Ayalon, G., Bingol, B., Sheng, M., Hinds, D., Behrens, T.W., Singleton, A.B., Bhagale, T.R., Graham, R.R., 2017. A meta-analysis of genome-wide association studies identifies 17 new Parkinson's disease risk loci. *Nature Genetics*. **49**, 1511-1518.

Chen, X. & Ding, H., 2011. Increased Expression of the Tail-Anchored Membrane Protein SLMAP in Adipose Tissue from Type 2Tally HoDiabetic Mice. *Experimental Diabetes Research*. **2011**, 1-10.

Chiara, Z., Andrea, C., Dorotea, R., Leavitt Blair, R., Donato, G., Luciano, C., MacDonald Marcy, E., Friedlander Robert, M., Vincenzo, S., Hayden Michael, R., Timmusk Tõnis, Simonetta, S., Elena, C., 2001. Loss of Huntingtin-Mediated BDNF Gene Transcription in Huntington's Disease. *Science*. **293**, 493-498.

Christine, C.W., Bankiewicz, K.S., Van Laar, A.D., Richardson, R.M., Ravina, B., Kells, A.P., Boot, B., Martin, A.J., Nutt, J., Thompson, M.E., Larson, P.S., 2019. Magnetic resonance imaging-guided phase 1 trial of putaminal AADC gene therapy for Parkinson's disease. *Annals of Neurology*. **85**, 704-714.

Chu, A.M. & Davis, R.W., 2008. High-Throughput Creation of a Whole-Genome Collection of Yeast Knockout Strains. In Osterman, A. L. & Gerdes, S. Y., eds, *Microbial Gene Essentiality: Protocols and Bioinformatics*. Humana Press. 205-220.

Churchill, G.A. & Doerge, R.W., 1994. Empirical threshold values for quantitative trait mapping. *Genetics (Austin)*. **138**, 963-971.

Ciarmiello, A., Cannella, M., Lastoria, S., Simonelli, M., Frati, L., Rubinsztein, D.C., Squitieri, F., 2006. Brain White-Matter Volume Loss and Glucose Hypometabolism Precede the Clinical Symptoms of Huntington's Disease. *The Journal of Nuclear Medicine (1978)*. **47**, 215-222.

Coulom, H. & Birman, S., 2004. Chronic Exposure to Rotenone Models Sporadic Parkinson's Disease in *Drosophila melanogaster*. *The Journal of Neuroscience*. **24**, 10993-10998.

Cubillos, F.A., Billi, E., Zörgö, E., Parts, L., Fargier, P., Omholt, S., Blomberg, A., Warringer, J., Louis, E.J., Liti, G., 2011. Assessing the complex architecture of polygenic traits in diverged yeast populations. *Molecular Ecology*. **20**, 1401-1413.

Dash, D. & Mestre, T.A., 2020. Therapeutic Update on Huntington's Disease: Symptomatic Treatments and Emerging Disease-Modifying Therapies. *Neurotherapeutics*. **17**, 1645-1659.

Davis, W.M., 2004. ApE: A plasmid Editor.

Dawson, T.M., Golde, T.E., Lagier-Tourenne, C., 2018. Animal models of neurodegenerative diseases. *Nature Neuroscience*. **21**, .

Delfino, L., Mason, R.P., Kyriacou, C.P., Giorgini, F., Rosato, E., 2020. Rab8 Promotes Mutant HTT Aggregation, Reduces Neurodegeneration, and Ameliorates Behavioural Alterations in a *Drosophila* Model of Huntington's Disease. *Journal of Huntington's Disease*. **9**, 253-263.

Dhekne, H.S., Yanatori, I., Gomez, R.C., Tonelli, F., Diez, F., Schüle, B., Steger, M., Alessi, D.R., Pfeffer, S.R., 2018. A pathway for Parkinson's Disease LRRK2 kinase to block primary cilia and Sonic hedgehog signaling in the brain. *eLife*. **7**, .

DiFiglia, M., Sapp, E., Chase, K.O., Davies, S.W., Bates, G.P., Vonsattel, J.P., Aronin, N., 1997. Aggregation of Huntingtin in Neuronal Intracellular Inclusions and Dystrophic Neurites in Brain. *Science*. **277**, 1900-1993.

Duan, S., et al, 2018. The origin and adaptive evolution of domesticated populations of yeast from Far East Asia. Springer Science and Business Media LLC.

Duennwald, M.L., Jagadish, S., Muchowski, P.J., Lindquist, S., 2006. Flanking Sequences Profoundly Alter Polyglutamine Toxicity in Yeast. *Proceedings of the National Academy of Sciences - PNAS*. **103**, 11045-11050.

Duffy, J.B., 2002. GAL4 system in drosophila: A fly geneticist's swiss army knife. *Genesis (New York, N.Y. : 2000)*. **34**, 1-15.

Duffy, P.E. & Tennyson, V., 1965. Phase and electron microscopic observations of Lewy Bodies and Melanin Granules in the Substantia Nigra and Locus Caeruleus in Parkinson's Disease. *Journal of Neuropathology & Experimental Neurology*. **24**, 398–414.

Dugger, B.N. & Dickson, D.W., 2017. Pathology of neurodegenerative diseases. *Cold Spring Harbor Perspectives in Biology*. **9**, a028035.

Duran, J., Saez, I., Gruart, A., Guinovart, J.J., Delgado-García, J.M., 2013. Impairment in Long-Term Memory Formation and Learning-Dependent Synaptic Plasticity in Mice Lacking Glycogen Synthase in the Brain. *Journal of Cerebral Blood Flow and Metabolism*. **33**, 550-556.

Faragó, A., Zsindely, N., Bodai, L., 2019. Mutant huntingtin disturbs circadian clock gene expression and sleep patterns in Drosophila. *Scientific Reports*. **9**, .

Farrer, M., Kachergus, J., Forno, L., Lincoln, S., Wang, D., Hulihan, M., Maraganore, D., Gwinn-Hardy, K., Wszolek, Z., Dickson, D., Langston, J.W., 2004. Comparison of kindreds with parkinsonism and α-synuclein genomic multiplications. *Annals of Neurology*. **55**, 174-179.

Fiermonte, G., Paradies, E., Todisco, S., Marobbio, C.M.T., Palmieri, F., 2009. A Novel Member of Solute Carrier Family 25 (SLC25A42) Is a Transporter of Coenzyme A and Adenosine 3',5'-Diphosphate in Human Mitochondria. *The Journal of Biological Chemistry*. **284**, 18152-18159.

Fisher, R.A., 1919. The causes of human variability. *The Eugenics Review*. **10**, 213-220.

Frank, S., 2009. Tetrabenazine as anti-chorea therapy in Huntington Disease: an open-label continuation study. Huntington Study Group/TETRA-HD Investigators. *BMC Neurology*. **9**, 62.

Fujita, M., Umemura, M., Takehiko, †, , Y., Jigami, Y., 2006. Shugoshin 2 regulates localization of the chromosomal passenger proteins in fission yeast mitosis. *Molecular Biology of the Cell*. **17**, 5253.

GeM-HD Consortium, 2019. CAG repeat not polyglutamine length determines timing of Huntington's disease onset. *178*, 887-900.

Gietz, R.D. & Schiestl, R.H., 2007. Quick and easy yeast transformation using the LiAc/SS carrier DNA/PEG method. *Nature Protocols*. **2**, 35-37.

Giordano, E., et al, 2002. RNAi Triggered by Symmetrically Transcribed Transgenes in *Drosophila melanogaster*. Oxford University Press (OUP).

Giorgini, F., Guidetti, P., Nguyen, Q., Bennett, S.C., Muchowski, P.J., 2005. A genomic screen in yeast implicates kynurenine 3-monooxygenase as a therapeutic target for Huntington disease. *Nature Genetics*. **37**, 526-531.

Giorgini, F. & Muchowski, P.J., 2009. Exploiting Yeast Genetics to Inform Therapeutic Strategies for Huntington's Disease. *Yeast Functional Genomics and Proteomics*. Totowa, NJ: Humana Press. 161-174.

Giorgini, F. & Muchowski, P.J., 2006. Screening for Genetic Modifiers of Amyloid Toxicity in Yeast. In Kheterpal, I. & Wetzel, R., eds, *Amyloid, Prions, and Other Protein Aggregates, Part B*. San Diego, United States: Elsevier Science Publishing Co Inc. 201-222.

Gitler, A.D., Bevis, B.J., Shorter, J., Strathearn, K.E., Hamamichi, S., Su, L.J., Caldwell, K.A., Caldwell, G.A., Rochet, J., McCaffery, J.M., Barlowe, C., Lindquist, S., 2008. The Parkinson's Disease Protein α -Synuclein Disrupts Cellular Rab Homeostasis. *Proceedings of the National Academy of Sciences - PNAS*. **105**, 145-150.

Goffeau, A., Barrell, B.G., Bussery, H., Davis, R.W., Dujon, B., Feldmann, H., Galibert, F., Hoheisel, J.D., Jacq, C., Johnston, M., Louis, E.J., Mewes, H.W., Murakami, Y., Philippson, P., Tettelin, H., Oliver, S.G., 1996. Life with 6000 genes. *Science*. **274**, 546-567.

Goody, R.S., Müller, M.P., Wu, Y., 2017. Mechanisms of action of Rab proteins, key regulators of intracellular vesicular transport. *Biological Chemistry*. **398**, 565-575.

Graham, R.K., Deng, Y., Slow, E.J., Haigh, B., Bissada, N., Lu, G., Pearson, J., Shehadeh, J., Bertram, L., Murphy, Z., Warby, S.C., Doty, C.N., Roy, S., Wellington, C.L., Leavitt, B.R., Raymond, L.A., Nicholson, D.W., Hayden, M.R., 2006. Cleavage at the Caspase-6 Site Is Required for Neuronal Dysfunction and Degeneration Due to Mutant Huntingtin. *Cell*. **125**, 1179-1191.

Green, E.W., Campesan, S., Breda, C., Sathyasaikumar, K.V., Muchowski, P.J., Schwarcz, R., Kyriacou, C.P., Giorgini, F., 2012. Drosophila eye color mutants as therapeutic tools for Huntington disease. *Fly (Austin, Tex.)*. **6**, 117-120.

Green, E.W. & Giorgini, F., 2012. Choosing and using Drosophila models to characterize modifiers of Huntington's disease. *Biochemical Society Transactions*. **40**, 739-745.

Greene, J.C., Whitworth, A.J., Kuo, I., Andrews, L.A., Feany, M.B., Pallanck, L.J., 2003. Mitochondrial Pathology and Apoptotic Muscle Degeneration in Drosophila parkin Mutants. *Proceedings of the National Academy of Sciences - PNAS*. **100**, 4078-4083.

Gruber-Bzura, B.M., Krzysztoń-Russjan, J., Bubko, I., Syska, J., Jaworska, M., Zmysłowski, A., Rosłon, M., Drozd, J., Drozd, E., Majorczyk, E., Anuszevska, E.L.,

2017. Role of thiamine in Huntington's disease pathogenesis: In vitro studies. *Advances in Clinical and Experimental Medicine : Official Organ Wroclaw Medical University.* **26**, 751-760.

Gulbranson, D.R., Davis, E.M., Demmitt, B.A., Ouyang, Y., Ye, Y., Yu, H., Shen, J., 2017. RABIF/MSS4 is a Rab-stabilizing holdase chaperone required for GLUT4 exocytosis. *Proceedings of the National Academy of Sciences.* **114**, E8224–E8233.

Gusella, J.F. & MacDonald, M.E., 2006. Huntington's disease: seeing the pathogenic process through a genetic lens. *Trends of Biochemical Science.* **31**, 533-540.

Gusella, J.F., Wexler, N.S., Conneally, P.M., Naylor, S.L., Anderson, M.A., Tanzi, R.E., Watkins, P.C., Ottina, K., Wallace, M.R., Sakaguchi, A.Y., Young, A.B., Shoulson, I., Bonilla, E., Martin, J.B., 1983. A polymorphic DNA marker genetically linked to Huntington's disease. *Nature.* **306**, 234–238.

Haitina, T., Lindblom, J., Renström, T., Fredriksson, R., 2006. Fourteen novel human members of mitochondrial solute carrier family 25 (SLC25) widely expressed in the central nervous system. *Genomics (San Diego, Calif.).* **88**, 779-790.

Hasan Siddique, Y., Rahul, Varshney, H., Mantasha, I., Shahid, M., 2021. Effect of luteolin on the transgenic Drosophila model of Huntington's disease. *Computational Toxicology.* **17**, 100148.

HDCRG, 1993. A novel gene containing a trinucleotide repeat that is expanded and unstable on Huntington's disease chromosomes. *Cell.* **72**, 971-983.

Healy-Stoffel, M., Ahmad, S.O., Stanford, J.A., Levant, B., 2013. Altered nucleolar morphology in substantia nigra dopamine neurons following 6-hydroxydopamine lesion in rats. *Neuroscience Letters.* **546**, 26-30.

Hepowit, N.L., Pereira, K.N., Tumolo, J.M., Chazin, W.J., MacGurn, J.A., 2020. Identification of ubiquitin Ser57 kinases regulating the oxidative stress response in yeast. *eLife.* **9**, e58155.

Hernández, I.H., Cabrera, J.R., Santos-Galindo, M., Sánchez-Martín, M., Domínguez, V., García-Escudero, R., Pérez-Álvarez, M.J., Pintado, B.N., Lucas, J.J., 2020. Pathogenic SREK1 decrease in Huntington's disease lowers TAF1 mimicking X-linked dystonia parkinsonism. *Brain.* **143**, 2207–2219.

Hiatt, S.M., Thompson, M.L., Prokop, J.W., Lawlor, J.M.J., Gray, D.E., Bebin, E.M., Rinne, T., Kempers, M., Pfundt, R., van Bon, B.W., Mignot, C., Nava, C., Depienne, C., Kalsner, L., Rauch, A., Joset, P., Bachmann-Gagescu, R., Wentzensen, I.M., McWalter, K., Cooper, G.M., 2019. Deleterious Variation in BRSK2 Associates with a Neurodevelopmental Disorder. *American Journal of Human Genetics.* **104**, 701-708.

Homma, Y., Hiragi, S., Fukuda, M., 2021. Rab family of small GTPases: an updated view on their regulation and functions. *The FEBS Journal.* **288**, 36-55.

Hou, J., Sigwalt, A., Fournier, T., Pflieger, D., Peter, J., de Montigny, J., Dunham, M., Schacherer, J., 2016. The Hidden Complexity of Mendelian Traits across Natural Yeast Populations. *Cell Reports (Cambridge)*. **16**, 1106-1114.

Howard, M., Murakami, Y., Pagnamenta, A., Daumer-Haas, C., Fischer, B., Hecht, J., Keays, D., Knight, S.L., Kölsch, U., Krüger, U., Leiz, S., Maeda, Y., Mitchell, D., Mundlos, S., Phillips, J., Robinson, P., Kini, U., Taylor, J., Horn, D., Kinoshita, T., Krawitz, P., 2014. Mutations in PGAP3 Impair GPI-Anchor Maturation, Causing a Subtype of Hyperphosphatasia with Mental Retardation. *American Journal of Human Genetics*. **94**, 278-287.

Huntington Study Group, 2006. Tetrabenazine as antichorea therapy in Huntington disease: a randomized controlled trial. *Neurology*. **66**, 366-372.

Huntington, G., 1872. On chorea. George Huntington, M.D. *The Journal of Neuropsychiatry and Clinical Neurosciences*. **15**, 109-112.

Hwang, J. & Pallas, D.C., 2014. STRIPAK complexes: Structure, biological function, and involvement in human diseases. *The International Journal of Biochemistry & Cell Biology*. **47**, 118-148.

Inoue, E., Mochida, S., Takagi, H., Higa, S., Deguchi-Tawarada, M., Takao-Rikitsu, E., Inoue, M., Yao, I., Takeuchi, K., Kitajima, I., Setou, M., Ohtsuka, T., Takai, Y., 2006. SAD: A Presynaptic Kinase Associated with Synaptic Vesicles and the Active Zone Cytomatrix that Regulates Neurotransmitter Release. *Neuron (Cambridge, Mass.)*. **50**, 261-275.

Inoue, M., Yagashita, S., Itoh, Y., Amano, N., Matsushita, M., 1996. Coexistence of paired helical filaments and polyglucosan bodies in the same neuron in an autopsy case of Alzheimer's disease. *Acta Neuropathol.* **92**, 511–514.

InterMine, 2021. *Saccharomyces Genome Database (SGD) YeastMine*. [online]. Available at: <https://yeastmine.yeastgenome.org/yeastmine/bag.do>.

Itzen, A., Pylypenko, O., Goody, R.S., Alexandrov, K., Rak, A., 2006. Nucleotide exchange via local protein unfolding-structure of Rab8 in complex with MSS4. *The EMBO Journal*. **25**, 1445-1455.

Jackson, G.R., Salecker, I., Dong, X., Yao, X., Arnheim, N., Faber, P.W., MacDonald, M.E., Zipursky, S.L., 1998. Polyglutamine-Expanded Human Huntingtin Transgenes Induce Degeneration of Drosophila Photoreceptor Neurons. *Neuron*. **21**, 633–642.

Jankovic, J. & Tan, E.K., 2020. Parkinson's disease: etiopathogenesis and treatment. *Journal of Neurology, Neurosurgery and Psychiatry*. **91**, 795-808.

Javadpour, P., Dargahi, L., Ahmadiani, A.A., Ghasemi, R., 2019. To be or not to be: PP2A as a dual player in CNS functions, its role in neurodegeneration, and its

interaction with brain insulin signaling. *Cellular and Molecular Life Sciences*. **76**, 2277–2297.

Jesse, S., Bayer, H., Alupei, M.C., Zügel, M., Mulaw, M., Tuorto, F., Malmsheimer, S., Singh, K., Steinacker, J., Schumann, U., Ludolph, A.C., Scharffetter-Kochanek, K., Witting, A., Weydt, P., Iben, S., 2017. Ribosomal transcription is regulated by PGC-1alpha and disturbed in Huntington's disease. *Scientific Reports*. **7**, 8513-10.

Jiang, M., Wang, J., Fu, J., Du, L., Jeong, H., West, T., Xiang, L., Peng, Q., Hou, Z., Cai, H., Seredenina, T., Arbez, N., Zhu, S., Sommers, K., Qian, J., Zhang, J., Mori, S., Yang, X.W., Tamashiro, K.L.K., Aja, S., Moran, T.H., Luthi-Carter, R., Martin, B., Maudsley, S., Mattson, M.P., Cichewicz, R.H., Ross, C.A., Holtzman, D.M., Krainc, D., Duan, W., 2011. Neuroprotective role of Sirt1 in mammalian models of Huntington's disease through activation of multiple Sirt1 targets. *Nature Medicine*. **18**, 153-158.

Karamanos, T.K., Kalverda, A.P., Thompson, G.S., Radford, S.E., 2015. Mechanisms of amyloid formation revealed by solution NMR. *Progress in Nuclear Magnetic Resonance Spectroscopy*. **88-89**, 86-104.

Kay, C., Collins, J.A., Wright, G.E.B., Baine, F., Miedzybrodzka, Z., Aminkeng, F., Semaka, A.J., McDonald, C., Davidson, M., Madore, S.J., Gordon, E.S., Gerry, N.P., Cornejo-Olivas, M., Squitieri, F., Tishkoff, S., Greenberg, J.L., Krause, A., Hayden, M.R., 2018. The molecular epidemiology of Huntington disease is related to intermediate allele frequency and haplotype in the general population. *American Journal of Medical Genetics Part B: Neuropsychiatric Genetics*. **177**, .

Keleman, K., Micheler, T. and VDRC project members, 2009. RNAi-phiC31 construct and insertion data submitted by the Vienna Drosophila RNAi Center.

Kiral, F.R., Kohrs, F.E., Jin, E.J., Hiesinger, P.R., 2018. Rab GTPases and Membrane Trafficking in Neurodegeneration. *Current Biology*. **28**, R471-R486.

Knaus, A., Awaya, T., Helbig, I., Afawi, Z., Pendziwiat, M., Abu-Rachma, J., Thompson, M.D., Cole, D.E., Skinner, S., Annese, F., Canham, N., Schweiger, M.R., Robinson, P.N., Mundlos, S., Kinoshita, T., Munnich, A., Murakami, Y., Horn, D., Krawitz, P.M., 2016. Rare Noncoding Mutations Extend the Mutational Spectrum in the PGAP3 Subtype of Hyperphosphatasia with Mental Retardation Syndrome. *Human Mutation*. **37**, 737-744.

Kobayashi, T., Heck, D.J., Nomura, M., Horiuchi, T., 1998. Expansion and contraction of ribosomal DNA repeats in *Saccharomyces cerevisiae*: requirement of replication fork blocking (Fob1) protein and the role of RNA polymerase I. *Genes & Development*. **12**, 3821-3830.

Koushika, S.P., Lisbin, M.J., White, K., 1996. ELAV, a Drosophila neuron-specific protein, mediates the generation of an alternatively spliced neural protein isoform. *Current Biology*. **6**, 1634-1641.

Kreiner, G., Bierhoff, H., Armentano, M., Rodriguez-Parkitna, J., Sowodniok, K., Naranjo, J.R., Bonfanti, L., Liss, B., Schütz, G., Grummt, I., Parlato, R., 2013. A neuroprotective phase precedes striatal degeneration upon nucleolar stress. *Cell Death and Differentiation*. **20**, 1455-1464.

Krobitsch, S. & Lindquist, S., 2000. Aggregation of Huntingtin in Yeast Varies with the Length of the Polyglutamine Expansion and the Expression of Chaperone Proteins. *Proceedings of the National Academy of Sciences - PNAS*. **97**, 1589-1594.

Krüger, R., Kuhn, W., Muller, T., Woitalla, D., Graeber, M., Kosel, S., Przuntek, H., Epplen, J.T., Schols, L., Rieess, O., 1998. Ala30Pro mutation in the gene encoding a-synuclein in Parkinson's disease. *Nature Genetics*. **18**, 106-108.

Kumar, A., Vaish, M., Ratan, R.R., 2014. Transcriptional dysregulation in Huntington's disease: a failure of adaptive transcriptional homeostasis. *Drug Discovery Today*. **19**, 956-962.

Landles, C., Sathasivam, K., Weiss, A., Woodman, B., Moffitt, H., Finkbeiner, S., Sun, B., Gafni, J., Ellerby, L.M., Trottier, Y., Richards, W.G., Osmand, A., Paganetti, P., Bates, G.P., 2010. Proteolysis of Mutant Huntingtin Produces an Exon 1 Fragment That Accumulates as an Aggregated Protein in Neuronal Nuclei in Huntington Disease. *The Journal of Biological Chemistry*. **285**, 8808-8823.

Langbehn, D., Brinkman, R., Falush, D., Paulsen, J., Hayden, M., 2004. A new model for prediction of the age of onset and penetrance for Huntington's disease based on CAG length. *Clinical Genetics*. **65**, 267-277.

Laquerriere, R., et al, 1957. Bi.ol. (in the press).

Larkin, A., Marygold, S.J., Antonazzo, G., Attrill, H., dos Santos, G., Garapati, P.V., Goodman, J., Gramates, L., Millburn, G., Strelets, V.B., Tabone, C.J., Thurmond, J., 2021. FlyBase: updates to the *Drosophila melanogaster* knowledge base. *Nucleic Acids Research*. **49**, D899-D907.

Lázaro, D.F., Rodrigues, E.F., Langohr, R., Shahpasandzadeh, H., Ribeiro, T., Guerreiro, P., Gerhardt, E., Kröhnert, K., Klucken, J., Pereira, M.D., Popova, B., Kruse, N., Mollenhauer, B., Rizzoli, S.O., Braus, G.H., Danzer, K.M., Outeiro, T.F., 2014. Systematic Comparison of the Effects of Alpha-synuclein Mutations on Its Oligomerization and Aggregation. *PLoS Genetics*. **10**, e1004741.

Lee, J.M., Ramos, E.M., Orobello, S., Di Donato, S., Gomez-Tortosa, E., Ayuso, C., Suchowersky, O., Trent, R.J.A., McCusker, E., Novelletto, A., Lee, J.H., Frontali, M., Jones, R., Ashizawa, T., Frank, S., Saint-Hilaire, M.H., Hersch, M.B., Zanko, A., Gillis, T., Luente, D., Rosas, H.D., Harrison, M.B., Abranson, R.K., Marder, K., Sequeiros, J., Paulsen, J.S., Landwehrmeyer, G.B., Myers, R.H., McDonald, M.E., Gusella, J.F., Mysore, J.S., Hayde, M.R., Warby, S.C., Morrison, P., Nance, M., Ross, C.A., Margolis, R.L., 2012. CAG repeat expansion in Huntington disease determines age at onset in a fully dominant fashion. *Neurology*. **78**, 690-695.

Lee, J., Hwang, Y.J., Boo, J.H., Han, D., Kwon, O.K., Todorova, K., Kowall, N.W., Kim, Y., Ryu, H., 2011. Dysregulation of upstream binding factor-1 acetylation at K352 is linked to impaired ribosomal DNA transcription in Huntington's disease. *Cell Death and Differentiation*. **18**, 1726-1735.

Lee, J., Hwang, Y.J., Ryu, H., Kowall, N.W., Ryu, H., 2014. Nucleolar dysfunction in Huntington's disease. *Biochimica Et Biophysica Acta. Molecular Basis of Disease*. **1842**, 785-790.

Lee, J., Wheeler, V., Chao, M., Vonsattel, J., Pinto, R., Lucente, D., Abu-Elneel, K., Ramos, E., Mysore, J., Gillis, T., MacDonald, M., Gusella, J., Harold, D., Stone, T., Escott-Price, V., Han, J., Vedernikov, A., Holmans, P., Jones, L., Kwak, S., Mahmoudi, M., Orth, M., Landwehrmeyer, G., Paulsen, J., Dorsey, E., Shoulson, I., Myers, R., 2015. Identification of Genetic Factors that Modify Clinical Onset of Huntington's Disease. *Cell*. **162**, 516-526.

Lesage, S., Deramecourt, V., Jacoupy, M., Hassoun, S., Pujol, C., Maurage, C., Sahbatou, M., Liebau, S., Bilgic, B., Emre, M., Erginol-Unaltuna, N., Guven, G., Tison, F., Tranchant, C., Corvol, J., Krack, P., Hernandez, D., Gibbs, J., Hardy, J., Wood, N., Durr, A., Deleuze, J., Tazir, M., Destée, A., Lohmann, E., Corti, O., Brice, A., Lesage, S., Tison, F., Vidailhet, M., Corvol, J., Agid, Y., Anheim, M., Bonnet, A., Borg, M., Broussolle, E., Durif, F., Krack, P., Klebe, S., Lohmann, E., Véritin, M., Viallet, F., Brice, A., Majounie, E., Corvol, J., Nalls, M., Ben-Shlomo, Y., Berg, D., Bhatia, K., de Bie, R.A., Bochdanovits, Z., Bonin, M., Bras, J., Brockmann, K., Chen, H., Counsell, C., Dexter, D., van Dijk, K., Dong, J., Escott-Price, V., Evans, J., Gray, E., Guerreiro, R., Hollenbeck, A., Holmans, P., Hu, M., Hudson, G., Jónsson, P., Langford, C., Lees, A., Lorenz, D., Lubbe, S., Lungu, C., Martinez, M., Mätzler, W., McNeill, A., Moorby, C., O'Sullivan, S., Owen, M., Pearson, J., Perlmuter, J., Plagnol, V., Ravina, B., Rivadeneira, F., Ryten, M., Schapira, A., Sharma, M., Sheerin, U., Sidransky, E., Spencer, C.A., Stefánsson, K., Strange, A., Talbot, K., Trabzuni, D., Traynor, B., van de Warrenburg, B., Williams-Gray, C., Winder-Rhodes, S., Morris, H., Hardy, J., 2016. Loss of VPS13C Function in Autosomal-Recessive Parkinsonism Causes Mitochondrial Dysfunction and Increases PINK1/Parkin-Dependent Mitophagy. *American Journal of Human Genetics*. **98**, 500-513.

Lewy, F.H., 1912. Paralysis agitans. Part 1: Pathologische Anatomie. In Lewandowsky, M., ed, *Spezielle Neurologie I*. Berlin: Julius Springer. 920-933.

Li, Z., Karlovich, C.A., Fish, M.P., Scott, M.P., Myers, R.M., 1999. A Putative Drosophila Homolog of the Huntington's Disease Gene. *Human Molecular Genetics*. **8**, 1807-1815.

Liti, G. & Louis, E.J., 2012. Advances in Quantitative Trait Analysis in Yeast. *PLoS Genetics*. **8**, e1002912.

Londin, E., Yadav, P., Surrey, S., Kricka, L.J. and Fortina, P., 2013. Use of Linkage Analysis, Genome-Wide Association Studies, and Next-Generation

Sequencing in the Identification of Disease-Causing Mutations. *Pharmacogenomics*. Totowa, NJ: Humana Press. 127-146.

Louis, E.J. & Haber, J.E., 1989. Nonrecombinant Meiosis I Nondisjunction in *Saccharomyces cerevisiae* Induced by tRNA Ochre Suppressors. *Genetics (Austin)*. **123**, 81-95.

Louvel, H., Gillet-Markowska, A., Liti, G., Fischer, G., 2013. A set of genetically diverged *Saccharomyces cerevisiae* strains with markerless deletions of multiple auxotrophic genes. *Yeast*. **31**, 91-101.

Lunkes, A., Lindenberg, K.S., Ben-Haiem, L., Weber, C., Devys, D., Landwehrmeyer, G.B., Mandel, J., Trottier, Y., 2002. Proteases Acting on Mutant Huntington Generate Cleaved Products that Differentially Build Up Cytoplasmic and Nuclear Inclusions. *Molecular Cell*. **10**, 259–269.

Maddison, D.C., Alfonso-Núñez, M., Swaibh, A.M., Breda, C., Campesan, S., Allcock, N., Straatman-Iwanowska, A., Kyriacou, C.P., Giorgini, F., 2020. A novel role for kynurenine 3-monooxygenase in mitochondrial dynamics. *PLOS Genetics*. **16**, e1009129.

Madero-Pérez, J., Fdez, E., Fernández, B., Lara Ordóñez, A.J., Blanca Ramírez, M., Gómez-Suaga, P., Waschbüsch, D., Lobbestael, E., Baekelandt, V., Nairn, A.C., Ruiz-Martínez, J., Aiastui, A., López de Munain, A., Lis, P., Comptdaer, T., Taymans, J., Chartier-Harlin, M., Beilina, A., Gonnelli, A., Cookson, M.R., Greggio, E., Hilfiker, S., 2018. Parkinson disease-associated mutations in LRRK2 cause centrosomal defects via Rab8a phosphorylation. *Molecular Neurodegeneration*. **13**, 3.

Maitra, U., Harding, T., Liang, Q., Ciesla, L., 2021. GardeninA confers neuroprotection against environmental toxin in a *Drosophila* model of Parkinson's disease. *Communications Biology*. **4**, 162.

Marston, A.L., 2014. Chromosome Segregation in Budding Yeast: Sister Chromatid Cohesion and Related Mechanisms. *Genetics (Austin)*. **196**, 31-63.

Mason, R.P. & Giorgini, F., 2011. Modeling Huntington disease in yeast. Perspectives and future directions. *Prion*. **5**, 269-276.

Mason, R.P., Casu, M., Butler, N., Breda, C., Campesan, S., Clapp, J., Green, E.W., Dhulkhed, D., Kyriacou, C.P., Giorgini, F., 2013. Glutathione peroxidase activity is neuroprotective in models of Huntington's disease. *Nature Genetics*. **45**, 1249-1254.

McEwen, R.S., 1918. *Drosophila* and its mutants. *The Journal of Experimental Zoology*. **25**, 49.

McGurk, L., Berson, A., Bonini, N.M., 2015. *Drosophila* as an In Vivo Model for Human Neurodegenerative Disease. *Genetics (Austin)*. **201**, 377-402.

Menezes, R., Tenreiro, S., Macedo, D., Santos, C.N., Outeiro, T.F., 2015. From the baker to the bedside: yeast models of Parkinson's disease. *Microbial Cell*. **2**, 262-279.

Merriin, A.B., Zhang, X., He, X., Newnam, G.P., Chernoff, Y.O., Sherman, M.Y., 2002. Huntington Toxicity in Yeast Model Depends on Polyglutamine Aggregation Mediated by a Prion-Like Protein Rnq1. *The Journal of Cell Biology*. **157**, 997-1004.

Metzler, M., Gan, L., Mazarei, G., Graham, R.K., Liu, L., Bissada, N., Lu, G., Leavitt, B.R., Hayden, M.R., 2010. Phosphorylation of huntingtin at Ser421 in YAC128 neurons is associated with protection of YAC128 neurons from NMDA-mediated excitotoxicity and is modulated by PP1 and PP2A. *The Journal of Neuroscience*. **30**, 14318-14329.

Miller, D.W., Hague, S.M., Clarimon, J., Baptista, M., Gwinn-Hardy, K., Cookson, M.R., Singleton, A.B., 2004. α -Synuclein in blood and brain from familial Parkinson disease with SNCA locus triplication. *Neurology*. **62**, 1835-1838.

Miller-Fleming, L., Giorgini, F., Outeiro, T.F., 2008. Yeast as a model for studying human neurodegenerative disorders. *Biotechnology Journal*. **3**, 325-338.

Miluzio, A., Ricciardi, S., Manfrini, N., Alfieri, R., Oliveto, S., Brina, D., Biffo, S., 2016. Translational control by mTOR-independent routes: how eIF6 organizes metabolism. *Biochemical Society Transactions*. **44**, 1667–1673.

Monckton, D.G., 2021. The Contribution of Somatic Expansion of the CAG Repeat to Symptomatic Development in Huntington's Disease: A Historical Perspective. *Journal of Huntington's Disease*. **10**, 7-33.

Morton, A.J., et al, 2018. Huntington's Disease_CNS - Brain (MMHCC)_GSE857. [online]. Available at: [https://maayanlab.cloud/Harmonizome/gene_set/Huntington's+Disease_CNS+-+Brain+\(MMHCC\)_GSE857/GEO+Signatures+of+Differentially+Expressed+Genes+for+Diseases](https://maayanlab.cloud/Harmonizome/gene_set/Huntington's+Disease_CNS+-+Brain+(MMHCC)_GSE857/GEO+Signatures+of+Differentially+Expressed+Genes+for+Diseases) [accessed July 2020].

Morton, A.J., Hunt, M.J., Hodges, A.K., Lewis, P.D., Redfern, A.J., Dunnett, S.B., Jones, L., 2005. A combination drug therapy improves cognition and reverses gene expression changes in a mouse model of Huntington's disease. *The European Journal of Neuroscience*. **21**, 855-870.

Morton, A.J., Wood, N.I., Hastings, M.H., Hurelbrink, C., Barker, R.A., Maywood, E.S., 2005. Disintegration of the Sleep-Wake Cycle and Circadian Timing in Huntington's Disease. *The Journal of Neuroscience*. **25**, 157-163.

Muchowski, P.J., Schaffar, G., Sittler, A., Wanker, E.E., Hayer-Hartl, M.K., Hartl, F.U., 2000. Hsp70 and Hsp40 Chaperones Can Inhibit Self-Assembly of Polyglutamine Proteins into Amyloid-Like Fibrils. *Proceedings of the National Academy of Sciences - PNAS*. **97**, 7841-7846.

Mueller, K.A., Glajch, K.E., Huizenga, M.N., Wilson, R.A., Granucci, E.J., Dios, A.M., Tousley, A.R., Iuliano, M., Weisman, E., LaQuaglia, M.J., DiFiglia, M., Kegel-Gleason, K., Vakili, K., Sadri-Vakili, G., 2018. Hippo Signaling Pathway Dysregulation in Human Huntington's Disease Brain and Neuronal Stem Cells. *Scientific Reports*. **8**, 11355-13.

Myers, R.H., Leavitt, J., Farrer, L.A., Jagadeesh, J., McFarlana, H., Mastromarco, C.A., Mark, J., Gusella, J.F., 1989. Homozygote for Huntington disease. *American Journal of Human Genetics*. **45**, 615-618.

Nalls, M.A., Blauwendraat, C., Vallerga, C.L., Heilbron, K., Bandres-Ciga, S., Chang, D., Tan, M., Kia, D.A., Noyce, A.J., Xue, A., Bras, J., Young, E., Von Coelln, R., Simón-Sánchez, J., Schulte, C., Sharma, M., Krohn, L., Pihlstrøm, L., Siitonen, A., Iwaki, H., Leonard, H., Faghri, F., Gibbs, J.R., Hernandez, D.G., Scholz, S.W., Botia, J.A., Martinez, M., Corvol, J., Lesage, S., Jankovic, J., Shulman, L.M., Sutherland, M., Tienari, P., Majamaa, K., Toft, M., Andreassen, O.A., Bangale, T., Brice, A., Yang, J., Gan-Or, Z., Gasser, T., Heutink, P., Shulman, J.M., Wood, N.W., Hinds, D.A., Hardy, J.A., Morris, H.R., Gratten, J., Visscher, P.M., Graham, R.R., Singleton, A.B., Adarnes-Gómez, A.D., Aguilar, M., Aitkulova, A., Akhmetzhanov, V., Alcalay, R.N., Alvarez, I., Alvarez, V., Bandres-Ciga, S., Barrero, F.J., Bergareche Yarza, J.A., Bernal-Bernal, I., Billingsley, K., Blauwendraat, C., Blazquez, M., Bonilla-Toribio, M., Botía, J.A., Boungiorno, M.T., Bras, J., Brice, A., Brockmann, K., Bubb, V., Buiza-Rueda, D., Cámara, A., Carrillo, F., Carrión-Claro, M., Cerdan, D., Chelban, V., Clarimón, J., Clarke, C., Compta, Y., Cookson, M.R., Corvol, J., Craig, D.W., Danjou, F., Diez-Fairen, M., Dols-Icardo, O., Duarte, J., Duran, R., Escamilla-Sevilla, F., Escott-Price, V., Ezquerra, M., Faghri, F., Feliz, C., Fernández, M., Fernández-Santiago, R., Finkbeiner, S., Foltyne, T., Gan-Or, Z., Garcia, C., García-Ruiz, P., Gasser, T., Gibbs, J.R., Gomez Heredia, M.J., Gómez-Garre, P., González, M.M., Gonzalez-Aramburu, I., Guelfi, S., Guerreiro, R., Hardy, J., Hassin-Baer, S., Hernandez, D.G., Heutink, P., Hoenicka, J., Holmans, P., Houlden, H., Infante, J., Iwaki, H., Jesús, S., Jimenez-Escríg, A., Kaishybayeva, G., Kaiyrzhanov, R., Karimova, A., Kia, D.A., Kinghorn, K.J., Koks, S., Krohn, L., Kulisevsky, J., Labrador-Espinosa, M.A., Leonard, H.L., Lesage, S., Lewis, P., Lopez-Sendon, J.L., Lovering, R., Lubbe, S., Lungu, C., Macias, D., Majamaa, K., Manzoni, C., Marín, J., Marinus, J., Martí, M.J., Martinez, M., Martínez Torres, I., Martínez-Castrillo, J.C., Mata, M., Mencacci, N.E., Méndez-Del-Barrio, C., Middlehurst, B., Mínguez, A., Mir, P., Mok, K.Y., Morris, H.R., Muñoz, E., Nalls, M.A., Narendra, D., Noyce, A.J., Ojo, O.O., Okubadejo, N.U., Pagola, A.G., Pastor, P., Perez Errazquin, F., Periñán-Tocino, T., Pihlstrom, L., Plun-Favreau, H., Quinn, J., R'bibo, L., Reed, X., Rezola, E.M., Rizig, M., Rizzu, P., Robak, L., Rodriguez, A.S., Rouleau, G.A., Ruiz-Martínez, J., Ruz, C., Ryten, M., Sadykova, D., Scholz, S.W., Schreglmann, S., Schulte, C., Sharma, M., Shashkin, C., Shulman, J.M., Sierra, M., Siitonen, A., Simón-Sánchez, J., Singleton, A.B., Suarez-Sanmartin, E., Taba, P., Tabernero, C., Tan, M.X., Tartari, J.P., Tejera-Parrado, C., Toft, M., Tolosa, E., Trabzuni, D., Valldeoriola, F., Van Hilten, J.J., Van Keuren-Jensen, K., Vargas-González, L., Vela, L., Vives, F., Williams, N., Wood, N.W., Zharkinbekova, N., Zharmukhanov, Z., Zholdybayeva, E.,

Zimprich, A., Ylikotila, P., Shulman, L.M., Von Coelln, R., Reich, S., Savitt, J., Agee, M., Alipanahi, B., Auton, A., Bell, R.K., Bryc, K., Elson, S.L., Fontanillas, P., Furlotte, N.A., Huber, K.E., Hicks, B., Jewett, E.M., Jiang, Y., Kleinman, A., Lin, K., Litterman, N.K., McCreight, J.C., McIntyre, M.H., McManus, K.F., Mountain, J.L., Noblin, E.S., Northover, C.A.M., Pitts, S.J., Poznik, G.D., Sathirapongsasuti, J.F., Shelton, J.F., Shringarpure, S., Tian, C., Tung, J., Vacic, V., Wang, X., Wilson, C.H., Anderson, T., Bentley, S., Dalrymple-Alford, J., Fowdar, J., Gratten, J., Halliday, G., Henders, A.K., Hickie, I., Kassam, I., Kennedy, M., Kwok, J., Lewis, S., Mellick, G., Montgomery, G., Pearson, J., Pitcher, T., Sidorenko, J., Silburn, P.A., Vallerga, C.L., Visscher, P.M., Wallace, L., Wray, N.R., Xue, A., Yang, J., Zhang, F., 2019. Identification of novel risk loci, causal insights, and heritable risk for Parkinson's disease: a meta-analysis of genome-wide association studies. *The Lancet Neurology*. **18**, 1091–1102.

Nalls, M.A., Pankratz, N., Lill, C.M., Do, C.B., Hernandez, D.G., Saad, M., DeStefano, A.L., Kara, E., Bras, J., Sharma, M., Schulte, C., Keller, M.F., Arepalli, S., Letson, C., Edsall, C., Stefansson, H., Liu, X., Pliner, H., Lee, J.H., Cheng, R., Ikram, M.A., Ioannidis, J.P.A., Hadjigeorgiou, G.M., Bis, J.C., Martinez, M., Perlmutter, J.S., Goate, A., Marder, K., Fiske, B., Sutherland, M., Xiromerisiou, G., Myers, R.H., Clark, L.N., Stefansson, K., Hardy, J.A., Heutink, P., Chen, H., Wood, N.W., Houlden, H., Payami, H., Brice, A., Scott, W.K., Gasser, T., Bertram, L., Eriksson, N., Foroud, T., Singleton, A.B., 2014. Large-scale meta-analysis of genome-wide association data identifies six new risk loci for Parkinson's disease. *Nature Genetics*. **46**, 989-995.

NIH, 2019. Prion Diseases. [online]. Available at: <https://www.niaid.nih.gov/diseases-conditions/prion-diseases> [accessed 30/09/2020].

Nunomura, A., Honda, K., Takeda, A., Hirai, K., Zhu, X., Smith, M.A., Perry, G., 2006. Oxidative damage to RNA in neurodegenerative diseases. *Journal of Biomedicine & Biotechnology*. **2006**, 82323-6.

Nuoffer, C., Wu, S.K., Dascher, C., Balch, W.E., 1997. Mss4 does not function as an exchange factor for Rab in endoplasmic reticulum to Golgi transport. *Molecular Biology of the Cell*. **8**, 1305-1316.

Online Mendelian Inheritance in Man, OMIM, 2021. MIM Number: 168600. [online]. Available at: <https://omim.org/>.

Online Mendelian Inheritance in Man, OMIM, 2020. MIM Number: 143100. [online]. Available at: <https://omim.org/>.

Outeiro, T.F. & Lindquist, S., 2003. Yeast Cells Provide Insight into Alpha-Synuclein Biology and Pathobiology NIH Public Access. *Science*. **302**, 1772-1775.

Özsoy, E.D., Yilmaz, M., Patlar, B., Emecen, G., Durmaz, E., Magwire, M.M., Zhou, S., Huang, W., Anholt, R.R.H., Mackay, T.F.C., 2021. Epistasis for head morphology in *Drosophila melanogaster*. *G3*. **0**.

Parkinson, J., 1817. An Essay on the Shaking Palsy. *J Neuropsychiatry Clin Neurosci.* **14**, 223-236.

Parlato, R. & Kreiner, G., 2013. Nucleolar activity in neurodegenerative diseases: a missing piece of the puzzle? *Journal of Molecular Medicine (Berlin, Germany).* **91**, 541-547.

Parlato, R., Kreiner, G., Erdmann, G., Rieker, C., Stotz, S., Savenkova, E., Berger, S., Grummt, I., Schutz, G., 2008. Activation of an Endogenous Suicide Response after Perturbation of rRNA Synthesis Leads to Neurodegeneration in Mice. *The Journal of Neuroscience.* **28**, 12759-12764.

Parlato, R. & Liss, B., 2014. How Parkinson's disease meets nucleolar stress. *Biochimica Et Biophysica Acta. Molecular Basis of Disease.* **1842**, 791-797.

Parsons, M.P. & Raymond, L.A., 2015. Chapter 20 - Huntington Disease. *Neurobiology of Brain Disorders.* Elsevier Inc. 303-320.

Peña-Altamira, L.E., Polazzi, E., Monti, B., 2013. Histone Post-translational Modifications in Huntington's and Parkinson's Diseases. *Current Pharmaceutical Design.* **19**, 5085-5092.

Peters, T.W., Nelson, C.S., Gerencser, A.A., Dumas, K.J., Tavshanjian, B., Chang, K.C., Lithgow, G.J., Hughes, R.E., 2018. Natural Genetic Variation in Yeast Reveals That NEDD4 Is a Conserved Modifier of Mutant Polyglutamine Aggregation. *G3 (Bethesda, Md.).* **8**, 3421-3431.

Piccini, P., Morrish, P.K., Turjanski, N., Sawle, G.V., Burn, D.J., Weeks, R.A., Mark, M.H., Maraganore, D.M., Lees, A.J., Brooks, D.J., 1997. Dopaminergic Function in Familial Parkinson's Disease: X Clinical and 18F-Dopa Positron Emission Tomography Study. *Annals of Neurology.* **41**, 222-229.

Plomin, R., Haworth, C., Davis, O., 2009. Common disorders are quantitative traits. *Nat Rev Genet.* **10**, 872-878.

Polymeropoulos, M.H., Higgins, J.J., Globe, L.I., Johnson, W.G., Ide, S.E., Di Iorio, G., Sanges, G., Stenroos, E.S., Pho, L.T., Schaffer, A.A., Lazzarini, A.M., Nussbaum, R.L., Duvoisin, R.G., 1996. Mapping of a Gene for Parkinson's Disease to Chromosome 4q21-q23. *Science.* **274**, 1197-1199.

Polymeropoulos, M.H., Lavedan, C., Leroy, E., Ide, S.E., Dehejia, A., Dutra, A., Pike, B., Root, H., Rubenstein, J., Boyer, R., Stenroos, E.S., Chandrasekharappa, S., Athanasiadou, A., Papapetropoulos, T., Johnson, W.G., Lazzarini, A.M., Duvoisin, R.C., Di Iorio, G., Golbe, L.I., Nussbaum, R.L., 1997. Mutation in the $\{\alpha\}$ -Synuclein Gene Identified in Families with Parkinson's Disease. *Science.* **276**, 2045-2047.

Raben, N., Danon, M., DiMauro, S., Plotz, P., Lu, N., Lee, E., Shliselfeld, L., Skurat, A.V., Roach, P.J., Lawrence, J.C., Musumeci, O., Shanske, S., 2001.

Surprises of genetic engineering: A possible model of polyglucosan body disease. *Neurology*. **56**, 1739-1745.

Rai, A., Singh, P.K., Singh, V.K., Kumar, V., Mishra, R., Thakur, A.K., Mahadevan, A., Shankar, S.K., Jana, N.R., Ganesh, S., 2018. Glycogen synthase protects neurons from cytotoxicity of mutant huntingtin by enhancing the autophagy flux. *Cell Death and Disease*. **9**, .

Reiner, A., Dragatsis, I. and Dietrich, P., 2011. Genetics and Neuropathology of Huntington's Disease. *International Review of Neurobiology*. United States: Elsevier Science & Technology. 325-372.

Richards, P., Didszun, C., Campesan, S., Simpson, A., Horley, B., Young, K.W., Glynn, P., Cain, K., Kyriacou, C.P., Giorgini, F., Nicotera, P., 2011. Dendritic spine loss and neurodegeneration is rescued by Rab11 in models of Huntington's disease. *Cell Death and Differentiation*. **18**, 191-200.

Rieker, C., Engblom, D., Kreiner, G., Domanskyi, A., Schober, A., Stotz, S., Neumann, M., Yuan, X., Grummt, I., Schütz, G., Parlato, R., 2011. Nucleolar Disruption in Dopaminergic Neurons Leads to Oxidative Damage and Parkinsonism through Repression of Mammalian Target of Rapamycin Signaling. *The Journal of Neuroscience*. **31**, 453-460.

Rodrigues, F.B., Byrne, L.M., Lowe, A.J., Tortelli, R., Heins, M., Flik, G.G., Johnson, E.B., De Vita, E., Scahill, R.I., Giorgini, F., Wild, E.J., 2021. Kynurenone pathway metabolites in cerebrospinal fluid and blood as potential biomarkers in Huntington's disease. *Journal of Neurochemistry*. **158**, 539-553.

Roos, R.A.C., 2010. Huntington's disease: a clinical review. *Orphanet Journal of Rare Diseases*. **5**, .

Ross, C. & Tabrizi, S.J., 2011. Huntington's disease: from molecular pathogenesis to clinical treatment. *10*, 83-98.

Rouillard, A.D., Gundersen, G.W., Fernandez, N.F., Wang, Z., Monteiro, C.D., McDermott, M.G., Maayan, A., 2016. The harmonizome: a collection of processed datasets gathered to serve and mine knowledge about genes and proteins. *Database : The Journal of Biological Databases and Curation*. **2016**, baw100.

Sathasivam, K., Neueder, A., Detloff, P.J., Housman, D.E., Batea, G.P., Gipson, T.A., Landles, C., Benjamin, A.C., Bondulich, M.K., Smith, D.L., Faull, R.L.M., Roos, R.A.C., Howland, D., 2013. Aberrant splicing of HTT generates the pathogenic exon 1 protein in Huntington disease. *Proceedings of the National Academy of Sciences - PNAS*. **110**, 2366-2370.

Saudou, F. & Humbert, S., 2016. The Biology of Huntingtin. *Neuron (Cambridge, Mass.)*. **89**, 910-926.

Schrader, C., Capelle, H.-., Knife, T.M., Blahak, C., Bazner, H., Lutjens, G., Dressler, D., Krauss, J.K., 2011. GPi-DBS may induce a hypokinetic gait disorder with freezing of gait in patients with dystonia. *Neurology*. **77**, 483-488.

Schulte, J. & Littleton, J.T., 2011. The biological function of the Huntington protein and its relevance to Huntington's Disease pathology. *Current Trends in Neurology*. **5**, 65-78.

Shahmoradian, S.H., Lewis, A.J., Genoud, C., Hench, J.r., Moors, T.E., Navarro, P.P., Castaño-Díez, D., Schweighauser, G., Graff-Meyer, A., Goldie, K.N., Sütterlin, R., Huisman, E., Ingrassia, A., Gier, Y.d., Rozemuller, A.J.M., Wang, J., Paepe, A.D., Erny, J., Staempfli, A., Hoernschemeyer, J., Großerüschkamp, F., Niedieker, D., el-Mashtoly, S.F., Quai, M., van IJcken, Wilfred F. J., Bonifati, V., Gerwert, K., Bohrmann, B., Frank, S., Britschgi, M., Stahlberg, H., van de Berg, Wilma D. J., Lauer, M.E., 2019. Lewy pathology in Parkinson's disease consists of crowded organelles and lipid membranes. *Nature Neuroscience*. **22**, 1099-1109.

Shahnawaz, M., Mukherjee, A., Pritzkow, S., Mendez, N., Rabadia, P., Liu, X., Hu, B., Schmeichel, A., Singer, W., Wu, G., Tsai, A., Shirani, H., Nilsson, K.P.R., Low, P.A., Soto, C., 2020. Discriminating α -synuclein strains in Parkinson's disease and multiple system atrophy. *Nature (London)*. **578**, 273-277.

Shamseldin, H.E., et al, 2016. Mutation of the mitochondrial carrier SLC25A42 causes a novel form of mitochondrial myopathy in humans. Springer Science and Business Media LLC.

Shao, L. & Hewitt, M.C., 2010. The kinetic isotope effect in the search for deuterated drugs. *Drug News & Perspectives*. **23**, 398-404.

Sherman, B.T., Lempicki, R.A., Huang, D.W., 2008. Systematic and integrative analysis of large gene lists using DAVID bioinformatics resources. *Nature Protocols*. **4**, 44-57.

Sherman, F., 2002. Getting started with yeast. *Methods in Enzymology*. United States: Elsevier Science & Technology. 3-41.

Singleton, A.B., Farrer, M., Lincoln, S., Crawley, A., Hanson, M., Maraganore, D., Adler, C., Cookson, M.R., Muenter, M., Babptista, M., Miller, D., Blacanto, J., Johnson, J., Hardy, J., Gwinn-Hardy, K., Singleton, A., Hague, S., Kachergus, J., Hulihan, M., Peuralllna, T., Dutra, A., Nussbaum, R., 2003. α -Synuclein Locus Triplication Causes Parkinson's Disease. *Science (American Association for the Advancement of Science)*. **302**, 841.

Skovronsky, D.M., Lee, V.M., Trojanowski, J.Q., 2006. Neurodegenerative diseases: new concepts of pathogenesis and their therapeutic implications. *Annual Review of Pathology*. **1**, 151-170.

Sontag, J. & Sontag, E., 2014. Protein phosphatase 2A dysfunction in Alzheimerâ€™s disease. *Frontiers in Molecular Neuroscience*. **7**.

Spillantini, M.G., Crowther, R.A., Jakes, R., Hasegawa, M., Goedert, M., 1998. α-Synuclein in filamentous inclusions of Lewy bodies from Parkinson's disease and dementia with Lewy bodies (ubiquitin/sarkosyl-insoluble filaments/immunoelectron microscopy). *Neurobiology Communicated by Max F. Perutz, Medical Research Council.* **95**, 6469–6473.

Steffan, J.S., Agrawal, N., Pallos, J., Rockabrand, E., Trotman, L.C., Slepko, N., Illes, K., Lukacsovich, T., Zhu, Y., Cattaneo, E., Pandolfi, P.P., Thompson, L.M., Marsh, J.L., 2004. SUMO Modification of Huntingtin and Huntington's Disease Pathology. *Science.* **304**, 100-104.

Steger, M., Diez, F., Dhekne, H.S., Lis, P., Nirujogi, R.S., Karayel, O., Tonelli, F., Martinez, T.N., Lorentzen, E., Pfeffer, S.R., Alessi, D.R., Mann, M., 2017. Systematic proteomic analysis of LRRK2-mediated Rab GTPase phosphorylation establishes a connection to ciliogenesis. *eLife.* **6**, e31012.

Steger, M., Tonelli, F., Ito, G., Davies, P., Trost, M., Vetter, M., Wachter, S., Lorentzen, E., Duddy, G., Wilson, S., Baptista, M.A., Fiske, B.K., Fell, M.J., Morrow, J.A., Reith, A.D., Alessi, D.R., Mann, M., 2016. Phosphoproteomics reveals that Parkinson's disease kinase LRRK2 regulates a subset of Rab GTPases. *eLife.* **5**, e12813.

Steinert, J.R., Campesan, S., Richards, P., Kyriacou, C.P., Forsythe, I.D., Giorgini, F., 2012. Rab11 rescues synaptic dysfunction and behavioural deficits in a Drosophila model of Huntington's disease. *Human Molecular Genetics.* **21**, 2912-2922.

Suster, M.L., Seugnet, L., Bate, M., Sokolowski, M.B., 2004. Refining GAL4-driven transgene expression inDrosophila with a GAL80 enhancer-trap. *Genesis (New York, N.Y. : 2000).* **39**, 240-245.

Tauber, E., Miller-Fleming, L., Mason, R.P., Kwan, W., Clapp, J., Butler, N.J., Outeiro, T.F., Muchowski, P.J., Giorgini, F., 2011. Functional Gene Expression Profiling in Yeast Implicates Translational Dysfunction in Mutant Huntingtin Toxicity. *The Journal of Biological Chemistry.* **286**, 410-419.

Taylor, M.B. & Ehrenreich, I.M., 2014. Higher-order genetic interactions and their contribution to complex traits. *Trends in Genetics.* **31**, 34-40.

Telenius, H., Greenberg, C., Adam, S., Clarke, L.A., Theilmann, J., Ives, E.J., Hayden, M.R., Kremer, B., Andrew, S.E., Zeisler, J., Goldberg, Y.P., 1994. Somatic and gonadal mosaicism of the Huntington disease gene CAG repeat in brain and sperm. *Nature Genetics.* **6**, 409-414.

Thomas, E.A., Coppola, G., Desplats, P.A., Tang, B., Soragni, E., Burnett, R., Gao, F., Fitzgerald, K.M., Borok, J.F., Herman, D., Geschwind, D.H., Gottesfeld, J.M., 2008. The HDAC Inhibitor 4b Ameliorates the Disease Phenotype and Transcriptional Abnormalities in Huntington's Disease Transgenic Mice. *Proceedings of the National Academy of Sciences - PNAS.* **105**, 15564-15569.

Tretiakoff, C., 1919. *Contribution a L'étude de L'anatomie Pathologique de Locus Niger de Soemmerling*. Ph. D. Université de Paris, Paris.

Tuite, M.F., 2019. Yeast models of neurodegenerative diseases. *Progress in Molecular Biology and Translational Science*. **168**, 351-379.

Ugur, B., Chen, K., Bellen, H.J., 2016. Drosophila tools and assays for the study of human diseases. *Disease Models & Mechanisms*. **9**, 235-244.

Visscher, P.M., Brown, M.A., McCarthy, M.I., Jian, Y., 2012. Five years of GWAS discovery. *American Journal of Human Genetics*. **90**, 7-24.

Visscher, P.M. & Goddard, M.E., 2019. From R.A. Fisher's 1918 Paper to GWAS a Century Later. *Genetics*. **211**, 1125–1130.

Vittori, A., Breda, C., Repici, M., Orth, M., Roos, R.A.C., Outeiro, T.F., Giorgini, F., Hollox, E.J., 2014. Copy-number variation of the neuronal glucose transporter gene SLC2A3 and age of onset in Huntington's disease. *Human Molecular Genetics*. **23**, 3129-3137.

Wang, Q., Liu, W., Liti, G., Wang, S., Bai, F., 2012. Surprisingly diverged populations of *Saccharomyces cerevisiae* in natural environments remote from human activity. *Molecular Ecology*. **21**, 5404-5417.

Wang, X. & Davis, R.L., 2021. Early Mitochondrial Fragmentation and Dysfunction in a Drosophila Model for Alzheimer's Disease. *Molecular Neurobiology*. **58**, 143-155.

Wang, Y., Wan, B., Li, D., Zhou, J., Li, R., Bai, M., Chen, F., Yu, L., 2012. BRSK2 is regulated by ER stress in protein level and involved in ER stress-induced apoptosis. *Biochemical and Biophysical Research Communications*. **423**, 813-818.

Warby, S.C., Chan, E.Y., Metzler, M., Gan, L., Singaraja, R.R., Crocker, S.F., Robertson, H.A., Hayden, M.R., 2005. Huntingtin phosphorylation on serine 421 is significantly reduced in the striatum and by polyglutamine expansion in vivo. *Human Molecular Genetics*. **14**, 1569-1577.

Warner, T.T. & Schapira, A.H.V., 2003. Genetic and Environmental Factors in the Cause of Parkinson's Disease. *Annals of Neurology*. **53**, S16–S25.

Weldon, W.F.R., 1902. Mendel's laws of alternative inheritance in peas. *Biometrika*. **1**, 228-233.

Wellington, C.L., Ellerby, L.M., Gutekunst, C., Rogers, D., Warby, S., Graham, R.K., Loubser, O., van Raamsdonk, J., Singaraja, R., Yang, Y., Gafni, J., Bredesen, D., Hersch, S.M., Leavitt, B.R., Roy, S., Nicholson, D.W., Hayden, M.R., 2002. Caspase Cleavage of Mutant Huntingtin Precedes Neurodegeneration in Huntington's Disease. *The Journal of Neuroscience*. **22**, 7862-7872.

Werner, A., et al, 2015. Cell-fate determination by ubiquitin-dependent regulation of translation. Springer Science and Business Media LLC.

Wexler, N.S., Young, A.B., Tanzi, R.E., Travers, H., Starosta-Rubinstein, S., Penney, J.B., Snodgrass, S.R., Shoulson, I., Gomez, F., Ramos Arroyo, M.A., Penchaszadeh, G.K., Moreno, H., Gibbons, K., Faryniarz, A., Hobbs, W., Anderson, M.A., Bonilla, E., Conneally, P.M., Gusella, J.F., 1987. Homozygotes for Huntington's disease. *Nature*. **326**, 194–197.

White, J.A., Anderson, E., Zimmerman, K., Zheng, K.H., Rouhani, R., Gunawardena, S., 2015. Huntingtin differentially regulates the axonal transport of a sub-set of Rab-containing vesicles in vivo. *Human Molecular Genetics*. **24**, 7182-7195.

Willingham, S., Outeiro, T.F., DeVit, M.J., Lindquist, S.L., Muchowski, P.J., 2003. Yeast Genes That Enhance the Toxicity of a Mutant Huntingtin Fragment or $\{\alpha\}$ -Synuclein. *Science*. **302**, 1769-1772.

Wojtecki, L., Groiss, S.J., Hartmann, C.J., Elben, S., Omlor, S., Schnitzler, A., Vesper, J., 2016. Deep Brain Stimulation in Huntington's Disease—Preliminary Evidence on Pathophysiology, Efficacy and Safety. *Brain Sciences*. **6**, .

Wood, A.R., Esko, T., Yang, J., Vedantam, S., Pers, T.H., Gustafsson, S., Chu, A.Y., Estrada, K., Luan, J., Kutalik, Z., Amin, N., Buchkovich, M.L., Croteau-Chonka, D.C., Day, F.R., Duan, Y., Fall, T., Fehrman, R., Ferreira, T., Jackson, A.U., Karjalainen, J., Lo, K.S., Locke, A.E., Mägi, R., Mihailov, E., Porcu, E., Randall, J.C., Scherag, A., Vinkhuyzen, A.A.E., Westra, H., Winkler, T.W., Workalemahu, T., Zhao, J.H., Absher, D., Albrecht, E., Anderson, D., Baron, J., Beekman, M., Demirkan, A., Ehret, G.B., Feenstra, B., Feitosa, M.F., Fischer, K., Fraser, R.M., Goel, A., Gong, J., Justice, A.E., Kanoni, S., van der Velde, N., Hovingh, G.K., Kastelein, J.J.P., 2014. Defining the role of common variation in the genomic and biological architecture of adult human height. *Nature Genetics*. **46**, 1173-1186.

Xia, J., Lee, D.H., Taylor, J., Vandelft, M., Truant, R., 2003. Huntingtin contains a highly conserved nuclear export signal. *Human Molecular Genetics*. **12**, 1393-1403.

Yengo, L., Sidorenko, J., Kemper, K.E., Zheng, Z., Wood, A.R., Weedon, M.N., Frayling, T.M., Hirschhorn, J., Yang, J., Visscher, P.M., 2018. Meta-analysis of genome-wide association studies for height and body mass index in ~700000 individuals of European ancestry. *Human Molecular Genetics*. **27**, 3641-3649.

Yuan, X., Zhou, Y., Casanova, E., Chai, M., Kiss, E., Gröne, H., Schütz, G., Grummt, I., 2005. Genetic Inactivation of the Transcription Factor TIF-IA Leads to Nucleolar Disruption, Cell Cycle Arrest, and p53-Mediated Apoptosis. *Molecular Cell*. **19**, 77-87.

Yue Hu, 2020. *Quantitative genetics of complex traits: solutions for studying the genetic basis of variation in yeast*. Ph. D. University of Leicester.

Zabrocki, P., Hoof, C.V., Goris, J., Thevelein, J.M., Winderickx, J., Wera, S., 2002. Protein phosphatase 2A on track for nutrient-induced signalling in yeast. *Molecular Microbiology*. **43**, 835-842.

Zhang, J., Perry, G., Smith, M.A., Robertson, D., Olson, S.J., Graham, D.G., Montine, T.J., 1999. Parkinson's Disease Is Associated with Oxidative Damage to Cytoplasmic DNA and RNA in Substantia Nigra Neurons. *The American Journal of Pathology*. **154**, 1423-1429.

Zheng, Z. & Diamond, M.I., 2012. Huntington Disease and the Huntingtin Protein. *Progress in Molecular Biology and Translational Science*. Netherlands: 189-214.

Zhou, J., Zhou, B.O., Lenzmeier, B.A., Zhou, J., 2009. Histone deacetylase Rpd3 antagonizes Sir2-dependent silent chromatin propagation. *Nucleic Acids Research*. **37**, 3699-3713.